# Thermodynamic and Heat Transfer Modeling of a Scroll Pump

by

Sankar Sunder

Submitted to the Department of Mechanical Engineering
in partial fulfillment of the requirements for the degree of

Doctor of Philosophy

at the

MASSACHUSETTS INSTITUTE OF TECHNOLOGY

Sept 1996
[February 1997]



Author .....
Department of Mechanical Engineering
Sept 2, 1996

Certified by....
.....
Joseph L. Smith, Jr.
Professor of Mechanical Engineering
Thesis Supervisor

Accepted by .....
Ain A. Sonin
Chairman, Departmental Committee on Graduate Students

This Thesis is Dedicated to my Grandparents,

Mrs. Janaki and Mr. S. Srinivasan,
Mrs. Sundari and Mr. S. Sankar.

From,
Their First Grandchild to earn a Ph.D

# Thermodynamic and Heat Transfer Modeling of a Scroll Pump

by

Sankar Sunder

Submitted to the Department of Mechanical Engineering
on Sept 2, 1996, in partial fulfillment of the
requirements for the degree of
Doctor of Philosophy

## Abstract

This thesis deals with the modeling and prediction of the internal processes of a scroll pump. The thesis is broadly divided into 3 distinct parts.

In the first part, we present a lumped parameter model of a scroll pump. Such a model takes the pump inlet state and discharge pressure as inputs and iteratively calculates the thermodynamic states of all intermediate stages of compression. Wall temperatures and closed process polytropic coefficient are also calculated. The model uses lumped parameter formulations of suction heat transfer, leakage into suction, leakage into the closed process, discharge heat transfer and discharge-to-suction wall heat transfer, while neglecting closed process heat transfer and frictional losses. Heat transferred from discharge side walls to suction side walls is through a combination of radial conduction through the bases of the fixed and orbiting scrolls, and kissing heat transfer.

In the second part of the thesis, we analyze kissing heat transfer which is a novel mechanism of conduction through transient contact between wraps of a scroll pump. We model kissing heat transfer as conduction through transient contact between semi-infinite bodies (wraps of scroll pump). The effectiveness of kissing heat transfer depends upon the angle of contact (and time of transient contact) between wraps of the scroll pump. Contact angles were estimated based on considerations of hertzian stresses. Lumped parameter heat transfer conductance calculations then suggest that while convection plays a major role in transferring heat on the discharge and suction sides of the pump, heat transfer at portions internal to the pump is likely to be in the form of conduction through the bases of the fixed and orbiting scrolls, and kissing heat transfer. Experiments were conducted on a specially modified and instrumented scroll compressor, which revealed the existence of large heat fluxes (and temperature differences) across the wraps of the fixed scroll. Such heat fluxes are symptomatic of kissing heat transfer and can't feasibly be explained by convection. Kissing heat transfer contact angles estimated from experimental data are roughly of the same order of magnitude as our physically based assumptions. The presence of significant heat fluxes across scroll wraps along with the experimental estimation of realistic kiss-

ing heat transfer contact angles together provide compelling evidence of the existence of kissing heat transfer between the wraps of a scroll pump.

In the third part of the thesis, we develop a distributed parameter model of a scroll pump. The distributed parameter model solves the partial differential equations governing continuity and energy for the gas in a scroll pump. Since such gas interacts with the metal parts of the pump, the energy interactions to the metal are also separately modeled. Metal side simulations demonstrate that radial conduction on the base of the fixed and orbiting scrolls and kissing heat transfer between wraps of the scrolls, are crucial in explaining the angular asymmetries in experimentally observed scroll wall temperature profiles. Gas side simulations help validate the assumptions of the lumped parameter model. They show that leakage and heat transfer are crucial sources of irreversibility to the suction processes of a scroll pump. Closed process calculations demonstrate that the bulk of closed cycle irreversibility can be ascribed to leakage and that closed cycle heat transfer can be neglected. Based on data from a number of simulations of the pump, correlations are developed to obtain the lumped parameter formulation of leakage phenomena in the scroll pump. Leakage into suction is found to depend principally on the suction density, while that into the closed pocket depends on pressure difference across the pump as well as discharge density.

The distributed parameter model of the scroll pump enables us to study the internal processes of a scroll pump in detail. The lumped parameter model, however is the model of choice for quick and easily computable prediction of scroll pump performance.

Thesis Supervisor: Joseph L. Smith, Jr.
Title: Professor of Mechanical Engineering

Thesis Supervisor: Gerald L. Wilson
Title: Professor of Electrical Engineering

Thesis Supervisor: Peter Griffith
Title: Professor of Mechanical Engineering

Thesis Supervisor: John H. Lienhard
Title: Professor of Mechanical Engineering

# Acknowledgments

## Professional Acknowledgements

First and foremost, I would like to express my sincerest gratitude to Prof. Joseph Smith, who has been my mentor and teacher for the last six years. It has been an honor and a privilege working under him.

I am deeply indebted to Prof. Gerald Wilson, who made this research project possible, and to Prof. Peter Griffith and Prof. John Lienhard for being on my thesis committee, and for guiding me as necessary.

The work that went into this thesis was entirely supported by research grants from Carrier Corporation, Syracuse. I would like to thank Carrier for giving me an opportunity to work on a relevant industrial problem for a Ph.D thesis. Many thanks go to Dr. Ezzat Khalifa, Mr. Bill Bush and Mr. Alex Lifsom of Carrier for promptly answering my questions and providing me with any information that I requested. I would also like to acknowledge the help of engineers at United Technologies Research Center (UTRC) in my research.

My colleagues at the Carrier Research Group at MIT have been a great source of inspiration for me. I would like to thank Dr. Steve Umans for his patience and persistence with my non-convergent computer programs. I would also like to thank Dave Otten, Tolga Ozgen and Patrick Leung for their help. Special thanks go to Mike Demaree and Bob Gertsen for their excellent workmanship in building my experiment.

I would like to thank Greg Nellis for his invaluable suggestions in developing an algorithm for the distributed parameter pump model.

I would like to thank my friends at the cryogenics lab (my second home for the last six years) for everything. Its been great fun interacting with Ed Ognibene, Bill Grassmyer, Greg Nellis, Hayong Yun, Brian Bowers, Ashok Patel and Hua Lang. Thanks also to Doris Elsemiller and Leslie Regan for their invaluable administrative help.

## Personal Acknowledgements

During the course of the last six years, I have made many friends at MIT, each of who has contributed positively to my experience at graduate school.

Many thanks to SRV with who I have wasted innumerable hours discussing everything from control theory to politics to the thermodynamics of economics ( on which I haven't lost hope as yet).

Thanks to Sumanth for all the fun times and good advice. We'll still write our famous paper on the Tang hall effect some day.

Thanks to Anandi for being a patient listener and indulging me my fantastic notions of doing cutting-edge economics research.

I wish Sumanth, SRV and Anandi well as they embark on their respective academic careers.

Thanks to Pradeep, Srikar and Gokul for being reliable roommates and solid friends.

Thanks also to TAV, Rizwan and Anant for each making my stay at MIT more enjoyable.

I have made many other good friends through my association with Sangam, the Indian Students' Association at MIT. I'd like to thank them all for their companionship.

My (over)active social life at MIT has probably been partially responsible for any delays with my thesis. However, I absolve my friends of any guilt on this count.

I'd like to thank my aunt Mrs. Ganga Krishnan and my sister-in-law, Priya for their affection and the many home-cooked meals that I have enjoyed at their home over the last two years.

Finally, I would like to thank my parents and grandparents for instilling in me an appreciation for education and a quest for excellence. It has always been my endeavor to live up to their high expectations.

This thesis is dedicated to my grandparents from their first grandchild to earn a Ph.D.

# Contents

# Chapter 1

# Introduction

## 1.1 Background

The concept for a scroll pump was proposed by Leon Creux [4] over 70 years ago. The geometric complexity of the machine however ensured that it did not start to be manufactured until very recently. Of late, however, scroll compressors are finding increasing use in HVAC systems. There are currently at least half a dozen major manufacturers of scroll compressors with many others waiting to invest in this technology. The reasons for this popularity are twofold. First of all, such compressors have a major advantage in terms of compactness, and are well-suited to the design of hermetically sealed machines that are integrated with the motors that drive the pumps of such compressors. A second important reason for their increasing prevalence is that the use of Numerically Controlled (NC) machines and modern machine tools has led to very reliable manufacture and alignment of the high precision parts that are necessary in the fabrication of such a system. Since the complex geometry of the machine was a major obstacle in the manufacture of these machines, a lot of work has gone into understanding the geometry and in rendering it manufacturable. An elegant generalized description of the principle of conjugacy for the surfaces of a scroll pump can be found in [2]. An extension of this principle has found use in the design of hybrid scroll geometries as described in [3]. While much work has concentrated on understanding scroll geometries, much of the research in evaluating scroll pump



**There is no text material missing here.**
**Pages have been incorrectly numbered.**

thermodynamic performance has been experimental and piecemeal in nature. Various sources of inefficiencies in scroll pumps have been listed in [2], but there has been no systematic attempt to model inefficiencies and irreversibilities in scroll pumps as they occur, so as to predict pump thermodynamic performance. This thesis attempts to fill such a void.

In this chapter, we first motivate the need for a predictive tool for scroll pump performance, followed briefly by a tutorial on scroll geometry as well as a brief synopsis of the rest of the thesis document.

## 1.2 Motivation for Scroll Pump Modeling

The primary motivation for scroll pump modeling is threefold - for use in making electromechanical design tradeoffs, for use in compressor protection algorithms and for use as a design tool for new generations of scroll pumps.

### 1.2.1 Electromechanical Design Tradeoffs

Scroll compressors go through a wide range of operating conditions. In order to optimize compressor design, we need to be able to predict the performance of these machines under these operating conditions. Such prediction would be of great value as a design tool with which to make design tradeoffs. The scroll compressor, however, is a complex machine with interacting electrical, thermodynamic and thermal processes that together affect overall machine performance. Within the shell of a scroll compressor, the scroll pump coexists in a hermetic environment with a motor and with the bearings that support the drive shaft. The pump's thermodynamic performance affects the motor as this determines the power demanded by the machine. Motor performance in turn also affects pump performance as the pump and motor are part of the same thermal environment. Volumetric efficiency of the pump and system capacity are affected by the state of gas entering the pump, which in turn is affected by the temperature of the motor windings and the bearing losses. The interaction of electrical, thermal and thermodynamic effects within the hermetic en-

vironment is the subject of an interdisciplinary study at MIT. Prediction of thermal and thermodynamic performance of the pump is an essential part of this program. Such a program aids in weighing the different design tradeoffs to be made in scroll compressor design, such as the advantage of running the motor colder and at higher electrical efficiency versus the lower pump volumetric efficiency to be suffered as a result. Other goals of the compressor system simulation are the prediction of EER under other design changes such as a smaller motor or direct cooling of the pump. Details of the fluid mechanics and heat transfer mechanisms in the hermetic motor within the scroll compressor shell can be found in [7] and [9]. Details of the motor loss distribution model can be found in [11].

### 1.2.2 Compressor Protection Algorithms

In addition to the compressor system simulation project, another project that is active at MIT involves the use of microprocessors to design "Smart Compressors." This program uses microprocessors and strategically placed sensors to monitor compressor performance and to protect it from operating at conditions which are damaging to the machine, thus rendering overdesign of the machine redundant. The methodology behind such a protection scheme involves estimating the state of the machine based on sensor input with the aid of first-principles based models of various parts of the machine. A thermodynamic and heat transfer model of the scroll pump is necessary here to predict the mass flow rate of refrigerant into the machine (which in turn aids in predicting pressure drops in the heat exchanger as well as cooling capacity of the machine), the wall temperatures of the scroll wraps, as well as the pressures at various stages of the compression process. It is necessary to monitor wrap temperatures so that the differential thermal expansion of the pump between suction and discharge doesn't get so large as to cause the scrolls of the pump to lift off at the suction side. Similarly, pressure prediction is needed to prevent the pump from reaching operating conditions where pressure forces on the wraps reach fracture levels.

### 1.2.3 Scroll Compressor Design Tool

A scroll pump model will also come in handy as a design tool for new generations of scroll pumps. Newer designs of scroll pumps involve hybrid scroll geometries that promise major savings in material costs and machining costs while providing high volume ratios. A scroll pump model that can be modified to incorporate the new geometry will aid in predicting performance of the new machines at various operating conditions, before such machines are even built. The scroll pump model will also aid in determining the optimal dishing of scroll wraps without resorting to many experiments. New concepts for scroll compressors with variable speeds and variable capacity can also be simulated on a computer before actually building such machines.

## 1.3 Geometry of a Scroll Pump

In this section, we will describe the principle of operation of a scroll pump, and also point out some specific details of scroll pump geometry that will be alluded to in other sections of the thesis.

The basic principle behind the operation of a scroll compressor is the continuous compression of gas in the volume formed between the conjugate (pinch) points of an eccentrically orbiting involute spiral (also known as the orbiting scroll) within the walls of a stationary involute spiral (also known as the fixed scroll). High precision sealing is necessary between fixed and orbiting scrolls in order that compressed gas does not leak within the pump, during the compression process. The specific mathematical requirements for a pair of surfaces to form conjugate contact is described in [2], and need not allude specifically to the involute spiral of a circle. For the purposes of this description, however, we will assume that the fixed and orbiting scrolls are involute spirals of a circle.

### 1.3.1 Fixed Scroll

The general form of the equations for the inner and outer walls of a fixed scroll are as shown below. Here, $x_{fo}$ and $y_{fo}$ are the $x$ and $y$ coordinates of the outer wall of the fixed scroll wrap at spiral angle $\beta$, while $x_{fi}$ and $y_{fi}$ are those associated with the inner walls of the fixed scroll wrap. In the equations below, $r_g$ refers to the radius of the generating circle of the involute spiral.

$$x_{fo}(\beta) = -r_g(cos(\beta) + \beta sin(\beta)) \tag{1.1}$$

$$y_{fo}(\beta) = -r_g(sin(\beta) - \beta cos(\beta)) \tag{1.2}$$

The outer wall of the fixed scroll is defined for the spiral angle range of $\beta = \beta_{i,s}$ to $\beta = \beta_{i,e}$. Here, $\beta_{i,s}$ and $\beta_{i,e}$ refer to the starting and and ending spiral angle locations of the conjugate sections of the inner pocket of the scroll pump.

$$x_{fi}(\beta) = -r_g(cos(\beta) + (\beta - \beta_0)sin(\beta)) \tag{1.3}$$

$$y_{fi}(\beta) = -r_g(sin(\beta) + (\beta - \beta_0)cos(\beta)) \tag{1.4}$$

The inner wall of the fixed scroll is defined for the spiral angle range of $\beta = \beta_{o,s}$ to $\beta = \beta_{o,e}$. Here, $\beta_{o,s}$ and $\beta_{o,e}$ refer to the starting and and ending spiral angle locations of the conjugate sections of the outer pocket of the scroll pump.

We notice that the equation for the inner wall of the fixed scroll wrap differs from that of the outer wall by the addition of the $\beta_0$ term to the spiral equations. The $\beta_0$ term is referred to as the wall thickness angle for reasons that will become clear.

At any angle $\beta$, the distance between a point on the inner fixed scroll wall and the corresponding point on the outer fixed scroll wall is given by

$$t = \sqrt{(x_{fo} - x_{fi})^2 + (y_{fo} - y_{fi})^2} = r_g\beta_0 = constant \tag{1.5}$$

Thus, the wall thickness of the fixed scroll wall wrap is found to be a constant for all values of the spiral angle $\beta$.

The spirals corresponding to the fixed scroll wraps are plotted on figure 1-1. From the graph, we observe that the range of spiral angle, $\beta$ for which the outer wall is defined differs from that for the inner wall. Specifically,

$$\beta_{o,s} = \beta_{i,s} + 180°$$

$$\beta_{o,e} = \beta_{i,e} + 180°$$

The $\beta$ range for the outer pocket of the scroll lags (is higher than) the $\beta$ range for the inner scroll pocket by 180°, because the start of suction (and compression) for the outer pocket is displaced from the suction port by 180°.

### 1.3.2 Orbiting Scroll

Now, we define the equations corresponding to the orbiting scroll wraps of a scroll pump. Once again, we define the equations in terms of the spiral angle $\beta$ and the radius of the generating circle, $r_g$. Also. $x_{oo}$, $y_{oo}$, $x_{oi}$ and $y_{oi}$ refer respectively to the $x$ and $y$ coordinates of the outer and inner walls of the orbiting scroll.

$$x_{oi}(\beta) = r_g(cos(\beta) + (\beta - \beta_0)sin(\beta)) \tag{1.6}$$

$$y_{oi}(\beta) = r_g(sin(\beta) - (\beta - \beta_0)cos(\beta)) \tag{1.7}$$

The inner wall of the orbiting scroll is defined between $\beta = \beta_{o,s} + 180°$ and $\beta = \beta_{o,e} + 180°$.

$$x_{oo}(\beta) = rg(cos(\beta) + \beta sin(\beta)) \tag{1.8}$$

$$y_{oo}(\beta) = rg(sin(\beta) - \beta cos(\beta)) \tag{1.9}$$

The outer wall of the orbiting scroll is defined between $\beta = \beta_{i,s} - 180°$ and $\beta = \beta_{i,e} - 180°$.

We observe that the equations for the orbiting scroll also indicate a constant wall thickness of $t = r_g\beta_0$, but that the spiral form is different from that of the fixed scroll,

as are the ranges of the spiral angle $\beta$ for which the orbiting scroll wraps are defined. In order to bring the spiral equations to the same form as that of the fixed scroll, we subject the orbiting scroll equations to coordinate transformations of $\hat{\beta} = \beta - 180°$ for the inner wall, and $\hat{\beta} = \beta + 180°$ for the outer wall. These transformations change the equations of the orbiting scroll to a spiral form similar to that of the fixed scroll, and also make the $\beta$ ranges for the orbiting scroll walls identical to their conjugate pairs on the fixed scroll. The equations of the orbiting scroll in the transformed form (with the $\hat{\beta}$ terms replaced by $\beta$) are as listed below.

$$x_{oi}(\beta) = -r_g(cos(\beta) + (\beta + 180° - \beta_0)sin(\beta)) \tag{1.10}$$

$$y_{oi}(\beta) = -r_g(sin(\beta) - (\beta + 180° - \beta_0)cos(\beta)) \tag{1.11}$$

The inner wall of the orbiting scroll is now defined between $\beta = \beta_{o,s}$ and $\beta = \beta_{o,e}$, which is the identical range for which its conjugate partner, the outer wall of the fixed scroll is defined.

$$x_{oo}(\beta) = -r_g(cos(\beta) + (\beta - 180°)sin(\beta)) \tag{1.12}$$

$$y_{oo}(\beta) = -r_g(sin(\beta) - (\beta - 180°)cos(\beta)) \tag{1.13}$$

The outer wall of the orbiting scroll is now defined between $\beta = \beta_{i,s}$ and $\beta = \beta_{i,e}$, which is the identical range for which its conjugate partner, the inner wall of the fixed scroll is defined.

The equations of the orbiting scroll are plotted on figure 1-2.

### 1.3.3 Conjugacy

Now that the equations of the orbiting scroll are of the same form as those of the fixed scroll, we can demonstrate what conjugacy means in the context of a scroll pump. Consider the distance between a point at spiral angle $\beta$ on the inner wall of the fixed scroll, and a point at angle $\beta$ (in the newly transformed coordinates) on the outer

wall of the orbiting scroll. The distance is calculated as

$$r_{orb} = \sqrt{(x_{oo} - x_{fi})^2 + (y_{oo} - y_{fi})^2} = r_g(180^\circ - \beta_0) = constant \qquad (1.14)$$

Thus, every point at angular position $\beta$ on the inner wall of the fixed scroll is at a constant distance of $r_{orb}$ from its corresponding point (referred to as its conjugate point) on the outer wall of the orbiting scroll. Similarly, every point at angular position $\beta$ on the outer wall of the fixed scroll is a constant distance of $r_{orb}$ from its conjugate partner on the inner wall of the orbiting scroll. The fixed and orbiting scrolls are jointly plotted on figure 1-3.

Now, if we displace the orbiting scroll by a distance $r_{orb}$ in any direction $\theta$, we will observe that there are points on the orbiting scroll that come into tangential contact with the fixed scroll. Specifically, points on the inner wall of the orbiting scroll at locations $\beta = \theta$, $\beta = \theta + 360^\circ$, $\beta = \theta + 720^\circ$ etc. come into contact with their conjugate points on the outer wall of the fixed scroll. Simultaneously, points on the outer wall of the orbiting scroll at locations $\beta = \theta + 180^\circ$, $\beta = \theta + 540^\circ$, $\beta = \theta + 900^\circ$ etc. come into contact with their conjugate points on the inner wall of the fixed scroll. Such contact is illustrated on figure 1-4. Each of these contact points is also referred to as a pinchpoint of the scroll pump. We observe that the space between any two consecutive pinchpoints (corresponding to a conjugate pair of scroll wraps) forms a sealed pocket. We also observe that the pinchpoints at the largest values of $\beta$ are exposed to the suction side of the scroll pump while those at the smallest values of $\beta$ are exposed to the discharge side of the scroll pump.

The principle of operation of a scroll pump then is simply the entrapment and compression of gas within the sealed pockets of a scroll pump. This is accomplished by the orbiting motion of the moving (orbiting) scroll (at a radius of $r_{orb}$) about its mean position between the wraps of the fixed scroll. The motion of the scroll is prevented from being rotational by the presence of an oldham coupling that constrains the orbiting scroll. Various stages of the compression process are shown in figures 1-5(a) - 1-5(f). From these figures, we notice that the scroll wraps are drawn for $\beta$

ranges that are larger than those in the previous figures (since scroll wraps need to have a finite thickness associated with them). However, the scroll conjugate range is still as defined before. Further, the outer pocket on the scroll pump is offset from the inner pocket (and pump suction) by about 180°.

The compression cycle is characterized by three processes, namely suction, the closed process and discharge. During suction, pinchpoints first form at spiral angles $\beta_{o,s}$ and $\beta_{i,s}$, and are exposed to suction gas. As the compression cycle continues, these pinchpoints move inwards into the pump (smaller $\beta$ values), forming volumes that are open to the suction state at one end, while they are sealed at the pinchpoints on the other end. At the end of 360° of rotation, the original (leading edge) pinchpoints have moved to angular locations $\beta_{o,s} - 360°$ and $\beta_{i,s} - 360°$ respectively. Simultaneously, (trailing edge) pinchpoints also form at angular locations $\beta_{o,s}$ and $\beta_{i,s}$, thus creating pockets that are totally sealed off between leading edge and trailing edge pinchpoints. Thus, the process of suction comes to an end with gas having been sucked into the pump during the course of one rotation and the gas pockets becoming sealed off. As the compression process now continues, the pinchpoints continue to move towards lower $\beta$ values, with the volume of the sealed pockets steadily diminishing. This process of the sealed off gas pocket volume diminishing constitutes the closed process of the scroll pump. Eventually, the leading edge pinchpoints reach the angular locations $\beta_{o,e}$ and $\beta_{i,e}$ where the scrolls cease to have conjugate contact. From this moment onwards, the pockets each have one sealed edge corresponding to the trailing edge pinchpoints, but are exposed to the discharge side of the pump on the other side. This constitutes the process of discharge where the pocket eventually diminishes to zero volume while expelling all its gas in the process.

### 1.3.4 Outer Pocket Vs Inner Pocket

As shown in the figures, the start of the outer pocket of the scroll pump is offset from the pump suction and the inner pocket by 180°. This is necessary so that the pump can operate with just one suction inlet port rather than separate suction ports for inner and outer pockets. The outer wall of the passageway for the 180° between the

suction port and the start of the outer pocket (i.e. the walls of the inner wall of the fixed scroll) are however not defined as involute spirals. This is necessary as otherwise the orbiting spiral walls would achieve conjugate contact with the outer wall even for this range of $\beta$s, which lies outside the range of $\beta$ for which the conjugate surfaces are defined. We do not permit conjugate contact for this 180° passageway to the outer pocket (henceforth referred to in this thesis as the Outer Suction Pathway) in order to maintain symmetry with the inner pocket. An outer suction pathway with conjugate contact would imply an outer pocket with a larger volume ratio than the inner pocket. The larger volume ratio in turn would lead to larger local pressures in the outer pocket than the inner pocket and therefore to asymmetric gas pressure forces in the pump.

The non-conjugacy of the outer suction pathway implies that gas entering the outer pocket has to pass through 180° of a channel between orbiting and fixed scroll walls even before it enters the outer pocket. During this "pre-suction", gas headed for the outer pocket is subject to heat transfer from the walls and leakage thus rendering its state different from corresponding gas in the inner pockets.

## 1.4 Irreversibilities in the Compression Process

### 1.4.1 Stages of Compression

The stages of compression in a scroll pump as described above can also be represented on a $P - V$ diagram as shown in figure 1-6. In this diagram, we plot the composite of the processes for the gas in both inner and outer pockets as it progresses from the suction port of the scroll pump to the discharge. The suction process is characterized by a constant pressure process when suction pockets form, and the pocket volumes steadily expand for one full revolution of the pump. At the end of suction, the suction pockets are completely sealed off from the suction port. The closed process then ensues with gas in the sealed-off pockets undergoing compression to a lower volume. At the end of the closed process, the pressure of gas in the pockets is higher

than that at suction but different (higher or lower) from that in the discharge port. The process of pump discharge is therefore preceded by an instantaneous blow-in / blow-out process when the gas pockets just open to the discharge tube, and experience a pressure equilibration process with the discharge tube. This pressure equilibration process is characterized by gas rushing in (blowing in) or rushing out (blowing out) to equalize pressures with the discharge tube. The discharge process which follows blow-in / blow-out is characterized by pocket volumes diminishing to zero and expelling gas from the scroll pump at discharge pressure.

### 1.4.2 Ideal Scroll Pump Process

The thermodynamic cycle described above is susceptible to irreversibilities that reduce its efficiency. Sources of irreversibility that affect pump performance are heat transfer, leakage, friction and mixing due to non-uniformities in gas properties. An ideal scroll pump process is characterized by the absence of most of these sources of irreversibility. In an ideal process, suction will occur with no leakage, heat transfer or friction, followed by an isentropic closed process of compression. At the end of the closed process, however, there is an inevitable irreversibility associated with blow-in / blow-out. This is because the closed process end pressure will in general be different from the discharge pressure. While the former pressure is a characteristic of the geometry of the scroll pump, the latter is determined by the operating condition at which the system operates. The irreversible blow-in / blow-out process is followed by an adiabatic, frictionless process of discharge. Thus, the only irreversibility in an ideal cycle is that associated with the pressure equilibration.

### 1.4.3 Pump Irreversibilities - A Lumped Parameter Formulation

Real scroll pump processes differ from the ideal scroll pump process because some or all of the irreversibilities listed above manifest themselves in significant fashion so as to affect pump performance. In order to be able to predict pump performance, any

model of the scroll pump ought to incorporate all significant sources of irreversibility and simulate the entire process in a thermodynamically consistent fashion. A lumped parameter model of a scroll pump process is described in chapter 2 of this thesis. Such a model has the advantage of being simple and fast to compute. It assumes uniformity of the gas in both pockets of the pump (like the $P - V$ diagram), and divides the process into essentially 4 discrete time-steps, namely suction, the closed process, blow-in/blow-out, and discharge. In the lumped parameter model, we model processes associated with heat transfer and leakages at various stages of compression and irreversibilities associated with blow-in / blow-out. Irreversibilities due to non-uniformity of gas in the pockets are neglected (indeed non-uniformities are not allowed to happen in a lumped parameter model). We also neglect friction as we believe it to be fairly small. In the absence of friction, the principal source of irreversibilities in a scroll pump process is the transfer of energy from one part of the pump to the other. As refrigerant enters a scroll pump and gets compressed, its temperature also rises. Gas that comes in to the pump at a low temperature and low pressure, leaves the pump at a high pressure and high temperature. This difference in gas temperatures and pressures between suction and discharge serves as the source of internal energy transfer within a scroll pump. Direct leakage of gas from high pressure, high temperature regions to low pressure, low temperature regions of the scroll is one mechanism of energy transfer, while heat transfer from discharge side to suction side is the second mode of energy transfer. Both these modes of internal energy transfer affect the thermodynamic processes within the pump. Here, we briefly describe these energy transfer mechanisms as incorporated into the the lumped parameter model for the different stages of compression.

### 1.4.4 Suction

Heat transfer to the suction side raises specific volume of gas as it is getting sucked into the pump, lowering the mass flow rate of refrigerant into the pump, and thus, lowering capacity and volumetric efficiency. Leakage into suction has an identical effect in that it also reduces the mass flow rate of refrigerant into the pump. In the

lumped parameter model, we model the suction gas as undergoing heat transfer with the wall of the scroll pump. Leakage to suction is also modeled with gas leaking into the suction from the closed process of compression that is simultaneously occurring for the scroll pockets that preceded the suction pockets.

### 1.4.5 Closed Process

During the closed processes of the pump, leakage, friction and heat transfer all serve as mechanisms of irreversibility in the pump. Entropy increase during the closed process causes the closed cycle reversible work to increase, relative to that of an isentropic closed process. In the lumped parameter model, we model the closed process as being polytropic and incorporate only the principal source of closed cycle irreversibility, which we show to be leakage from the discharge side of the pump. A work balance on experimental data from a scroll compressor demonstrates that friction cannot be large enough to account for the bulk of closed cycle irreversibility. Estimations of closed cycle convection coefficients, as well as analysis of pump P-V data demonstrate that unidirectional heat transfer cannot also be the principal mode of closed process entropy increase. While we incorporate leakage from the discharge process to the closed process in the model, we also include leakage that occurs from the closed process to the suction process.

### 1.4.6 Blow in / Blow out

At the end of the closed process, gas in the scroll pockets is not typically at discharge pressure. Therefore, the discharge process is usually preceded by a process of pressure equilibration when gas blows in / out of the scroll pockets and brings it into pressure equilibrium with the discharge tube of the compressor. In the lumped parameter model, we model the blow in / blow out processes as being instantaneous and adiabatic.

### 1.4.7 Discharge

Gas within a scroll pump attains its highest temperature at the end of the blow in / blow out processes. As this gas gets discharged from the pump, it transfers heat to the scroll walls at positions close to the discharge side of the pump. We incorporate such heat transfer into the lumped parameter model of a scroll pump.

### 1.4.8 Wall Interactions

Heat transfer from discharge to suction involves interactions between the refrigerant and the walls of the scroll pump. The walls of the scroll pump, which are affected by the presence of the gas, get warmer as one progresses from the suction side wall to sections of the wall closer to discharge. The hottest part of the wall, however, attains a temperature that is lower than the hottest gas within the pump, while the coldest portion of the wall reaches a temperature that is higher than the coldest (suction) gas temperature. Thus, there is a crossover point on the wall, at which the wall starts to transfer heat to the suction gas that was transferred to the wall from discharge gas. This continuum of wall temperatures from the suction to the discharge sides of the pump is lumped into two temperatures meant to capture mean wall temperatures for the suction and discharge sides respectively. Mechanisms of heat transfer between discharge and suction walls include conduction through the metal of the scrolls, convection through the closed process, and a novel mechanism of transient conduction through the scroll wraps which we refer to as kissing heat transfer (briefly described below). Lumped parameter analysis of heat transfer conductances reveals that internal convection is an unimportant mode of heat transfer relative to kissing heat transfer and conduction. The lumped parameter model for discharge to suction heat transfer therefore incorporates only wall conduction and kissing heat transfer. The wall model is thus characterized by 1) heat transfer to the discharge-side wall from discharge gas, 2) heat transfer from discharge-side wall to suction-side wall by a combination of kissing heat transfer and wall conduction, and 3) heat transfer from the suction-side wall to suction gas.

### 1.4.9 Closed Loop Iteration

Given the geometric parameters, suction state and discharge pressure for the pump, the lumped parameter model goes through a process of closed loop iteration to predict thermal performance of the scroll pump. Figure 1−7 shows a schematic of the lumped parameter model.

## 1.5 Kissing Heat Transfer

As mentioned briefly in the previous section, lumped heat transfer conductance calculations reveal that kissing heat transfer conductance is an important mode of heat transfer within a scroll pump. Chapter 3 of the thesis describes the analysis for this mode of heat transfer and also discusses the results of an experiment to observe kissing heat transfer within a scroll pump. Here, we briefly describe this mode of heat transfer and mention the relevant results from the experiment.

Kissing heat transfer is a novel mode of heat transfer specific to the geometry and periodicity of a scroll pump (see figure 1 – 8). Every location $X$ on the orbiting scroll comes into transient contact with a point $X''$ on a hot wrap of the fixed scroll followed 180° later by transient contact with point $X'$ on a cold wrap of the fixed scroll. This periodic, transient, alternating contact of the orbiting scroll between hot and cold wraps of the fixed scroll, serves as a mechanism of heat transfer within a scroll pump, and is referred to here as "Kissing Heat Transfer."

Kissing heat transfer serves to increase the effective radial thermal conductivity of the scroll pump and manifests itself in the form of significant temperature gradients across scroll wraps.

In order to observe and experimentally verify the existence of kissing heat transfer, an experiment was conducted on a specially instrumented scroll compressor. This machine was fitted with sensors that enabled us to observe temperature profiles of the metal of the fixed scroll, as well as temperature differences across scroll wrap walls. Temperature profiles from the experiment showed that there are indeed significant temperature gradients across the wraps of the fixed scroll, and that the heat fluxes

associated with such gradients cannot be feasibly explained by convection. Further, estimation of contact angles between fixed and orbiting scrolls, based on experimental data, gave values that are smaller but of the same order of magnitude as those estimated by analytical techniques.

The presence of significant temperature gradients across fixed scroll wraps, and the estimation of "realistic" contact angles based on experimental data, together provide compelling evidence of the existence of kissing heat transfer. The kissing heat transfer coefficient is part of the wall heat transfer conductance that is incorporated into the lumped parameter model of the scroll pump.

## 1.6 Distributed Parameter Model of Scroll Pump

The lumped parameter model developed incorporates sources of pump irreversibility selectively, while neglecting other sources of irreversibility. A significant problem with experimental data from scroll pumps is that it is not possible to distinguish various forms of irreversibility in the machine, but only to observe the effect of their totality on the performance of the machine. For example, since both suction heat transfer and leakage to suction lower volumetric efficiency of the pump, it is not possible to ascribe exact proportions of irreversibility to each of these modes based on experimental data. Similarly, with closed process irreversibility, it is possible to state with confidence that friction and heat transfer cannot each be the chief sources of closed cycle entropy generation. It is not possible, however to rule them out in entirety. The various processes at play within a scroll pump are by their very nature phenomena that are distributed over space (over the length of the scroll), and unsteady (since gas temperatures swing during the course of a cycle). A distributed parameter model was therefore developed to model various sources of irreversibility in tandem, and to quantify their relative importance. Another important reason for the development of the distributed parameter model was to be able to obtain the correct lumped parameter formulation of inherently distributed phenomena such as leakage.

The methodology of the distributed parameter model was to simulate the unsteady thermo-fluid processes of the gas in isolation, and to interact it with the thermal processes of a steady-state wall. Simulations proceeded iteratively till the energy transfers between the gas and wall are locally (and globally) self-consistent. The methodology of the solution of the computational fluid dynamic equations is described in chapter 4 of the thesis.

## 1.7 Results of Distributed Parameter Model

The results of the distributed parameter model are described in chapter 5 of the thesis. The results of the distributed parameter model in brief are that heat transfer and leakage turn out to be significant sources of irreversibility for the suction process. For the closed process however, heat transfer turns out not to be very significant at all, thus confirming our earlier suspicion that leakage accounts for most of the irreversibilities associated with the closed process. The simulations demonstrate that the gas process associated with the outer pocket is slightly different from that of the inner pocket. The starting state for the closed process of the outer pocket is at a higher temperature than that for the inner pocket owing to heat transfer and leakage into the outer suction pathway. The polytropic coefficient associated with the outer pocket is however almost identical to that for the inner pocket. The wall temperature profile simulations demonstrate that kissing heat transfer is a necessary mode of heat transfer required to explain some of the characteristics of the wall temperature profiles obtained from the kissing heat transfer experiment, and that kissing heat transfer through the wraps of the pump plays an analogous role to radial conduction through the base of fixed and orbiting scrolls of the pump. Correlations obtained from leakage profiles simulated for a number of operating conditions also give us the appropriate lumped parameter approximation to leakage phenomena.

## 1.8 Outline of the Thesis

The chapters of this thesis have been written to each be self-contained. Therefore, the reader that is interested in lumped parameter modeling will be well-advised to skip straight over to chapter 2. Similarly, kissing heat transfer and distributed parameter modeling are described in fairly self-contained form in chapters 3 and 4. Results of the distributed parameter model are described in chapter 5. Chapter 6 presents the conclusions of the thesis.

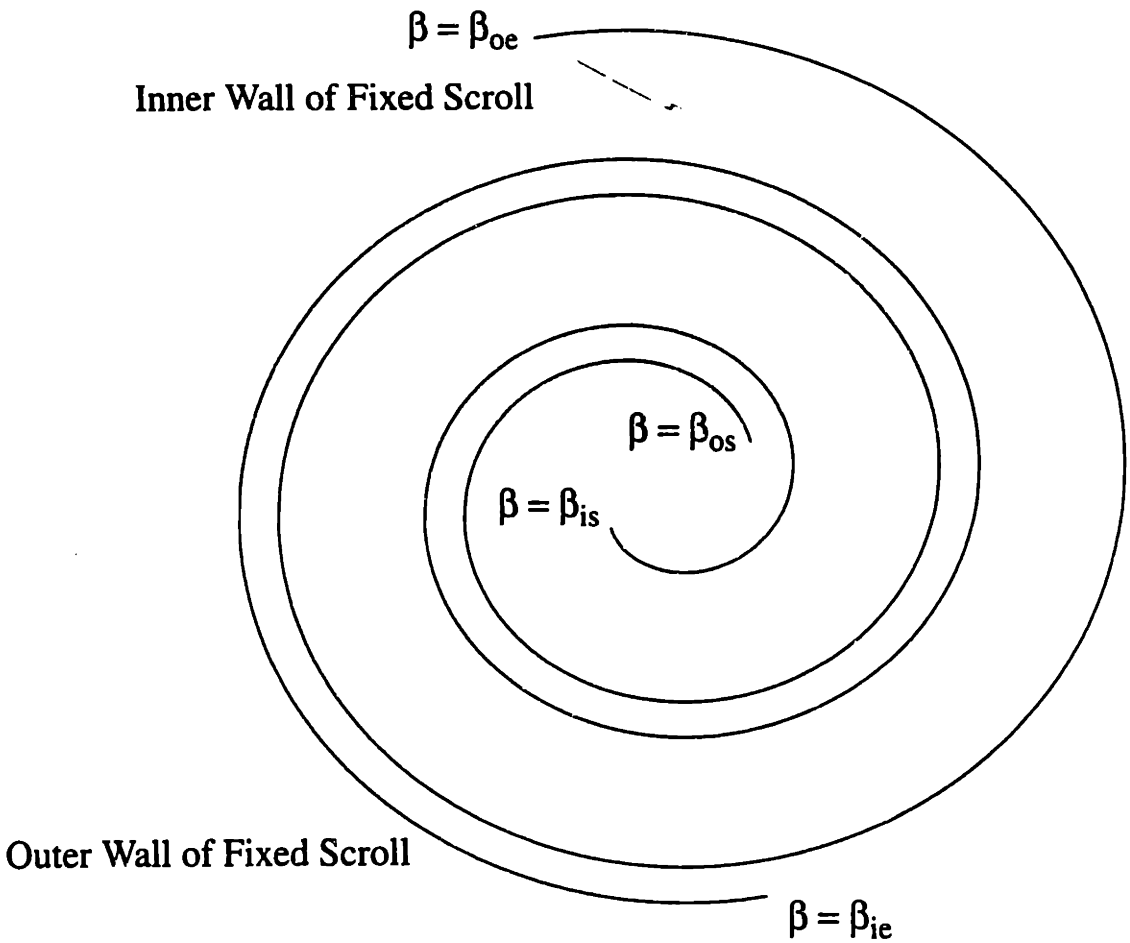


Figure 1-1: Geometry of Fixed Scroll

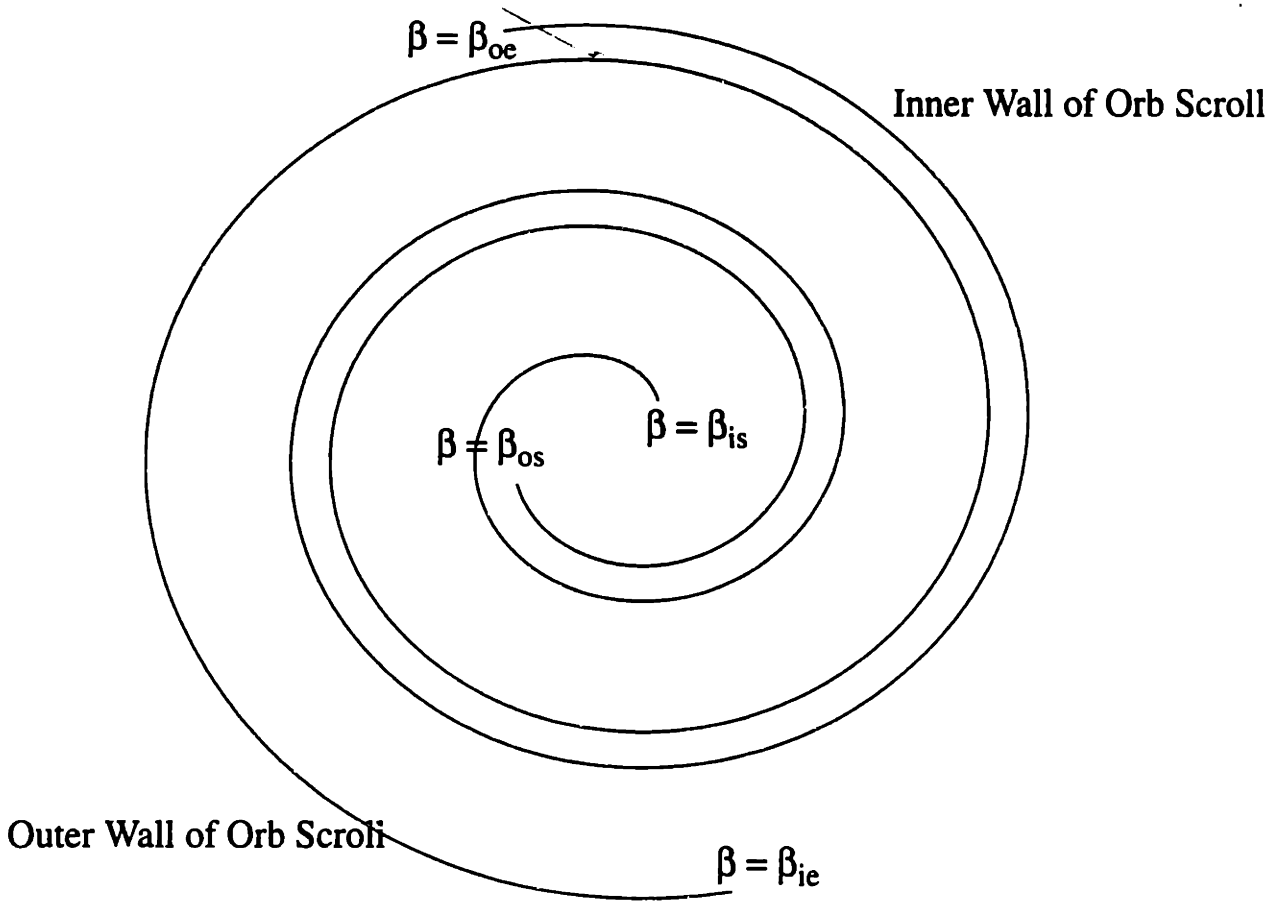


Figure 1-2: Geometry of Orbiting Scroll

Orbiting Scroll - Dotted Lines
Fixed Scroll - Solid Lines

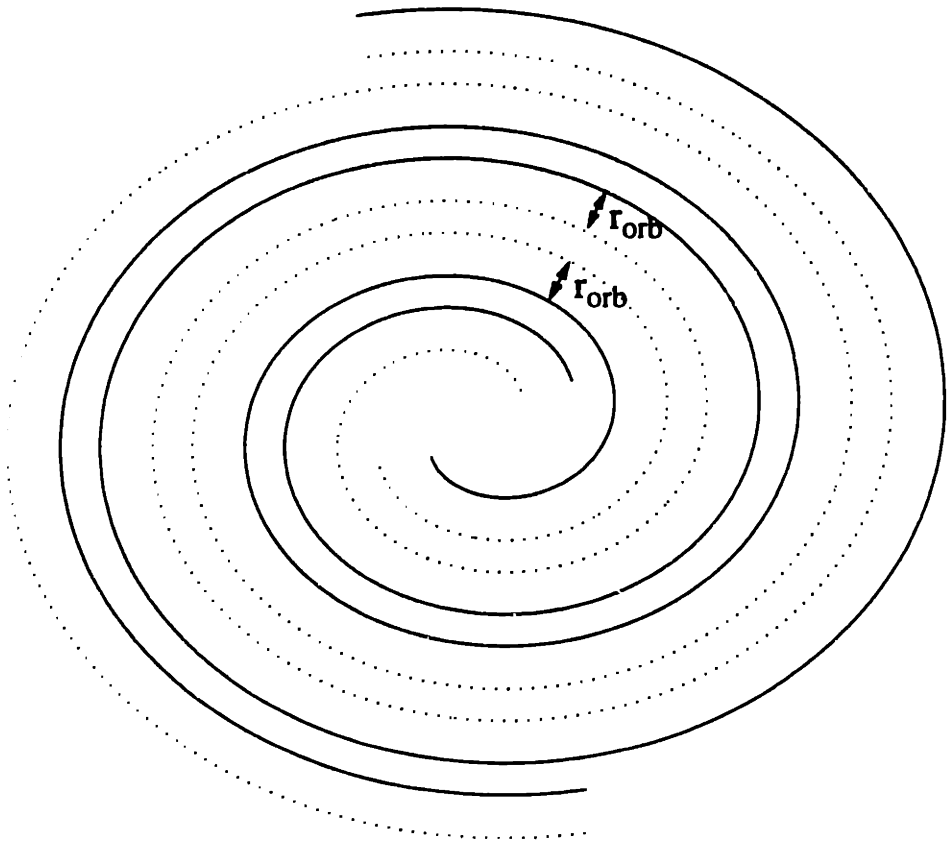


Figure 1-3: Orbiting Scroll and Fixed Scroll Plotted Together

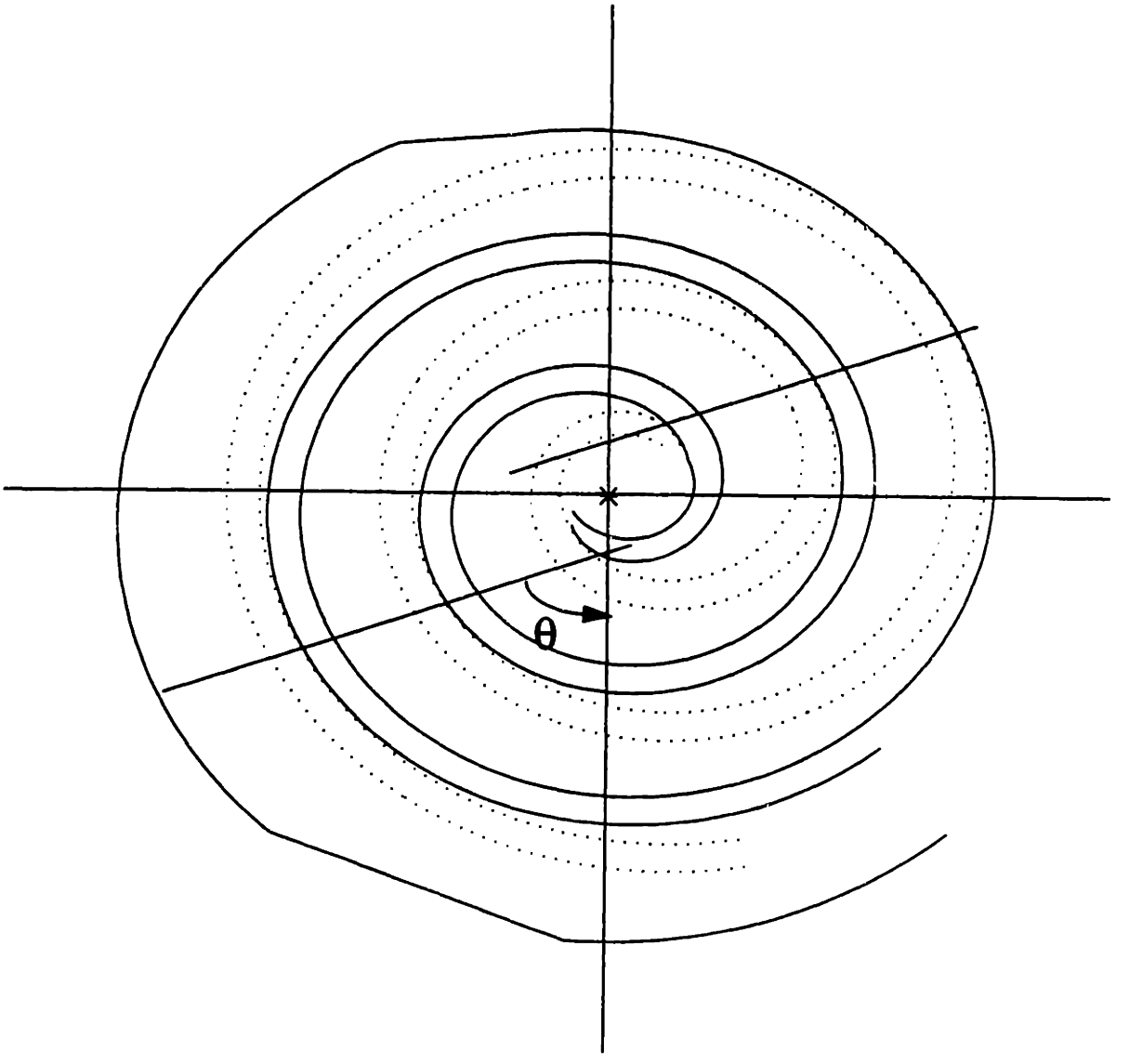


Figure 1-4: Pinchpoints Created by Displacement of Orbiting Scroll by distance $r_{orb}$ in direction $\theta$.

**Fig 1-5(a)**

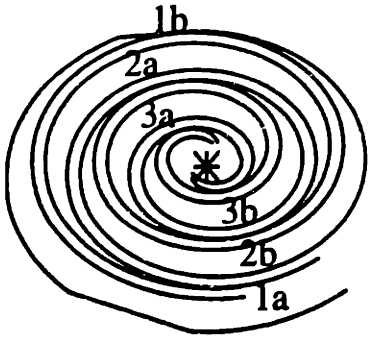


Position I
1a, 1b Starting Suction
2a, 2b Starting Closed Process
3a, 3b Advanced Stages of
Closed Process

**Fig 1-5(b)**

Outer Suction Pathway

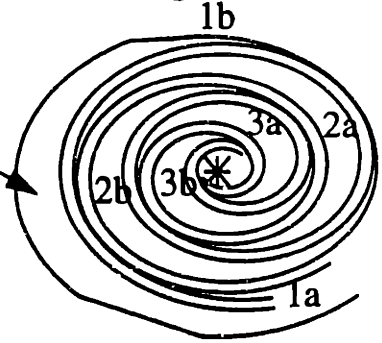


Position II
1a, 1b Suction
2a,2b Closed Process
3a, 3b Finishing Closed
Process

**Fig 1-5(c)**

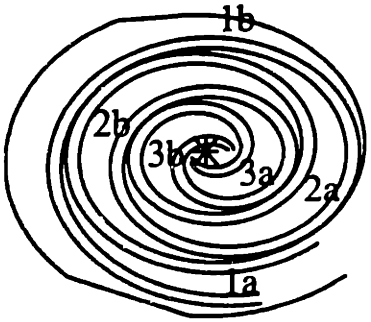


Position III
1a, 1b Suction
2a, 2b Closed Process
3a, 3b Discharge Process

At any instant, there are a pair
of pockets undergoing suction,
their predecessors undergoing
a closed process, whose predecessors
in turn are either going through
final stages of the closed process
or are going through discharge

**Fig 1-5(d)**

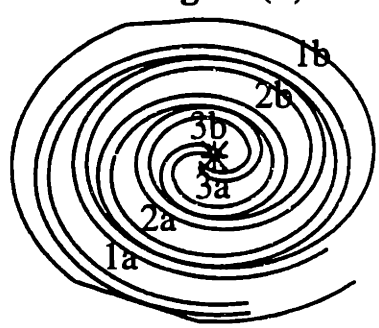


Position IV
1a, 1b Suction
2a, 2b Closed Process
3a, 3b Discharge Process

**Fig 1-5(e)**

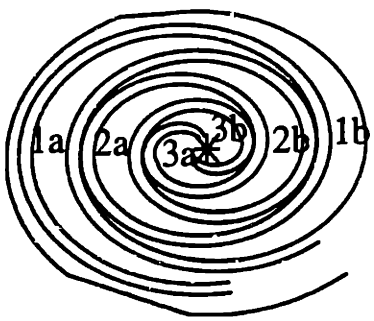


Position V
1a, 1b Suction
2a, 2b Closed Process
3a, 3b Discharge Process

**Fig 1-5(f)**

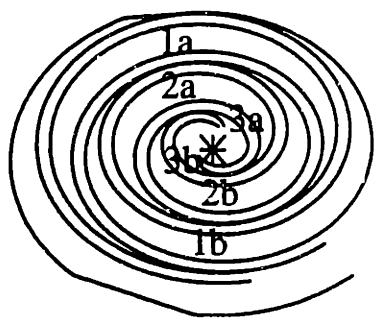


Position VI
1a, 1b Suction Ending
2a, 2b Closed Process
3a, 3b Discharge Process

**Figure 1-5 - Stages of the Compression Process**

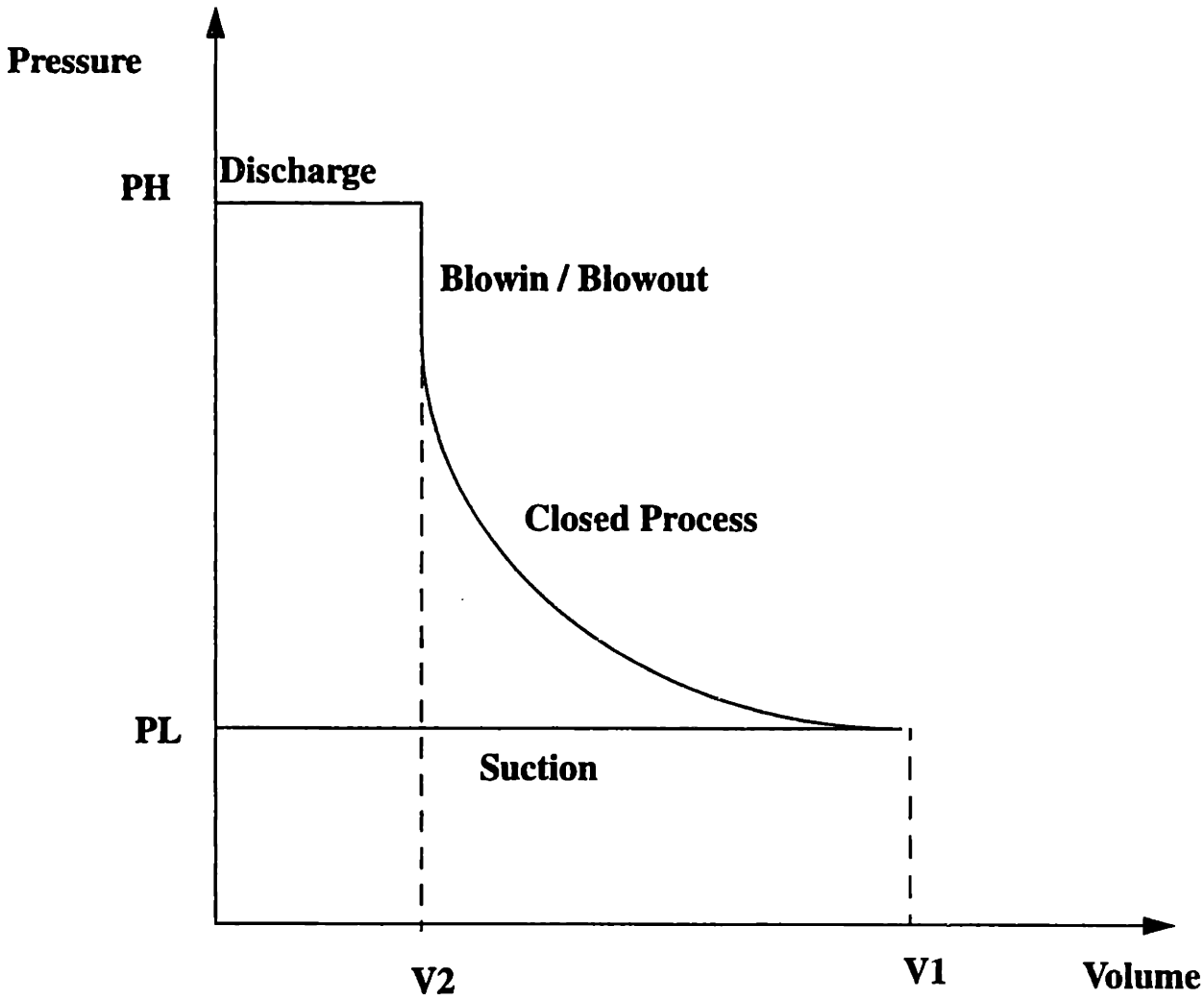


**Figure 1-6 - Stages of Compression on a P-V Diagram**

# Figure 1-7: Schematic of Lumped Parameter Pump Model

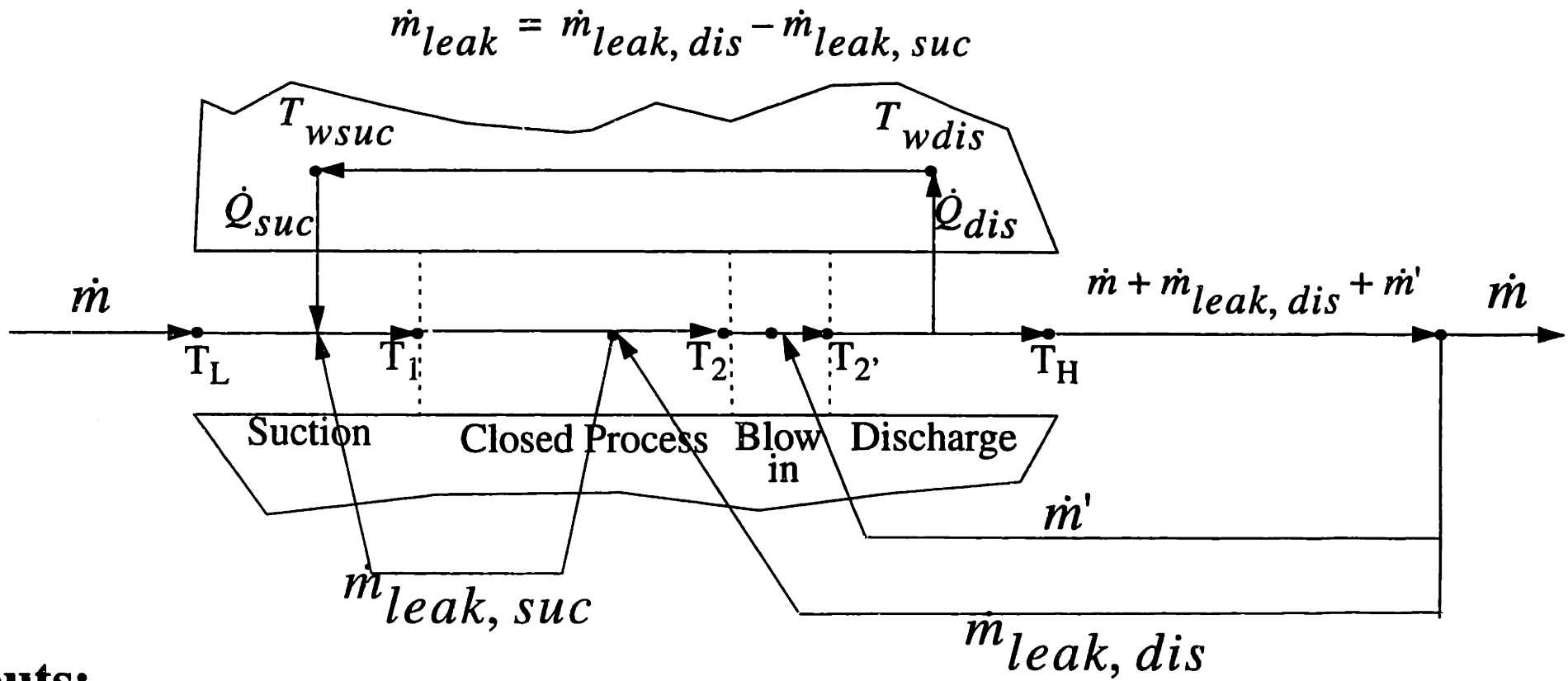


## Inputs:

**Suction Pressure $P_L$ Suction Temperature $T_L$**

**Discharge Pressure $P_H$ Pump Speed N**

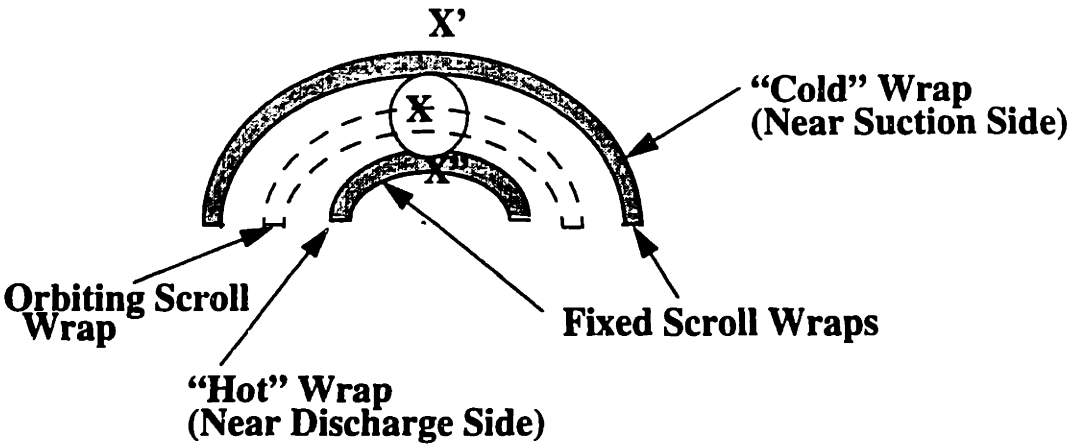


X' and X" are points of Contact for X within the course of one Eccentric Rotation of the Orbiting Scroll

Kissing Heat Transfer Modeled as
Transient Conduction Between Semi-Infinite Bodies

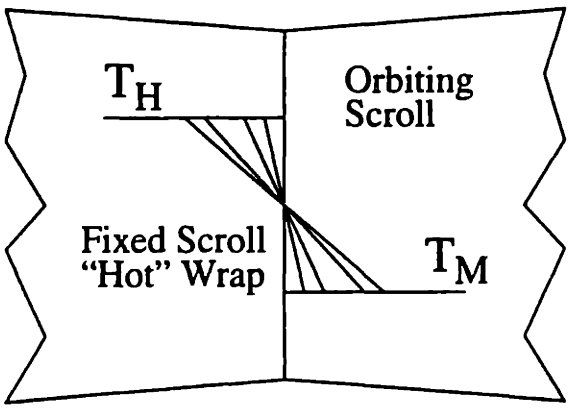


**Orbiting Scroll Kisses Hot Wrap of Fixed Scroll for time t**

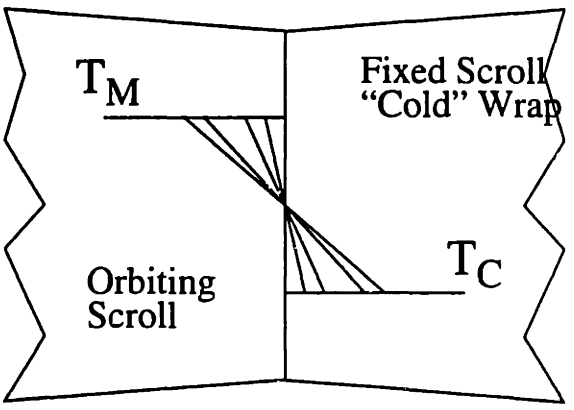


**Then Orbiting Scroll Kisses Cold Wrap of Fixed Scroll for time t**

Figure 1-8 - Mechanism of Kissing Heat Transfer

# Chapter 2

# Lumped Parameter Thermodynamic and Heat Transfer Modeling of a Scroll Pump

## 2.1 Introduction

In this chapter, we present the thermodynamic principles and equations used in modeling the internal processes of a scroll pump. The model discussed below is a lumped parameter model in that it treats gas in the scroll pockets as having attained a uniform pressure and temperature. Further, the model does not distinguish between gas in the outer and inner pockets that undergo simultaneous compression in a scroll pump. The development of a lumped parameter model of a scroll pump is motivated by the fact that engineers often need to be able to predict the performance of a pump in quick order. Such predictions, which are meant to be accurate only to the first order don't need or can't afford the sophistication of full scale computational fluid dynamic calculations of pump processes. Lumped parameter models aid engineers in modeling the most important physical processes of engineering machinery without

necessarily worrying about high levels of precision.

Lumped parameter models are also advantageous in that model can be developed to selectively incorporate only "important" sources of irreversibilities. The model developed in this chapter incorporates the irreversible effects of wall heat transfer and leakage at suction. However, it neglects heat transfer associated with the closed process of the scroll pump and only incorporates irreversibilities associated with leakage into and out of the closed process. Blow-in and blow-out processes associated with the end of the closed process and start of pump discharge are modeled as being instantaneous and adiabatic. Heat transfer between wall and discharge gas is also modeled. Irreversibilities associated with friction are neglected for all phases of the pumping cycle. Heat transferred from the discharge side gas to the walls is modeled as being transferred back to the suction side wall through a combination of conduction through scroll bases and kissing heat transfer. This heat is then transferred from the suction side wall to the suction gas as modeled earlier.

## 2.2 Model Specifications

The inputs to the thermodynamic model described below are the state of gas at the start of the suction process, (pressure $P_L$, and temperature, $T_L$), the time-period $T$ of the motor and the discharge pressure, $P_H$.

Parameters of the model that would change for different compressors, but that are assumed to be known for a given scroll compressor are the volumes of the scroll pocket at the start ($V_1$) and end ($V_2$) of the closed process, gas to wall heat transfer conductance at suction ($UA_{suc}$) and discharge ($UA_{dis}$), leakage mass-flow rate from discharge to the closed process, $\dot{m}_{leak,dis}$, leakage mass-flow rate from the closed process to suction, $\dot{m}_{leak,suc}$, and the discharge to suction wall heat transfer conductance, $UA_{wall}$. The wall conductance alluded to here represents a combination of kissing heat transfer and conduction modes for the transfer of heat from the discharge side pump walls to the suction side pump walls.

The outputs of the model are the prediction of all intermediate states of the com-

pression process, (states 1, 2, 2′ and $H$) polytropic constant, $n$ of the closed process, work of compression, $\dot{W}_{comp}$, mass flow rate, $\dot{m}$ of refrigerant through the compressor, and lumped wall temperatures of the scroll at suction, $T_{w,suc}$ and discharge, $T_{w,dis}$.

The algorithm for the pump model and the numerical values of the parametric models used for an SC37 scroll pump are presented in Appendix $A$ to this thesis.

## 2.3 Stages of the Compression Process

The model divides the compression cycle (of period $T$) into 4 time-steps that are briefly described here. The suction process (from time $t = 0$ to time $t = t_1$) is characterized by gas entering the pump at state $L$ (pressure $P_L$, temperature $T_L$) and the volume of the compression pocket increasing from zero to a volume $V_1$. At the end of the suction process, the pocket seals off, and the gas within has reached a state 1 (pressure $P_1$, temperature $T_1$). The suction process is followed by a closed process (from time $t = t_1$ to time $t = t_2$) where the sealed-off pocket undergoes a reduction in Volume from $V_1$ to $V_2$. At the end of the closed process, gas in the pocket that was at state 1 has reached state 2 (pressure $P_2$, temperature $T_2$). The gas pressure $P_2$ is not in general equal to the discharge pressure $P_H$. Therefore, the unsealing of the pocket at the end of the closed process is accompanied by a constant volume blow-in / blow-out process (from time $t = t_2$ to time $t = t_{2'}$) of rapid pressure equilibration. If $P_2 < P_H$, the pocket undergoes a blow-in process, whereby gas rushes into the pockets from the discharge plenum and raises the pocket pressure to $P_H$, and gas temperature to $T_2'$. On the other hand, if $P_2 > P_H$, the pocket undergoes a blow-out process in which gas rushes out of the pocket till pressure inside the pocket reaches $P_H$, with the temperature of the gas reaching $T_2'$. At the end of the blow-in / blow-out process, gas is at state 2′ (pressure $P_H$, temperature $T_2'$). The process of discharge (from time $t = t_{2'}$ to time $t = t_3$) which follows the blow-in / blow-out processes involves the expulsion of gas from the pocket to the discharge plenum. Gas which starts the process of discharge at a state 2′ reaches state $H$ (pressure $P_H$, temperature $T_H$) at the end of discharge. During the process of discharge, pocket volume decreases from $V_2$

to zero. The time-scales described above are related to the time-period of one crank rotation $T$ (or time-period of the motor) in the following manner. $T = t_1 = t_3 - t_{2'}$, because the processes of pump suction and discharge each take place for the duration of one crank rotation.

The different stages of the compression process are shown on a P-V diagram in figure 2-1. The nomenclature of states used in the preceding section is the one adhered to throughout this chapter. The thermodynamic modeling of each of these processes is described in detail in the sections that follow.

As gas undergoes compression within the scroll pump, it exchanges heat with the wall of the fixed and orbiting scrolls. For the purposes of this model, the scroll walls are divided into two portions, each with a uniform and steady temperature. Scroll walls near the suction side of the compressor are at a uniform cool temperature of $T_{w,suc}$, while portions of the metal near the discharge side are assumed to be at a uniform hot temperature of $T_{w,dis}$.

The model described below really deals with the masses of gas that undergo compression within a scroll pump. In order that these masses may be connected to measurable mass flow rates of refrigerant in the inlet and discharge pipes of the machine, we average each of the processes of the machine over the time-period of one crank rotation. The equations of the model are thus finally described in terms of mass-flow rates of refrigerant.

## 2.4 Suction

The start of compression is characterized by a period of expansion when two pockets are in the process of being formed between the walls of the fixed scroll and the orbiting scroll. Both these pockets are open to the suction side of the compressor and undergo expansion due to the entry of suction gas. The pockets seal simultaneously soon after the point where the pocket volume reaches a maximum. Gas that is entering the pockets is at a mixed mean temperature of gas that circulates over the motor within the hermetic shell of the scroll compressor and gas that enters the scroll pump

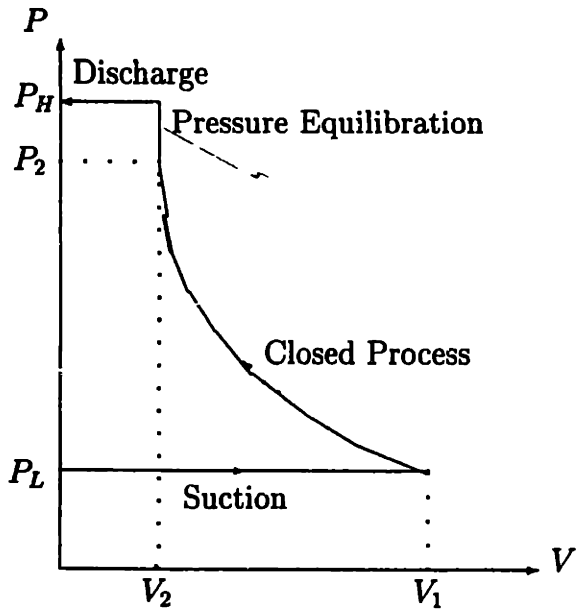


Figure 2-1: P-V Diagram of the Compression Process

directly from the suction port of the compressor. This mixed mean state of the gas is labelled here as the state $L$, with pressure $P_L$ and temperature $T_L$. The entering gas experiences a transfer of heat from the suction side scroll wall, which is at a hotter temperature $T_{w,suc}$. At the end of the suction process, gas within the pocket reaches state 1 (see figure 2-2). The thermodynamic equations governing the evolution of gas from state L to state 1 are listed below.

*Continuity* - Drawing an expanding control volume for the suction process as shown in figure 2-2.

$$\frac{\partial m_{Cv}}{\partial t} = \dot{m}_{in} + \dot{m}_{leak,in} \tag{2.1}$$

where, $m_{Cv}$ is the mass of gas in the control volume at any time, while $\dot{m}_{in}$ is the instantaneous flow rate of gas into the control volume, and $\dot{m}_{leak,in}$ is the instantaneous rate of leakage into suction from the closed process.

We now integrate the continuity equation between times $t = 0$ and $t = t_1 = T$ as

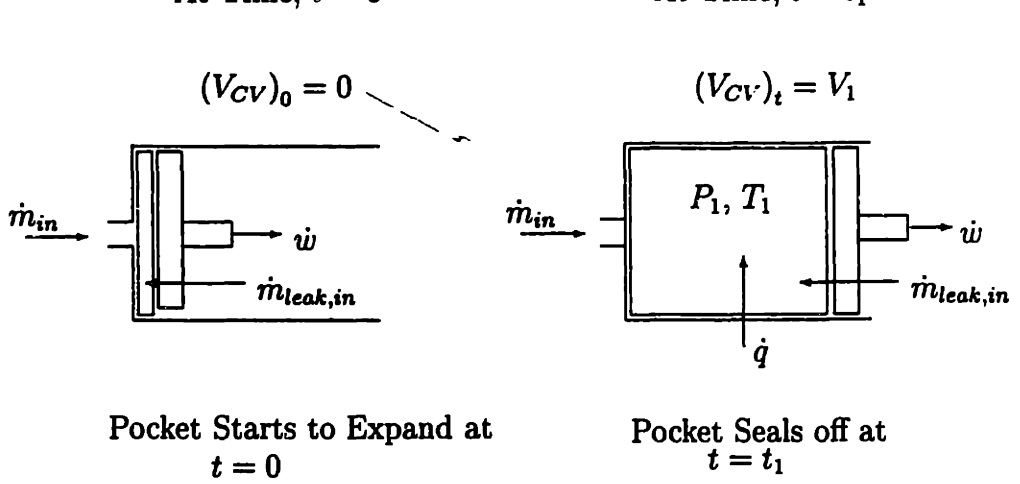


Figure 2-2: Schematic Diagram of the Suction Process

below:

$$(m_{Cv})_T - (m_{Cv})_0 = (m_{Cv})_{t_1} - (m_{Cv})_0 = \int_0^{t_1} (\dot{m}_{in} + \dot{m}_{leak,in})dt = (\dot{m} + \dot{m}_{leak,suc}) \cdot T \tag{2.2}$$

In the above equation, $(m_{Cv})_0 = 0$ because there is no gas in the pocket at the start of suction, while $(m_{Cv})_T = (m_{Cv})_{t_1}$ because the process of suction ends at time $t = t_1 = T$. $\dot{m}$ is the average (taken over the time-period of one crank rotation) mass flow rate of refrigerant entering the pump. $\dot{m}_{leak,suc}$ is the average (taken over the time-period of one crank rotation) leakage mass flow rate into the suction process. $\dot{m}$ also turns out to be the average mass flow rate of refrigerant entering the pump because the suction process occurs over one crank rotation.

Therefore,

$$\dot{m}_{leak,suc} + \dot{m} = \frac{(m_{Cv})_{t_1}}{T} \tag{2.3}$$

Since, gas in the pocket is at state 1 at time, $t_1$,

$$\dot{m} = \frac{V_1}{v_1 T} - \dot{m}_{leak,suc} \tag{2.4}$$

*First Law* - At any given instant, the first law balance on the control volume is

as listed below. Here, $\dot{q}$ is the instantaneous rate of heat transfer into the control volume, while $\dot{w}$ is the instantaneous work done by the gas in the control volume. $h_{in}$ is the specific enthalpy of gas entering the pump from suction while $h_{leak,in}$ is the instantaneous specific enthalpy of the leakage gas.

$$\frac{\partial(mu)_{Cv}}{\partial t} = \dot{q} - \dot{w} + \dot{m}_{in}h_{in} + \dot{m}_{leak,in}h_{leak,in} \tag{2.5}$$

Integrating over the time-period of the suction process as before, we get

$$(\dot{m}_{leak,suc} + \dot{m})(u_{Cv})_{t_1} = \dot{Q}_{suc} - \dot{W}_{suc} + \dot{m}h_{in} + H_{leak,suc} \tag{2.6}$$

Here, $\dot{Q}_{suc}$ is the average rate of heat transfer into the control volume during the process of suction, while $\dot{W}_{suc}$ is the average work done by the control volume during suction. $H_{leak,suc}$ is the enthalpy rate of leakage into suction averaged over one crank rotation. We also define $h_{leak,suc}$ to be the average (over one crank rotation) specific enthalpy associated with leakage into suction.

$$\dot{Q}_{suc} = \frac{1}{T} \cdot \int_0^T \dot{q}dt$$

$$\dot{W}_{suc} = \frac{1}{T} \cdot \int_0^T \dot{w}dt$$

$$H_{leak,suc} = \frac{1}{T} \cdot \int_0^T (\dot{m}_{leak,in}h_{leak,in})dt$$

$$h_{leak,suc} = \frac{H_{leak,suc}}{m_{leak,suc}}$$

Gas enters the control volume at state $L$, while gas in the control volume at time $t_1$ is at state 1. The suction work is positive because gas entering the control volume causes it to expand. If we assume that the pressure of the control volume remains constant at the suction pressure $P_L$, then

$$\dot{W}_{suc} = \frac{1}{T} \cdot \int_0^{V_1} P \cdot dV + \dot{W}_{fric,suc} = \frac{1}{T} \cdot P_L \cdot V_1 + \dot{W}_{fric,suc}$$

where $\dot{W}_{fric,suc}$ is the friction component of the suction work.

The first law can now be rewritten as

$$(\dot{m}_{leak,suc} + \dot{m})u_1 = \dot{Q}_{suc} - \frac{1}{T} \cdot P_L \cdot V_1 - \dot{W}_{fric,suc} + \dot{m}h_L + \dot{m}_{leak,suc}h_{leak,suc}$$

$$\Rightarrow (\dot{m}_{leak,suc}+\dot{m})(u_{Cv})_{t1}+\frac{(m_{Cv})_{t1}}{T}P_L(v_{Cv})_{t1}-\dot{m}h_L-\dot{m}_{leak,suc}h_{leak,suc} = \dot{Q}_{suc}-\dot{W}_{fric,suc}$$

$$\Rightarrow (\dot{m}_{leak,suc} + \dot{m})[u_1 + P_1 \cdot v_1] - \dot{m}h_L - \dot{m}_{leak,suc}h_{leak,suc} = \dot{Q}_{suc} - \dot{W}_{fric,suc} \quad (2.7)$$

Now, if we neglect friction, the first law equation reduces to

$$\dot{Q}_{suc} = \dot{m} \cdot (h_1 - h_L) + \dot{m}_{leak,suc} \cdot (h_1 - h_{leak,suc}) \quad (2.8)$$

Thus, under the assumptions of constant suction pressure and no friction, the suction heat transfer is simply the rise in enthalpy of gas entering the suction process. As seen from the equation, this rise in enthalpy accounts for the heat transferred to gas entering the pump as well as that leaking into the suction process.

*Volumetric Efficiency* - It is important to note here that the mass flow rate $\dot{m}$ is lowered by suction heat transfer as well as leakage into suction. In the absence of heat transfer and leakage mechanisms, gas in the pocket would still be at state $L$ at the end of suction, and therefore at a lower specific volume $v_L$. The resultant average mass flow rate would then be higher at

$$\dot{m}_{max} = \frac{V_1}{v_L T} > \frac{V_1}{v_1 T} - \dot{m}_{leak,suc} = \dot{m}$$

The reduction in mass flow rate of refrigerant through the pump as a result of irreversibilities at suction can be captured in the form of an efficiency parameter known as the volumetric efficiency. A scroll pump that is at a volumetric efficiency of 100% is one that does not suffer from the ill-effects of suction heat transfer and leakage and therefore admits the maximum mass flow rate associated with the suction state $L$. In contrast, a pump that is affected by suction heat transfer and leakage (like the one modeled here) has a volumetric efficiency of $\eta_v < 1$ where

$$\eta_v = \frac{\dot{m}}{\dot{m}_{max}} \tag{2.9}$$

*Suction Heat Transfer* - Since, suction heat transfer involves a transfer of heat from the fixed scroll wall at temperature, $T_{w,suc}$,

$$\dot{Q}_{suc} = \dot{m}(h_1 - h_L) = (UA)_{suc} \cdot (\Delta T)_{lm,suc} \tag{2.10}$$

Here, $UA_{suc}$ is the conductance of suction heat transfer, while $(\Delta T)_{lm,suc}$ is the log mean temperature difference associated with suction heat transfer.

$$(\Delta T)_{lm,suc} = \frac{T_1 - T_L}{ln(\frac{T_L - T_{w,suc}}{T_1 - T_{w,suc}})}$$

The above equations completely characterize the suction process, In Appendix $B$ of the thesis, we use experimental data from a scroll compressor to justify why the work of friction can be neglected.

## 2.5 Closed Process

At the start of the closed process (at time $t = t_1$), the two pockets formed during the process of suction completely seal off from the suction port of the scroll pump. From time $t = t_1$ to time $t = t_2$, the pockets remain sealed off from both suction and discharge, while undergoing a reduction in volume from $V_1$ to $V_2$ as shown in figure 3. The pocket gas pressure correspondingly rises from $P_1(= P_L)$ (at state 1) to $P_2$ (at state 2). The thermodynamic equations governing the closed process from state 1 to state 2 are listed below.

*Continuity* - Drawing a control volume around the closed pocket, we get

$$\frac{\partial m_{Cv}}{\partial t} = \dot{m}_{leak,in} - \dot{m}_{leak,out} \tag{2.11}$$

where $m_{Cv}$ is the mass of gas in the control volume at time $t$, $\dot{m}_{leak,in}$ is the instantaneous rate of leakage of gas into the closed pocket from the high pressure

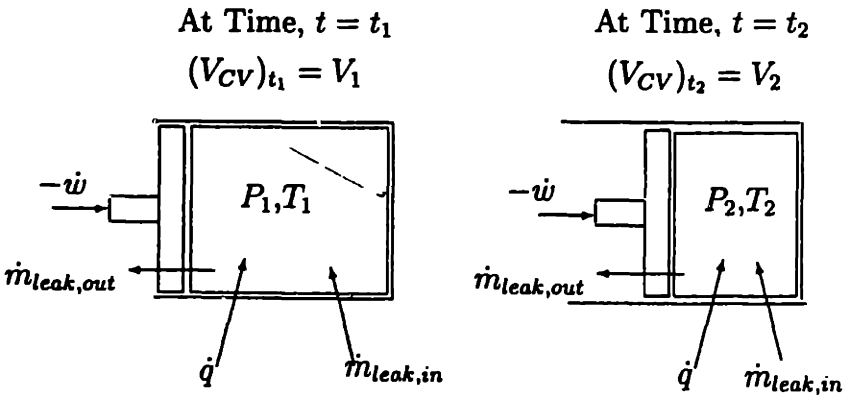


Figure 2-3: Schematic Diagram of The Closed Compression Process

(discharge) side of the pump, and $\dot{m}_{leak,out}$ is the instantaneous rate of leakage of gas out of the closed process into suction. Integrating the continuity equation over the duration of the closed process (between $t = t_1$ and $t = t_2$), we get

$$(m_{Cv})_{t_2} - (m_{Cv})_{t_1} = \int_{t_1}^{t_2} (\dot{m}_{leak,in} - \dot{m}_{leak,out})dt \tag{2.12}$$

Now dividing the equation by the time-period of crank rotation $T$, we get

$$\frac{(m_{Cv})_{t_2}}{T} = \dot{m} + \dot{m}_{leak,suc} + \dot{m}_{leak,dis} - \dot{m}_{leak,suc} = \dot{m} + \dot{m}_{leak,dis} \tag{2.13}$$

Here, $\dot{m}_{leak,dis}$ is the average (taken over time-period T) rate of mass leakage from discharge into the pocket, $\dot{m}_{leak,suc}$ is the average rate of mass leakage from the closed process into suction.

$$\dot{m}_{leak,dis} = \frac{\int_{t_1}^{t_2} \dot{m}_{leak,in} dt}{T}$$

$$\dot{m}_{leak,suc} = \frac{\int_{t_1}^{t_2} \dot{m}_{leak,out} dt}{T}$$

The above relations neglect any leakage that may occur to / from the closed process to succeeding / preceding pockets that are also undergoing a closed process. Thus, $\dot{m}_{leak,dis}$ and $\dot{m}_{leak\ suc}$ represent net leakage rates into and out of the closed

process.

Since, gas in the control volume is at state 2 at time $t_2$, the continuity equation can be rewritten as shown below.

$$\frac{(m_{Cv})_{t_2}}{T} = \frac{V_2}{v_2 T} = \dot{m} + \dot{m}_{leak,dis} \tag{2.14}$$

*First Law* - The energy balance on the control volume at any instant is as shown below. Here, $\dot{q}$ is the instantaneous rate of heat transfer into the control volume, $\dot{w}$ is the instantaneous work done by the gas in the control volume, $\dot{m}_{leak,in}h_{leak,in}$ is the instantaneous enthalpy transferred into the control volume by leakage, and $\dot{m}_{leak,out}h_{leak,out}$ is that transferred out of the control volume by leakage.

$$\frac{\partial (mu)_{Cv}}{\partial t} = \dot{q} - \dot{w} + \dot{m}_{leak,in}h_{leak,in} - \dot{m}_{leak,out}h_{leak,out} \tag{2.15}$$

Integrating the first law equation over the duration of the closed process as before, and dividing by the crank rotation time-period $T$, we have

$$\begin{aligned} \frac{1}{T} \cdot [(mu)_{Cv_{t_2}} - (mu)_{Cv_{t_1}}] &= \dot{Q}_{closed} - \dot{W}_{closed} + \dot{m}_{leak,dis}h_{leak,dis} \\ &\quad -\dot{m}_{leak,suc}h_{leak,suc} \\ &= \dot{Q}_{closed} - \dot{W}_{closed} + H_{leak} \end{aligned} \tag{2.16}$$

Here, $\dot{Q}_{closed}$ is the average rate of heat transfer into the control volume during the closed process, while $\dot{W}_{closed}$ is the average work done by the gas during the closed process. $h_{leak,dis}$ and $h_{leak,suc}$ are respectively the averaged specific enthalpies of the leakage flows into and out of the control volume, while $H_{leak}$ is the net flow rate of enthalpy into the control volume by leakage.

$$\dot{Q}_{closed} = \frac{\int_{t_1}^{t_2} \dot{q} dt}{T}$$

$$\dot{W}_{closed} = \frac{\int_{t_1}^{t_2} \dot{w} dt}{T}$$

$$h_{leak,dis} = \frac{1}{T}\frac{\int_{t_1}^{t_2}(\dot{m}_{leak,in}h_{leak,in})dt}{\dot{m}_{leak,dis}}$$

$$h_{leak,suc} = \frac{1}{T}\frac{\int_{t_1}^{t_2}(\dot{m}_{leak,out}h_{leak,out})dt}{\dot{m}_{leak,suc}}$$

$$H_{leak} = \dot{m}_{leak,dis}h_{leak,dis} - \dot{m}_{leak,suc}h_{leak,suc}$$

As with suction, the work term can be split into a reversible ($PdV$) term and an irreversible (non-$PdV$) term, which we attribute here completely to friction. The $PdV$ term here will be negative as the volume of the pocket decreases during the closed process. The friction term is defined to be positive in order to avoid confusion.

$$\dot{W}_{closed} = \frac{\int_{V_1}^{V_2} P \cdot dV}{T} - \dot{W}_{fric,closed}$$

At time $t_1$, gas in the control volume is at state 1, while at time $t_2$, it is at state 2. Using all this to rewrite the energy balance, we get

$$(\dot{m}+\dot{m}_{leak,dis})u_2-(\dot{m}+\dot{m}_{leak,suc})u_1 = \dot{Q}_{closed}-\frac{\int_{V_1}^{V_2} P \cdot dV}{T}+\dot{W}_{fric,closed}+H_{leak} \quad (2.17)$$

Proprietary data from UTRC's measurements on an SC37 scroll compressor reveals that the closed process generally follows a P-V trace characterized by the relation,

$$PV^n = constant \quad (2.18)$$

A reversible process that follows the same P-V trace is generally referred to as a polytropic process, and the constant $n$ is referred to as the polytropic coefficient. Such a process differs from an isentropic process between the same end pressures and volumes in that the exponent $n$ is in general different from the ratio of gas specific heats, $\gamma$. The polytropic coefficient, then is an indicator of entropy increase (if $n > \gamma$), or of entropy decrease (if $n < \gamma$) for the closed process. Entropy change in the control volume can be attributed to any of the three phenomena modeled above, namely heat transfer into / out of the gas, leakage into / out of the control volume, and irreversible

closed cycle work. In order to keep the model simple, we attempt to determine the most significant mechanism of entropy change in the closed process, and then neglect the relatively less important mechanisms.

### 2.5.1 Friction

In an isentropic closed process, the entropy of the compressed gas remains constant from the start to finish of the closed process. Such a process is ideal and unrealistic in that it doesn't consider the effects of friction between walls of the orbiting and fixed scrolls. Friction is a source of irreversibility that will result in an increase of system entropy during the closed process. Deviations from isentropy of the closed process can thus be partially attributed to friction. We show from a work balance calculation on proprietary data from a SC37 compressor that friction would have to be unreasonably large for it to account for all of the deviation from isentropy. Therefore, friction cannot be the principal source of entropy increase for the closed process. (See Appendix B)

### 2.5.2 Closed Cycle Heat Transfer

We now consider the possibility that closed cycle heat transfer is the important mechanism of entropy increase in the closed process. Such an explanation can be discarded principally because such heat transfer would require heat transfer coefficients that are unreasonably high. Indeed, lumped parameter heat transfer conductance estimations (made in the next chapter) show that convection between gas and walls for the closed process tends to be a higher thermal resistance mechanism than either conduction or kissing heat transfer. Also, unidirectional heat transfer between the gas and scroll walls is unphysical as the temperature of the scroll walls is hotter than the closed pocket gas at the beginning of the closed process, but lower than the gas temperature towards the end of the closed process. Bidirectional heat transfer would imply a polytropic constant that changed during the closed process, as we would need $n > \gamma$ at the beginning, and $n < \gamma$ towards the end. Such a trend of variation of polytropic

coefficient was however, not observed from UTRC's data. Thus, closed cycle heat transfer also cannot be the significant mechanism of entropy change for the closed process. (See Appendix C)

### 2.5.3 Leakage

Leakage of mass into the closed pocket from the high pressure discharge side and leakage of mass from the closed process to suction offer a third explanation for the departure of the closed process from isentropy. Since, friction and heat transfer cannot account for much of the deviation from isentropy, leakage can be used to account for such deviations. Using proprietary $P - V$ data for an SC37 compressor, we make an estimate of the net leakage mass flow rates (with the enthalpy associated with discharge) that would be necessary to account for all of the deviations from closed cycle isentropy. Our calculations show that the calculated $\dot{m}_{leak}$ correlates quite well with pressure difference across the scroll pump. This makes physical sense as pressure differences across the wraps would be the principal determinant of leakage through clearances in the scroll. (See Appendix D)

### 2.5.4 Attribution of all Closed Cycle Irreversibility to Leakage

Since we find friction and closed cycle heat transfer to be implausible mechanisms to cause the experimentally observed deviations of the closed cycle from isentropy, we identify leakage to be the principal mechanism of irreversibility in the closed process. In reality, each of the three mechanisms described above probably has a role to play in explaining closed cycle irreversibility. Our lumping of all the irreversibility into leakage is really an extra simplification made in the spirit of a lumped parameter model. In order for leakage phenomena to be incorporated as a source of irreversibility in the lumped parameter model, we need to have models for the leakage of mass into suction and into the closed process. Since leakage in the pump is essentially a distributed phenomenon governed by the unsteady spatial distributions of pressure

within the pump, we resort to a distributed parameter model of the pump out of which we derive the lumped parameter formulation of leakage (see chapters 4 and 5 of the thesis).

If we neglect closed cycle heat transfer and friction, and model the closed process to follow the P-V trace of a polytropic process, with coefficient $n$, the energy balance equation can be rewritten as shown below.

$$(\dot{m} + \dot{m}_{leak,dis})u_2 - (\dot{m} + \dot{m}_{leak,suc})u_1 = \frac{1}{T}\frac{P_L {V_1}^n}{n-1}({V_2}^{1-n} - {V_1}^{1-n}) + H_{leak} \qquad (2.19)$$

## 2.6 Blow-in/Blow-out

At the end of the closed process (at time $t = t_2$), gas in the pockets is at pressure $P_2$, which is in general not equal to the discharge pressure $P_H$. As a result, the pockets, which just start to unseal towards the discharge side, undergo a rapid blow-in or blow-out process (between $t = t_2$ and $t = t_{2'}$), whereby gas rushes in to the pocket (blow-in), or out of it (blow-out) to equilibrate pocket pressure to the discharge side. At the end of the blow-in / blow-out process, gas in the pockets reaches state 2', (pressure $P_H$, temperature $T_{2'}$), and is ready for the discharge process.

### 2.6.1 Blow-in

If $P_2 < P_H$, a blow-in process occurs, with gas rushing in to the pocket from the discharge side, till the pocket pressure reaches $P_H$, as shown in figure 4. The thermodynamic equations governing the blow-in process are listed below.

*Continuity* - Drawing a control volume for the blow-in process as shown in figure 4, we get

$$\frac{\partial m_{Cv}}{\partial t} = \dot{m}'_{blow-in} \qquad (2.20)$$

Here, $m_{Cv}$ is the mass of gas in the control volume at any instant, while $\dot{m}'_{blow-in}$

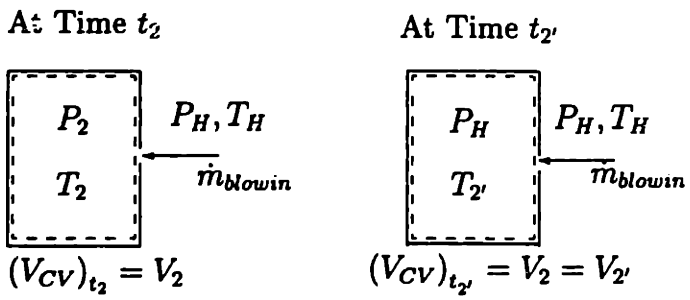


Figure 2-4: Blow-in Process

is the instantaneous blow-in mass flow rate. Integrating the continuity equation over the blow-in time-period,

$$(m_{Cv})_{t_{2'}} - (m_{Cv})_{t_2} = \int_{t_2}^{t_{2'}} \dot{m}'_{blow-in} dt \tag{2.21}$$

Dividing the equation by the crank rotation time-period $T$,

$$\frac{(m_{Cv})_{t_{2'}}}{T} = \dot{m} + \dot{m}_{leak,dis} + \dot{m}' \tag{2.22}$$

where $\dot{m}'$ is the average (taken over crank rotation time-period $T$) rate of blow-in mass into the pocket.

$$\dot{m}' = \frac{\int_{t_2}^{t_{2'}} \dot{m}'_{blow-in} dt}{T}$$

Since gas in the control volume is at state $2'$ at time $t = t_{2'}$, the continuity equation can be rewritten as

$$\frac{(m_{Cv})_{t_{2'}}}{T} = \frac{V_2}{v_{2'} T} = \dot{m} + \dot{m}_{leak,dis} + \dot{m}' \tag{2.23}$$

*First Law* - An energy balance on the control volume at any instant is shown below. Here, $\dot{q}$ is the heat transferred to the control volume at any instant, while $\dot{w}$ is the instantaneous rate of work done by the gas in the control volume. $\dot{m}'_{blow-in} h_{blow-in}$ is the enthalpy convected into the control volume at any instant by blow-in gas.

$$\frac{\partial(mu)_{Cv}}{\partial t} = \dot{q} - \dot{w} + \dot{m}'_{blow-in} h_{blow-in} \tag{2.24}$$

Since the time-scales associated with blow-in (between $t = t_2$, and $t = t_{2'}$) are too quick for any appreciable heat transfer to occur, the blow-in process can be modeled as being adiabatic (i.e.), $\dot{q} = 0$. As the volume of the control volume remains constant at $V = V_2$, the work transfer during the blow-in process is also zero, $\dot{w} = 0$. Integrating the first law equation over the blow-in time and dividing by $T$ as before, we get

$$\frac{((mu)_{Cv})_{t_{2'}} - ((mu)_{Cv})_{t_2}}{T} = \dot{m} h_{blow-in} \tag{2.25}$$

At time $t_{2'}$, gas in the control volume is at state $2'$, while at time $t_2$, it is at state 2. Since, blow-in occurs from the discharge side, the state of the blow-in gas is the same as state $H$ of discharge. Using this to rewrite the first law equation, we get

$$(\dot{m} + \dot{m}_{leak,dis} + \dot{m}')u_{2'} - (\dot{m} + \dot{m}_{leak,dis})u_2 = \dot{m}' h_H \tag{2.26}$$

### 2.6.2 Blow-out

If, at the end of closed process, $P_2 > P_H$, a blow-out process occurs where gas rushes out of the pocket until pressure inside the pocket equilibrates with the discharge pressure $P_H$. The blow-out process can be modeled as a control volume of initial pressure $P_2$, and volume $V_2$ at time $t = t_2$, expanding to a final volume $V_{2'}$ at time $t = t_{2'}$, while in the process reducing control volume pressure to $P_H$, as shown in figure 5. The thermodynamic equations governing blow-out are listed below.

*Continuity* - Since the mass of gas, $m_{Cv}$ in the control volume does not change during the blow-out process,

$$\frac{\partial m_{Cv}}{\partial t} = 0 \tag{2.27}$$

$$\Rightarrow (m_{Cv})_{t_{2'}} = (m_{Cv})_{t_2} \tag{2.28}$$

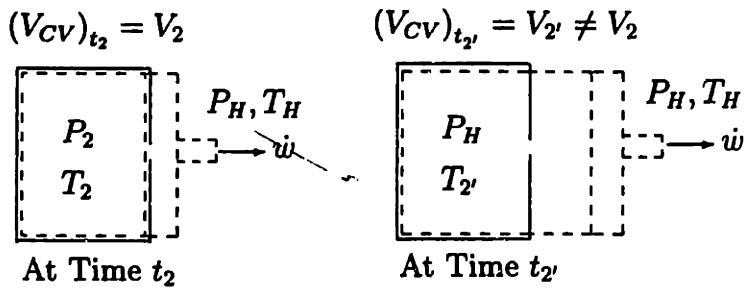


Figure 2-5: Blow-out Process

At time $t = t_{2'}$, the volume of the control volume is $V_{2'}$, and the gas inside is at state $2'$. Therefore,

$$\frac{(m_{Cv})_{t_{2'}}}{T} = \frac{V_{2'}}{v_{2'}T} = \dot{m} + \dot{m}_{leak,dis} \tag{2.29}$$

*First Law* - Writing the energy balance on the control volume at any instant, we get the following equation. Here, as usual, $\dot{q}$ is the instantaneous rate of heat transfer into the control volume, while $\dot{w}$ is the instantaneous rate of work done by the control volume.

$$\frac{\partial(mu)_{Cv}}{\partial t} = \dot{q} - \dot{w} \tag{2.30}$$

As the time-scales associated with blow-out are very small, we can model it to be an adiabatic process, $\dot{q} = 0$. The instantaneous work done by the control volume during blow-out is the work done by the control volume in expanding against a boundary pressure of $P_H$. Therefore,

$$\dot{w} = P_H \cdot \frac{dV}{dt}$$

Integrating the first law equation over time (between $t-t_2$ and $t = t_{2'}$, and dividing by the crank-rotation time-period $T$, we get

$$\frac{((mu)_{Cv})_{t_{2'}} - ((mu)_{Cv})_{t_2}}{T} = \frac{-P_H(V_{2'} - V_2)}{T} \tag{2.31}$$

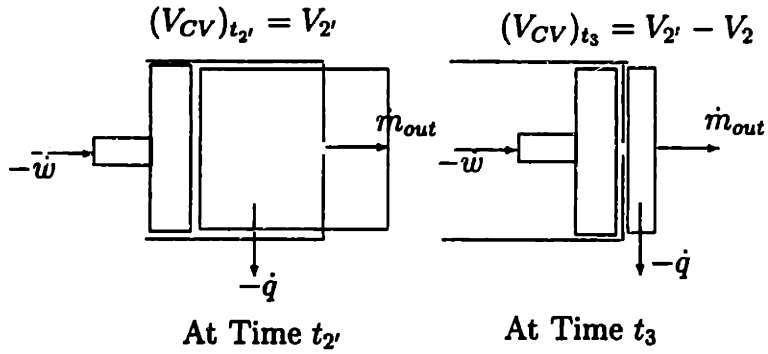


Figure 2-6: Schematic Figure of the Discharge Process

At time $t_{2'}$, gas in the control volume is at state 2', while it is at state 2 at time $t_2$. Using this, we rewrite the energy balance equation as shown below.

$$(\dot{m} + \dot{m}_{leak,dis}) \cdot (u_{2'} - u_2) = \frac{-P_H(V_{2'} - V_2)}{T} \tag{2.32}$$

## 2.7 Discharge

At the end of the blow-in/blow-out process, gas in the scroll pockets is at state 2' (pressure $P_H$ and temperature $T_{2'}$). Between time, $t = t_{2'}$, and the end of the compression cycle, $t = t_3$, the pockets undergo a process of discharge when pocket volume steadily diminishes to zero, and gas gets expelled from the scroll pockets into the discharge plenum. The exiting gas experiences a transfer of heat to the discharge side scroll wall, which is at a cooler temperature, $T_{w,dis}$. At the end of the discharge process, all gas from the scroll pockets has been expelled into the discharge plenum, and has reached the discharge state $H$ (pressure $P_H$, and temperature $T_H$) as shown in figure 6. The thermodynamic equations governing the discharge process are listed below.

We start the discharge process where the blow-in/blow-out process left off. Therefore, the start of discharge is characterized by a control volume of volume $V_{2'}$, with gas at state 2'. At the end of the discharge process, the pocket volume has diminished to zero, thus reducing the control volume to a volume of $V_{2'} - V_2$. In the process,

discharge gas (and all remaining gas in the control volume) has reached state $H$.

*Continuity* - Drawing a contracting control volume for the discharge process as shown in figure 6,

$$\frac{\partial m_{Cv}}{\partial t} = -\dot{m}_{out} \tag{2.33}$$

where $m_{Cv}$ is the mass of gas in the control volume at any instant, and $\dot{m}_{out}$ is the instantaneous flow rate of gas out of the control volume.

Integrating the control volume over time (between $t = t_{2'}$ and $t = t_3$), and dividing the equation by crank-rotation (and discharge) time-period $T$, we get

$$\frac{(m_{Cv})_{t_3} - (m_{Cv})_{t_{2'}}}{T} = -\frac{1}{T}\int_{t_{2'}}^{t_3} \dot{m}_{out} dt = -\dot{m}_{dis} \tag{2.34}$$

In the above equation, $(m_{Cv})_{t_3} = (V_{2'} - V_2)/v_H$ as gas left in the control volume at the end of discharge is at state $H$, and $\dot{m}_{dis}$ is the average (taken over the crank-rotation time-period $T$) mass flow rate of refrigerant exiting the pump.

Therefore,

$$\dot{m}_{dis} = \dot{m} + \dot{m}_{leak,dis} + \dot{m}' - \frac{V_{2'} - V_2}{T v_H} \tag{2.35}$$

Note here, that for a blow-out scenario, $\dot{m}' = 0$, while for a blow-in scenario, $V_{2'} = V_2$.

*First Law* - Performing an energy balance on the control volume at any instant, we get

$$\frac{\partial (mu)_{Cv}}{\partial t} = \dot{q} - \dot{w} - \dot{m}_{out} h_{out} \tag{2.36}$$

Here, $\dot{q}$ is the instantaneous rate of heat transfer into the control volume, while $\dot{w}$ is the instantaneous rate of work done by the control volume. Integrating the energy balance over time, we get

$$\frac{((mu)_{Cv})_{t_3} - ((mu)_{Cv})_{t_{2'}}}{T} = -\dot{Q}_{dis} - \dot{W}_{dis} - \dot{m}_{dis} h_{out} \tag{2.37}$$

Here, $\dot{Q}_{dis}$ is the average rate of heat transfer out of the control volume, and $\dot{W}_{dis}$ is the average rate of work done by the control volume during the discharge process.

$$\dot{Q}_{dis} = -\frac{\int_{t_{2'}}^{t_3} \dot{q} dt}{T}$$

$$\dot{W}_{dis} = \frac{\int_{t_{2'}}^{t_3} \dot{w} dt}{T}$$

Gas leaves the control volume at the discharge state $H$, while gas in the control volume at time $t_{2'}$ is at state 2'. The discharge work $\dot{W}_{dis}$ is negative because the volume of the control volume is steadily decreasing from $V_{2'}$ to $V_{2'} - V_2$. The pressure at the boundary of this contracting control volume is constant at discharge pressure, $P_H$ during this process. In order to avoid confusion, the frictional work, $\dot{W}_{fric,dis}$ is defined to be positive.

$$\dot{W}_{dis} = \frac{\int_{V_{2'}}^{V_{2'}-V_2} P \cdot dV}{T} - \dot{W}_{fric,dis}$$

Recalling that the discharge process takes place for one crank-rotation,

$$\Rightarrow \dot{W}_{dis} = -\frac{P_H \cdot V_2}{T} - \dot{W}_{fric,dis}$$

Recalling from the continuity equation that

$$\frac{((m)_{CV})_{t_{2'}}}{T} = \dot{m} + \dot{m}_{leak,dis} + \dot{m}' = \frac{V_{2'}}{v_{2'}T}$$

and

$$\frac{((m)_{CV})_{t_3}}{T} = \frac{V_{2'} - V_2}{v_H T} = \dot{m} + \dot{m}_{leak,dis} + \dot{m}' - \dot{m}_{dis}$$

The first law equation is

$$\frac{((mu)_{Cv})_{t_3} - ((mu)_{Cv})_{t_{2'}}}{T} = -\dot{Q}_{dis} - \dot{W}_{dis} - \dot{m}_{dis} h_{out}$$

which can be expanded as

$$(\dot{m}+\dot{m}_{leak,dis}+\dot{m}'-\dot{m}_{dis})u_H-(\dot{m}+\dot{m}_{leak,dis}+\dot{m}')u_{2'} = -\dot{Q}_{dis}+\frac{P_H V_2}{T}-\dot{W}_{fric,dis}-\dot{m}_{dis}h_H$$

which can in turn be simplified to the equation below

$$(\dot{m} + \dot{m}_{leak,dis} + \dot{m}')(u_{2'} + P_H v_{2'} - h_H) = \dot{Q}_{dis} - \dot{W}_{fric,dis} \tag{2.38}$$

If we neglect the work of friction, we then get

$$\dot{Q}_{dis} = (\dot{m} + \dot{m}_{leak,dis} + \dot{m}')(h_{2'} - h_H) \tag{2.39}$$

Thus, under the assumption of constant discharge pressure and no friction, the discharge heat transfer is simply the decrease in enthalpy of discharge gas.

Since, discharge heat transfer involves a transfer of heat to the scroll walls at a temperature, $T_{w,dis}$,

$$\dot{Q}_{dis} = \dot{m}_{dis}(h_{2'} - h_H) = (UA)_{dis} \cdot (\Delta T)_{lm,dis} \tag{2.40}$$

Here, $(UA)_{dis}$ is the conductance of discharge heat transfer, while $(\Delta T)_{lm,dis}$ is the log mean temperature difference associated with discharge heat transfer.

$$(\Delta T)_{lm,dis} = \frac{T_{2'} - T_H}{log(\frac{T_{2'}-T_{w,dis}}{T_H-T_{w,dis}})} \tag{2.41}$$

## 2.8 Heat Transfer from Discharge to Suction

In the preceding sections, we described a process where gas entering the scroll pump undergoes heat transfer with the scroll wall at the suction side resulting in a higher gas temperature at the start of the closed process, while gas at the discharge side undergoes a cooling process with the scroll wall near discharge. The process that results in the transfer of heat from the discharge gas to the suction gas to the suction gas is a combination of 2 coexisting processes, namely "kissing" heat transfer between

wraps of the orbiting and fixed scrolls, and conduction heat transfer through the scroll pump head from the discharge to the suction side. "Kissing" heat transfer is a mode of transient conduction between wraps of the scroll at discharge to wraps of the scroll at suction caused by transient contact between points on the fixed scroll and their conjugate points on the orbiting scroll. This mode is modeled and its existence proved experimentally using data from a specially instrumented SC37 pump. A third complementary mode of heat transfer would involve transfer of heat from the scroll walls to the closed pocket gas in the discharge side, and back to the scroll walls on the suction side. A calculation of the heat transfer coefficients associated with these three modes, for an SC37 compressor effectively rules out closed cycle convection from being a very significant mode of heat transfer. The kissing and conduction modes of heat transfer can both be lumped into one heat transfer conductance, $(UA)_{wall}$, which should only weakly depend on operating condition of the pump as thermal conductivity of the metal and thermal contact areas between orbiting and fixed scrolls depend weakly on operating condition. The following equations thus aid in closing the loop on thermodynamic model of the pump from suction to discharge.

$$\dot{Q}_{suc} = \dot{Q}_{dis \to suc} = \dot{Q}_{dis} \tag{2.42}$$

$$\dot{Q}_{dis \to suc} = (UA)_{wall} \cdot (T_{w,dis} - T_{w,suc}) \tag{2.43}$$

## 2.9 Parametric Models to be Used as Inputs to the Lumped Parameter Model

The parametric models of the pump are specific to the geometry of a pump and can be easily derived. While the volumes of the scroll pocket at the start ($V_1$) and the end ($V_2$) of the closed process are merely functions of the geometry of the scroll, heat transfer conductances and leakage models can be explicitly derived for each scroll pump. The heat transfer conductances associated with suction heat transfer

($UA_{suc}$), and discharge heat transfer ($UA_{dis}$) can be derived from pipe flow correlations as demonstrated in chapter 3 of the thesis. In general form, the heat transfer conductances above will depend upon the the mass flow rate of refrigerant through the pump ($\dot{m}$), the dimensions of the scroll passages, ($r_{orb}$ and $h_{wrap}$), and the area of walls exposed to suction ($A_{suc}$) and discharge ($A_{dis}$) respectively.

$$UA_{suc} = f(\dot{m}, r_{orb}, h_{wrap}, A_{suc})$$

$$UA_{dis} = f(\dot{m}, r_{orb}, h_{wrap}, A_{dis})$$

The discharge-to-suction heat transfer conductance ($UA_{wall}$) is simply a composite of two competing modes of heat transfer between discharge and suction side pump walls, namely kissing heat transfer and conduction. While the conductance associated with conduction through the scroll bases ($UA_{cond}$) is easily estimated assuming a cylindrical geometry of the scrolls, the kissing heat transfer coefficient ($UA_{kiss}$) is estimated from an analysis of data from the kissing heat transfer experiment described in chapter 3.

$$UA_{wall} = UA_{cond} + UA_{kiss}$$

Since leakage phenomena in the scroll pump are distributed phenomena, we develop lumped parameter leakage models as correlations from distributed parameter leakage models as described in chapters 4 and 5. Since, the models for leakage are based on orifice flow, leakage mass flow rates depend on the pressure difference across the orifice as well as the density of fluid on the high pressure side of the orifice. In developing lumped parameter formulations of leakage for the pump, we consider the pressure difference between discharge and suction sides of the pump ($P_H - P_L$), and the densities associated with discharge ($\rho_H$) and suction ($\rho_L$).

$$\dot{m}_{leak,suc} = f(P_H - P_L, \rho_H, \rho_L)$$

$$\dot{m}_{leak,dis} = f(P_H - P_L, \rho_H, \rho_L)$$

## 2.10 Conclusion

The methodology for creating lumped parameter models of each stage of the compression process has been described above. The equations derived here taken together form a closed loop lumped parameter model of the compression process. (see Appendix A) Given the input values and parametric models for a specific pump, using the model reduces to solving an algebraic system of equations, the solution of which uniquely describes the thermodynamic operation of a scroll pump.

# Chapter 3

# Kissing Heat Transfer Between the Wraps of a Scroll Pump

## 3.1 Introduction

In this chapter, we model the heat transfer processes taking place within a scroll pump. Lumped parameter estimation of heat transfer conductances suggested that the dominant modes of heat transfer within the pump are a combination of conduction through the fixed and orbiting scrolls, and a mechanism of transient conduction through the momentary contact (kissing) of conjugate points on the wraps of the orbiting and fixed scrolls. Our analysis further showed that convection between gas and wall is characterized by small heat transfer conductances and can therefore be neglected for substantial portions of the pumping process relative to conduction and kissing heat transfer.

In order to demonstrate the existence of kissing heat transfer, we conducted experiments to observe the fixed scroll metal temperature profile on a specially instrumented Carrier scroll compressor. Our experimental measurements revealed the existence of significant temperature gradients across the wraps of the fixed scroll. These temperature gradients are indicative of heat fluxes which are too large to be explained by convection between gas and wall, and are therefore considered to be evidence of the existence of kissing heat transfer. Further, kissing heat transfer contact angle esti-

mations based on experimental data are consistent with those predicted by analysis. We believe that kissing heat transfer explains a large portion of the loss of volumetric efficiency in scroll pumps, and that elimination of this mode of heat transfer is beneficial to improvements in pump operating efficiency.

In the next section of the chapter, we derive the lumped parameter heat transfer conductances associated with various modes of heat transfer within a scroll pump. This is followed by a section in which we describe the construction and instrumentation of the pump kissing heat transfer experiment. Thereafter, we discuss results of the experiment, followed finally by conclusions.

## 3.2 Nomenclature

$A_c$ Cross-sectional area of gas flow passage in pump

$A_i$ Heat transfer area of fixed scroll wrap at location $i$

$A_{orb}$ Heat transfer area of orbiting scroll wrap

$b$ Hertzian stress contact length

$dT$ Temperature difference for kissing heat transfer

$D_h$ Hydraulic Diameter of gas flow passage in pump

$E$ Modulus of elasticity of metal

$h$ Convection heat transfer coefficient

$h_{fix}$ Thickness of base of fixed scroll

$h_{orb}$ Thickness of base of orbiting scroll

$h_{wrap}$ Nominal height of scroll wrap

$K$ Thermal conductivity of metal

$K_g$ Thermal conductivity of refrigerant

$m$ Mass of orbiting scroll

$\dot{m}$ Mass flow rate of refrigerant

$Nu$ Nusselt number

$P$ Gas pressure

$Pr$ Prandtl number

$p$ Centrifugal force per unit scroll wrap length

$Re$ Reynold's number

$r_i$ Radius of fixed scroll at location $i$

$r_{orb}$ Radius of eccentric orbit of scroll

$T$ Gas temperature

$T_c$ Temperature of "cold" scroll wrap

$T_h$ Temperature of "hot" scroll wrap

$T_m$ Temperature of orbiting scroll wrap

$R_{conv}$ Thermal resistance associated with convection

$R_{fix}$ Thermal resistance associated with conduction across base of fixed scroll

$R_{kiss}$ Thermal resistance associated with kissing heat transfer

$R_{orb}$ Thermal resistance associated with conduction across base of orbiting scroll

$U_{conv}$ Thermal Conductance of convection per unit circumferential length

$U_{fix}$ Thermal Conductance of fixed scroll conduction per unit circumferential length

$U_{kiss}$ Thermal Conductance of kissing heat transfer per unit circumferential length

$U_{orb}$ Thermal Conductance of orbiting scroll conduction per unit circumferential length

$t$ Time

$\alpha$ Thermal diffusivity of metal

$\Delta T$ Temperature difference between cold and hot wraps

$\mu$ Absolute viscosity of refrigerant

$\mathcal{P}$ Perimeter of pump gas flow passage

$\tau$ Time period of one crank rotation of scroll pump

$\theta$ Kissing heat transfer contact angle

$\omega$ Angular velocity of scroll pump

## 3.3 Estimation of Heat Transfer Conductances

As refrigerant enters a scroll pump and gets compressed, its temperature also rises. Gas that comes in to the pump at a low temperature and low pressure, leaves the pump at a high pressure and high temperature. This difference in gas temperatures and pressures between suction and discharge serves as the source of internal energy transfer within a scroll pump. Direct leakage of gas from high pressure, high temperature regions to low pressure, low temperature regions of the scroll is one mechanism of energy transfer, while heat transfer from discharge side to suction side is the second mode of energy transfer. In this section, we concern ourself only with heat transfer modes, though we believe that internal leakages are also an important factor in lowering pump thermodynamic efficiency.

Heat transfer from discharge to suction involves interactions between the refrigerant and the walls of the scroll pump. The walls of the scroll pump, which are affected by the presence of the gas, get warmer as one progresses from the suction side wall to sections of the wall closer to discharge. The hottest part of the wall, however, attains a temperature that is lower than the hottest gas within the pump, while the coldest portion of the wall reaches a temperature that is higher than the coldest (suction) gas temperature. Thus, there is a crossover point on the wall, at which the wall starts to transfer heat to the suction gas that was transferred to it from the discharge gas.

Figure $3-1$ shows a schematic diagram of the various paths available for heat to get transferred from the hot discharge gas to the suction gas. Figure $3-2$ shows these heat transfer modes depicted in the form of a resistance network. In the subsections that follow, we attempt to quantify each of these resistances in order to determine the dominant modes of heat transfer within the scroll pump. Such an analysis while enhancing our understanding of the various mechanisms at play within a scroll pump,

also serves to identify sources of irreversibility within the pump. The three modes of heat transfer that are estimated below are conduction through the metal of the fixed and orbiting scrolls, convection between gas and wall of the pump, and kissing heat transfer (to be described in detail). Our analysis shows that while heat is convected to the walls at discharge and from them at suction, the major mode of heat transfer from hot sections of the wall to the cold sections of the wall is a combination of kissing heat transfer and conduction through the base of the fixed and orbiting scrolls respectively. This is because of the fact that conduction and kissing heat transfer provide a low thermal resistance pathway for heat to travel within the pump, relative to convection between hot wall and gas, followed by convection from gas to cold wall. This conclusion has an important ramification in that it indicates that heat transfer during the closed process within the scroll pump cannot be a major source of irreversibility and that the principal sources of deviation of the closed process polytropic constant, $n$ from the isentropic constant $\gamma$ lie elsewhere (presumably leakage and friction). It also demonstrates that, in kissing heat transfer, there lies a unique mechanism of heat transfer that in effect, enhances the radial thermal conductivity of the scroll.

In the following subsections, we take two radial locations within the scroll, namely positions 1 and 2 as indicated on figure $3-1$. We then estimate the thermal conductance associated with each mode of heat transfer between these two radial positions. While the numbers presented below are specifically applicable to the section of the fixed scroll between positions 1 and 2, the general trends from these estimations are equally applicable to the scrolls in general. All numerical calculations were done with a Carrier scroll pump in mind, since that is the pump we used in our experiments.

### 3.3.1 Conduction through Walls of Fixed and Orbiting Scrolls

The bases of the orbiting scroll and the fixed scroll are large chunks of metal that provide for a transfer of heat between hot and cold sections of the scroll metal. The mechanism of heat transfer here is simply radial conduction, whose lumped

conductance can be estimated assuming cylindrical symmetry of the scroll bases. We neglect any conduction through the spiral of the scrolls since this presents a heat transfer pathway that has a much higher resistance associated with it than radial conduction through the bases of the scroll. Conduction through the heavy metal of the fixed and orbiting scroll bases is modeled as radial conduction through a cylindrical resistance.

### Fixed Scroll

We take points 1 and 2 on the fixed scroll and determine the resistance associated with thermal conduction between the two points. For simplicity, we assume that the metal between 1 and 2 is at a uniform thickness, $h_{fixed}$ associated with the narrower section. This will give us a higher value of the thermal resistance than is real.

Radius of scroll at location 2, $r_2$=36.85 mm = 0.03685 m
Radius of scroll at location 1, $r_1$=21.45 mm = 0.02145 m
Thickness of the narrower section of the fixed scroll,

$$h_{fix}=12.70 \text{ mm} = 0.0127\text{m}$$

Average radius, $r_{ave}=29.15mm=0.02915m$
Thermal Conductivity of Cast Iron, $K=54\ W/m \cdot K$

For a cylindrical geometry, conduction resistance [1, p. 104] is given by

$$R_{Fix} = \frac{ln(\frac{r_2}{r_1})}{2\pi h_{fix} K} = 0.13K/W \tag{3.1}$$

Since our objective is to compare conduction through the fixed scroll to other modes of heat transfer, namely conduction through the orbiting scroll, convection and kissing heat transfer, we calculate the thermal conductance of each mode per unit circumferential length along the scroll wraps. This calculation is done based on the unit circumferential length at a radial location midway between locations 1 and 2.

The thermal conductance per unit circumferential length is then given as

$$U_{Fix} = (R_{Fix} \cdot 2\pi r_{ave})^{-1} = 43.5 W/m \cdot K \tag{3.2}$$

**Orbiting Scroll**

We now estimate the conductance associated with heat transfer across the base of the orbiting scroll between points 1 and 2. This calculation is identical to that for the fixed scroll, except for the fact that the base of the orbiting scroll is at a uniform thickness, $h_{orb} = 9.5mm$. Making the calculations as in the previous paragraph, we get

$$U_{orb} = 32.7 W/m \cdot K \tag{3.3}$$

### 3.3.2 Convection Between Gas and Walls

As gas progresses through the scroll getting compressed, its temperature and pressure go up. Here we quantify the thermal conductance associated with convection between gas and walls of the scrolls at location 1 transmitted through the gas and wall of the orbiting scroll to location 2.

For heat to progress through the gas between locations 1 and 2, it has to be convected across 4 boundary layers, i.e. convection between the hot wall of the fixed scroll at location 1 and hot gas, followed by convection between the hot gas and the wall of the orbiting scroll, followed by conduction through the thickness of the orbiting scroll (whose resistance can be neglected), followed by convection between the orbiting scroll and the cooler gas on its other side, followed finally by convection between the cool gas and the cold fixed scroll walls at location 2.

Assuming that the heat transfer coefficient, $h$ does not vary very much with location, the thermal resistance associated with convection [1, p. 104-110] is given by the following formula.

$$R_{conv} = \frac{1}{h}[1/A_1 + 2/A_{orb} + 1/A_2] \tag{3.4}$$

Here, $A_1$ is the area of the fixed scroll wrap at location 1 that is exposed to the hot gas while $A_2$ is the area of wrap exposed to the gas at location 2. $A_{orb}$ is the area of the orbiting scroll wrap, that is exposed to gas on each side (crudely assumed to be equal here), and is assumed to be the average of $A_1$ and $A_2$. The height of the scroll wrap is $h_{wrap}$=27$mm$.

$$A_1 = 2\pi r_1 h_{wrap} = 3.7 \times 10^{-3} m^2$$
$$A_2 = 2\pi r_2 h_{wrap} = 6.3 \times 10^{-3} m^2$$
$$A_{orb} = 5.0 \times 10^{-3} m^2$$

### Estimation of Convection Coefficient

Flow of refrigerant between the walls of a scroll pump is highly turbulent and can be thought of as unsteady flow through a channel of varying and non-uniform cross-section. The channel has a height, $h_{wrap}$ associated with the height of the scroll wraps, while the width of the channel varies from a maximum of $2r_{orb}$ to a minimum of *zero*, where $r_{orb}$ is the orbiting radius of the scroll pump. We simplify the model of this complex flow to one through a rectangular duct with uniform and non-varying channel width $r_{orb}$, and height $h_{wrap}$. The channel width $r_{orb}$ is the smaller of the two numbers (by an order of magnitude). Therefore, the governing dimension to determining Reynold's numbers ($Re$) and heat transfer coefficients is the hydraulic diameter of the duct ($D_h = \frac{4A_c}{\mathcal{P}} = 2r_{orb}$). Using standard pipe flow heat transfer correlations [6, p. 404] to determine the Nusselt number, $Nu$, we get

$$Nu = 0.023 Re^{0.8} Pr^{1/3} \tag{3.5}$$

where

$$Re = \frac{\dot{m} \cdot 2r_{orb}}{A_c \mu} \tag{3.6}$$

$A_c$=area of cross-section of the channel = $r_{orb} \cdot h_{wrap}$

$\mathcal{P}$=perimeter of the channel = $2r_{orb} + 2h_{wrap}$

$r_{orb}$=radius of the eccentric orbit= 3.7 mm = 0.0037 m

For a typical ARI condition ($P = 100psi$ and $T = 100F$)

The absolute viscosity [5] of R-22, $\mu$=134.1 $\mu poise$

The thermal conductivity [5] of R-22, $K_g$=0.0116 $W/m{\cdot}K$

The mass Flow rate of refrigerant through the pump,

$$\dot{m} = 500 \text{ lb/hr} = 0.063 \text{ kg/s}$$

The convection coefficient can then be calculated as below:

$$h = \frac{Nu \cdot K_g}{D_h} = 0.023(\dot{m})^{0.8}(\frac{2r_{orb}}{A_c \cdot \mu})^{0.8} \cdot \frac{Pr^{1/3}K_g}{2r_{orb}} \tag{3.7}$$

Plugging in the relevant values, we get

$$h = 870 \ W/m^2 \cdot K \tag{3.8}$$

### Conductance Calculation

The thermal resistance associated with convection can be estimated using the formula described before as $R_{conv} = 0.95 \ K/W$. In order to be able to compare different modes of heat transfer, as before, we compute the thermal conductance per unit circumferential length as

$$U_{conv} = [2\pi r_{ave} \cdot R_{conv}]^{-1} = 5.7W/m \cdot K \tag{3.9}$$

## 3.3.3 Kissing Heat Transfer

We now quantify the conductance associated with a third mode of heat transfer that is very specific to the geometry and the periodicity of scroll pumps, namely kissing heat transfer. In the sections that follow, we first describe the mechanism of this mode of heat transfer followed by a quantification of this mechanism in the scroll pump, between locations 1 and 2.

### Mechanism of Kissing Heat Transfer

The pumping action in a scroll pump is produced by the conjugate contact of points on the orbiting scroll with corresponding points on the fixed scroll. As the orbiting scroll orbits within adjacent scroll wraps of the fixed scroll, the location of conjugacy moves along in spiral angle [2]. The region between two consecutive conjugate points at any instant, encloses the volume of gas that is undergoing compression. As the orbiting scroll orbits, the distance between consecutive conjugate points decreases thus reducing the volume of the gas trapped inside and providing compression. Conjugate contact of any point in the orbiting scroll with its corresponding point on the fixed scroll is periodic. This means that any point such as point X, (see figure $3-5$) on the orbiting scroll that is in conjugate contact with a point, such as X' in the fixed scroll at time $t$, will once again be in contact with the same point at time, $t+\tau$, where $\tau$ is the time-period of one crank rotation of the pump (or the time-period for one orbit of the orbiting scroll). This also means that a point on the opposite side of the orbiting scroll will be in conjugate contact with the neighboring fixed scroll wrap at point X" at times, $t+\tau/2$, $t+3\tau/2$ etc. Thus, any point on the orbiting scroll that has contact with a hot wrap of the fixed scroll, also has contact with a neighboring cold wrap of the fixed scroll half a time-period (180°) later. This transient touching contact of the orbiting scroll with hot and cold wraps of the fixed scroll serves as a mechanism of heat transfer within the scroll pump, and is referred to in this thesis as "Kissing Heat Transfer".

### Modeling of Kissing Heat Transfer

The principal determinant of the magnitude of kissing heat transfer is the time of contact between conjugate pair points on the fixed and orbiting scroll. If the scroll surfaces were perfectly smooth and the geometry unaffected by stress, the time of contact between conjugate pairs would be infinitesimally small as the contact between scrolls would be along a line rather than an area. In such a situation, the amount of heat that might be transferred between fixed and orbiting scrolls might also tend

to zero. However, the actual situation within a scroll pump is far from ideal with surface roughness, oil films between the scrolls and hertzian stresses on the wrap surfaces (produced by centrifugal forces) all contributing towards making the time of contact between conjugate pairs non-zero. In the analysis that follows, we first assume that any point on the orbiting scroll is in conjugate contact with a point on the fixed scroll for $\theta/360$ of the time-period of crank rotation. This implies that there is a $\theta°$ angle subtended by contact between the wraps. After we estimate the kissing heat transfer conductance associated with a $\theta°$ angle of contact between wraps, we estimate the contact angle between wraps by a consideration of hertzian stresses and oil film thickness, and show it to be about 0.3° to 0.5°.

In estimating the kissing heat transfer coefficient between scroll wraps, we model the process as being one of transient conduction between two semi-infinite bodies of different temperatures. These temperatures are assumed to be constant with the rationale that the thermal penetration depth, $\sqrt{\alpha t}$ associated with the time-period of the scroll pump is much smaller than the thickness of its scroll wraps. For a semi-infinite body undergoing transient conduction with a constant temperature source, the instantaneous rate of heat transfer [6, p. 203] is given as

$$\dot{q}_s = \frac{K \cdot dT}{\sqrt{\pi \alpha t}} \tag{3.10}$$

We consider this to be the instantaneous heat flux from a hot fixed scroll wrap at temperature, $T_h$ to the orbiting scroll wrap at intermediate temperature, $T_m = (T_h + T_c)/2$ (to the first approximation) where $T_c$ is the temperature of the cold fixed scroll wrap that is in conjugate contact with the opposite side of the orbiting scroll wrap. The heat transfer temperature difference, $dT$ is then nothing but

$$dT = T_h - T_m = \frac{(T_h - T_c)}{2} = \Delta T/2 \tag{3.11}$$

Here $\Delta T = T_h - T_c$, and is the temperature difference between hot and cold fixed scroll wraps, i.e. the temperature difference between locations 1 and 2 on the fixed scroll. Assuming that the fixed scroll and the orbiting scroll wraps are in contact

for a time $t$, the total energy transferred between the hot fixed scroll wrap and the orbiting scroll is given by:

$$q_s = \int_0^t \dot{q}_s dt = \frac{K\Delta T}{\sqrt{\alpha\pi}} t^{1/2} \tag{3.12}$$

The average rate of kissing transfer between fixed and orbiting scrolls is then

$$\dot{q}_{kiss} = \frac{1}{\tau} \frac{K\Delta T}{\sqrt{\alpha\pi}} t^{1/2} \tag{3.13}$$

Here, the thermal diffusivity of cast iron, $\alpha = 7.22 \times 10^{-6}\ m^2/s$.
For $\theta°$ contact angle between scrolls, the contact time, $t = \tau\theta/360$,
while the time-period of the pump is $\tau$=1/60 $s$ (corresponding to 3600 rpm).
Plugging in the corresponding numbers, we then obtain

$$\dot{q}_{kiss} = 4629\theta^{1/2}\Delta T\ \frac{W}{m^2 \cdot K} \tag{3.14}$$

As the wrap has a length of $h_{wrap}$ = 27mm, the total kissing heat transfer per unit circumferential length of the scroll is

$$\dot{Q}_{kiss} = \dot{q}_{kiss} \cdot h_{wrap} = 126\theta^{1/2}\Delta T\ \frac{W}{m \cdot K} \tag{3.15}$$

The conductance per unit circumferential length associated with kissing heat transfer between the hot fixed scroll wrap and the orbiting scroll wrap is therefore,

$$U_{kiss} = 126\theta^{1/2}\ \ W/m \cdot K \tag{3.16}$$

If we model the kissing heat transfer between the orbiting scroll wrap and the cold fixed scroll wrap to be exactly identical (as an approximation), then we get that the conductance associated with kissing heat transfer between locations 1 and 2 on the fixed scroll is $U_{kiss} = 126\theta^{1/2}\ W/m \cdot K$. Note that the overall kissing heat transfer conductance is not halved when we also consider kissing heat transfer between orbiting

scroll, and the cool wrap of the fixed scroll. This is because the conductance calculated above was done on the basis of temperature difference ($\Delta T$) between locations 1 and 2 on the fixed scroll, rather than temperature difference between a wrap of the fixed scroll and the orbiting scroll.

These calculations were all made neglecting any contact resistance between conjugate surfaces, and by considering the local bulk temperatures of the scroll wraps to be constant.

### Contact Angle Estimation through Hertzian Stress Calculations

We now estimate the contact angles between orbiting and fixed scrolls assuming that the surfaces of both scroll wraps deform due to hertzian stresses. The stresses in turn are induced by the centrifugal force of the orbiting scroll in orbit. We model the contact of the orbiting and fixed scrolls as that of two solid cylinders in contact with a uniform load, $p$ per unit length, acting at the line of contact. The width of the contact between the two cylinders, $b$ can then be calculated using the formula [10, p. 516-517]:

$$b = 2.15\sqrt{\frac{p \cdot K_D}{E}} \tag{3.17}$$

where $p$ is the centrifugal force per unit length of scroll wrap.

$$p = \frac{m\omega^2 r_{orb}}{4 \cdot h_{wrap}} \tag{3.18}$$

We divide the centrifugal force by 4 because at any given time, there are at least 4 contact locations between orbiting and fixed scrolls. To the first order, each of these contact locations supports an equal part of the centrifugal load. $K_D$ is the weighted diameter of the contact location, as is conventionally used in hertzian stress calculations and is calculated as

$$K_D = \frac{D_1 \cdot D_2}{D_1 - D_2} \tag{3.19}$$

$D_1$ is the diameter of the larger cylinder (the scroll with larger local diameter at the point of contact), while $D_2$ is the diameter of the smaller cylinder. $E$ is the modulus of elasticity of cast iron, $E$=20 $\times$ $10^{10}$ Pa. The local contact angle, $\theta$ (in degrees) for orbiting or fixed scroll can then be calculated.

$$\theta_i = \frac{b}{2\pi r_i} \cdot 360° \tag{3.20}$$

where $r_i$ is the local radius of the fixed or the orbiting scroll. Table 3-1 lists results of our contact angle estimation for points 1 and 2 on the scroll. The calculations from this table show that contact angles range from 0.3°-0.5°.

The accuracy of our contact angle estimations here is affected by two factors. It tends to be underestimated due to the fact that the hertzian stress formulae applied here actually are for infinitely long cylinders in contact. Secondly, we assumed the geometry to be that of solid cylinders instead of hollow rings. This might tend to overestimate the contact angle.

### Effect of Oil Film Contact between Wraps

The scroll pump in operation has oil that lubricates the wrap surfaces. This oil performs the role of lubrication of the wraps, which also serve as the principal radial load bearing surfaces of the orbiting scroll at contact locations. The oil also serves the dual role of sealing any clearances between fixed and orbiting scrolls, thus helping minimize internal leakage between low and high pressure parts of the pump. If we assume that the wraps have uniform oil films that stick to their surfaces, the effective area of contact between orbiting and fixed scrolls at conjugacy is increased by the coalescence of the oil film sticking to either scroll wrap. If we now assume that the oil attached to each wrap is in local thermal equilibrium with the scroll wrap, then we could think of the kissing heat transfer contact angles as being increased by the presence of oil. For the oil itself to undergo kissing heat transfer, the term $K_{oil}/\sqrt{\alpha_{oil}}$ would have to be of the same order of magnitude as that for the metal. In fact, this term is at least an order of magnitude lower for oil than it is for cast iron. Kissing

heat transfer between oil films is therefore ruled out as being a major mode of heat transfer. There are however, other mechanisms by which the oil film enhances heat transfer between hot and cold scrolls - (1) direct thermal conduction across the oil films (with a negligibly small thermal resistance) or (2) actual mixing of hot and cold oil films which then changes the temperature of the surface of the scroll wrap and provides for a longer time-period in which heat transfer between wrap and oil film occurs. In figure 3-6 and table 3-2, we estimate the oil film contact area for the orbiting and fixed scrolls using only geometric considerations and neglecting any hydrodynamic effects on the oil between scroll wraps. Since, it is unclear as to the actual thickness of the oil film within the scroll pump, we perform this calculation for a range of oil film thicknesses. Oil enhanced contact angles of 5° to 15° between scrolls suggests that kissing heat transfer enhanced by the presence of oil films is another plausible mechanism of heat transfer between fixed and orbiting scrolls.

We observe from the graph that as the oil film thickness goes up, the oil contact angle between scrolls asymptotically reaches a maximum value at around 15°. Contact angles larger than this need oil film thicknesses that are very large, owing to the curvature effects of the fixed and orbiting scrolls.

### 3.3.4 Effect of Oil Film on Kissing Heat Transfer

Here, we consider the effect of the presence of the oil film on kissing heat transfer conductance. Specifically, we consider the possibility that fixed and orbiting scrolls are not in direct metal to metal contact, but are separated by the presence of an oil film. This oil film, which is very thin (less than 1.0 mils), is assumed to attain thermal equilibrium with the scrolls at the locations of contact. Kissing heat transfer is then characterized by transient conduction mechanisms of the kind described earlier as well as conduction across oil films, and conduction across the wraps of the orbiting scroll. In figure 3-7, we present the kissing heat transfer coefficient calculated as a function of oil film thickness for a range of contact angles. As expected, kissing heat transfer coefficient rises with contact angle. We find that oil film thickness also has a strong effect in determining the kissing heat transfer coefficient (kissing heat transfer

coefficient decreases as we increase oil film thickness).

In the absence of any specific knowledge of oil film thicknesses in the pump, or experimental estimations of scroll to scroll contact angle, we defer to our hertzian stress calculations and use the kissing heat transfer coefficient corresponding to a contact angle of 0.4° and direct metal to metal contact. The kissing heat transfer coefficient corresponding to this condition is $U_{kiss} = 80\ W/m \cdot K$.

### 3.3.5 Comparison of Modes of heat Transfer

Our estimation of heat transfer conductances demonstrates that convection between gas and wall is a very high thermal resistance mechanism of internal heat transfer, and that it is unlikely to be favored over a combination of thermal conduction through scroll bases, and kissing heat transfer. A caveat here is that while kissing heat transfer and conduction dominate the heat transfer from the hot parts of the scroll to the cold parts, there has to be a mechanism of convection between gas and wall to get the heat into the wall at the hot side and out of it into the gas at the cold side. Such convection is made possible by the fact that the kissing and conduction heat transfer pathways are not available at portions of the pump near discharge and suction ports. Thus convection becomes the dominant mode of heat transfer at suction and discharge, while kissing heat transfer and conduction dominate within the pump. A major implication of kissing heat transfer being a dominant mode of heat transfer within the pump is that large heat fluxes associated with this mode ought to be observed across the wraps of the scroll pump. These fluxes should in turn manifest themselves in the form of significant steady-state temperature gradients across the wraps of the fixed and orbiting scrolls.

## 3.4 Pump Heat Transfer Experiment

Our preliminary analysis of the lumped heat transfer conductances within a scroll pump indicates that kissing heat transfer is a major mode of heat transfer within the pump and that it should manifest in the form of significant heat fluxes across the scroll.

Since our results from the analysis of kissing heat transfer are highly dependent on an unobservable (and immeasurable) contact angle and contact time between orbiting and fixed scrolls, we decided to seek experimental verification of this mode of heat transfer. We performed an experiment on a specially instrumented Carrier scroll compressor to capture its temperature profile and to observe any heat fluxes that might manifest across scroll wraps. The following section describes the apparatus that was built to perform the experiment and explains the rationale behind the placement of sensors in this experiment. The results of the experiment are then reported in the next section. The principal result of the experiment is that there were significant temperature differences observed across scroll wraps. These temperature differences are evidence of heat fluxes that could not have come about due to convection between gas and wall, and are indicative of kissing heat transfer. The contact angles inferred from these measurements are smaller, but of the same order of magnitude as those estimated in the previous section.

### 3.4.1 Description of Apparatus

The apparatus used to perform the pump heat transfer experiment was a scroll compressor, manufactured by Carrier Corporation that was placed in a desuperheat loop to study its performance under a variety of controlled operating conditions.

A production compressor was modified as a bolted shell closure for access to the scroll pump. The production compressor was complete except for the final closure welds for the bottom and top end caps. The bolted closure use O-ring seal rings welded to the endcaps. The O-rings sealed on the OD of the shell at each end. The axial thrust on the endcaps was supported by external pressure plates and axial stay bolts external to the shell. Before the fixed scroll was disassembled from the crank case, dowel pins were installed to ensure alignment on reassembly. The internal thermocouple wires (a total of 48 pairs) were passed through a pressure-tight leadthrough welded into the top cap. The lead through was of the compression-type with 48 holes for two-wire thermocouple leads. The compression seal was made with a highly compressed teflon disk.

### 3.4.2 Placement and Positioning of Sensors

A set of 48 thermocouples were placed on the fixed scroll (and crank base) of the device. The rationale of the positioning of these sensors was to be able to observe the temperature profile of the metal in the pump, and to verify the existence of kissing heat transfer. Sensors were placed in spiral angle increments of 90° from the suction all the way to the discharge so as to be able to watch the temperatures of the metal evolve along the path of compression. Sensors were placed both at the base of the fixed scroll as well as at locations midway through the height of the scroll wraps. Sensors placed at the mid-point of the wraps were mounted as pairs on either side of the wrap wall. This was done in order to observe any temperature differences and heat fluxes that may result across the scroll wraps due to kissing heat transfer. The location of these sensors on the wraps was offset from the center of the fixed scroll by the radius of the orbit of the orbiting scroll, $r_{orb}$ in the direction perpendicular to the angular location on the scroll. This was done so that sensors that faced each other across the gap between scroll wraps also constitute a kissing pair, i.e. a given point on the orbiting scroll comes into transient contact with the fixed scroll wrap at both these locations during the course of a rotation. Such a placement enables experimental estimation of the kissing heat transfer coefficient between locations on the scroll. Measurement of temperature at the midpoint of wrap and the base of the scroll at the same spiral locations means that we can also determine if axial conduction (parallel to the axis of rotation) is an important mechanism of heat transfer within the scroll. Base temperatures at different angular locations also help determine the magnitude of radial conduction that occurs through the fixed scroll base. A set of 4 thermocouples were set up to measure the temperature of gas as it enters the pump. 2 of these thermocouples measure the temperature of the suction gas (gas that enters the compressor), while the other 2 measure the temperature of the (approximately) 20% of suction gas that gets diverted over the motor within the hermetic shell of the compressor. The suction state of the pump can be considered to a mixed mean average of these 2 temperatures. A set of 3 thermocouples was set up to measure

the temperature of gas as it progresses (and gets heated) through the outer suction pathway of the fixed scroll. These 3 sensors were mounted in a narrow section along the outer wall of the fixed scroll, that does not get swept through by the orbiting scroll. Finally, a set of 2 thermocouples measure the temperature of gas as it gets discharged from the pump. All metal temperatures are measured by thermocouples that are embedded in the metal and that are held in place by an epoxy, while gas temperatures are measured by thermocouples whose junctions are isolated from metal and left exposed to the gas stream. A schematic diagram showing the placement off all sensors is shown in figure 3 – 3.

Thermocouples that are positioned midway along the length of the scroll wraps were each placed in specially machined grooves along the length of the fixed scroll wraps. This was done by first locating the exact desired position of the sensor, using a rotary table and then machining grooves on the fixed scroll to extend up to the base of the scroll. Through holes were then drilled at these locations through the fixed scroll base. Thermocouple junctions were positioned in these grooves and the wire taken through these holes out the base of the fixed scroll. The thermocouples were each glued to their spots using an epoxy resin. Once the thermocouple junctions were securely glued on to position, the grooves and holes were all injected with epoxy so as to fill all spaces and hold the thermocouples within a pressure-tight environment. Each of the grooves that were machined to hold the thermocouples were deep enough to contain the thermocouples, but were considered shallow enough that they wouldn't disturb the local temperature profile by too much. Thermocouple junctions were embedded at a shallow depth from the surface of the epoxy so that they would measure the surface temperatures of the wraps, while still not being susceptible to any transient effects created by periodic contact between orbiting and fixed scroll wraps (i.e. beyond the thermal penetration depth). The grooves themselves were filled with epoxy to the level commensurate with the undisturbed scroll wrap surface so as to not cause undue leakage at the location of the grooves due to clearances between fixed and orbiting scrolls.

Thermocouples that were positioned on the base of the orbiting scroll, were each

placed in specially machined and precisely located blind holes on the base of the fixed scroll. These holes carried thermocouple wire from the exterior to precise locations at the roots of the scroll wraps. Once again, thermocouples were held in place, and all holes filled up with a slow-curing epoxy. Thermocouples measuring gas temperature were all taken in to the pump through holes drilled through the walls of the fixed scroll. These holes were filled up with epoxy but the junctions of these thermocouples were allowed to jut out of these holes and be directly exposed to gas.

Finally, the wires of all thermocouples that were epoxied in place, were taken to the exterior, through the compression leadthrough on the top end cap. The modified compressor was placed on a cart that was fitted with a desuperheat loop and a turbine flowmeter with which to measure mass flow rate of refrigerant through the experiment. Temperatures in the device were measured using a rotary thermocouple switch that could losslessly switch between thermocouples. Thermocouple signals were then put through a cold junction compensator, amplifier and low pass filter, and were finally read on a precise digital multimeter. Thermocouple pairs that were placed on opposite sides of a scroll wrap were measured in two ways. Firstly, there were positions on the rotary switch that enabled direct measurement of the absolute temperature of these thermocouples. Secondly, there were also uncompensated positions on the rotary switch that measured the differential voltage across these pairs. Such a measurement enables precise measurement of the temperature difference across scroll wraps.

## 3.5 Results from Pump Heat Transfer Experiment

This section presents the results of the pump heat transfer experiment and discusses the implication of some of the experimental observations. The pump heat transfer experiment was performed for 5 operating conditions over a wide range of suction pressures, (and thus mass flow rates) and pressure ratios. Relatively noisefree readings of temperature were recorded in each of these operating conditions. In figures 3−4 and

3 – 8, we report the data corresponding to the −10/90/10 (evaporator at a saturation pressure corresponding to −10° F, condenser at a saturation pressure corresponding to 90° F, and a 20° F superheat at suction) condition on the pump. Data for the other operating conditions exhibit similar trends, and are not reported here.

### 3.5.1 Temperature Profiles from Pump Heat Transfer Experiment

Unfortunately, some of the scroll wrap thermocouples in the experiment (see figure 3-3 for their locations on the experiment) did not work. These are the scroll wrap pair $TC19$ and $TC20$, $TC8$ (though its scroll wrap pair $TC9$ worked), and $TC10$, which gave very noisy readings. Fortunately, all the other thermocouples (including 4 scroll wrap pairs) did work very well, enabling us to get a fairly complete picture of the scroll pump temperature profile. Several common trends were observed from the data of the pump heat transfer experiment. These trends help us comprehend some of the heat transfer processes at play within a scroll pump.

Gas entering the scroll pump is at 2 distinct temperatures - a cold one associated with the suction state of the compressor, and a hot one associated with gas that has flown over the motor within the hermetic shell. It was observed that as expected, wall temperatures increased as one progressed angularly through the compression path. An exception to this that held true in each of the five operating conditions, was the presence of a cold spot associated with the suction port (as shown in figures 3-4 and 3-8). The presence of this spot indicates that there is a strong effect of the suction gas and therefore convection at portions of the scroll close to suction. The three thermocouples measuring gas temperature along the suction pathway indicated that the gas gets hotter as it progresses through the scroll. However, these thermocouples tend to closely mimic the wall temperatures at locations close to them, suggesting that these thermocouples may in fact be measuring wall temperatures as opposed to gas temperature. A comparison of scroll base and wrap temperatures reveals that the wraps are cooler than the base near suction but are hotter close to discharge.

However, the temperature gradients associated with these differences is very small, showing that axial conduction does not play a very significant role within a scroll pump. Most importantly, finite and significant temperature differences are observed across the scroll wraps in all of the operating conditions.

### 3.5.2 Analysis of Data from Experiment

In the section below, we examine the pump heat transfer experimental data corresponding to a pump operating condition of $-10/90$. This is a low mass flow rate (about 150 lb/hr), and high pressure ratio operating condition of the pump. The data from this setting is, however, fairly representative of the other operating conditions under which data was taken.

#### Kissing Heat Transfer Coefficients and Fluxes

Given that the thickness of the scroll wraps is $t_{wrap} = 1/8'' = 3.2 \times 10^{-3} m$, a temperature difference of $1°F$, $(5/9°C)$ across the scroll wraps corresponds to a heat flux of $\frac{K}{t_{wrap}} \cdot 5/9 = 9375\ W/m^2$. In table 3-3, we calculate heat fluxes and heat transfer coefficients corresponding to the actual $\Delta T$s observed across scroll wrap walls. Kissing heat transfer coefficients are calculated by taking the heat flux and dividing it by the temperature difference $(dT)$ between kissing pairs, i.e. pairs of thermocouples that are placed opposite each other across the channels of the fixed scroll. Since the heat flux through a wrap can be considered to be a result of kissing heat transfer to a cooler wrap (i.e.) one at an outer radius to the wrap, or from a hotter wrap (i.e.) one at an inner radius to the wrap, we calculate two kissing heat transfer coefficients corresponding to every $\Delta T$ across the wraps.

$$h_{kiss} = \frac{q''_{wrap}}{dT} \tag{3.21}$$

It was not possible to calculate kissing heat transfer coefficients for the scroll wrap pair corresponding to $TC17$ and $TC18$. This was because the thermocouples at the wrap inner to this wrap ($TC19$ and $TC20$) both did not work, while the temperature

at the wrap outer to this wrap ($TC16$) always measured temperatures greater than those of $TC17$, thus rendering kissing heat transfer between the two wraps unphysical. While this looks puzzling at first glance, we realized that there was nothing unphysical about this situation. $TC16$ and $TC17$ do not in fact constitute a kissing pair. The reason for this is that $TC16$ is situated on the outer suction path of the fixed scroll, whose walls have been machined so as not to provide conjugate sealing between orbiting and fixed scrolls at this location.

To determine if the heat fluxes calculated in table 3-4 are in fact attributable to convection rather than kissing heat transfer, we also calculate the convection coefficients that would be necessary in order to accomplish this. If heat were transferred all the way from the hot wrap to the cold wrap only by means of convection and conduction across scrolls, heat would need to be transferred over a sum total of 4 boundary layers and 1 conduction resistance, corresponding to the thickness of the orbiting scroll. If we neglect the conduction resistance, and neglect radial area changes, we get

$$h_{conv,4} = 4 \cdot h_{kiss} \tag{3.22}$$

On the other hand, if we considered the heat flux across the scroll wrap to have its origin in the orbiting scroll, and then be convected to the fixed scroll, then, the convection coefficient is given as

$$h_{conv,2} = 2 \cdot h_{kiss} \tag{3.23}$$

If the heat is considered to be transferred to or from the gas immediately neighboring the scroll wrap, then there is only one boundary layer in question and

$$h_{conv,1} = h_{kiss} \tag{3.24}$$

In each of these cases, we've assumed that convection coefficients don't change by a whole lot within the scrolls, and that gas temperatures can be assumed to be the weighted average of neighboring wall temperatures. As a basis of comparison, we

also provide the theoretically calculated estimation of the convection coefficient for the $-10/90$ case. As observed in table 3-4, all experimentally evaluated convection coefficients look implausibly high other than the calculation for the temperature difference across $TCs$, 2 and 3. Any heat that is transferred to the outer most wraps by means of kissing heat transfer, has no place to go but the gas, thus forcing convection to take place at this location.

A persistent feature with the data from the experiment is the fact that heat transferred across scroll wraps does not seem to be conserved all the way from discharge to suction. This suggests that perhaps there are internal portions of the scroll where convection between gas and wall occurs. This is possible because as one progresses along the length of the spiral from the suction side to the interior, there is a substantial portion of the scroll that sees suction gas (the first approx. 500° of the spiral), or discharge gas (the last 250° of the spiral) for varying amounts of time during the compression cycle. Suction heat transfer and discharge heat transfer are therefore not as localized as one might imagine. Perhaps, a kissing heat transfer experiment conducted on a scroll pump with a larger number of turns in it might display data that conserved the energy of kissing heat transfer all the way from discharge to suction.

### Contact Angles

Using the kissing heat transfer fluxes experimentally observed, it is possible to estimate the kissing heat transfer contact angles within the scroll. Performing an energy balance on a given section of scroll wrap, we see that total heat flux across the wall ought to be the sum of heat fluxes produced by kissing heat transfer and convection.

$$q''_{wrap} = q''_{conv} + q''_{kiss} = h_{conv} \cdot dT/4 + h_{kiss} \cdot dT \tag{3.25}$$

Here, $h_{kiss} = U_{kiss}\sqrt{\theta}$ where $U_{kiss}$ is the kissing heat transfer coefficient estimated assuming a 1° angle of contact between scrolls, and $\theta$ is the angle of contact between scrolls. The value of convection coefficient, $h_{conv}$ is one that was also calculated

theoretically. The contact angle, $\theta$ can then be calculated as

$$\theta = (\frac{q''_{wrap} - h_{conv}/4 \cdot dT}{U_{kiss} \cdot dT})^2 \tag{3.26}$$

Table 3-4 shows that the contact angles that were inferred from the experiment, are all of the order of about $0.1 - 0.3°$. This are slightly lower than the angles that were estimated based on considerations of Hertzian stresses. One reason why these contact angles might be lower than those estimated by hertzian stress calculations is that contact resistances and/or oil film thicknesses that we neglected in our estimation of contact angles may in fact be large enough to be affecting answers. Another limitation with our data is that the precise location of the thermocouples in the scroll wraps is not known (they were embedded in epoxy). As a result, temperature differences that were measured across scroll wraps might actually correspond to temperature differences across a fraction of the the thickness of the scroll wraps, leading our kissing heat transfer fluxes and coefficients to be underestimated.

Experimental estimation of "realistic" contact angles, along with the experimental verification of significant heat fluxes across the scroll wraps, provide compelling evidence of the existence of kissing heat transfer.

## 3.6 Conclusions

The thermodynamic effects of compression lead to a variation of gas temperature within a scroll pump, with suction gas entering cold, and discharge gas leaving the pump hot. The temperature difference across this gas within the compact confines of a scroll pump serve as a source of internal heat transfer from the discharge side of the pump, to the suction side. Such heat transfer is undesirable because it lowers pump volumetric efficiency and capacity. Lumped heat transfer conductance calculations suggest that while convection plays a major role in transferring heat on the discharge and suction sides of the pump, heat transfer at portions internal to the pump is likely to be in the form of conduction through the bases of the fixed and orbiting scrolls,

and kissing heat transfer. Kissing heat transfer conductances were estimated making assumptions about the contact angle (and contact time) between orbiting and fixed scrolls. Since these assumptions are not easily experimentally verifiable, we decided to conduct an experiment to observe kissing heat transfer in action.

Experiments were conducted on a specially modified and instrumented (Carrier) scroll compressor, which revealed the existence of large heat fluxes (and temperature differences) across the wraps of the fixed scroll. Such heat fluxes are symptomatic of kissing heat transfer and can't feasibly be explained by convection. Kissing heat transfer contact angles estimated from experimental data are roughly of the same order of magnitude as our physically based assumptions. The presence of significant heat fluxes across scroll wraps along with the estimation of realistic kissing heat transfer contact angles together provide compelling evidence of the existence of kissing heat transfer.

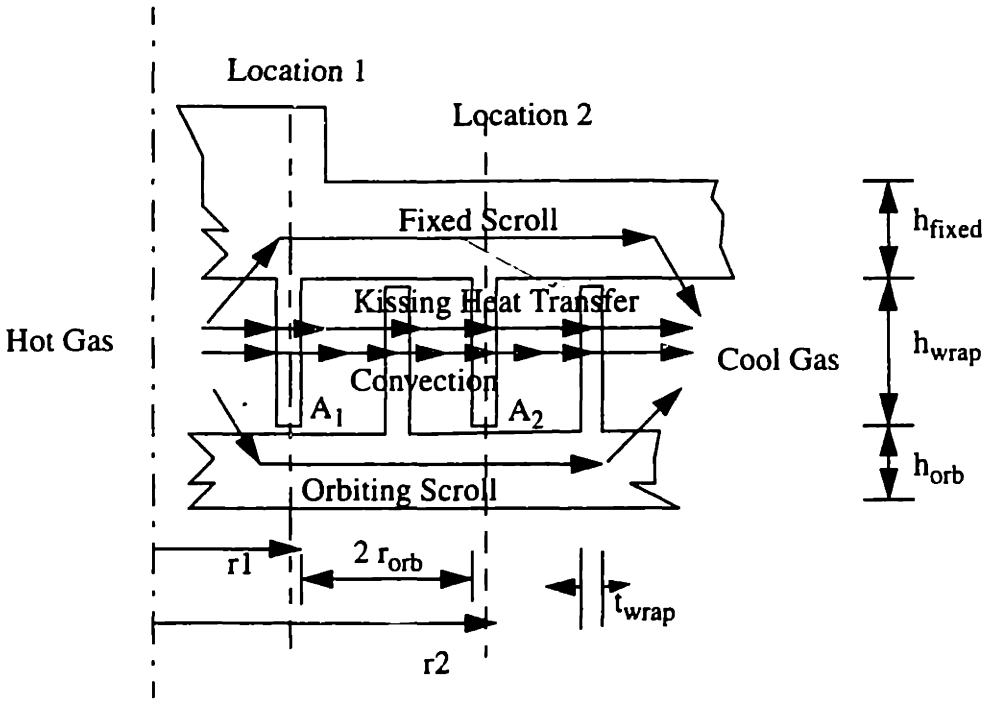


**Figure 3-1: Modes of Heat Transfer Within a Scroll Pump**

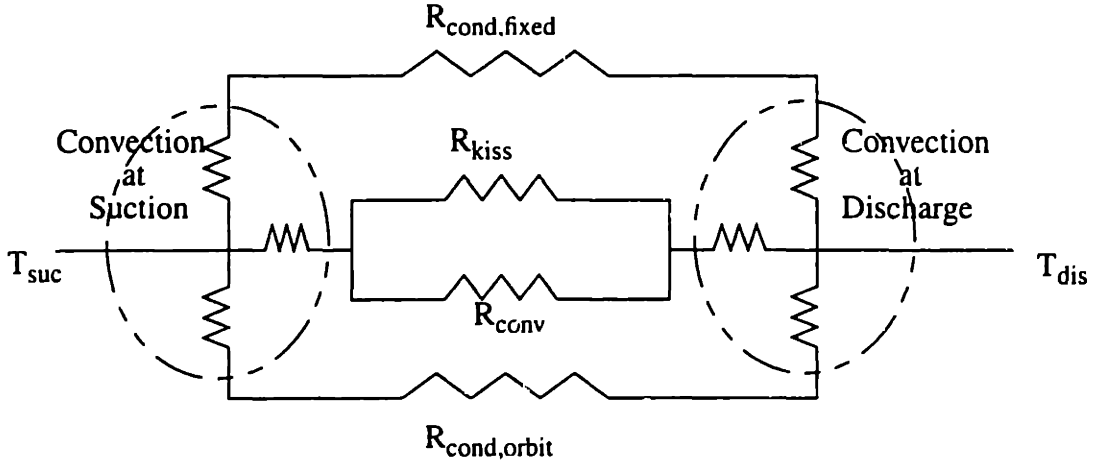


**Figure 3-2: Thermal Resistance Network for Scroll Pump**

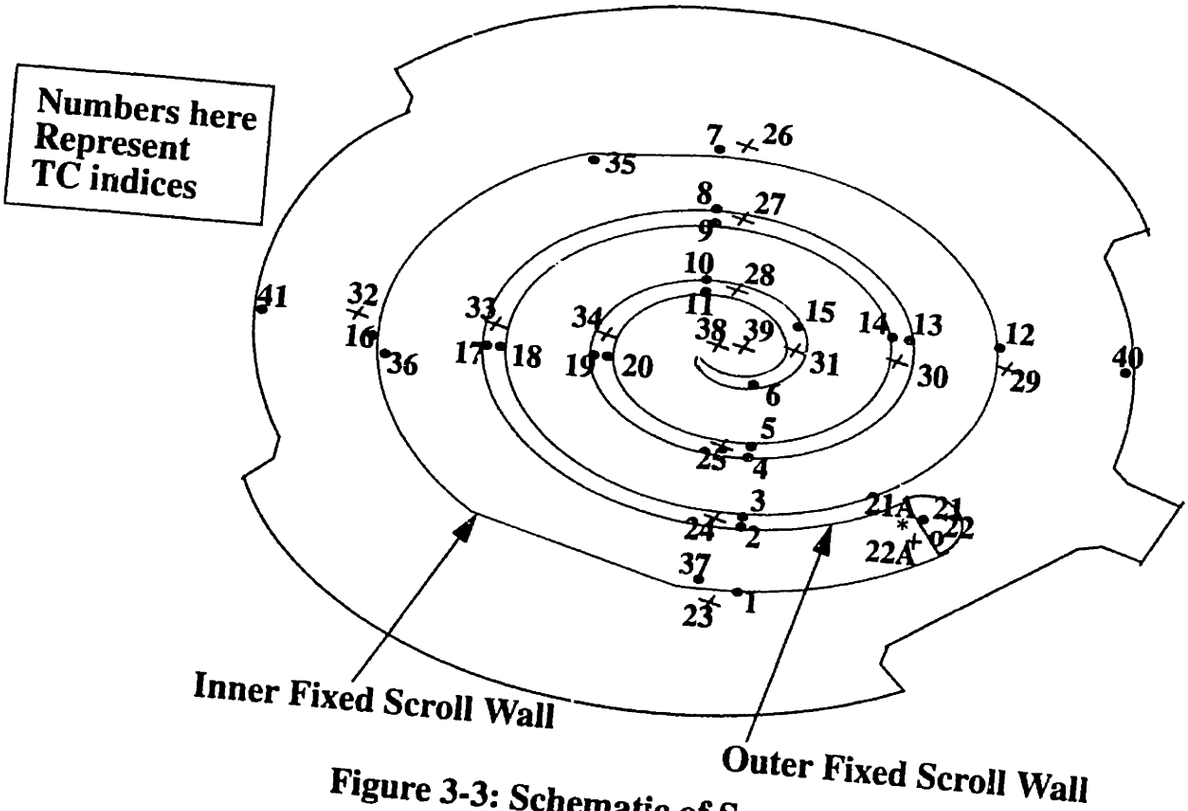


Figure 3-3: Schematic of Sensors on the Fixed Scroll

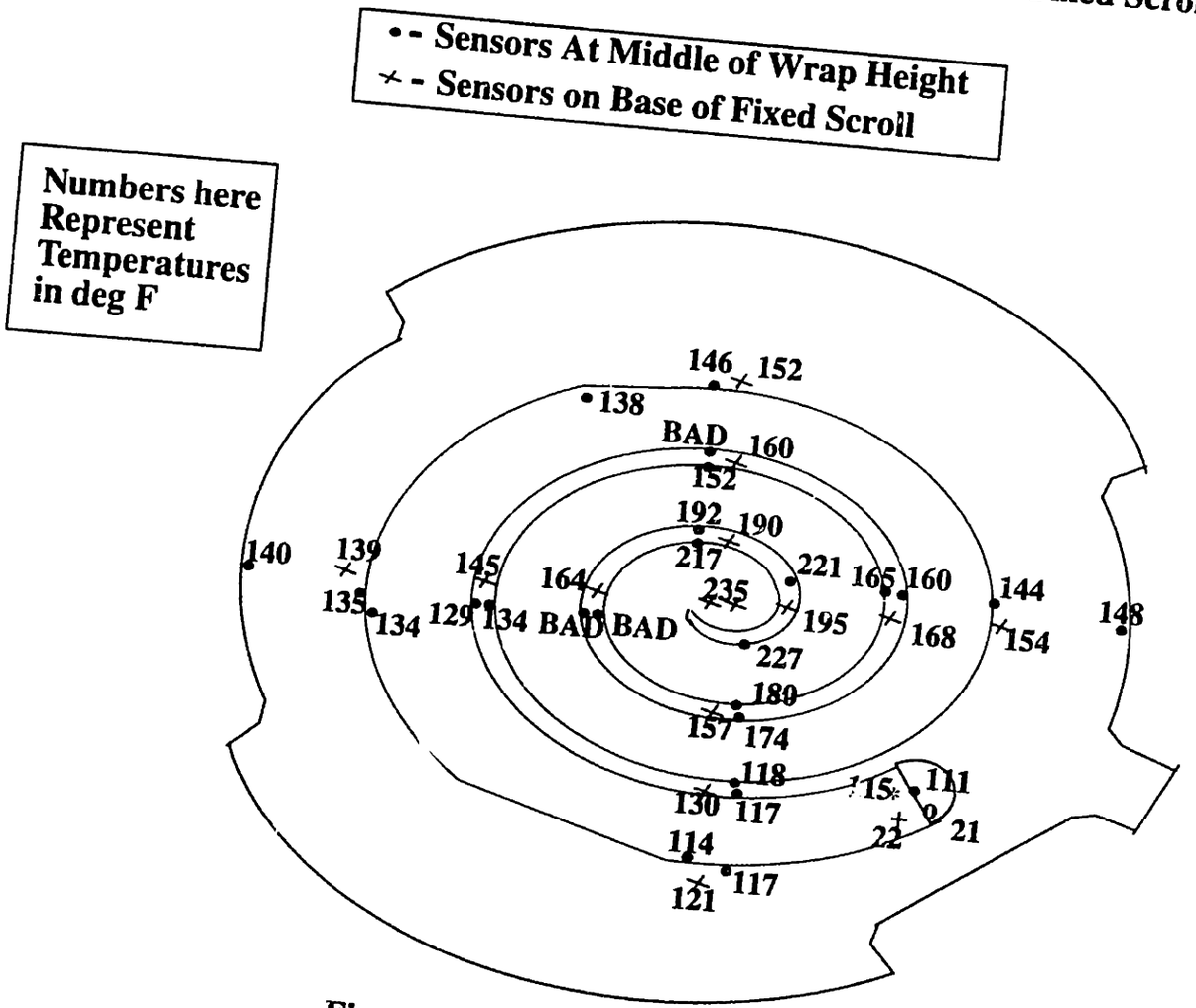


Figure 3-4: Data for the -10/90 Operating Condition

Figure 3-5 - Mechanism of Kissing Heat Transfer

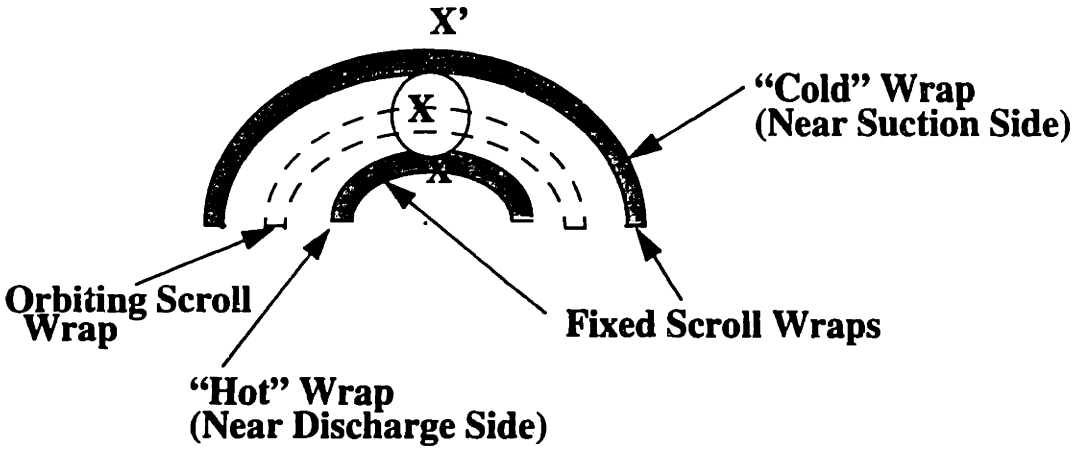


X' and X" are points of Contact for X within the course of one Eccentric Rotation of the Orbiting Scroll

Kissing Heat Transfer Modeled as
Transient Conduction Between Semi-Infinite Bodies

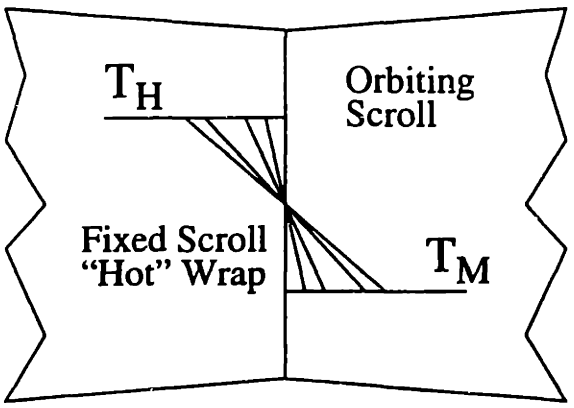


**Orbiting Scroll Kisses Hot Wrap of Fixed Scroll for time *t***

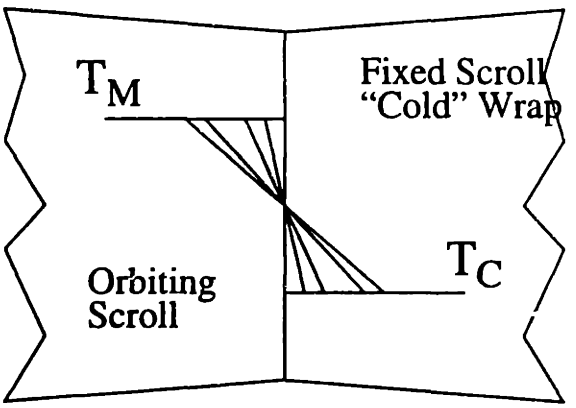


**Then Orbiting Scroll Kisses Cold Wrap of Fixed Scroll for time *t***

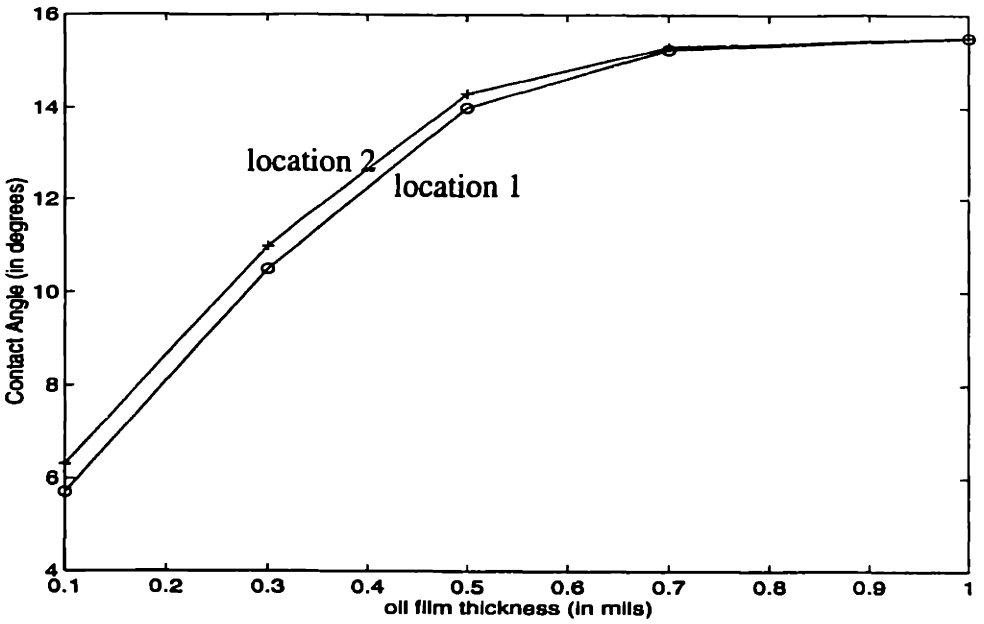


**Figure 3-6 - Effect of Oil Film Thickness on Kissing Heat Transfer Contact Angles**

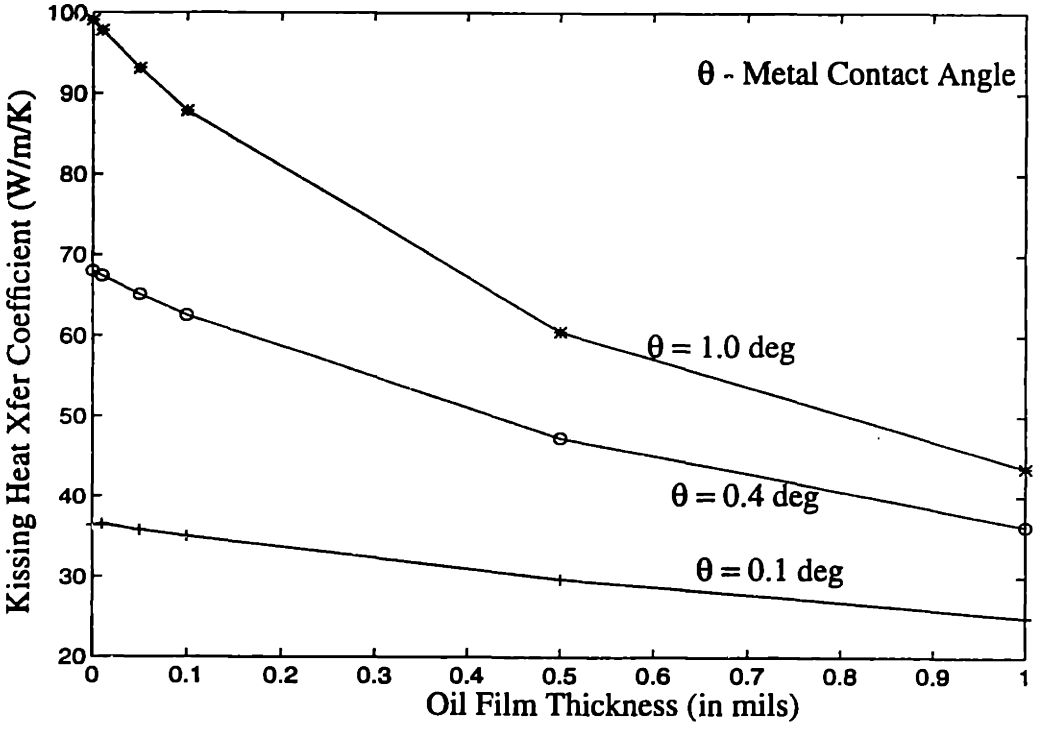


**Figure 3-7 - Kissing Heat Transfer Coefficient as Function of Oil Film Thickness and Metal Contact Angle**

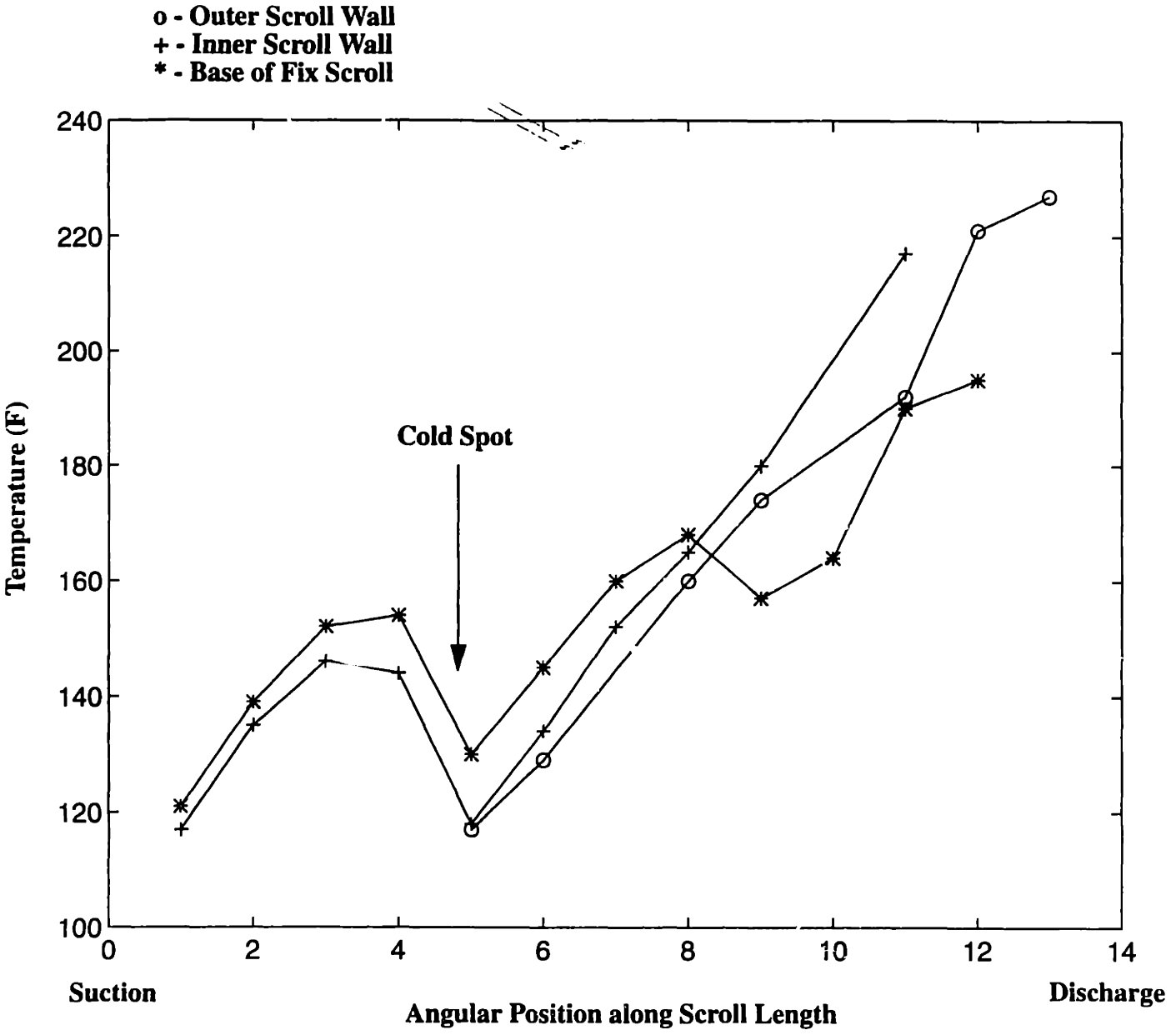


**Figure 3-8: Data From -10/90 Experiment Plotted Vs Angular Position**

| | | | | Contact Angle | |
|---|---|---|---|---|---|
| Location | $D_1$ (mm) | $D_2$(mm) | $K_D$ (mm) | $\theta_1$(deg) | $\theta_2$(deg) |
| 1 | 54 | 46 | 311 | 0.38 | 0.45 |
| 2 | 67 | 60 | 574 | 0.42 | 0.47 |

**Table 3-1: Kissing Heat Transfer Contact Angle Estimations Based on Hertzian Stresses**

| | Oil Film Thickness | | |
|---|---|---|---|
| Location | 0.1 mils | 0.5 mils | 1.0 mils |
| 1 | 6 deg | 14 deg | 15 deg |
| 2 | 6 deg | 13 deg | 15 deg |

**Table 3-2: Oil Wetted Contact Angle Between Scroll Wraps**

$h_{conv}$ (from theory) = 74 Btu/hr/ft$^2$/F

| $\Delta T_{wall}$ (F) | $T_H$ (F) | $T_C$ (F) | $q''_{wrap}$ Btu/hr/ft$^2$ | $h_{kiss}$ Btu/hr/ ft$^2$/F | $h_{conv,4}$ Btu/hr/ ft$^2$/F | $h_{conv,2}$ Btu/hr/ ft$^2$/F | Scroll Pair |
|---|---|---|---|---|---|---|---|
| 1 | 174 | 118 | 2972 | 53 | 212 | 106 | 2,3 |
| 6 | 174 | 118 | 17832 | 318 | 1272 | 636 | 4,5 |
| 6 | 227 | 180 | 17832 | 379 | 1516 | 758 | 4,5 |
| 5 | 160 | 144 | 14860 | 929 | 3716 | 1858 | 13,14 |
| 5 | 165 | 221 | 14860 | 265 | 1060 | 530 | 13,14 |

**Table 3-3: Kissing Heat Transfer Coefficients and Heat Fluxes for -10/90 Operating Conditon**

| Scroll Pair | dT (F) | $q''_{wrap}$ Btu/hr/ft$^2$ | $\theta$ (deg) |
|---|---|---|---|
| 2,3 | 56 | 2972 | 0.002 |
| 4,5 | 56 | 17832 | 0.15 |
| 4,5 | 47 | 17832 | 0.20 |
| 13,14 | 24 | 14860 | 0.54 |
| 13,14 | 56 | 14860 | 0.10 |

**Table 3-4: Contact Angles Estimated From Experiment for -10/90 Operating Condition**

# Chapter 4

# Distributed Parameter Thermodynamic and Heat Transfer Model of a Scroll Pump

## 4.1 Introduction

In this chapter, we describe the derivation of the equations to be used in simulating a distributed parameter model of the thermodynamic and heat transfer processes in a scroll pump. Such a model involves the solution of the thermo-fluid equations of the gas within the scroll pump, and an energy balance on the walls of the pump that interact with the gas. In this chapter, we first outline what we hope to accomplish out of such a model, followed by a derivation of the partial differential equations that describe the fluid processes. The method used to solve the gas equations (a semi-implicit stiff solver) is then described, followed by a description of the models used to describe the processes of the walls of the scroll pump. Finally, we outline the method of iteratively solving gas and wall equations so as to converge to the thermodynamically self-consistent states of a scroll pump. The results of such simulations and their implications to scroll pump modeling are presented in the next chapter of the thesis.

## 4.2 Motivation for Distributed Parameter Modeling

In the prior chapters of this thesis, we described a lumped parameter model of a scroll pump, and proposed a novel mechanism for heat transfer (kissing heat transfer) within a scroll pump. The lumped parameter model developed was intended to be a quick and easy-to-use simulation tool that could predict scroll pump performance under a variety of operating conditions. As a result, the model was set up with as many relevant approximations as possible, and with some sources of irreversibilities left unmodeled. In reality, the sources of irreversibility that were modeled are all distributed in space and time, but are approximated for simplicity as lumped phenomena. The principal advantage of a lumped parameter approach is that relatively good results can be obtained by solving an algebraic system of equations. In this chapter, we develop the equations and the methodology to simulate the distributed and unsteady processes at play within a scroll pump. The idea behind this approach is to simulate various sources of irreversibility individually and to be able to evaluate their relative importance in a scroll pump. The results of such a simulation enable us to check the validity of the various assumptions of the lumped parameter model. Such an exercise will also help identify any major source of irreversibility that has been left unmodeled in the lumped parameter model, or sources of irreversibility that have been erroneously exaggerated in importance in the lumped parameter formulation.

## 4.3 Derivation of Gas Equations

In the sections that follow, we derive the equations that describe the thermo-fluid processes of the gas within a scroll pump. For the purposes of the model described below, the control volumes used for gas thermodynamics and fluid mechanics are pseudo one-dimensional. This approximation of the gas processes is obtained by unwrapping the involute spirals of a scroll pump and assuming centrifugal and coriolis effects to be secondary to the volume change effects in the scroll. The basic building block of the

model is a control volume of varying cross-section (see figure 4-1). This control volume is pseudo one-dimensional because we only consider gradients of gas properties in the scroll unwrap direction, though we model the cross-sectional variations associated with the two-dimensional geometry of the control volumes. Many such control volumes taken together represent a column of gas (not necessarily of fixed mass) as it enters the pump (at suction), forms as a pocket of the scroll pump, undergoes compression, and finally exits the pump at discharge. Thus, we follow control volumes as they form during suction, through the closed compression process in the pump, blowin/blowout, and their eventual disappearance during the discharge process. The walls of the scroll pump exchange heat with the gas in each control volume, while gas in the control volumes leaks from higher pressure sections of the scroll to low pressure sections through clearances between the fixed and orbiting scrolls. In the sections below, we first derive the control volume equations of continuity, linear momentum and energy, with heat transfer and leakage neglected. Preliminary simulations with a stiff solver showed that momentum effects in the scroll pump are negligible. Therefore, the equations of the gas are then simplified to neglect momentum effects, and incorporate wall heat transfer and leakage effects. Even though momentum effects are negligible, we describe the derivation of these equations for completion, and for potential use in other applications where such effects may in fact turn out to be significant. The equations of continuity, momentum and energy along with an equation of thermodynamic state and appropriate boundary conditions for the gas, completely characterize the gas thermodynamics for a scroll pump. In our ensuing description, we refer to a contiguous collection of control volumes as a "pocket", even though it really is not a pocket during the suction and discharge processes.

### 4.3.1 Nomenclature

The terms used in the derivation of control volume equations are briefly defined below.

$\theta$ - angular position of the orbiting scroll

$\beta$ - spiral angle associated with any position on the scrolls

$\xi$ - pocket position index of a control surface within a scroll pocket

$u(\xi, t)$ - absolute speed of a control surface at position $\xi$ as a function of time

$A(\xi, t)$ - Cross-section of the control surface at position $\xi$ as a function of time

$V_{CV}(\xi, t)$ - Volume of the control volume around $\xi$ as a function of time

$\mathcal{V}(\xi, t)$ - Volume of the control volume around $\xi$ per unit $\xi$ as a function of time

$\rho(\xi, t)$ - density of fluid at the control surface at $\xi$ as a function of time

$v(\xi, t)$ - absolute velocity of fluid at the control surface at $\xi$ as a function of time

$\tilde{u}(\xi, t)$ - specific internal (thermodynamic) energy of fluid at the control surface at $\xi$ as a function of time

$e(\xi, t)$ - specific internal energy of fluid at the control surface at $\xi$ as a function of time; this includes kinetic energy as well as thermodynamic energy stored in the fluid.

$P(\xi, t)$ - Pressure of fluid at the control surface at $\xi$ as a function of time

$P_L$ - Quasi-static Pressure of the fluid at pump suction

$P_H$ - Quasi-static Pressure of the fluid at pump discharge

$T(\xi, t)$ - Temperature of fluid at the control surface at $\xi$ as a function of time

$\vec{v}_b$ - velocity of a point on the boundary of the control volume

### 4.3.2 Geometry of Control Surfaces

In modeling control volumes for the scroll we take advantage of the natural geometry of the scroll. Consider a situation when the orbiting scroll is at a rotational position of $\theta$ (recall that the scroll compression process occurs by eccentric rotation of the orbiting scroll within the fixed scroll boundaries). Pockets within the scroll form by contact between conjugate surfaces at spiral angles of $\beta = \theta$ and $\beta = \theta + 360°$. The

relative position of a control surface within a pocket can therefore be indexed by the spiral angle that is associated with it. We use a pocket position index $\xi$ to indicate the position of a control surface within a pocket, as shown in figure 4-2. A position of $\xi = 1.0$ indicates a control surface at the leading edge of the pocket (at a spiral angle of $\beta = \theta$), while a position of $\xi = 0$ would indicate to a control surface at the trailing edge of the pocket, namely at a spiral angle of $\beta = \theta + 360°$. Analogically, a control surface at a spiral angle of $\beta = \theta + 180°$, will be indexed by $\xi = 0.5$.

This method of indexing control surfaces is a natural choice for the closed process, when we have pinchpoints associated with the spiral angles $\beta = \theta$ and $\beta = \theta + 360°$. However, this method can also be modified to index control surfaces during the processes of suction and discharge. During the process of suction, the pocket (which is really only a geometrically contiguous ensemble of control volumes at this stage) has a leading edge (at a spiral angle of $\beta = \theta$) where fixed and orbiting scrolls pinch, but doesn't have a corresponding trailing edge pinchpoint. The relative position of a control surface at this stage can still be indexed by the parameter $\xi$, simply by proceeding as if there were a trailing edge pinchpoint at the spiral angle of $\beta = \theta + 360°$. Similarly, during the process of discharge, the gas "pockets" have a pinchpoint associated with the trailing edge at a spiral angle of $\beta = \theta + 360°$, but no leading edge pinchpoint. In this case also, control surfaces can be indexed assuming the existence of a pinchpoint at the spiral angle of $\beta = \theta$, and using the same methodology as with pockets during the closed process. The principal difference then between the suction and discharge processes on the one hand and the closed process on the other is the fact that we have control surfaces for the full range of $\xi = 0 \cdots 1$ for the latter, but only an incomplete set for the former.

The pocket index parameter $\xi$, however only indexes the relative position of a control surface inside a pocket within the scroll pump. In order to compute its absolute position, as well as geometric attributes such as cross-section area, velocity of motion and volume, we have to resort to the kinematics of the pump. Since velocities of the surfaces, areas of cross-section of the control surfaces, and volumes of the control volumes change with time, we refer to them as $A(\xi, t)$, $u(\xi, t)$ and

$V_{CV}(\xi, t)$ respectively. Methods of determining $A$, $u$ and $V_{CV}$ will be described in the next subsection.

### 4.3.3 Differential Formulation

#### Geometry of Differential Control Volume

We consider the differential control volume enclosed by control surfaces at positions, $\xi$, and $\xi + \Delta\xi$. At any given instant of time $t$, the absolute positions of the vertices of the control volume ABCD (as shown in figure 4-3) are given by $\vec{r}_A = \vec{r}_o(\xi, t)$, $\vec{r}_B = \vec{r}_i(\xi, t)$, $\vec{r}_C = \vec{r}_o(\xi + \Delta\xi, t)$ and $\vec{r}_D = \vec{r}_i(\xi + \Delta\xi, t)$. Here, the subscripts $o$ and $i$ for the position vectors refer to the fact that every control volume has associated with it an "outer" wall, and an "inner" wall. Using a Taylor series approximation, and neglecting higher order terms in $\Delta\xi$, we can rewrite $\vec{r}_C$ and $\vec{r}_D$ as follows:

$$\vec{r}_C = \vec{r}_o(\xi, t) + \frac{\partial \vec{r}_o}{\partial \xi}\Delta\xi \tag{4.1}$$

$$\vec{r}_D = \vec{r}_i(\xi, t) + \frac{\partial \vec{r}_i}{\partial \xi}\Delta\xi \tag{4.2}$$

To compute the area (or volume per unit height) of this control volume, we approximate the control volume with the quadrilateral $ABCD$, whose area we then compute vectorially. The area of the quadrilateral is simply the sum of the area of the two triangles, $ABD$, and $BDC$.

$$V_{CV} = Ar(ABCD) = Ar(ABD) + Ar(BDC) \tag{4.3}$$

Representing this vectorially,

$$V_{CV} = \frac{1}{2}|\vec{r}_{BA} \times \vec{r}_{AD}| + \frac{1}{2}|\vec{r}_{DC} \times \vec{r}_{CB}| \tag{4.4}$$

Neglecting higher order terms in $\Delta\xi$, this can be rewritten as

$$V_{CV} = |\frac{1}{2}(\frac{\partial \vec{r_o}}{\partial \xi} + \frac{\partial \vec{r_i}}{\partial \xi}) \times (\vec{r_o} - \vec{r_i})|\Delta\xi \tag{4.5}$$

The Volume of the control volume per unit height per unit $\xi$ is then given by $\mathcal{V}$, where

$$V_{CV} = \mathcal{V}\Delta\xi \tag{4.6}$$

and

$$\mathcal{V} = |\frac{1}{2}(\frac{\partial \vec{r_o}}{\partial \xi} + \frac{\partial \vec{r_i}}{\partial \xi}) \times (\vec{r_o} - \vec{r_i})| \tag{4.7}$$

The cross-section of a control surface per unit height at position $\xi$ is simply given as

$$A(\xi, t) = |\vec{r_o}(\xi, t) - \vec{r_i}(\xi, t)| \tag{4.8}$$

while the speed of motion of the control surface is given as

$$u(\xi, t) = \frac{1}{2}|\frac{\partial[\vec{r_o}(\xi, t) + \vec{r_i}(\xi, t)]}{\partial t}| \tag{4.9}$$

### Continuity

Mass in the control volume changes over time due to mass fluxes into/out of the control volume. Temporarily, we neglect any mass flux in to the control volume due to leakage. Gas enters the control volume through the control surface at position $\xi$, and leaves through the control surface at position $\xi + \Delta\xi$ (see figure 4-1). A mass balance on the control volume yields the following equation of continuity.

$$\frac{\partial}{\partial t}(\rho V_{CV}) + (\rho + \frac{\partial \rho}{\partial \xi}\Delta\xi)(v + \frac{\partial v}{\partial \xi}\Delta\xi - u - \frac{\partial u}{\partial \xi}\Delta\xi)(A + \frac{\partial A}{\partial \xi}\Delta\xi) - (\rho(v-u)A) = 0 \tag{4.10}$$

Simplifying and dropping higher order terms in $\Delta\xi$, this equation becomes

$$\frac{\partial}{\partial t}(\rho\mathcal{V}) + \frac{\partial}{\partial \xi}(\rho(v-u)A) = 0 \tag{4.11}$$

### Linear Momentum

The linear momentum of fluid in the control volume changes over time because of momentum fluxes into/out of the control volume, and because of the application of other forces. The only source of external force considered here is the force exerted on the control surfaces by fluid pressure (see figures 4-1 and 4-4). Viscous forces are neglected, as are momentum fluxes due to leakage. An x-direction (scroll unwrap direction) momentum balance on the control volume yields the following equation.

$$\begin{aligned}\Sigma F &= (\rho+\frac{\partial\rho}{\partial\xi}\Delta\xi)(v+\frac{\partial v}{\partial\xi}\Delta\xi-u-\frac{\partial u}{\partial\xi}\Delta\xi)(v+\frac{\partial v}{\partial\xi}\Delta\xi)(A+\frac{\partial A}{\partial\xi}\Delta\xi)\\ &\quad -\rho v(v-u)A+\frac{\partial}{\partial t}(\rho v V_{CV})\end{aligned} \tag{4.12}$$

The term $\Sigma F$, which is fully attributable to pressure forces can be expanded as below.

$$\Sigma F = P\cdot A-(P+\frac{\partial P}{\partial\xi}\Delta\xi)(A+\frac{\partial A}{\partial\xi}\Delta\xi)+(P+\frac{\partial P}{\partial\xi}\frac{\Delta\xi}{2})(\frac{\partial A}{\partial\xi}\Delta\xi) \tag{4.13}$$

Writing the Taylor series for P and A in $\xi$, and neglecting higher order terms in $\Delta\xi$, the equation for $\Sigma F$ simplifies as follows.

$$\Sigma F=-\frac{\partial P}{\partial\xi}A\Delta\xi \tag{4.14}$$

The momentum balance equation can now be rewritten, using the Taylor series of $\rho$, $v$, $u$ and $A$ in $\xi$, and neglecting higher order terms in $\Delta\xi$.

$$-\frac{\partial P}{\partial\xi}A=\frac{\partial}{\partial t}(\rho v\mathcal{V})+\frac{\partial}{\partial\xi}(\rho v(v-u)A) \tag{4.15}$$

### Energy

The internal energy of fluid in the control volume changes due to energy fluxes into/out of the control volume, due to heat transfer with the surroundings, and due to work interactions of the control volume with the surroundings. If we neglect heat transfer and frictional work, the only work interaction experienced by the control

volume is the indicated work caused by volume change of the control volume in a pressure field. An energy balance on the control volume then yields the following equation, where the energy terms due to gravitation have been neglected. Note that kinetic energy terms have however been incorporated as $e = \tilde{u} + \frac{1}{2}v^2$

$$[(\rho + \frac{\partial \rho}{\partial \xi}\Delta\xi)(e + \frac{\partial e}{\partial \xi}\Delta\xi) + P + \frac{\partial P}{\partial \xi}\Delta\xi](A + \frac{\partial A}{\partial \xi}\Delta\xi)(v + \frac{\partial v}{\partial \xi}\Delta\xi - u - \frac{\partial u}{\partial \xi}\Delta\xi)$$
$$-[\rho e + P]A(v - u) + \dot{W}_p + \frac{\partial}{\partial t}(\rho e V_{CV}) = 0$$

The indicated work, $\dot{W}_P$ due to deformation of the control volume can be further expanded. The integral below has to consider the motion of the boundaries in all directions, not just in the scroll unwrap direction.

$$\dot{W}_P = \int P\vec{v}_b \cdot \hat{n} dA \tag{4.16}$$

This is the term that will reduce to $P\frac{\partial(V_{CV})}{\partial t}$ in a uniform pressure field. This is because the term $\int \vec{v}_b \cdot \hat{n} dA$ is simply the rate of change of Volume of the control volume, namely $\frac{\partial(V_{CV})}{\partial t}$. The work integral in the presence of a non-uniform pressure field (neglecting higher order terms in $\xi$) therefore can be reduced to the following form:

$$\dot{W}_P = P\frac{\partial(V_{CV})}{\partial t} + \frac{\partial P}{\partial \xi} uA\Delta\xi \tag{4.17}$$

Once again, neglecting higher order terms in $\Delta\xi$, the energy equation can be rewritten as:

$$\frac{\partial}{\partial t}(\rho e \mathcal{V}) + \frac{\partial}{\partial \xi}[(\rho e + P)(v - u)A] + P\frac{\partial \mathcal{V}}{\partial t} + \frac{\partial P}{\partial \xi} uA = 0 \tag{4.18}$$

### 4.3.4 Thermodynamic State Equation

At any instant of time, the fluid properties in the control volume follow an equation of state for the refrigerant gas. This equation couples the continuity, momentum and energy equations.

$$(P, T) = f(\tilde{u}, \rho) \tag{4.19}$$

### 4.3.5 Boundary Conditions

#### Pinchpoints

Control Volumes that end at pinchpoints need to be treated differently from control volumes that have flow on both control surfaces. At these control volumes, we impose the boundary condition that $v(\xi, t) = u(\xi, t)$ for the control surface corresponding to the pinch. Additionally, we neglect spatial pressure variation for the pinched control volumes so that $\frac{\partial P}{\partial \xi} = 0$ for these control volumes. Care should also be taken in evaluating the volume per unit $\xi$, $\mathcal{V}$ for these control volumes. This is because the methodology of spatial discretization may affect the answer. Recall that we defined $\mathcal{V}$ as

$$\mathcal{V} = |\frac{1}{2}(\frac{\partial \vec{r_o}}{\partial \xi} + \frac{\partial \vec{r_i}}{\partial \xi}) \times (\vec{r_o} - \vec{r_i})| \tag{4.20}$$

At a pinchpoint, $\vec{r_o} - \vec{r_i} = 0$. So if the discretization scheme is centered around the pinchpoint, the volume $\mathcal{V}$ will be spuriously evaluated to be zero. An additional point to note is that for increased accuracy of volume computation, it might be worthwhile to abandon the formula listed above and actually compute the vectorial area of the quadrilaterals / triangles corresponding to every control volume, not just the ones with pinchpoints. The process of evaluating quadrilateral areas is one that naturally fits with the process of spatial discretization that is to be used in numerically solving the PDEs.

#### Suction and Discharge

Trailing edge control volumes that have just been formed during the suction process, and leading edge control volumes that are just about to be destroyed during discharge are exposed to the conditions of the suction and discharge tubes respectively. In imposing suction and discharge boundary conditions on the problem, we make the quasi-static assumption in suction and discharge tubes, (ie) that the total pressures in these tubes remains constant throughout the suction and discharge processes. The boundary conditions imposed on suction and discharge respectively are as listed below.

For the trailing edge control volume at any time $t$ during suction,

$$P + \frac{1}{2}\rho v^2 = P_L \tag{4.21}$$

For the leading edge control volume at any time $t$ during discharge,

$$P + \frac{1}{2}\rho v^2 = P_H \tag{4.22}$$

### 4.3.6 Computation of the System of Equations

The system of four equations (equations 11, 15, 19 and 20) listed above in conjunction with appropriate boundary and initial conditions completely determine the thermodynamics and fluid mechanics for the refrigerant gas in a scroll pump. A natural choice of state variables for the numerical solution of the above equations are the mass per unit $\xi$, $\rho\mathcal{V}$, the linear momentum per unit $\xi$, $\rho v\mathcal{V}$, and the internal energy per unit $\xi$, $\rho e\mathcal{V}$. Geometric parameters of the problem such as the instantaneous cross-sectional area $A(\xi, t)$ of a control surface, and the control surface velocities $u(\xi, t)$ are inputs to the problem that are characterized by scroll geometry.

The above system of equations is a stiff system with eigen values of different orders of magnitude (pressure waves tend to move much faster than continuity and energy differences). As a result, explicit numerical methods were all found to be unstable for anything but the smallest time-steps. In order to render computation more stable, and to avoid the usage of minute time-steps, we implemented a semi-implicit (stiff) solver that was used in conjunction with a refrigerant properties routine to directly solve for the primitive variables of the problem, namely the density, $\rho(\xi, t)$, absolute fluid velocity $v(\xi, t)$, and the specific internal energy $\tilde{u}(\xi, t)$. The results of the simulation showed that momentum effects were negligible in the pocket. This manifested itself in the form of essentially uniform pressures in all the control volumes of a pocket for all the three stages of compression, namely suction, closed process and discharge. The use of momentum effects, however also created numerical problems in the form of spurious temperature effects that it created in the control volumes near pinch points.

Such locations of the pocket represent points where the one dimensionality approximation is most deficient. Spuriously high (or low) values of gas temperature therefore get predicted at such points by the minute pressure differences perpetuated at such locations by the momentum equation (recall that at a pinch point control volume, fluid enters at one side but does not leave at the other). Since gas temperatures represent a part of the information we are trying to secure through a distributed parameter model, we decided to abandon the small momentum effects in our simulation. The alternative would have been to two dimensionalize the equations of control volumes corresponding to pinch points. Since the momentum effects were so small to begin with, we determined that it was not worth the effort to try to continue to predict spatial variations in pressure within a control volume.

### 4.3.7 Gas Process Equations After Neglecting Momentum Effects

In order to rewrite the gas process equations after neglecting momentum effects, all that we have to do is impose uniform pressure in the control volumes, get rid of the momentum equation (since it now conveys no new information), and neglect the influence kinetic energy has on the internal energy of the gas. The gas equations then reduce to the forms presented below. Note here that the single equation equating pressure in all of the control volumes takes the place of the momentum equation. The role of fluid flow across control surfaces is then simply to jointly fulfill continuity and energy equations while also maintaining pressure equilibria.

$$\frac{\partial}{\partial t}(\rho\mathcal{V}) + \frac{\partial}{\partial \xi}(\rho(v-u)A) = 0; \tag{4.23}$$

$$\frac{\partial}{\partial t}(\rho\mathcal{V}\tilde{u}) + \frac{\partial}{\partial \xi}(\rho h(v-u)A) + P\frac{\partial \mathcal{V}}{\partial t} = 0; \tag{4.24}$$

$$P(t) = P(\rho(\xi,t), \tilde{u}(\xi,t)) \tag{4.25}$$

The boundary conditions at suction and discharge also get correspondingly mod-

ified with kinetic energy effects now being neglected on the gas.

$$P(t) = P_L \tag{4.26}$$

$$P(t) = P_H \tag{4.27}$$

For the closed process, the pressure in the pocket is uniform but changes with time, and is determined by the solution of the energy, continuity and state equations.

### Incorporation of Leakage and Heat Transfer

The equations are further modified to incorporate leakage and heat transfer effects. Mass leaking into and out of control volumes affects the mass balance on a control volume, while the enthalpy that such leakage conveys also affects energy balance. Heat transfer with walls, however has a direct effect only on energy balance of a control volume.

$$\frac{\partial}{\partial t}(\rho\mathcal{V}) + \frac{\partial}{\partial \xi}(\rho(v-u)A) + \dot{m}_{leak,in} - \dot{m}_{leak,out} = 0; \tag{4.28}$$

$$\frac{\partial}{\partial t}(\rho\mathcal{V}\tilde{u}) + \frac{\partial}{\partial \xi}(\rho h(v-u)A) + P\frac{\partial \mathcal{V}}{\partial t} + \dot{m}_{leak,in}h_{lak,in} - \dot{m}_{leak,out}h_{leak,out} + \dot{Q}_{in} = 0; \tag{4.29}$$

Here, in order that the equations remain dimensionally consistent $\dot{m}_{leak,in}$, and $\dot{m}_{leak,out}$ are the instantaneous and local mass flow rates of leakage calculated on a per unit $\xi$ basis. Similarly, $\dot{Q}_{in}$ is the local instantaneous heat transferred to the gas calculated on a per unit $\xi$ basis.

## 4.3.8 Leakage Models

Internal leakage in the scroll pump is modeled as being caused by pressure differences across clearance gaps between fixed and orbiting scrolls. Such clearances occur throughout the length of the scroll wraps in the form of tip clearances i.e. clearances between the tip of the wraps of one scroll, and the base of the other scroll. Clearances

are also likely to manifest at the pinchpoints of the pump between wraps of the fixed and orbiting scrolls (see figures 4-5(a) and 4-5(b)). Instantaneous mass flow rates of leakage for every control volume are calculated by equations for compressible flow across an orifice. The pressure differences across the orifice are an output of the entire pump model simulation, but for the purposes of calculation are simply taken as the outputs from the previous iteration of the pump model. The mass flow rate of leakage across an orifice of area $A_{gap}$ from a pressure of $P_{high}$ to a region of pressure, $P_{low}$ is given by the following equation.

$$\dot{m} = KYA_{gap}\sqrt{\rho g_c(P_{high} - P_{low})} \tag{4.30}$$

Here, $K$ and $Y$ are curve-fit parameters that allow this equation to be used for compressible flow, while $g_c$ is the acceleration due to gravity. Typically, the product $KY$ takes a value of about 0.5 for the flow conditions in a scroll pump. In our leakage relation, we implicitly assume that the pressure difference across wraps is not too large i.e. $(P_{high} < 2P_{low})$ so that we don't have a situation of choked flow.

The clearance area, $A_{gap}$ for tip clearance on one side of a control volume can be calculated as $A_{gap} = h_{tip}l_{CV}$ where $l_{CV}(\xi, t)$ is the length of the side surface of the control volume, while $h_{tip}$ is the clearance gap between tip of one scroll wrap and the base of the other scroll. Similarly, $A_{gap}$ for clearance gaps at the pinchpoints can be calculated as $A_{gap} = h_{wrap}h_{flank}$ where $h_{wrap}$ is the height of the scroll wraps, and $h_{flank}$ is the clearance between wraps at a pinchpoint.

In order to substitute leakage mass flow rates back into the continuity and energy equations, the mass flow rates calculated using the orifice flow equations have to be converted to a per unit $\xi$ basis by dividing the mass flow rates by the appropriate $\Delta\xi$ for the control volume. The enthalpy of the leakage mass flow is simply that associated with the source of leakage i.e. the high pressure side of the orifice.

### 4.3.9 Heat Transfer

The gas in each control volume is in thermal contact with the walls of the fixed and orbiting scrolls that border the control volume. Since the thermal time-constants associated with the metal are considerably longer than the time-period of the scroll pump, it is safe to assume that the metal of the pump has a local temperature that is invariant with time as long as the operating condition on the scroll pump does not change. Since the metal is exposed to gas temperatures that range from the cold suction state to the relatively hot discharge state, the metal is likely to have a temperature distribution that is dependent on its interaction with the gas. In one of the following sections of this chapter, we describe a modeling procedure to estimate this temperature distribution. For the moment, however, we assume that the steady state temperature distribution of the metal is known. Here, we describe the instantaneous heat transfer processes that occur between gas and the walls of a control volume, for use in the energy equation (see figure 4-6). The gas at an instantaneous temperature of $T(\xi, t)$ is flanked by a section of the orbiting scroll wrap, at a steady temperature of $T_{ow}(\beta)$, a section of the fixed scroll wrap at a temperature of $T_{fw}(\beta)$, a section of the orbiting scroll base, which is at a temperature of $T_{ob}(\beta)$, and a section of the fixed scroll base, which is at a temperature of $T_{fb}(\beta)$. Here $\beta$ is the spiral angle corresponding to the wall sections of the control volume. The areas of the wall section exposed to the gas are $A_{ow}(\beta)$, $A_{fw}(\beta)$, $A_{ob}(\beta)$, and $A_{fb}(\beta)$ respectively. While the wall temperatures are steady, the temperatures of gas in a control volume vary with time, as do the areas of heat transfer. This happens because of the fact that control volumes themselves move within the pump, and are exposed to different sections of the wall at different times. To account for this fact, we also index wall temperatures and heat transfer areas as being functions of the pocket position index, $\xi$, and time, $t$. The heat transferred to the gas at any instant of time, calculated on a per unit $\xi$ basis is then given by the following equation.

$$\begin{aligned}\dot{Q}_{wall} &= \frac{1}{\Delta\xi} \cdot [hA_{ow}(\xi,t) \cdot (T_{ow}(\xi,t) - T(\xi,t)) + hA_{fw}(\xi,t) \cdot (T_{fw}(\xi,t) - T(\xi,t)) \\ &\quad + hA_{ob}(\xi,t) \cdot (T_{ob}(\xi,t) - T(\xi,t)) + hA_{fb}(\xi,t) \cdot (T_{fb}(\xi,t) - T(\xi,t))]\end{aligned}$$

The convection coefficient, $h$ here is assumed to be uniform at every position within the pump. This equation will, however remain unchanged even if the convection coefficient were in fact assumed to vary with position and time in the scroll pump.

## 4.4 Stiff Solver Algorithm

In this section, we describe the algorithm used to solve the fluid equations derived in the previous section. The technique used here is an adaptation of the semi-implicit method since such techniques are good at dealing with systems of stiff equations, and at providing unconditional stability even with the use of relatively large time-steps. Specifically, the method outlined here is closest to the one described in [12].

### 4.4.1 Spatial Discretization

Stiff solvers deal with systems of ordinary differential equations. Hence, the first task to render the fluid equations in a form suited to stiff computation is the method of spatial discretization, since this will determine the exact form of the ordinary differential equations (in time) that can then be solved using a semi-implicit solver. We discretize the spatial terms in the partial differential equations while keeping the method of derivation of these equations in mind. We therefore, choose to solve for the instantaneous density, $\rho(\xi,t)$, and the temperature, $T(\xi,t)$, by averaging these properties for an entire control volume, while we compute velocities, $v(\xi,t)$ of the fluid at the control surfaces (see figure 4-7). The continuity and momentum equations can then be rewritten as shown below.

$$\begin{aligned}\frac{\partial(\rho\mathcal{V})}{\partial t} &= \rho_{CS,1}(v_1(\xi,t)-u_1(\xi,t))A_1(\xi,t)-\rho_{CS,2}(v_2(\xi,t)-u_2(\xi,t))A_2(\xi,t)\\ &\quad +\dot{m}_{leak,in}-\dot{m}_{leak,out} \qquad (4.31)\\ \frac{\partial(\rho\tilde{u}\mathcal{V})}{\partial t} &= \rho_{CS,1}h_{CS,1}(v_1(\xi,t)-u_1(\xi,t))A_1(\xi,t)\\ &\quad -\rho_{CS,2}h_{CS,2}(v_2(\xi,t)-u_2(\xi,t))A_2(\xi,t)\\ &\quad +\dot{m}_{leak,in}h_{leak,in}-\dot{m}_{leak,out}h_{leak,out}-P\frac{\partial calV}{\partial t}+\dot{Q}_{wall,in} \qquad (4.32)\end{aligned}$$

In determining the fluxes of mass and energy into the control volume, we keep the real physics of the problem in mind. Thus, any fluid that passes through a control surface has the fluid property of the gas upstream of it. Thus, the density, $\rho_{CS}(\xi, t)$ and the specific enthalpy, $h_{CS}(\xi, t)$ of fluid in the flux terms is determined by the fluid upstream of the gas at the control surface. This feature becomes important especially in situations when the direction of flux is opposite in direction from that indicated in the figures i.e. when $(v(\xi, t) < u(\xi, t))$. Simulations done without heeding this feature tended to give unintuitive results at best, while becoming unstable at other instances.

Since each of these ordinary differential equations is the result of discretization of the PDEs for each of the control volumes, we have twice as many equations as control volumes. This, represents a well-posed system of equations for suction, the closed process and discharge simulations as we will now demonstrate.

### Suction

We model suction as a process when control volumes get formed at the mouth of the scroll pump (near the suction tube), and move and deform as they move along into the scroll pump. The process of suction ends with the orbiting scroll and the fixed scroll wraps becoming conjugate near the mouth of the scroll pump, thus having created a pocket of gas that is sealed off from suction (see figure 4-8). In our model, we assume that one control volume gets created at every time-step of computation. Therefore, we divide the suction process into as many time-steps as the number of control volumes we have in spatial discretization. At the end of the $i$th timestep, we have $i$ control volumes, the last one of which has just been created from zero volume, while the other $i - 1$ control volumes have undergone deformation and have moved further into the scroll. Since the suction process is open to the suction tube, and we have assumed uniform spatial pressure within a pocket, the pressure in all of the control volumes remains constant at the suction pressure, $P_L$ throughout the process of suction. The unknowns to be solved during the suction process are therefore, only the velocity of fluid at each control surface and the temperature of fluid at the center

of each control volume. Since the pressure is known, knowledge of the temperature alone will completely specify the state of gas in each control volume of the suction process. As mentioned earlier, our method of discretization solves for the velocity of the fluid at each control surface, while it solves for the gas properties at the center of each control volume. At the $i$th time-step, there are $i$ control volumes, which means there are $i+1$ control surfaces, and $i$ centers of the control volumes. Of the $i+1$ control surfaces, however, one of them corresponds to the pinchpoint through which fluid is not allowed to flow. Therefore, we only have to solve for fluid velocities at $i$ control surfaces, and gas properties at the center of $i$ control volumes. Thus, we have a system of $2i$ equations that have to be simultaneously solved for $2i$ variables. This represents a well-posed system.

### Closed Process

At the end of the suction process, we have the ensemble of control volumes undergoing a closed process, (i.e) with no mass entering or leaving the pocket, except by leakage. The number of control volumes for the entire duration of the closed process is constant and is equal to the number of control volumes corresponding to the last step of suction. Figure 4-9 shows the closed process as it progresses from start to finish. For the closed process, as with suction, we solve for gas properties at the centers of control volumes, while we solve for fluid velocities at the control surfaces. Given an ensemble of $n$ control volumes, we have $n+1$ control surfaces. However, two of these control surfaces correspond to pinch points, as a result of which we only have to solve for the velocities at $n-1$ control surface. As before, we have to solve for gas temperature at $n$ centers of control volumes. The closed process, however differs crucially from the suction and discharge processes, in that pocket pressure at intermediate time-steps in the closed process are unknown and have to be solved for. The pocket pressure thus represents another variable to solved for during closed process calculations. Thus, we use the $2n$ equations of continuity and energy (with the state equation constraint), to solve for $n-1$ fluid velocities, $n$ gas temperatures and 1 gas pressure at each time-step, which represents a total of $2n$ unknowns. Thus, the closed process model

also represents a well-posed system.

### Discharge

We model the discharge process as the reverse of the suction process, with one control volume being destroyed (going to zero volume) with every time-step as it reaches the discharge tube of the pump. As with suction, the pressure of gas in the pockets is known and is simply held to be constant at the discharge pressure $P_H$. As with suction, the number of control volumes changes with time, except for the fact that in discharge, the number of control volumes decreases with time instead of increasing as with suction (see figure 4-10). At any given time-step, where there are $i$ control volumes, we solve the fluid equations to solve for $i$ velocities (there is no need to solve for the velocity of fluid at the trailing edge pinchpoint), and for $i$ gas temperatures, using the $2i$ equations of continuity and energy for the control volumes. The crucial difference between suction and discharge lies in the processes of blow-in / blow-out that occur at the first time-step of discharge. In the 0th time-step of discharge, the pocket has a pressure, $P_2$ corresponding to the last time-step of the closed process. Since this pressure is in general, not equal to the discharge pressure, the first time-step of discharge involves a high velocity blow-in or blow-out of gas into or out of the pocket to equalize pressures with the discharge tube. In a system where momentum effects are not neglected, the blow-in / blow-out process will lead to the creation of pressure waves that propagate back and forth throughout the process of discharge. Since, we neglect momentum effects, we don't capture this (real) phenomenon.

## 4.4.2 Stiff Solver

In this section, we outline the semi-implicit stiff solver algorithm that we use to solve the fluid equations. For the purposes of illustration, we represent the system of fluid ordinary differential equations (ODEs) in the following form.

$$\frac{\partial \vec{y}(t)}{\partial t} = \vec{f}(\vec{x}(t), \vec{\Gamma}(t)) \tag{4.33}$$

where

$$\vec{y}(t) = (\rho_1(t)\mathcal{V}_1(t), \rho_1(t\tilde{u}_1(t)\mathcal{V}_1(t), \rho_2(t)\mathcal{V}_2(t), \rho_2(t)\tilde{u}_2(t)\mathcal{V}_2(t), ...)^T \tag{4.34}$$

while

$$\vec{x}(t) = (v_1, T_1, v_2, T_2, ...)^T \tag{4.35}$$

The vector $\vec{\Gamma}(t)$ is simply the vector of geometric parameters of the pocket at time, $t$. We use a trapezoidal method to discretize this system of equations in time, thus getting the following algebraic system.

$$\frac{\vec{y}^{n+1} - \vec{y}^n}{\Delta t} = \frac{\vec{f}(\vec{x}^n, \vec{\Gamma}^n) + \vec{f}(\vec{x}^{n+1}, \vec{\Gamma}^{n+1})}{2} \tag{4.36}$$

Now, we can use any numerical method to solve the system of equations for the primitive variables, $\vec{x}(t)$. Specifically, the method we use is a Newton-Rapshon iteration, which is briefly described below. Since, the Newton-Raphson method is an iterative method, we describe below how one progresses from the $m$th iteration to the $m+1$th iteration. In order to do this, we have to write the taylor series expansion of each of the terms in the algebraic system of equations. In all the taylor series expansions, we keep only the zeroth and first order terms, neglecting all higher order terms.

$$\vec{x}_{m+1}^{n+1} = \vec{x}_m^{n+1} + \delta\vec{x}_m^{n+1} \tag{4.37}$$

$$\vec{y}_{m+1}^{n+1} = \vec{y}_m^{n+1} + [B] \cdot \delta\vec{x}_m^{n+1} \tag{4.38}$$

where the matrix, $[B]$ is the Jacobian of the $\vec{y}$ vector relative to the $\vec{x}$ vector.

$$[B] = [\frac{\partial y_i}{\partial x_j}] \tag{4.39}$$

$$\vec{f}(\vec{x}_{m+1}^{n+1}, \vec{\Gamma}^{n+1}) = \vec{f}(\vec{x}_m^{n+1}, \vec{\Gamma}^{n+1}) + [A] \cdot \delta\vec{x}_m^{n+1} \tag{4.40}$$

Here, the matrix, $[A]$ is the Jacobian of the functions, $\vec{f}$, with respect to the primitive variables, $\vec{x}$.

$$[A] = [\frac{\partial f_i}{\partial x_j{}_m^{n+1}}] \tag{4.41}$$

Putting all these expressions together and solving, we get

$$([B] - \frac{\delta t}{2}[A]) \cdot \delta \vec{x}_m^{n+1} = \vec{y}^n - \vec{y}_m^{n+1} + \frac{\delta t}{2} \cdot [\vec{f}(\vec{x}^n, \vec{\Gamma}^n) + \vec{f}(\vec{x}_m^{n+1}, \vec{\Gamma}^{n+1})] \tag{4.42}$$

This equation can be used to iterate for the primitive variables, $\vec{x}^{n+1}$ at every time-step, till the iteration step, $\delta \vec{x}_m^{n+1}$ vanishes.

In general, both matrices $[A]$ and $[B]$ tend to be sparse since the equations of continuity and energy for each control volume tend to be affected only by velocities and temperatures of gas at neighboring control volumes. As a result, matrix inversion of $([B] - \frac{\delta t}{2}[A]$ at every iteration tends not to be a very computationally intensive process. The algorithm tends to be unconditionally stable in the solution of the algebraic system as long as care is taken to watch for flow reversals, and compensate for such conditions as described earlier. This becomes important as it influences the signs of the pivoting terms of the jacobian matrix, thus becoming crucial to numerical stability. Therefore, the use of the Newton-Raphson method in conjunction with the semi-implicit method helps us solve for the vector $\vec{x}(t)$. Since this vector represents a vector of the control surface velocities $v_i$, and the control volume temperatures $T_i$, we are able to directly solve for the primitive variables of the system of fluid equations.

## 4.5 Modeling of Scroll Walls

This section describes the model of the scroll walls that interact with the gas in a scroll pump. The gas that is in contact with any portion of the scroll sees temperature swings that are periodic with the time-period of the pump. These temperature swings are however not mirrored on walls of the pump because the time constant associated with the bulk of the metal is much greater than the time-period of crank rotation. Therefore, we model the scroll walls as having reached a steady temperature

distribution caused as a result of its interaction with the gas in the pump. In order to simplify our analysis, we also model the gas as having a steady temperature equal to the time-averaged gas temperature at every location within the pump. Such an averaging procedure helps us capture the average heat transferred from gas to wall over a time-period, and thus calculate the resultant temperature distribution in the walls.

In keeping with the one-dimensional nature of the gas model, we model the walls also in a one-dimensional fashion. The wall model can be subdivided into 4 parts, namely models for the wraps of the fixed scroll, base of the fixed scroll, wraps of the orbiting scroll, and base of the orbiting scroll. The single dimension along which the walls are modeled is the spiral angle, $\beta$ of the involute spirals for the orbiting and fixed scrolls.

### 4.5.1 Wraps of the Fixed and Orbiting Scroll

The wraps of the fixed and orbiting scrolls are modeled as a collection of differential metal elements at spiral angles starting from the start of the involute spiral at $\beta = \beta_{start}$ to the end of the spiral at $\beta = \beta_{end}$ (See figure 4-11). Each differential element at angle $\beta$ is completely characterized by its local wrap thickness $w_{wrap}(\beta)$, the wrap height $h_{wrap}$, and interactions with its neighboring wrap elements. The orbiting scroll has a uniform wrap thickness of $t_{wrap}$, as does the major portion of the fixed scroll. The outer wall of the fixed scroll, however has a non-uniform wall thickness, and is modeled as a "thick" wrap with varying wrap thickness $w_{wrap}(\beta)$. Each differential element on the wraps is modeled to be at a uniform and steady temperature, while undergoing thermal interactions with its neighboring gas and wall elements. Each differential element undergoes convection with gas on either side, conduction with neighboring differential elements, and kissing heat transfer with its conjugate differential element on the other scroll. In addition, the scroll wraps are also connected to their corresponding locations on the scroll base by the metal of the wraps. For the metal of the element to be at a steady temperature, the total energy transferred to the element should be equal to the energy transferred from it. Figure

4-12 shows a schematic of all the heat interactions undergone by elements of the fixed and orbiting scroll wraps.

### Convection with Neighboring Gas

Every section of wrap undergoes convective heat transfer with its neighboring gas. Every wrap element (except for the outer walls of the fixed scroll) is exposed to gas both at its inner and its outer surfaces. The inner surface of every position on the fixed scroll wrap is exposed to gas from the outer scroll pocket, while it is exposed to gas from the inner scroll pockets at its outer surface. Conversely, every location on the wraps of the orbiting scroll is exposed to inner pocket gas on its inner surface and outer pocket gas on its outer surface. The heat transferred to each wrap element (averaged over the time-period of the pump) is then given by the following equations:

$$\dot{Q}_{conv,ow} = h_{conv} A_{ow}(\beta)(T_{go}(\beta+360°) - T_{ow}(\beta)) + h_{conv} A_{ow}(\beta)(T_{gi}(\beta) - T_{ow}(\beta)) \quad (4.43)$$

$$\dot{Q}_{conv,fw} = h_{conv} A_{fw}(\beta)(T_{gi}(\beta) - T_{fw}(\beta)) + h_{conv} A_{fw}(\beta)(T_{go}(\beta) - T_{fw}(\beta)) \quad (4.44)$$

Here, $T_{ow}(\beta)$ and $T_{fw}(\beta)$ are the temperatures of the wrap elements of the orbiting scroll and fixed scroll at the spiral angle $\beta$, $A_{ow}(\beta)$ and $A_{fw}(\beta)$ are the heat transfer areas of the fixed and orbiting scroll wrap elements at spiral angle $\beta$, while $T_{gi}(\beta)$ and $T_{go}(\beta)$ are the time-averaged gas temperatures at spiral angle $\beta$ (see figure 4-13). Note that in the above equation, we don't distinguish between the areas of the inner and outer surfaces of each wrap element. This is tantamount to neglecting the effect of the wrap thickness on the circumference of the wrap element.

### Conduction with Neighboring Wrap Elements

Each wrap element at spiral angle, $\beta$ undergoes conductive heat transfer with its neighboring wrap elements, i.e. the wrap elements at spiral angles, $\beta - \Delta\beta$, and $\beta + \Delta\beta$. The heat conducted to the wrap element is given by the following equations. Here, $l^+(\beta)$ is the length of spiral between the center of the current wrap element with that at $\beta + \Delta\beta$, while $l^-(\beta)$ is that corresponding to the wrap element at $\beta - \Delta\beta$ (see

figure 4-14).

$$\dot{Q}_{cond,ow} = -\frac{kh_{wrap}t_{wrap}}{l^{+}_{ow}(\beta)}(T_{ow}(\beta+\Delta\beta)-T_{ow}(\beta)) - \frac{kh_{wrap}t_{wrap}}{l^{-}_{ow}(\beta)}(T_{ow}(\beta-\Delta\beta)-T_{ow}(\beta)) \tag{4.45}$$

$$\dot{Q}_{cond,fw} = -\frac{kh_{wrap}t_{wrap}}{l^{+}_{fw}(\beta)}(T_{fw}(\beta+\Delta\beta)-T_{fw}(\beta)) - \frac{kh_{wrap}t_{wrap}}{l^{-}_{fw}(\beta)}(T_{fw}(\beta-\Delta\beta)-T_{fw}(\beta)) \tag{4.46}$$

Once again, we state the equations of wrap conduction both for orbiting and fixed scroll wrap elements.

### Kissing Heat Transfer

Wrap elements on each scroll undergo transient contact with their conjugate points on the other scroll. The inner surface of a point on the orbiting scroll wrap at spiral angle, $\beta$ is conjugate with a location at spiral angle, $\beta$ on the outer surface of the fixed scroll, while the outer surface of the wrap at the same angle, $\beta$ is conjugate with the inner surface of the fixed scroll wrap at a spiral angle of $\beta + 360°$ (see figure 4-15). The kissing heat transfer corresponding to a wrap element at spiral angle $\beta$ is given by the following equations.

$$\dot{Q}_{kiss,ow} = h_{kiss}A_{ko,1}(\beta)\cdot(T_{fw}(\beta+360°) - T_{ow}(\beta)) + h_{kiss}A_{ko,2}(\beta)\cdot(T_{fw}(\beta) - T_{ow}(\beta)) \tag{4.47}$$

$$\dot{Q}_{kiss,fw} = h_{kiss}A_{kf,1}(\beta)\cdot(T_{ow}(\beta-360°) - T_{fw}(\beta)) + h_{kiss}A_{kf,2}(\beta)\cdot(T_{ow}(\beta) - T_{fw}(\beta)) \tag{4.48}$$

Here, $h_{kiss}$ is the kissing heat transfer coefficient, while $A_{ko,1}$, $A_{ko,2}$, $A_{kf,1}$ and $A_{kf,2}$ are the kissing heat transfer areas for the orbiting and fixed scroll wrap elements respectively. We approximate the kissing heat transfer areas as simply being equal to the mean of the areas of the surfaces in conjugate contact.

$$A_{ko,1}(\beta) = (A_{ow}(\beta) + A_{fw}(\beta+360°))/2 \tag{4.49}$$

$$A_{ko,2}(\beta) = (A_{ow}(\beta) + A_{fw}(\beta))/2 \tag{4.50}$$

$$A_{kf,1}(\beta) = (A_{ow}(\beta - 360°) + A_{fw}(\beta))/2 \tag{4.51}$$

$$A_{kf,2}(\beta) = (A_{ow}(\beta) + A_{fw}(\beta))/2 \tag{4.52}$$

### Conduction with Neighboring Base Elements

A scroll wrap element at spiral angle, $\beta$ is in thermal communication with the base of the scroll at the same wrap angle through the metal of the wraps (see figure 4-16). Thus, heat is conducted between wraps and base at all spiral angles. Since the wraps are thin, the thermal resistance associated with this mode tends to be quite large at most locations. However, the outer most turn of the fixed scroll wrap has thick walls that provide a low resistance connection between wraps and base, thus making this mode of heat transfer crucial at least at the outer most sections of the fixed scroll. The heat conducted into a wrap element from the base at spiral angle $\beta$ is given by the following equation. Here, in order to keep things general, we refer to the thickness of the thermal conduction path as $w_{wrap}$ rather than $t_{wrap}$ which is the thickness of the scroll wraps at all angular locations other than the outer most sections of the fixed scroll.

$$\dot{Q}_{base,o} = -\frac{k w_{wrap} l_{CV}(\beta)}{h_{wrap}}(T_{ob}(\beta) - T_{ow}(\beta)) \tag{4.53}$$

$$\dot{Q}_{base,f} = -\frac{k w_{wrap} l_{CV}(\beta)}{h_{wrap}}(T_{fb}(\beta) - T_{fw}(\beta)) \tag{4.54}$$

Here, $T_{ob}(\beta)$ refers to the temperature of the orbiting scroll base at spiral angle $\beta$, while $T_{fb}(\beta)$ is the temperature of the fixed scroll base at spiral angle $\beta$.

### Overall Energy Balance

For the wraps of the orbiting and fixed scrolls to be at a steady temperature, the total energy transfer to a scroll wrap element must be equal to that transferred from it. Thus, every scroll wrap element has an energy balance of the following form.

$$\dot{Q}_{conv,o}(\beta) + \dot{Q}_{cond,o}(\beta) + \dot{Q}_{kiss,o}(\beta) + \dot{Q}_{base,o}(\beta) = 0 \tag{4.55}$$

$$\dot{Q}_{conv,f}(\beta) + \dot{Q}_{cond,f}(\beta) + \dot{Q}_{kiss,f}(\beta) + \dot{Q}_{base,f}(\beta) = 0 \tag{4.56}$$

### 4.5.2 Base of the Fixed and Orbiting Scrolls

Now, we write the equations corresponding to the base of the fixed and orbiting scrolls. As with the wraps, we divide the base into differential elements, once again at incremental values of the spiral angle, $\beta$. Using only one dimension, i.e. the spiral angle may seem odd to model a two-dimensional geometry like one associated with the base of a scroll. Such a description, however, suffices when we consider the fact that the principal characteristics of a base element - its radial location $r(\beta)$, its width $b$, its local thickness $w_{base}(\beta)$, and its neighbors are all adequately indexed by the spiral angle $\beta$ (See figure 4-17). Every element on the base of a scroll undergoes radial conduction with base elements at neighboring radial locations. Elements also undergo conduction in the azimuthal direction with elements at neighboring spiral angles. As with elements of the wraps, they also undergo convection with gas corresponding to the inner and outer pockets of gas. Conduction between base and wrap elements constitutes the last mode of heat transfer. Each of these modes is briefly described below. Figure 4-18 shows a schematic of all the energy interactions experienced by a base element at spiral angle $\beta$.

#### Convection with Neighboring Gas

Every base element undergoes heat transfer with gas that flows past the element. Such gas undergoes periodic swings in temperature associated with thermodynamic processes that occur with every period in the pump. However, like the wrap elements, the base elements also have large thermal time constants relative to the period of the pump, and therefore can be modeled as having reached a steady-state temperature. Every base element on the fixed scroll at spiral angle, $\beta$ (except for elements at the outer most radii, which are only exposed to the outer pocket gas at angle $\beta$) convects heat with gas in both the outer and inner pockets at spiral angle, $\beta$, while the corresponding element on the orbiting scroll convects with gas in the inner pocket

at spiral angle, $\beta$, while it convects heat with gas in the outer pocket at spiral angle, $\beta + 360°$. The equations governing convective heat transfer to the a base element at angle, $\beta$ element are listed below. Here, $\dot{Q}_{conv,f}(\beta)$ and $\dot{Q}_{conv,o}(\beta)$ are the rates of heat transferred to the base elements of the fixed and orbiting scrolls at angle, $\beta$. $T_{gi}(\beta)$ and $T_{go}(\beta)$ are time-averaged temperatures of gas at spiral angle, $\beta$ in the inner and outer pockets respectively, while $A_{oo}(\beta)$, $A_{oi}(\beta)$, $A_{fo}(\beta)$ and $A_{fi}(\beta)$ are the heat transfer areas of the orbiting and fixed scroll base elements at its outer and inner radii, respectively.

$$\dot{Q}_{conv,o} = h_{conv}A_{oo}(\beta)\cdot(T_{go}(\beta+360°) - T_{ob}(\beta) + h_{conv}A_{oi}(\beta)\cdot(T_{gi}(\beta) - T_{ob}(\beta)) \quad (4.57)$$

$$\dot{Q}_{conv,f} = h_{conv}A_{fo}(\beta)\cdot(T_{gi}(\beta) - T_{ob}(\beta) + h_{conv}A_{fi}(\beta)\cdot(T_{go}(\beta) - T_{ob}(\beta)) \quad (4.58)$$

### Radial Conduction

Elements on the base of both scrolls undergo radial conduction with elements that radially neighbor these elements. Here, we approximate the radial conduction as that corresponding to an angular section of a cylinder between the centers of the two elements that exchange heat. The width of the angular section is $\Delta\beta$, which is simply the angular increment of spiral angle at which we consider base elements. The height of the cylinder is approximated to be the average thickness, $w_{base}(\beta)$ of the scroll base corresponding to the locations of the two control volumes considered. While base thickness is constant for the orbiting scroll, it tends to vary with location with the fixed scroll, as a result such an approximation becomes necessary. The average thickness for the purpose of this estimation is referred to as $w^{+}_{base}(\beta)$ for outward radial conduction in a base element, while its referred to as $w^{-}_{base}(\beta)$ for inward radial conduction. The radius of the scroll at spiral angle $\beta$ is $r_{ob}(\beta)$ for the orbiting scroll, and $r_{fb}(\beta)$ for the fixed scroll respectively. In the equations below, $\dot{Q}_{rcond,f}$ and $\dot{Q}_{rcond,o}$ are rates of heat transferred into a base element at angle $\beta$ through radial

conduction.

$$\dot{Q}_{rcond,o} = \frac{k\Delta\beta w^{+}_{base}(\beta)}{log\frac{r_{ob}(\beta+360^{\circ})}{r_{ob}(\beta)}}(T_{ob}(\beta+360^{\circ}) - T_{ob}(\beta)) + \frac{k\Delta\beta w^{-}_{base}(\beta)}{log\frac{r_{ob}(\beta)}{r_{ob}(\beta-360^{\circ})}}(T_{ob}(\beta-360^{\circ}) - T_{ob}(\beta)) \tag{4.59}$$

### Azimuthal Conduction

Elements on the base of a scroll also conduct heat to elements at neighboring angular locations. Such conduction in the azimuthal direction is described here. Here, as with radial conduction, we use $w^{+}_{base}(\beta)$ and $w^{-}_{base}(\beta)$ to refer to the average thickness of the base elements between consecutive base elements in the positive and negative azimuthal directions respectively. The width of each base element is $b$. In addition, $l^{+}(\beta)$ and $l^{-}(\beta)$ are respectively the the conduction lengths between consecutive base elements in the positive and negative azimuthal directions. $\dot{Q}_{acond,o}(\beta)$ is the heat transferred by azimuthal conduction to an orbiting scroll base element at spiral angle $\beta$, while $\dot{Q}_{acond,f}$ is the heat transferred to a fixed scroll base element at angle $\beta$.

$$\dot{Q}_{acond,o} = -\frac{kbw^{+}_{base}(\beta)}{l^{+}(\beta)}(T_{ob}(\beta+\Delta\beta) - T_{ob}(\beta)) - \frac{kbw^{-}_{base}(\beta)}{l^{-}(\beta)}(T_{ob}(\beta-\Delta\beta) - T_{ob}(\beta)) \tag{4.60}$$

$$\dot{Q}_{acond,f} = -\frac{kbw^{+}_{base}(\beta)}{l^{+}(\beta)}(T_{fb}(\beta+\Delta\beta) - T_{fb}(\beta)) - \frac{kbw^{-}_{base}(\beta)}{l^{-}(\beta)}(T_{fb}(\beta-\Delta\beta) - T_{fb}(\beta)) \tag{4.61}$$

### Conduction with Wrap Elements

The last mode of heat transfer that we consider for the base elements is conductive heat transfer with wrap elements at the same spiral angle. This mode of heat transfer was modeled as one of the modes of heat transfer to wraps of a scroll pump. Here, we simply change signs on the equation used there to describe the heat transfer rate $\dot{Q}_{wrap,o}(\beta)$ and $\dot{Q}_{wrap,f}(\beta)$ to base elements on the orbiting and fixed scrolls at angle $\beta$ from their corresponding wrap element locations.

$$\dot{Q}_{wrap,o} = -\frac{kw_{wrap}l_{CV}(\beta)}{h_{wrap}}(T_{ow}(\beta) - T_{ob}(\beta)) \tag{4.62}$$

$$\dot{Q}_{wrap,f} = -\frac{kw_{wrap}l_{CV}(\beta)}{h_{wrap}}(T_{fw}(\beta) - T_{fb}(\beta)) \tag{4.63}$$

**Overall Energy Balance**

As with the wraps, in order for the base elements to have attained a steady temperature distribution, total heat transfer into each element should be equal to the heat transferred out of it. This is written in equation form for each location on the fixed and orbiting scroll base as shown below.

$$\dot{Q}_{conv,o}(\beta) + \dot{Q}_{rcond,o}(\beta) + \dot{Q}_{acond,o}(\beta) + \dot{Q}_{wrap,o}(\beta) = 0 \tag{4.64}$$

$$\dot{Q}_{conv,f}(\beta) + \dot{Q}_{rcond,f}(\beta) + \dot{Q}_{acond,f}(\beta) + \dot{Q}_{wrap,f}(\beta) = 0 \tag{4.65}$$

### 4.5.3 Calculation of Time-Averaged Gas Temperature at every location within the scroll

In the models for computation of the steady state temperature distributions of the walls of a scroll pump, we only use the time-averaged temperatures of gas at every location within the pump. This is done because the walls are modeled to have already reached a steady-state as a result of their interaction with the gas. Such interaction of metal with oscillating gas temperatures can be approximated as the interaction of metal with gas temperatures that are averaged over the period of a crank rotation of the pump. Thus, average temperatures at every spiral angle $\beta$ are calculated as follows.

$$T_{gi}(\beta) = \int_0^\tau T_{gi}(\beta, t)dt \tag{4.66}$$

$$T_{go}(\beta) = \int_0^\tau T_{go}(\beta, t)dt \tag{4.67}$$

Here, $T_{gi}(\beta, t)$ and $T_{go}(\beta, t)$ are the gas temperatures of the inner and outer pocket at spiral angle $\beta$ at time $t$, while the figures without the $t$ index are the average of such temperatures taken over the time period $\tau$ at the angular location $\beta$. Thus we use outputs of the gas-side calculations (namely $T_{gi}(\beta, t)$ and $T_{go}(\beta, t)$) to calculate

the time-averaged gas temperatures $T_{gi}(\beta)$ and $T_{go}(\beta)$ which are then used as inputs to the metal-side calculations.

## 4.6 Distinguishing Between Inner and Outer Pocket of the Scroll

The inner and outer pockets of a scroll pump are geometrically symmetric since they are both formed of identical sections of the involute spirals that constitute the fixed and orbiting scrolls. The inner pocket is formed between the inner wall of the orbiting scroll wraps and the outer wall of the fixed scroll wraps. Simultaneously, at a spiral angle that is 180° greater, the outer pocket is formed by conjugate contact between the outer wall of the orbiting scroll wrap and the inner wall of the fixed scroll wrap. The section of inner orbiting scroll wall that forms part of the inner pocket is exactly identical in dimension to the inner fixed scroll wall that forms the outer pocket, while outer fixed scroll wall sections that form the inner pocket are identical to outer orbiting scroll wall sections of the outer pocket. Owing to this symmetry, it becomes very easy to treat the inner and outer pockets as nearly identical for gas side simulations. The outer pocket however, crucially differs from the inner pocket in one sense. This is due to the fact that gas in the outer pocket flows through non-conjugate sections of the scroll pump walls for almost 180° before it reaches the conjugate sections of the pocket that are identical to the inner pocket (see figure 4-19). This flow of gas through non-conjugate sections of the pump, henceforth referred to as the outer suction pathway, is however subject to at least two sources of irreversibility that gas in the inner pockets are not subject to. The walls of the orbiting scroll wraps that form the outer suction pathway allow gas to leak into this pathway from the closed process of the inner pocket while gas in this path is also subject to heat transfer from the walls of the pathway that are in general hotter than the gas. As a result, the entropy and temperature of gas in the outer pocket is higher than that associated with pump suction even before it reaches conjugate sections of the outer

pocket. We model these sources of irreversibility as energy (and mass transfer) to a through-flow system, thus neglecting the oscillatory features of the outer suction pathway. While such modeling does not capture the exact state of the gas at the start of conjugacy for the outer pocket at every instant of time, it does serve to capture the average state of gas at the mouth of the outer pocket, thus enabling us to model the outer pocket in a manner similar to the inner pocket except with a suction state at a hotter temperature than that associated with the inner pocket.

## 4.7 Solution Procedure

In this chapter, we have described methods of modeling the gas and walls of a scroll pump separately, with wall temperatures being inputs to the gas process, while gas temperatures are inputs to the wall calculations. Here, we briefly outline the method for iteratively solving the pump model to its thermodynamically self-consistent operating states.

First of all, we perform the gas side simulations assuming no leakage or heat transfer. We use the outputs of this simulation to calculate the average gas temperatures at every location in the pump, which we then use as inputs into the wall model to calculate the steady-state temperature distribution of the scroll walls. The pressure distribution that arises out of the initial gas simulation, is also used to calculate mass flow rates and enthalpies of leakage for various parts of the gas process. Now, we use the calculated wall temperatures and leakages to recalculate the gas process this time without neglecting leakage and heat transfer processes. The outputs of this calculation are then used to recalculate wall temperatures and leakages, which are then used as inputs to the next iteration of gas process calculations. Such a process of iteration goes on till we arrive at invariant distributions of wall temperatures, leakages and gas states. The invariant distribution that is arrived at in such a manner will be thermodynamically self-consistent and will constitute the output of the distributed parameter scroll pump model.

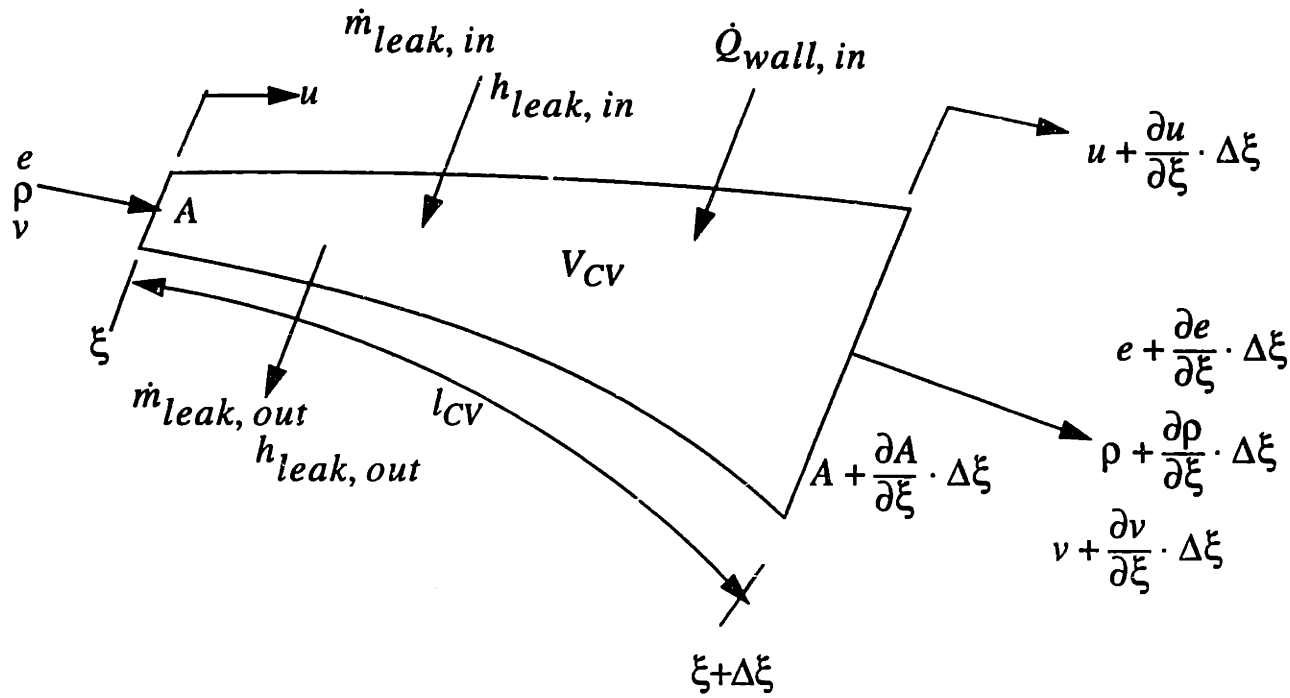


$\rho$, $v$, $u$, $e$, $A$, $V_{cv}$ are all functions of time.

**Figure 4-1: Differential Control Volume**

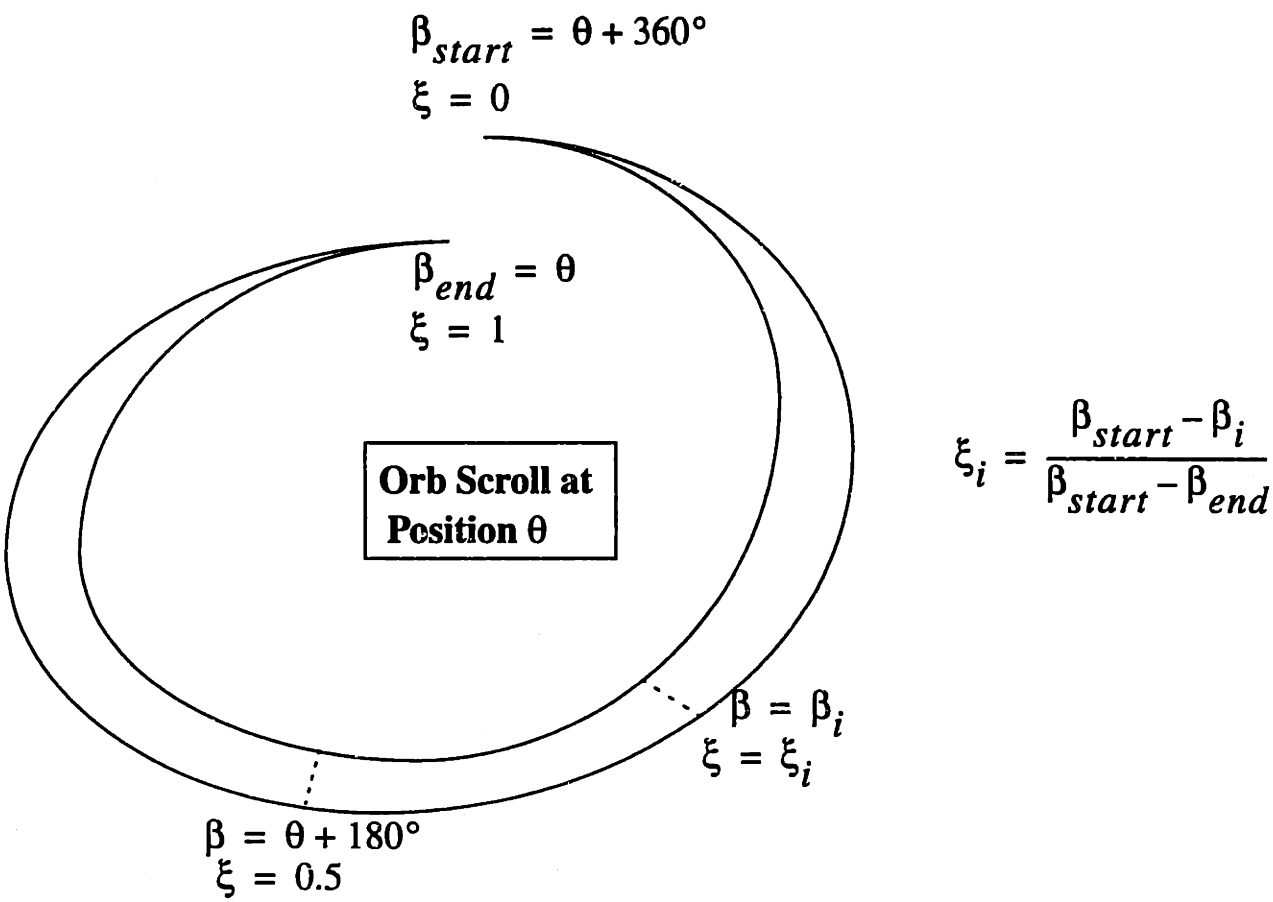


**Figure 4-2: Relative Positions of Control Surfaces Within a Pocket**

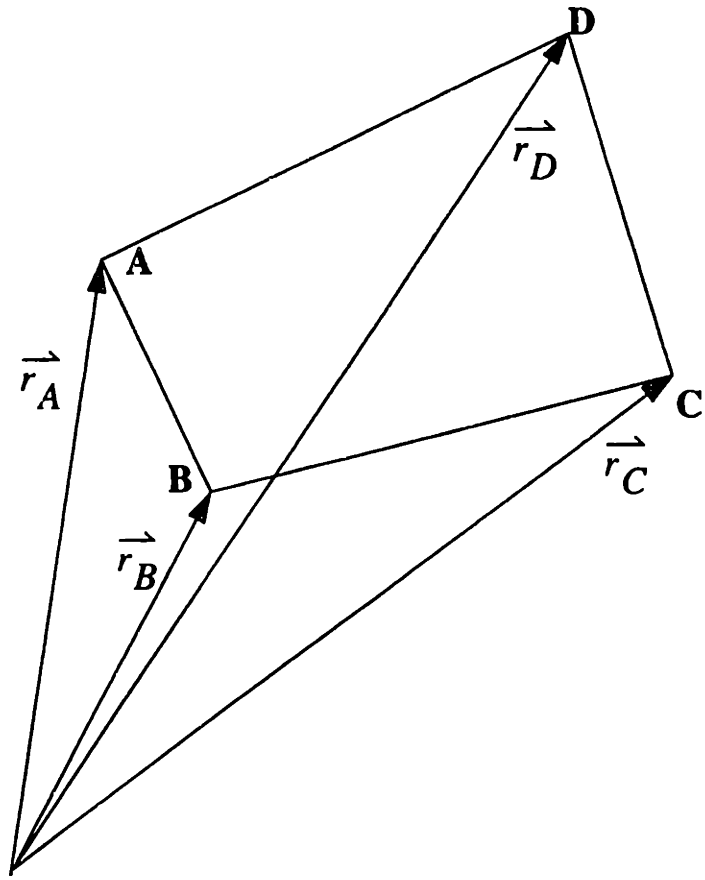


**Figure 4-3: Vectorial Description of Differential Control Volume**

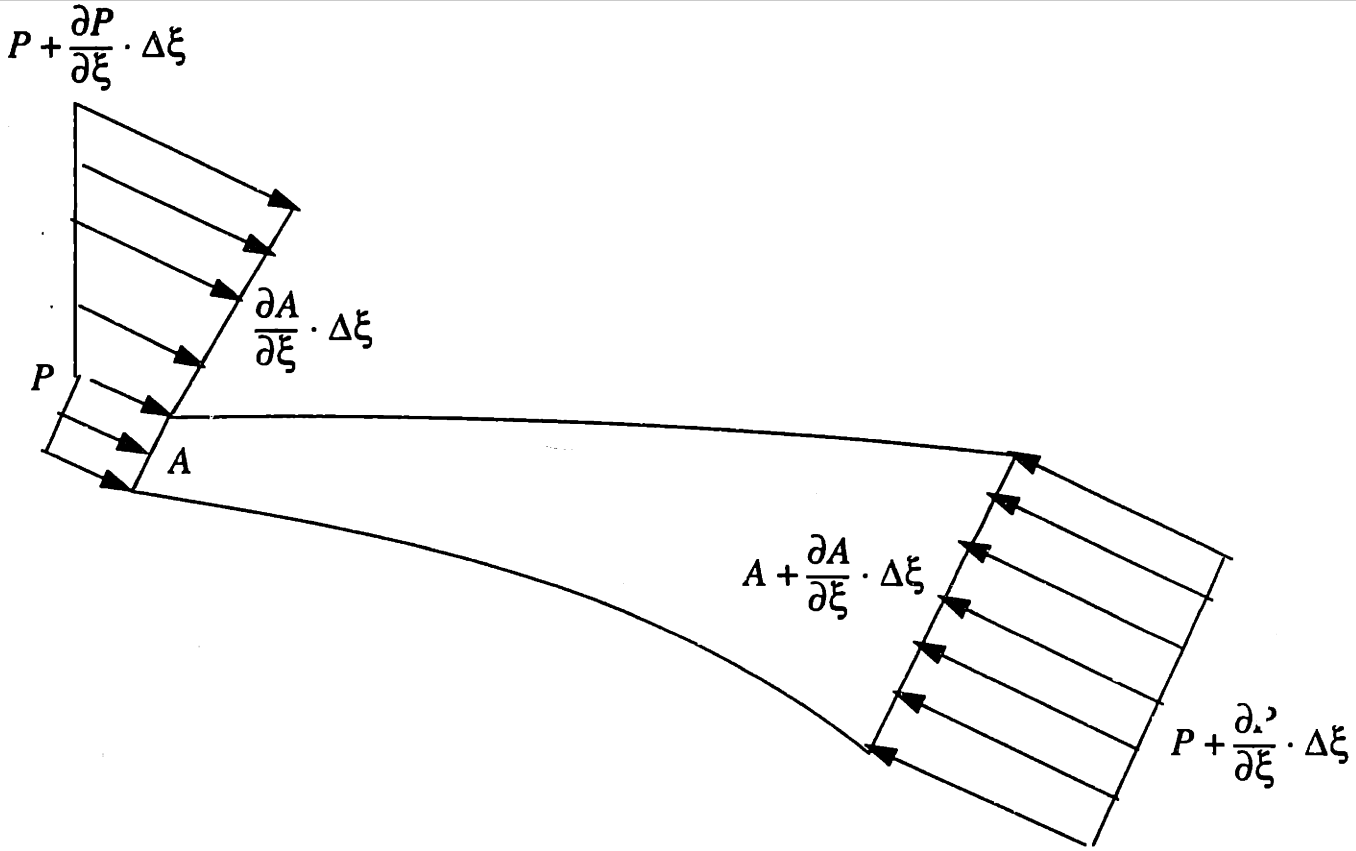


**Figure 4-4: Pressure Forces on a Control Volume**

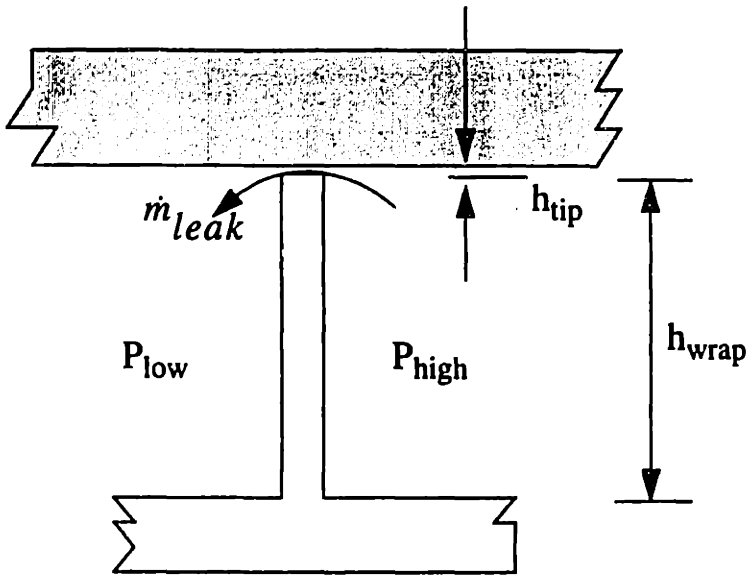


(a) Leakage Across Tips of Scroll

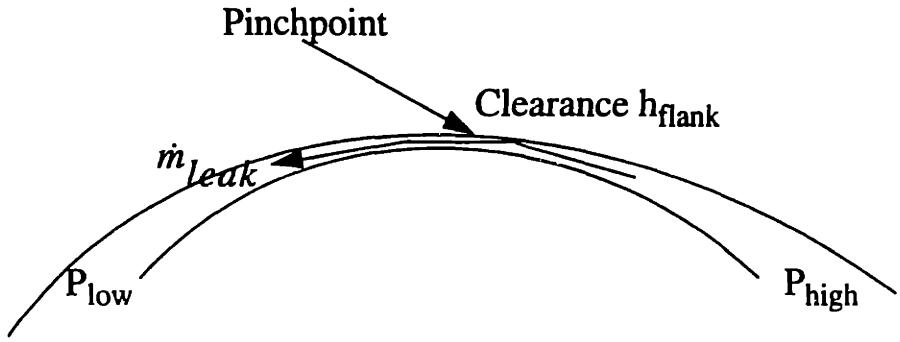


(b) Leakage Across Flanks at a Pinchpoint

**Figure 4-5: Leakage Modeled as Flow Across Orifices**

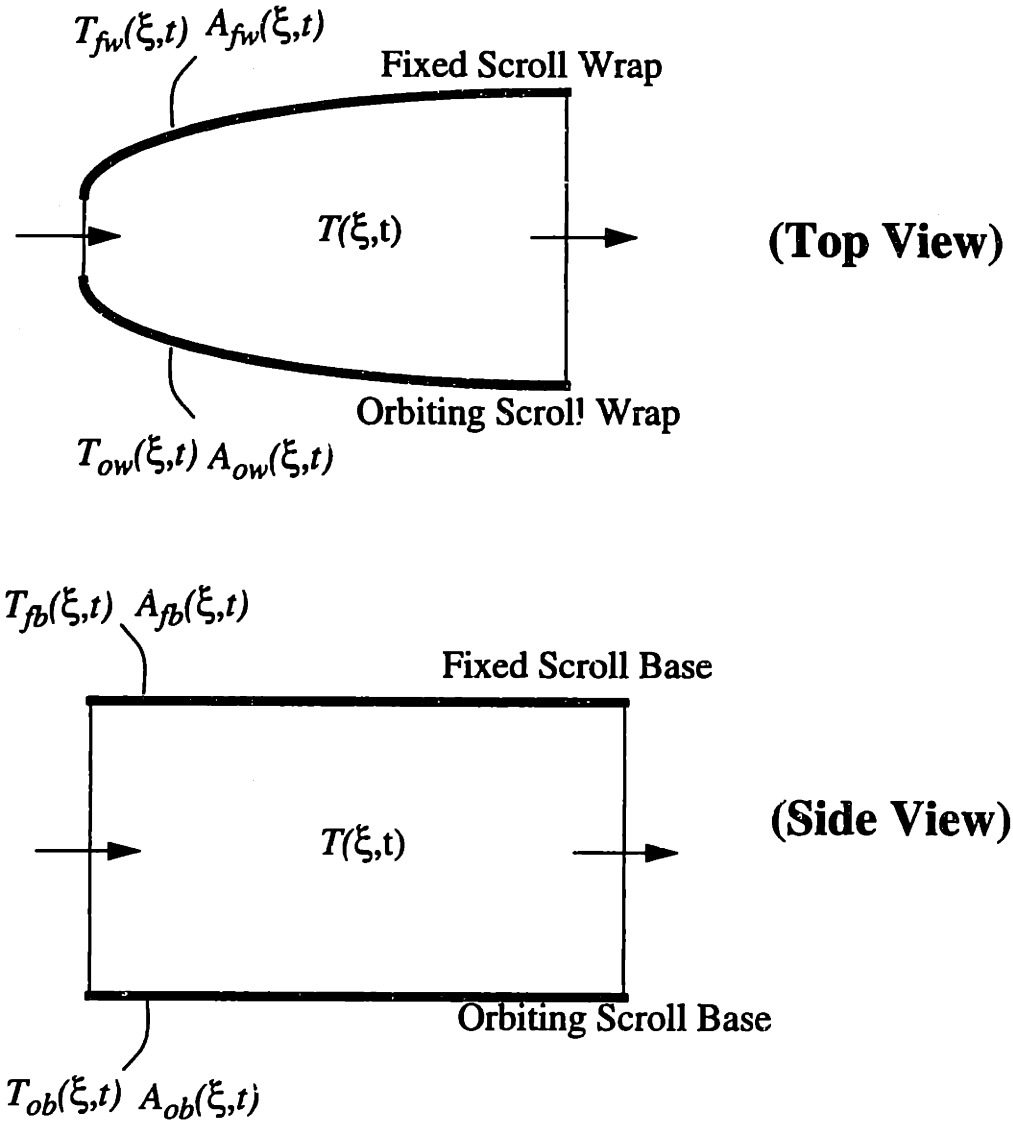


$$\dot{Q}_{wall,\,in} = hA_{ow}(\xi,t)\cdot[T_{ow}(\xi,t)-T(\xi,t)] + hA_{fw}(\xi,t)\cdot[T_{fw}(\xi,t)-T(\xi,t)]$$
$$+hA_{ob}(\xi,t)\cdot[T_{ob}(\xi,t)-T(\xi,t)] + hA_{fb}(\xi,t)\cdot[T_{fb}(\xi,t)-T(\xi,t)]$$

**Figure 4-6: Heat Transfer Between Gas and Walls of a Control Volume**

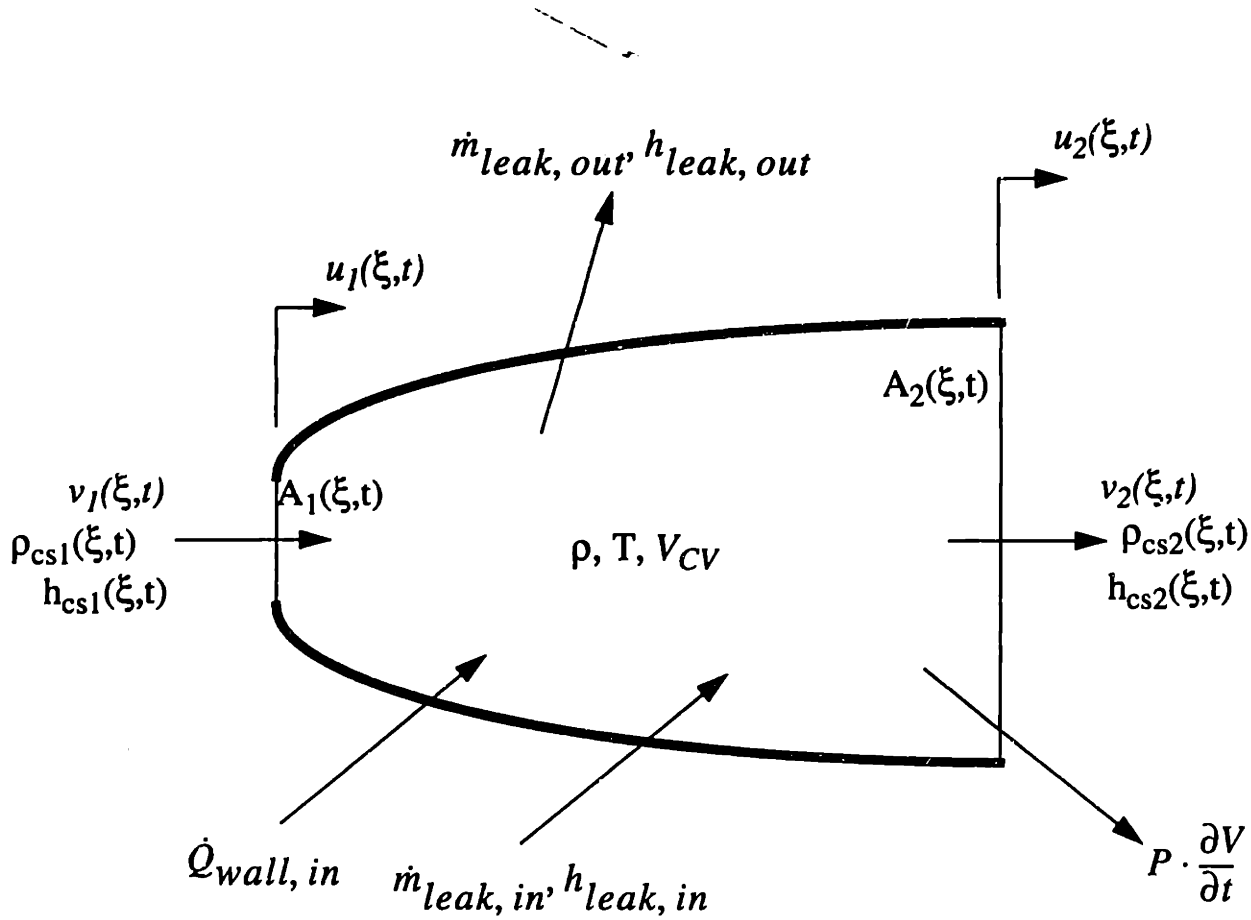


We Solve for velocities at control surfaces, but for densities and temperatures at the centers of control volumes.

**Figure 4-7: Control Volume After Spatial Discretization**

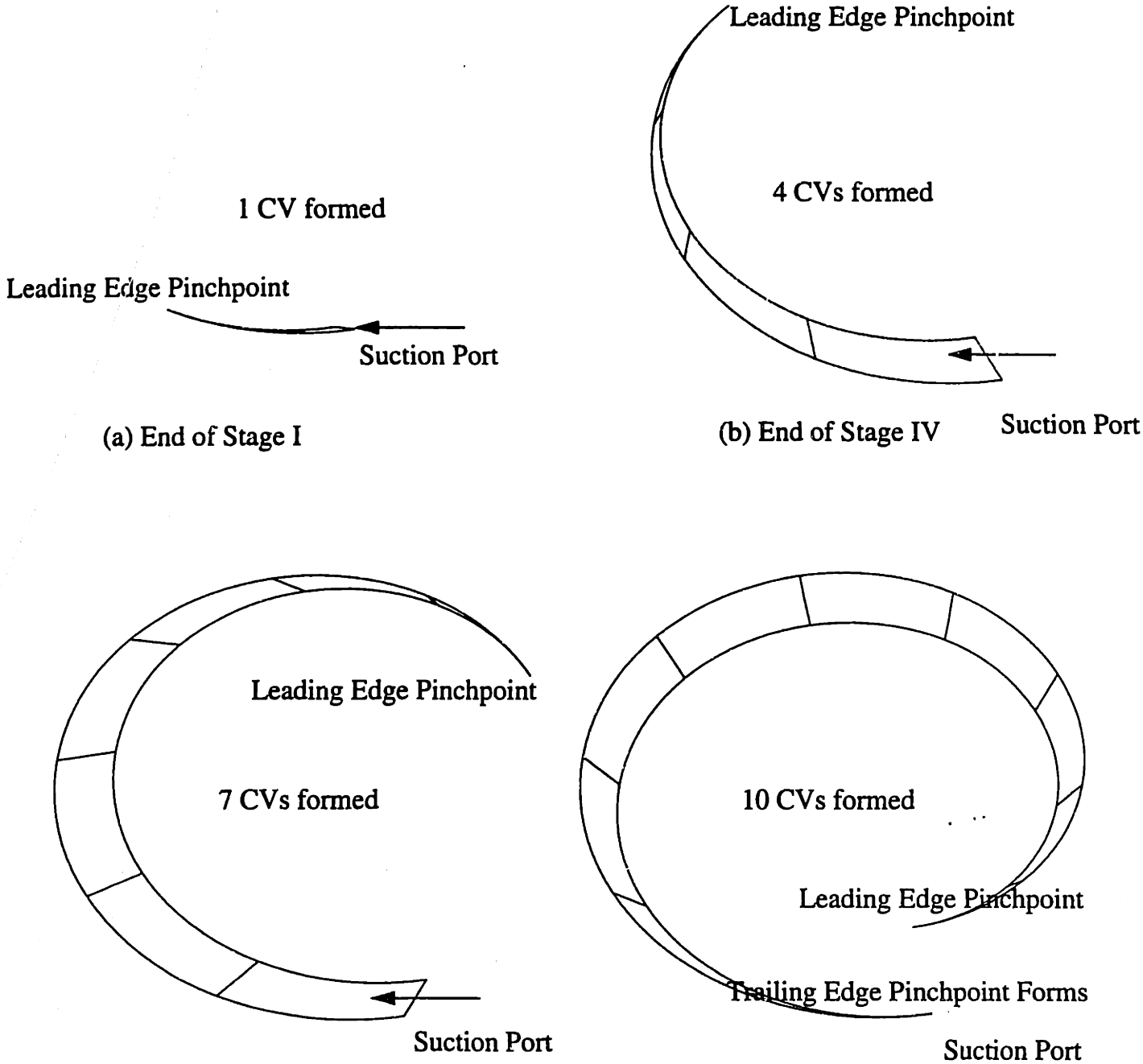


Suction Divided Into Ten Stages. At each stage, one control volume gets formed. At end of 10th stage, trailing edge pinchpoint forms thus ending the suction process.

**Figure 4-8: Stages of Suction**
**(Drawn to Scale)**

(a) Start of Closed Process

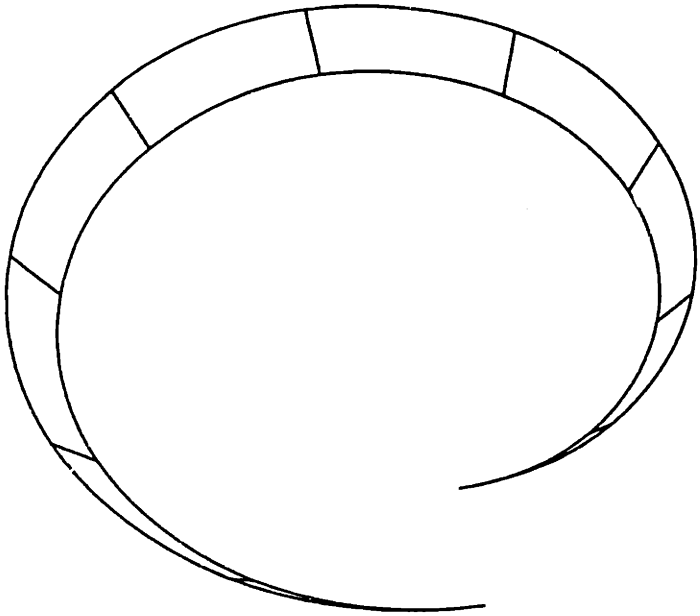

(b) Intermediate Stage I of Closed Process

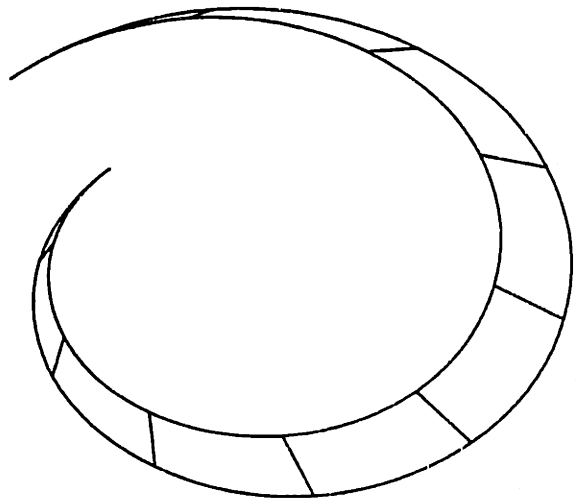

(c) Intermediate Stage II of Closed Process

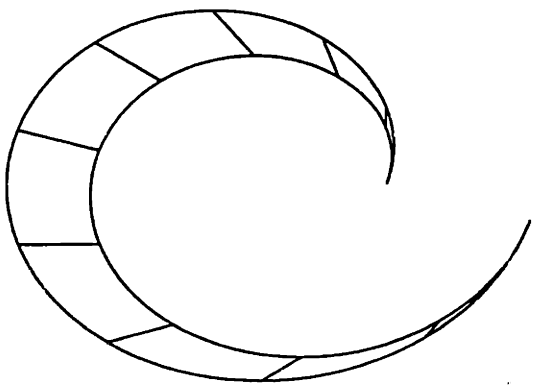

(d) End of the Closed Process

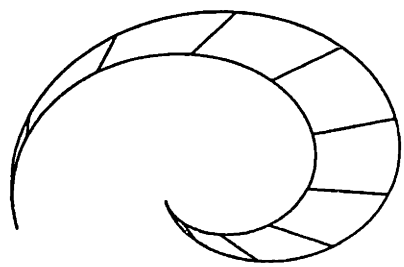

As Closed Process Proceeds, the fully sealed off pocket moves inward within the pump and diminishes in volume. Here, we show the start of the closed process, followed by 3 stages leading to the end of the closed process.

**Figure 4-9: Stages of Closed Process**
**(Drawn to Scale)**

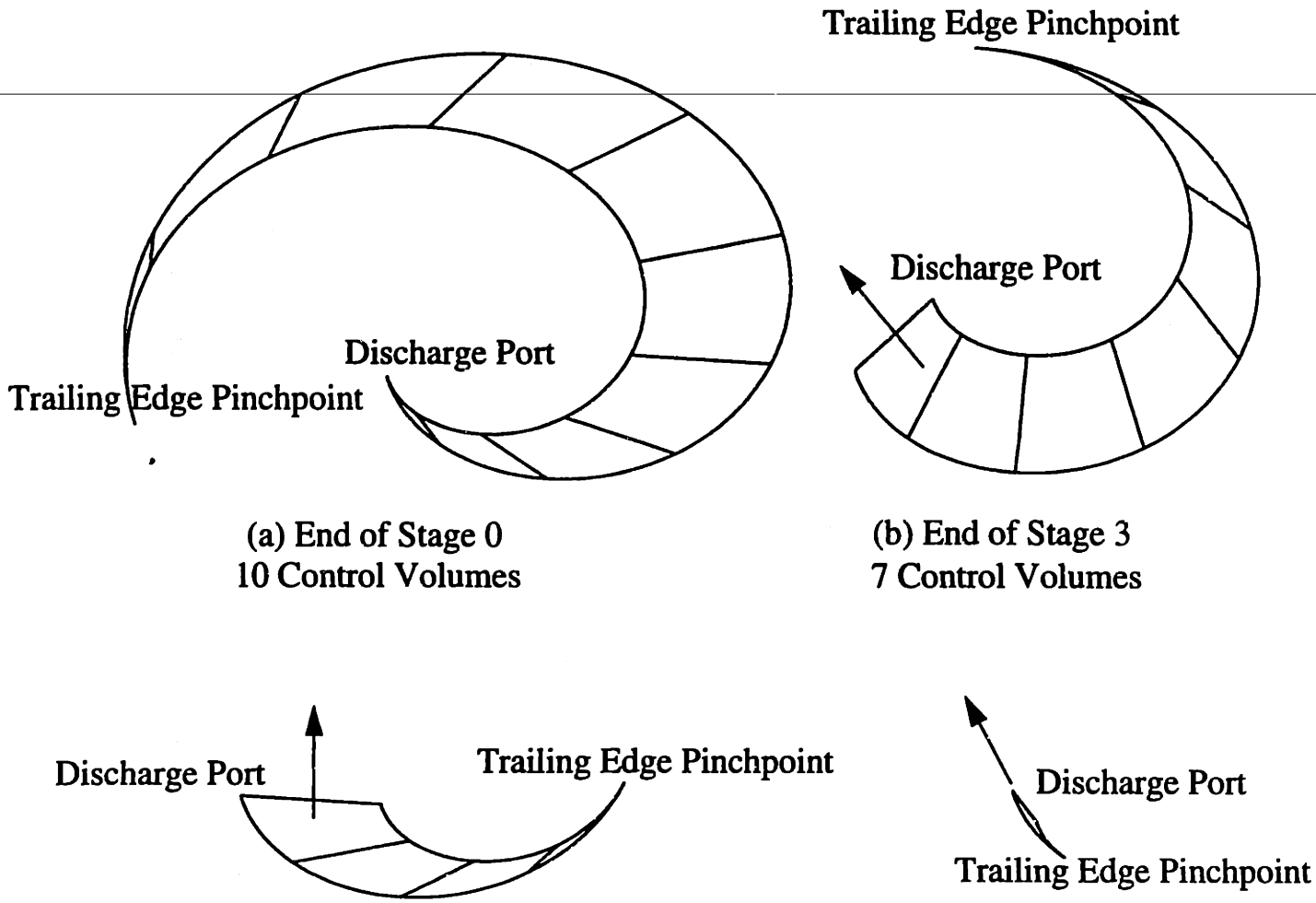


The Discharge Process Here is Divided Into 10 Stages. At Each Stage, one Control Volume gets Destroyed, and the Pocket Volume Shrinks. At the End of 10 Stages, Pocket Volume Has Shrunk to Zero and all Gas has been Expelled to the Discharge Port.

**Figure 4-10: Stages of Discharge (Drawn to Scale)**

Fixed Scroll Between $\beta_{f,start}$ and $\beta_{f,end}$. Outer 360° of fixed scroll modeled as "Thick Wraps"
Orbiting Scroll Between $\beta_{o,start}$ and $\beta_{o,end}$. Wrap Thickness is uniform.

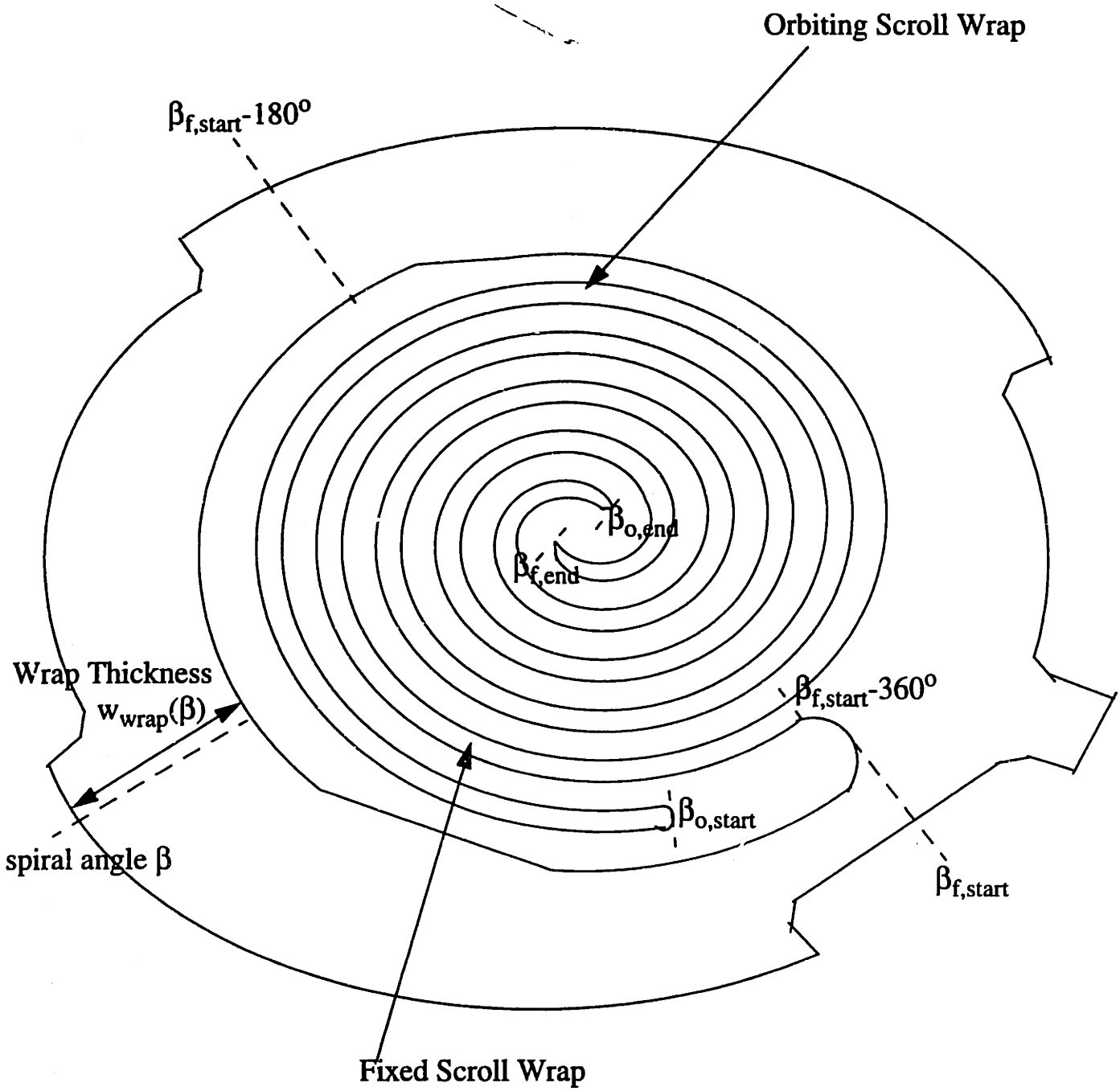


Every wrap location at angle β is completely characterized by the wrap thickness, $w_{wrap}(\beta)$, its height, $h_{wrap}$ and its interactions with neighboring elements.

**Figure 4-11: Scroll Wraps Modeled One-Dimensionally along Spiral Angle β.**

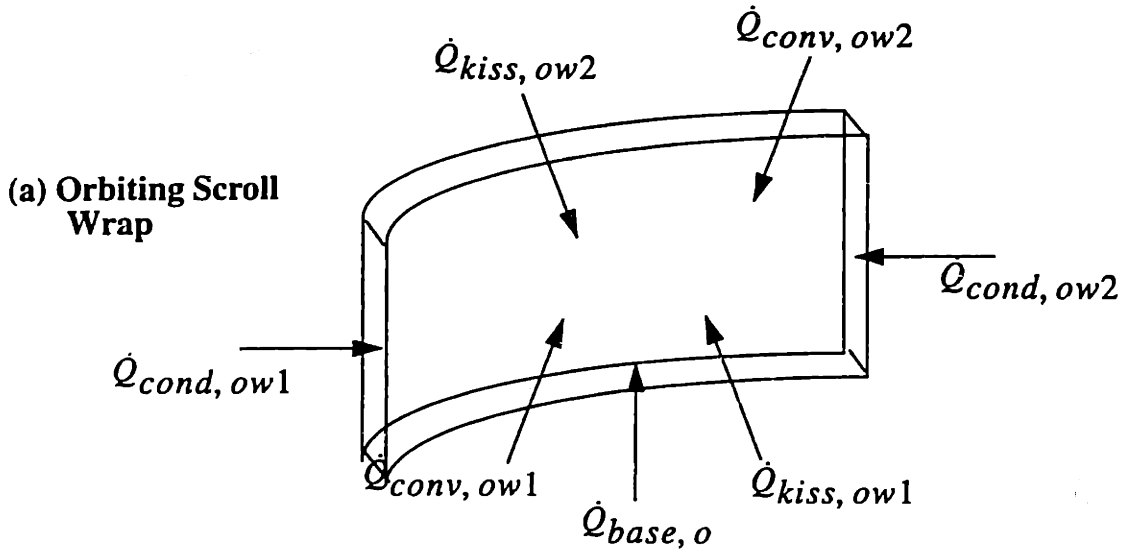


$$\dot{Q}_{cond,\,ow1} + \dot{Q}_{cond,\,ow2} + \dot{Q}_{conv,\,ow1} + \dot{Q}_{conv,\,ow2} + \dot{Q}_{base,\,o} + \dot{Q}_{kiss,\,ow1} + \dot{Q}_{kiss,\,ow2} = 0$$

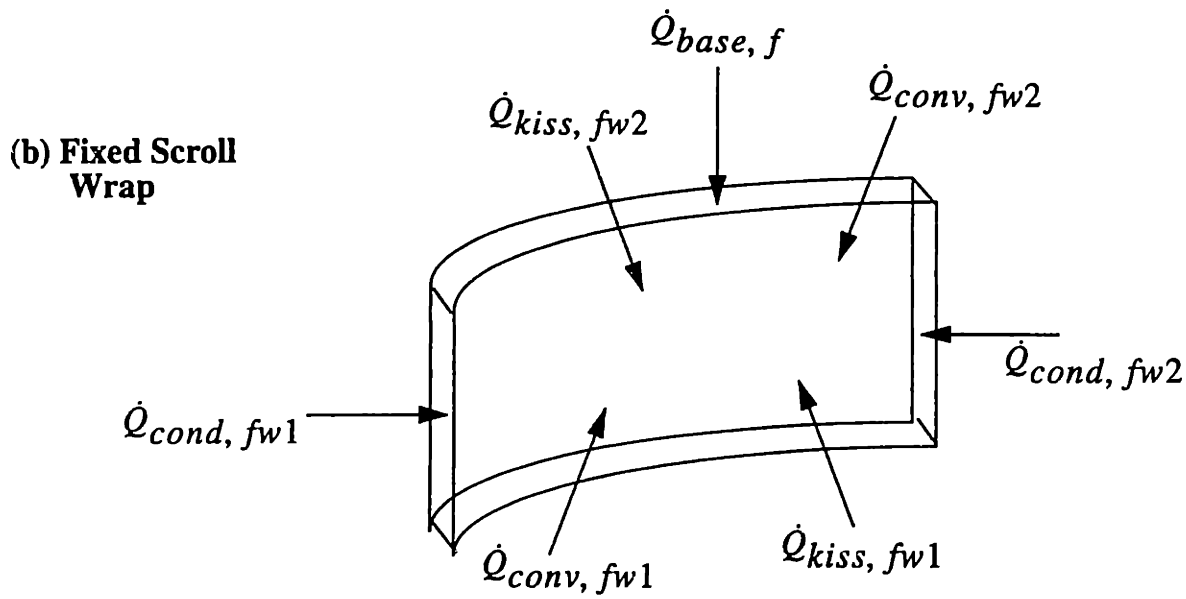


$$\dot{Q}_{cond,\,fw1} + \dot{Q}_{cond,\,fw2} + \dot{Q}_{conv,\,fw1} + \dot{Q}_{conv,\,fw2} + \dot{Q}_{base,\,f} + \dot{Q}_{kiss,\,fw1} + \dot{Q}_{kiss,\,fw2} = 0$$

**Figure 4-12: Differential Elements on Wraps of Scroll**

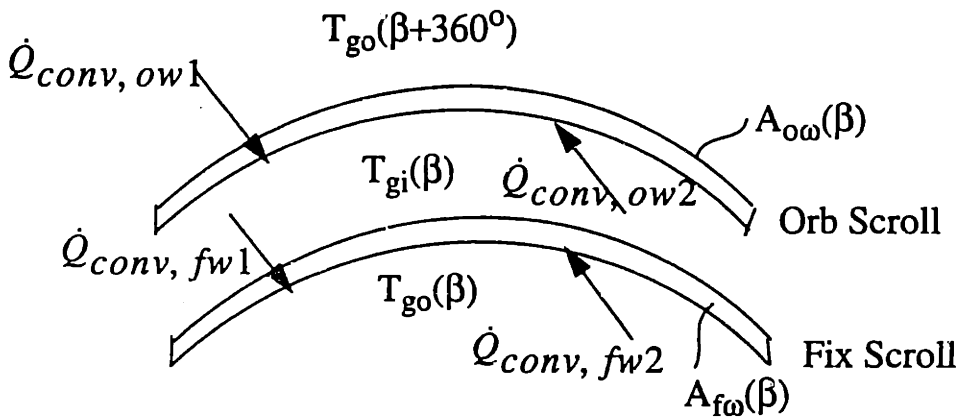


$$\dot{Q}_{conv,\,cw1} = h_{conv} A_{ow}(\beta) \cdot \langle T_{go}(\beta + 360°) - T_{ow}(\beta) \rangle$$

$$\dot{Q}_{conv,\,ow2} = h_{conv} A_{ow}(\beta) \cdot \langle T_{gi}(\beta) - T_{ow}(\beta) \rangle$$

$$\dot{Q}_{conv,\,fw1} = h_{conv} A_{fw}(\beta) \cdot \langle T_{gi}(\beta) - T_{fw}(\beta) \rangle$$

$$\dot{Q}_{conv,\,fw2} = h_{conv} A_{fw}(\beta) \cdot \langle T_{go}(\beta) - T_{fw}(\beta) \rangle$$

**Figure 4-13: Convection Between Scroll Wraps and Gas**

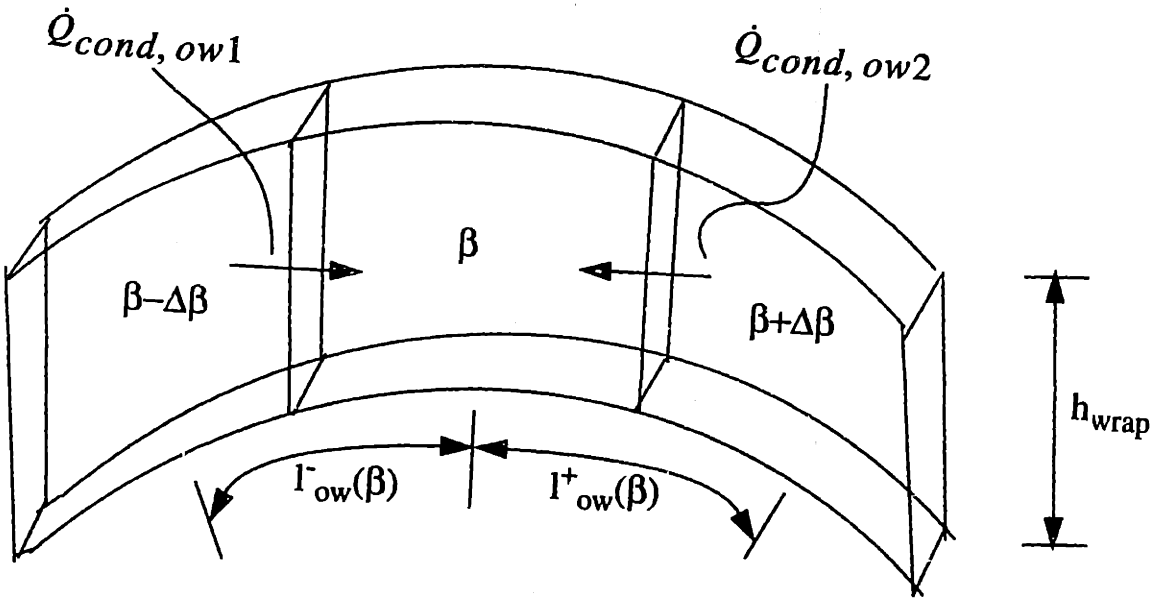


(a) Orbiting Scroll Wrap

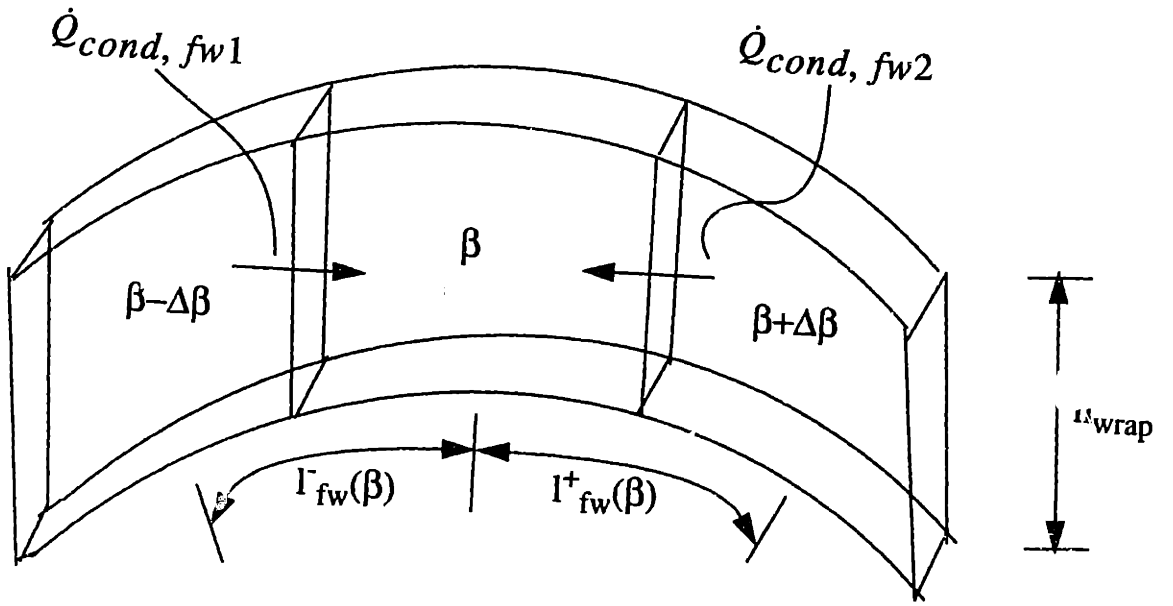


(b) Fixed Scroll Wrap

**Figure 4-14: Conduction Between Neighboring Wrap Elements**

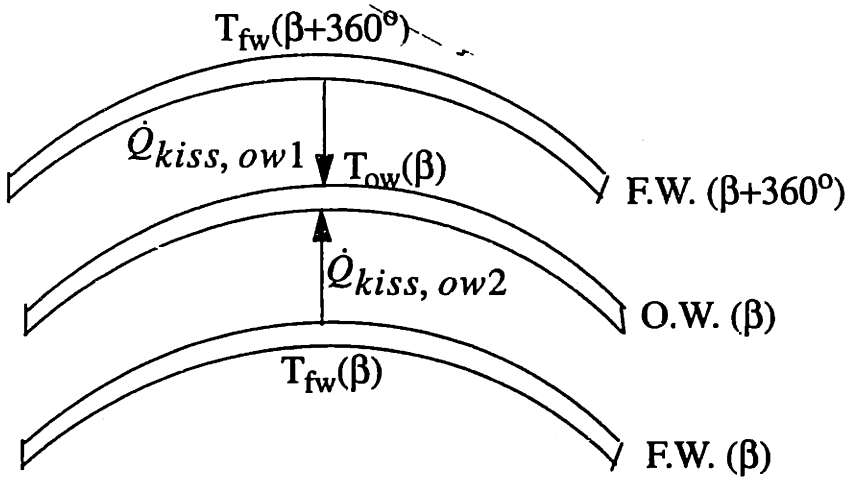


(a) Kissing Heat Transfer to Orb Scroll Wrap Element at β

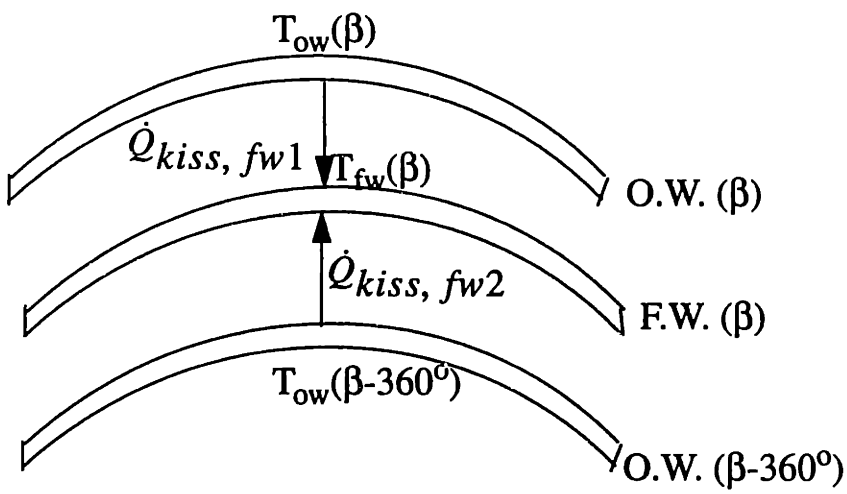


(b) Kissing Heat Transfer to Fix Scroll Wrap Element at β

**Figure 4-15: Kissing Heat Transfer Between Wraps**

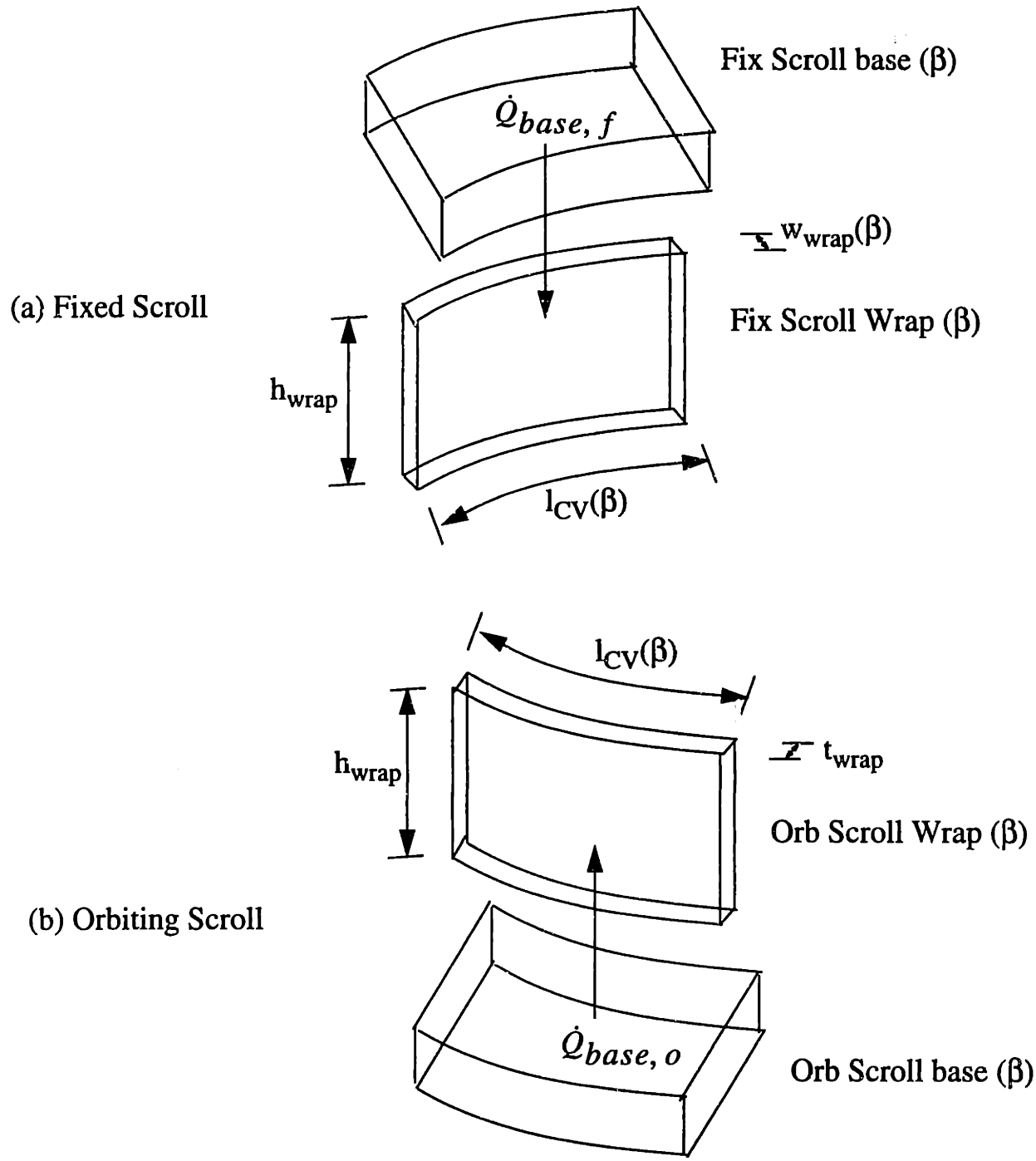


**Figure 4-16: Conduction Between Base and Wraps of Scroll**

Scroll Base is Discretized One-Dimensionally on the Basis of β

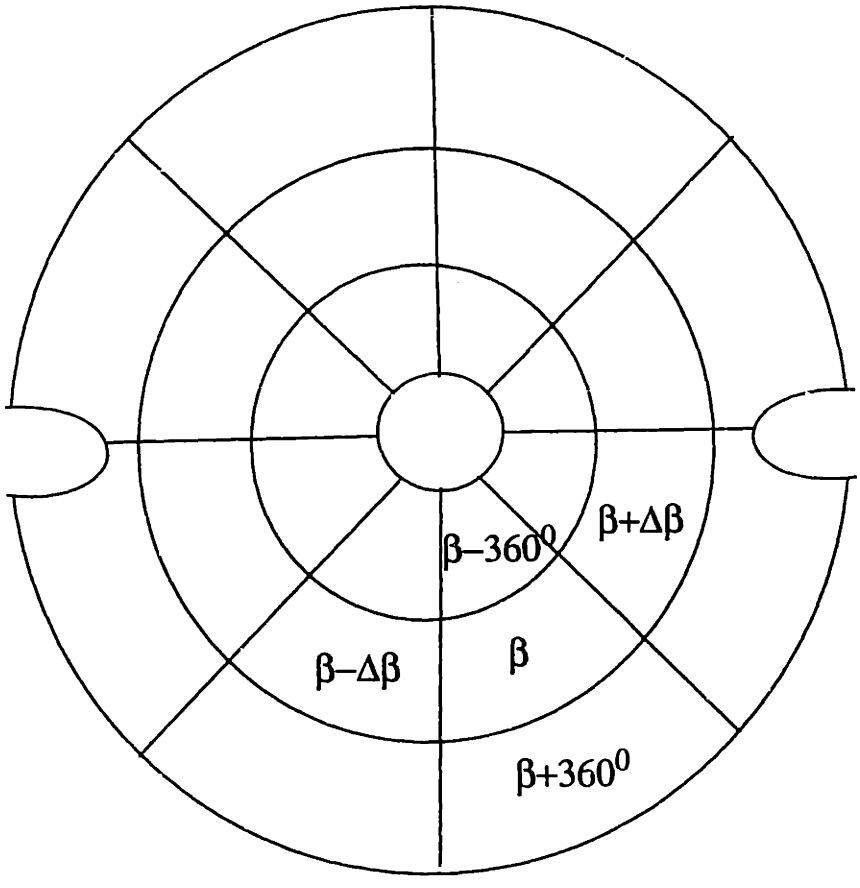


Every Element at location β is Completely Characterized by Its Radius r(β), its thickness $w_{base}(\beta)$, its width b, and its interaction with neighboring elements.

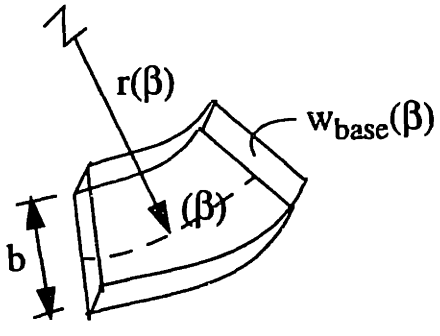


**Figure 4-17: One-Dimensional Discretization of Scroll Base**

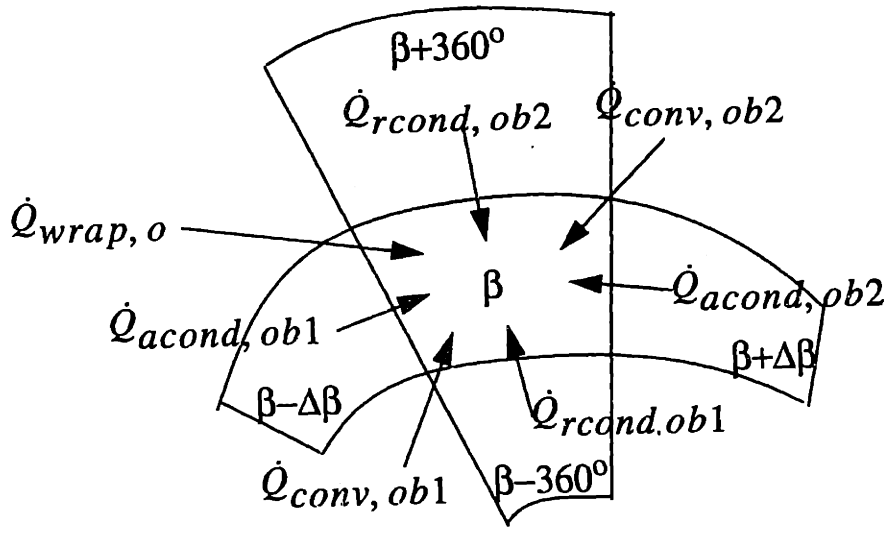


**(a) Orbiting Scroll Base**

$$\dot{Q}_{acond,\,ob1} + \dot{Q}_{acond,\,ob2} + \dot{Q}_{conv,\,ob1} + \dot{Q}_{conv,\,ob2} + \dot{Q}_{wrap,\,o} + \dot{Q}_{rcond,\,ob1} + \dot{Q}_{rcond,\,ob2} = 0$$

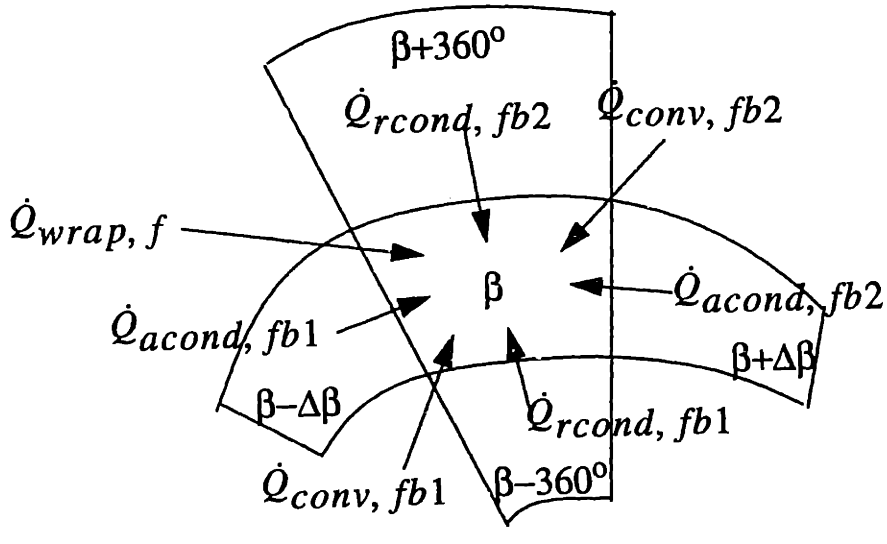


**(b) Fixed Scroll Base**

$$\dot{Q}_{acond,\,fb1} + \dot{Q}_{acond,\,fb2} + \dot{Q}_{conv,\,fb1} + \dot{Q}_{conv,\,fb2} + \dot{Q}_{wrap,\,f} + \dot{Q}_{rcond,\,fb1} + \dot{Q}_{rcond,\,fb2} = 0$$

**Figure 4-18: Energy Balance on Elements in the Bases of the Scroll**

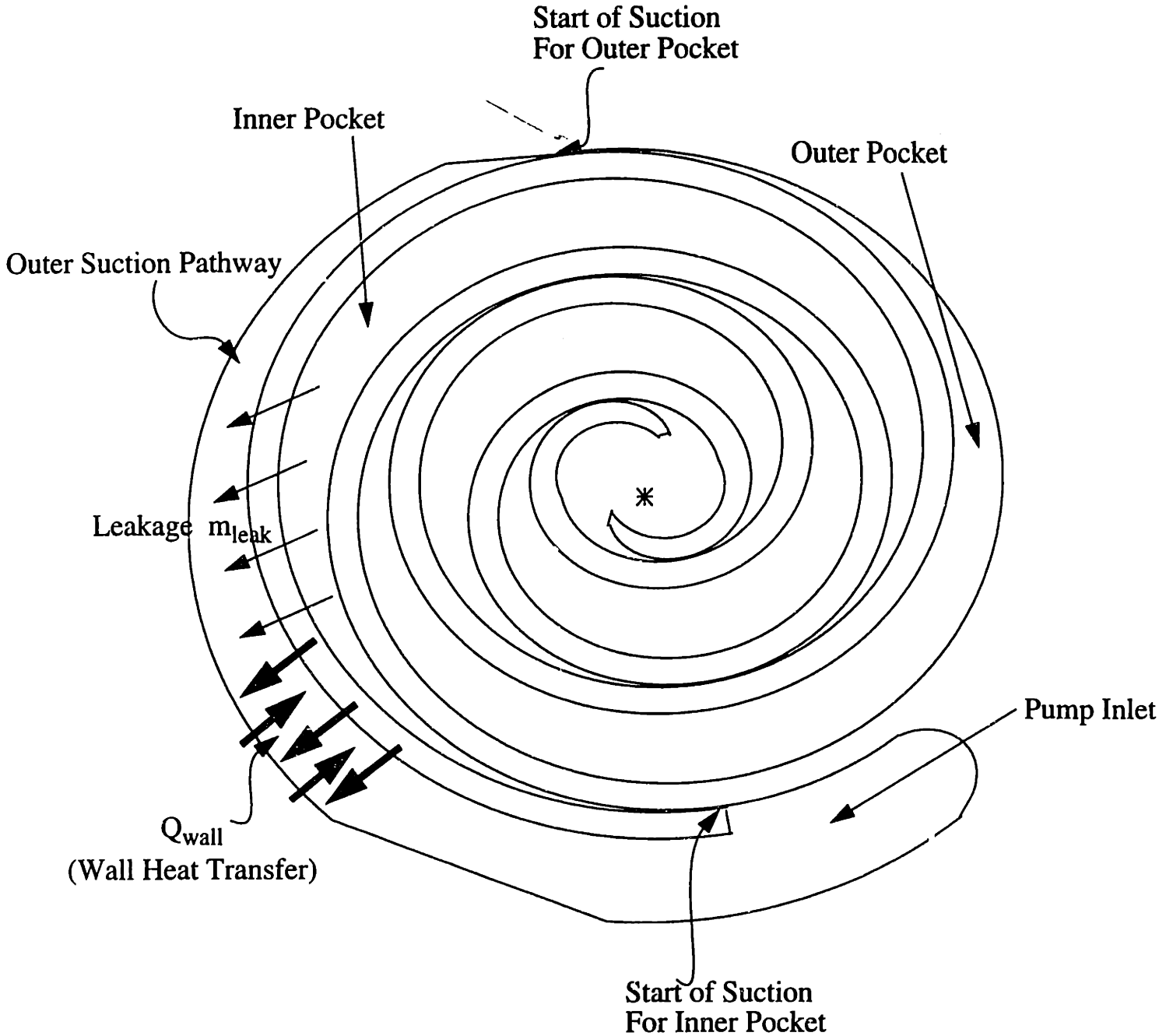


Gas in Outer Suction Pathway is Subject to Leakage and Heat Transfer Before It Reaches the Mouth of the Outer Suction Pocket

**Figure 4-19: Outer Suction Pathway of Scroll Pump**

# Chapter 5

# Results of Distributed Parameter Scroll Pump Model

## 5.1 Introduction

In this chapter, we present the results of the distributed parameter scroll pump model whose development was described in the previous chapter. First, we present the results for two conditions ARI-C and CHEER assuming no extraneous sources of irreversibility (other than blowin / blowout phenomena). Later, we incrementally add heat transfer and leakage to the model and demonstrate the effects of these sources of irreversibility on the performance of the pump. As part of the simulations, we also capture the wall temperature profile and show it to be qualitatively similar to the wall temperature data from the kissing heat transfer experiment.

## 5.2 Summary of Results

A quick summary of the results of the distributed parameter model are the following:

1. Kissing heat transfer tends to increase effective radial conductivity of the pump and thus lowers temperature differences across the walls of the pump from suction to discharge. Simulation of the wrap temperature profile without kiss-

ing heat transfer causes the cold spot associated with suction to disappear. Similarly, simulation of the base temperature profile without radial conduction causes the asymmetry associated with suction to disappear in the base temperature profile. The fact that angular asymmetry is such a dominant characteristic of wall temperature profiles observed from experiments is evidence that both kissing heat transfer and radial conduction on the base are very important modes of heat transfer in the pump.

2. Axial Conduction between wraps and base of the scroll is an important mode of heat transfer especially at the outer radii of the fixed scroll, as the resistance associated with this mode of heat transfer is relatively low at the thick outer walls of the fixed scroll.

3. Both heat transfer and leakage affect the mass flow rate of the machine significantly. This result indicates that suction heat transfer and leakage into suction are both important sources of irreversibility that cannot be neglected in a lumped parameter model of the pump.

4. For the closed cycle, as expected, leakage and heat transfer both contribute to the increase of the closed cycle polytropic coefficient. However, the effect of leakage is much greater than that of heat transfer indicating that the neglecting closed cycle heat transfer in the lumped parameter model is a reasonable approximation to make.

5. The inner and outer pockets differ in geometric layout, which affects the thermodynamic performance of the two pockets in two important ways. Firstly, the mass flow rate associated with the outer pocket is lower than that of the inner pocket because of the effects of leakage and heat transfer in the outer suction pathway. Secondly, the leakage profile from the outer pocket tends to be different from that for the inner pocket. Leakage out of the closed process of the inner pocket tends to be greater than that corresponding to the outer pocket due to the presence of the outer suction pathway. However, leakage from

discharge into the closed process of the inner pocket also tends to be greater than that corresponding to the outer pocket owing to the fact that the wrap length corresponding to the pressure difference is higher for the inner pocket than it is for the outer pocket. As a result, the net leakage (leakage in - leakage out) for both pockets tends to be about equal, thus leading to almost identical polytropic coefficients for both pockets. The gas temperatures for the outer pocket, however tend to be higher than that corresponding to the inner pocket as the outer pocket starts its closed process at a higher average gas temperature.

6. In order that the predictive capabilities of the lumped parameter model be improved, we present correlations that could be used to incorporate the effects of leakage in the lumped parameter model. Such correlations are based on simulation of a wide range of operating conditions, and serve to capture the correct lumped parameter formulation of the distributed internal leakage phenomena.

## 5.3 Inputs to the Distributed Parameter Model

In simulating the processes of gas within a scroll pump, we numerically solve the partial differential equations (PDEs) corresponding to gas continuity and energy balance, as were derived in the previous chapter. Simultaneously, we also solve for the metal wall temperature profile by solving equations of energy balance for the scroll pump walls in interaction with the gas. Iterative solutions of the gas and wall temperatures eventually converge to thermodynamically self-consistent gas and wall states. In order to solve the equations for the gas and wall, several models are necessary as inputs to the system, and are listed below.

1. The kinematics as well as geometry of the scroll pump are required as described in the previous chapter. Various quantities such as control surface velocities, cross-sectional areas, volumes of control volumes and heat transfer areas are calculated from a description of the pump geometry and kinematics.

2. We specify a correlation for convective heat transfer between gas and walls of the pump. We assume a uniform heat transfer coefficient throughout the pump, and use pipe-flow correlations as described in chapter 3 of the thesis. The heat transfer coefficient is assumed to depend only on the mass flow rate of refrigerant into the machine and takes the form, $h_{conv} = 1.26\dot{m}^{0.8}$ in $(Btu/hr/ft^2/^\circ F)$, where $\dot{m}$ is the mass flow rate specified in $lb/hr$.

3. We specify a kissing heat transfer coefficient of $h_{kiss} = 200\ Btu/hr/ft^2/^\circ F$, which is a conservative value for the kissing heat transfer coefficient estimated from the kissing heat transfer experiment.

4. We specify models for internal leakage based on orifice flow correlations as described in the previous chapter. The only matter remaining was to specify the orifice clearance gap itself. By a process of trial and error in matching the simulated values of the polytropic coefficient and mass flow rate for the CHEER operating condition with that obtained by experiments, we arrived at a discharge-side clearance of 0.3 mils for the pump, while the suction side clearance was assumed to be 0.05 mils. These clearances are reasonable assumptions to make since the wraps of the scroll are dished to about 0.8 mils between suction and discharge. Our assumption of these clearances was also justified by the fact that simulated values of mass flow rates and polytropic coefficients for other operating conditions of the pump also seemed to give good agreement with experiments.

## 5.4 Wall Temperature Profile

Here, we present the wall temperature profiles obtained by taking an average gas temperature profile as an input and separately turning "on" or "off" various modes of wall heat transfer. The principal point of such an exercise is that it lets us comprehend the effect of each mode of heat transfer separately. In this section, the average gas temperatures at every location in the pump are taken as being given though

they themselves have to be calculated out of gas side calculations. In describing wall temperature profiles, we simulate the $-10/90/10$ operating condition on a scroll pump, since this is one operating condition for which experimental wall temperature data is available from the kissing heat transfer experiment.

1. In the most basic simulation, we allow convection between gas and the pump walls as well as conduction along the walls in the circumferential direction. However, we neglect axial conduction between base and wraps, neglect kissing heat transfer between wraps of the fixed and orbiting scroll, and neglect radial conduction in the walls of the base of the fixed and orbiting scrolls. The resultant temperature profiles are then the mostly monotonic graphs shown in figure 5-1(a) and 5-1(b). It is educational to compare the temperature profile of the fixed scroll from figure 5-1(a) to the data obtained from the kissing heat transfer experiment in figure 5-4. We observe that none of the characteristic non-monotonicities (or humps) in the base and wrap temperature profiles are reproduced by the simulation. It must be noted that we don't have experimental data on the temperature profiles of the orbiting scroll. Hence, all comparisons of experiment and simulations are done only for the fixed scroll.

2. When we add radial conduction as a mode of heat transfer on the base, and kissing heat transfer as a mode of radial heat transfer in the wraps, the temperature profiles that we get from the simulation are those shown in figures 5-2(a) and 5-2(b). The most important difference between these graphs and the ones in figures 5-1(a) and 5-1(b), are the characteristic humps on the base and wrap temperature profiles. The wrap temperatures exhibit a cool spot associated with a position 360° inwards from the suction port of the pump. Thereafter, the wrap temperature profile becomes monotonically increasing with angular distance from the suction port. The base temperature profile on the other hand exhibits the effects of the suction port asymmetry all the way from suction through to discharge. This is due to the fact that the radial conductance of the base of the fixed scroll remains fairly high all the way from suction to

discharge, while kissing heat transfer conductance tends to start getting lower as one progresses from suction through to discharge. The higher radial thermal conductance of the fixed scroll base also contributes to the base being more isothermal than the wraps of the scroll. The temperature profiles obtained from the simulations are still, however different from those obtained in the experiment in one crucial aspect, which is the divergence of wrap and base temperatures all the way from suction to discharge.

3. Finally, we turn on axial conduction also as an extra mode of thermal communication between wraps and the base of the fixed and orbiting scrolls. The temperature profile that is obtained is that shown in figures 5-3(a) and 5-3(b). The simulated temperature profile in figure 5-3(a) is now very similar to that obtained for the walls of the fixed scroll from the kissing heat transfer experiment. Figure 5-4 plots the wall temperature profiles obtained from experiment and simulation on the same graph, in order that they can be compared. We observe that axial conduction plays a major role in bringing wrap and base temperatures of the fixed scroll closer to each other, thus making the simulations of figure 5-3 different from those of figure 5-2. This mode of heat transfer is especially significant at the outer most wall of the fixed scroll where wall thickness is large enough for axial conduction to be a major mode of heat transfer. While the temperature profiles obtained from simulation are now qualitatively similar to those obtained from the experiment, they still differ in some aspects. Specifically, we note that the experimental values of fixed scroll wrap and base temperatures near discharge are higher than the corresponding values obtained by simulation. We think that this difference occurs because our simulations assume a uniform convective heat transfer coefficient at all points within the pump. Since densities and mass flow rates (due to leakage and blow-in/blow-out mass) are higher at discharge than at suction, it is likely that heat transfer coefficients at discharge are higher than those at suction. In the interests of keeping the distributed parameter model simple, we restrict ourselves to a uni-

form convective coefficient.

The lessons drawn from these simulations of the wall temperature profile are then that radial conduction in the base and kissing heat transfer in the wraps play the analogous role of increasing effective radial thermal conductivity of the metal, thus leading to the presence of "cold spots" associated with the suction port of the pump. Axial conduction between base and wraps is also found to be an important mode of heat transfer.

## 5.5 Gas Processes

We now simulate the gas processes with various sources of irreversibilities modeled, and consider the effect of these irreversibilities on the gas side simulations. The gas side simulations are distinctly divided into 3 parts, namely suction, the closed process and discharge. The 3 stages of compression for the inner pocket differ from those of the outer pocket, due to differences in starting thermodynamic states, heat transfer and leakage profiles. Such differences will be pointed out in the section below. For the purposes of this chapter, we simulate two of the most common compressor test conditions, namely $ARI-C$ (45/130/65), and $CHEER$ (45/100/65). These are both test conditions with suction pressure set to the saturation pressure corresponding to $45°F$, and with a $20°F$ superheat at compressor suction. The discharge pressure for $ARI - C$ is the saturation pressure corresponding to $130°F$, while it is that corresponding to $100°F$ for $CHEER$. The lessons learned from the simulations of these two operating conditions are equally applicable to other operating conditions. Of the two operating conditions, $ARI-C$ represents a blow-in condition on the pump, while $CHEER$ represents a blow-out condition. Simulation results for $ARI - C$ and $CHEER$ are summarized in tables 5-1 and 5-2 respectively.

One of the results that we hope to get out of a distributed parameter model is the equivalent lumped parameter formulation of leakage phenomena. In order to arrive at leakage correlations (for leakage into the closed cycle, and for leakage into suction), we simulate a wide variety of operating conditions and arrive at empirical relationships

that can then be used in lumped parameter models.

### 5.5.1 Suction

1. First, we simulate the suction process without any sources of irreversibility modeled. $ARI-C$ was simulated with a pump inlet temperature of $83°F$, while $CHEER$ was simulated with a pump inlet temperature of $80°F$. Unsurprisingly, the volumetric efficiency of the scroll pump (with reference to the pump inlet state) was predicted to be 100%, with no increase in gas temperature predicted for the process of suction (see figures 5-5 and 5-10). The resultant mass flow rates ($\dot{m}$) and gas temperatures at the end of suction ($T_1$) are those shown in Tables 5-1 and 5-2 below.

2. Now, we simulate the suction process for the inner pocket with heat transfer modeled, but with no leakage effects incorporated into the process. It must be noted that the model now incorporates heat transfer for all stages of compression, not just suction. This is done so that the overall pump model remains energy consistent. As expected, the mass flow rate of refrigerant into the pump falls, while gas temperature in the pockets rises. The mass flow rates and temperatures are shown in Tables 5-1 and 5-2 below. A comparison with the experimental observed mass flow rates of the $ARI$ and $CHEER$ conditions indicate that heat transfer alone is not sufficient to account for the loss in volumetric efficiency of the scroll pump. This can be also be interpreted as evidence that leakage into suction is an important source of irreversibility that ought not to be neglected,

   A plot of the suction pocket average temperature vs pocket volume (in figures 5-5 and 5-10) reveals an interesting feature about the pattern of heat transfer. The average temperature of gas in the suction pocket first reaches a high value at the start of suction owing to the fact that a small volume of gas entering the pump is exposed to a large surface area of hot suction side scroll pump walls. Thereafter, as more gas enters the pump, the average pocket temperature actually falls

(though it never falls lower than the pump inlet temperature), followed by a gradual rise in average gas temperature. The last stages of suction, which are characterized by diminishing pocket volume is where the last spurt of gas temperature heating seems to take place. While it may be tempting to ascribe this final rise in temperature to a thermodynamic artifact (due to $P-V$ work of the diminishing suction pocket volume), such an explanation can be discarded because our gas equations neglected momentum effects thus forcing the suction pocket to remain at suction pressure even as its volume is diminishing.

3. Leakage effects are now incorporated into the model. It must be noted that leakage is at this stage incorporated into all stages of the model starting from suction to discharge. This is done in order to keep mass and energy flows in the model consistent. In modeling leakage into suction, we assume a tip clearance between scrolls of approximately 0.05 mils (thousandths of an inch). This is a reasonable clearance to assume since the wraps of the scroll pump are dished to a height difference of 0.8 mils between suction and discharge. As a result of simulating leakage effects into suction, the mass flow rate of refrigerant into the suction pocket falls even further, while the average temperature of gas in the pocket rises to a higher value than the temperature obtained with only suction heat transfer. The mass flow rates and temperatures corresponding to this case are listed on Tables 5-1 and 5-2, and indicate that leakage in combination with heat transfer is sufficient to account for the volumetric efficiency loss of the machine. For the $ARI-C$ condition, we observe that leakage and heat transfer each play about equal parts in explaining the reduction of mass flow rate into the inner pocket of the machine. For the $CHEER$ operating condition on the other hand, leakage plays a more important role than does heat transfer in reducing mass flow rates in the inner pocket of the machine.

Figures 5-5 and 5-10 show plots of the average gas temperature of the suction pocket against pocket volume. As observed from the graph, the temperatures display the same qualitative characteristics as those obtained with leakage ne-

glected. The average gas temperatures for this case however always exceed those obtained in the previous simulation. In simulating other pump operating conditions that are not reported here, we find that scroll tip clearances of 0.03 mils to 0.07 mils are always sufficient to explain volumetric efficiency losses for the scroll pump. In the interests of consistency, we restrict ourselves to a suction side tip clearance of 0.05 mils.

4. The outer suction pathway of the scroll undergoes leakage and heat transfer, which cause the average state of gas at the start of the conjugate sections of the outer pocket to be at higher temperature than that corresponding to the inner state. We simulate the outer suction pathway as simply being a channel where leakage and heat transfer occur, and observe that the suction gas attains a higher temperature even before it reaches the sections of the pump where the outer pocket starts to undergo suction (as defined by the surfaces of the fixed and orbiting scrolls becoming conjugate). For both $ARI-C$ and $CHEER$, gas temperature increases by about $5°F$ between start and end of the outer suction pathway.

5. As with the inner pocket, we incrementally add on sources of irreversibility in the form of leakage and heat transfer to the gas in the outer pocket, and evaluate its impact on pump volumetric efficiency and mass flow rate, the results of which are shown in tables 5-1 and 5-2. Unlike the inner suction pocket, we observe that heat transfer and leakage play equally important roles in lowering refrigerant mass flow rate for $CHEER$, with heat transfer accounting for about 2/3 of loss in mass flow rate for the $ARI-C$ operating condition.

6. A general trend observed from simulation of a large number of operating conditions is that suction heat transfer becomes very significant for high load operating conditions, while leakage into suction becomes significant as suction pressure rises. $ARI-C$ is a high load operating condition with high temperature differences across the pump, which is why suction heat transfer tends to be important at this operating condition in comparison to $CHEER$ which is a low

load operating condition, with low temperature differences across the pump. Both $ARI - C$ and $CHEER$ have (identically) high suction pressures, thus making leakage into suction fairly important to both operating conditions.

7. Table 5-3 shows the leakage into suction calculated for 6 operating conditions of the pump ranging from a low suction pressure corresponding to $-10°F$ on the evaporator to a high suction pressure corresponding to $55°F$ on the evaporator. A regression of the leakage mass flow rate versus pressure difference across the pump and suction density reveals almost no dependence on the former, and a very strong dependence on the latter. This can be explained by the fact that the outer wraps of the scroll don't see a pressure difference across them that is very dependent on overall pump pressure ratio. Any mass that leaks across such a pressure difference however is at a density (and pressure) that is fairly close to that of suction. This dependence on density shows up in the regression in the form shown below.

$$\dot{m}_{leak,suc} = 4.46\rho_L \qquad R^2 = 0.99$$

This expression is one that can directly be plugged into a lumped parameter model of the pump. For the purposes of the lumped parameter model, we assume that leakage into suction is characterized by an enthalpy that is the arithmetic mean of that for corresponding suction and discharge states.

### 5.5.2 Closed Process

1. We now simulate the closed process, with sources of irreversibility added incrementally. First of all, we simulate the closed process without any sources of irreversibility modeled. As expected, the results of the simulation are identical to what we might expect from an isentropic closed process. The resultant polytropic exponent for the entire closed process is simply the isentropic exponent, which leads to a closed process end pressure that is considerably less than that observed experimentally (for both $ARI - C$ and $CHEER$ operating

conditions). This implies that that sources of entropy are clearly important to the closed process and that they do need to be incorporated into a closed process model. Average closed pocket gas temperatures are plotted as a function of pocket volume in figures 5-6 and 5-11 for ARI-C and CHEER respectively, and both exhibit a clear and non-surprising trend of pocket temperature rising with diminishing pocket volume.

2. We incorporate heat transfer effects to the closed process of the inner pocket. In figures 5-6 and 5-11, we plot the average pocket temperatures as a function of pocket volume. As observed from the graphs, the temperature plot seems to proceed in a parallel fashion to that obtained from the isentropic simulation other than for a bulge at the center. This is a symptom of heat being transferred to the gas at the early stages of the closed cycle, followed by heat being transferred away from it towards the end. The net heat transferred to the closed cycle is therefore quite small and is insufficient to alter the closed cycle polytropic coefficient significantly. A plot of the $P - V$ process for the simulations can be seen in figures 5-9 and 5-14 respectively, which conclusively demonstrate that closed process heat transfer cannot account for much of the irreversibility associated with the closed process of a scroll pump. We note the starting temperature of the gas for this simulation is higher than that corresponding to the case with no heat transfer. This is because heat transfer is modeled for this simulation, not just for the closed process, but for all stages of compression. As a result, gas in the pump pocket at the send of suction (or start of the closed process) is at a higher temperature than that corresponding to the siulation with no heat transfer effects.

3. We finally incorporate leakage effects into the closed process for the inner pocket. As with heat transfer effects, we simultaneously incorporate leakage effects into all stages of compression. Leakage to the closed pocket occurs from portions of the outer pocket undergoing advanced stages of the closed process (for about 20% of the time), and from the discharge portions of the outer pocket. Leakage

also occurs from the inner pocket's closed process to the suction process of the outer pocket, and to the outer suction pathway of the outer pocket. As mentioned earlier, we use a tip clearance of 0.3 mils to calculate leakage rates into the closed process from discharge, while we use a tip clearance of 0.05 mils to calculate leakages out of the closed pocket. Figures 5-6 and 5-11 show plots of the closed cycle average gas temperature as a function of pocket volume. A comparison of the temperature profiles obtained for this simulation versus those obtained for the isentropic and heat transfer simulations demonstrate that leakage produces a clear net influx of energy (and entropy) into the closed cycle. The effect of leakage is also clearly observable in the $P-V$ plots of figures 5-9 and 5-14, which clearly demonstrate that leakage accounts for the bulk of closed cycle irreversibility, thus justifying our assumption of neglecting closed cycle heat transfer in a lumped parameter model of the scroll pump.

4. The outer pocket's closed process differs from that of the inner pocket in two important ways. Firstly, the starting state of the closed process for the outer pocket tends to be hotter than that corresponding to the inner pocket. This difference is ascribable to the fact that the gas in the outer pocket undergoes heat transfer and leakage in the outer suction pathway followed later by the suction process. The gas in the inner pocket on the other hand, does not undergo heat transfer and leakage before the suction process.

   A second aspect in which the outer pocket differs from the inner pockets is in leakage profiles. Gas from the inner closed process leaks for a portion of time to the outer suction process, while it leaks at other times to the outer suction pathway. On the other hand, the closed process in the outer pocket only leaks to the suction process of the inner pocket. There is no leakage from the outer pocket corresponding to leakage from the inner pocket to the outer suction pathway. Thus, there is less leakage out of the outer pocket's close process than that corresponding to the inner pocket.

   The lower leakage out of the closed process of the outer pocket, however seems

to be compensated by a lower leakage into the closed process than that corresponding to the the inner pocket. The reason for this is that the scroll wraps across which mass leaks are smaller in length for the outer pocket than they are for the inner pocket. Thus, leakages into the closed process of the outer pocket are also lower in magnitude than corresponding leakages to the inner pocket.

As a result of both leakages in and out of the outer pocket's closed process being less than that corresponding to the inner pocket, the net leakage into the outer pocket's closed process tends to be almost identical to that of the inner pocket. And since it is leakage that is the predominant determinant of the polytropic coefficient of the closed process, the pressure profiles of the inner and outer pockets are remarkably identical. The only major difference between inner and outer pockets then tends to be in the gas temperatures that are higher for the processes of the outer pocket than they are for the inner pocket.

5. As with the process of suction, we are interested in deriving a physically based correlation for leakage into the closed process, since such a relationship finds direct use in the lumped parameter scroll pump model. Table 5-4 displays the leakages observed from simulations of 6 operating conditions of the scroll pump. Unlike leakage into suction, leakage into the closed process is affected by the pressure difference across the pump. Indeed its principal source is the discharge side of the pump, while its principal sink is the closed process, whose intermediate pressures depend heavily on the suction pressure. Therefore, we regress the leakage mass flow rates observed against pressure difference and density of fluid at the discharge side.

$$\dot{m}_{leak,dis} = 1.73\sqrt{\rho_H \Delta P} \qquad R^2 = 0.99$$

As before, the expression obtained above is one that finds direct use in lumped parameter models of the scroll pump.

### 5.5.3 Discharge

1. We now simulate the discharge process. The discharge process is characterized at the beginning by a pressure equilibration process whereby gas blows in or out of the pockets to equilibrate pressure with the discharge tube. In the two conditions we simulate, *ARI* is a blowin process, while *CHEER* is a blowout process (provided sources of irreversibility are incorporated into the model for the closed process). The discharge process, when simulated without leakage or heat transfer tends to be an isothermal process as characterized by the pocket temperature profiles shown in figures 5-7 and 5-12 respectively. Since a blow-in process is characterized by a sudden addition of high temperature mass into a fixed volume (corresponding to the end of the closed process), blow-in is characterized by an immediate rise in average pocket gas temperature (as in figure 5-7). Blow-out on the other hand involves a reduction of mass from a fixed volume in order to bring it to a lower pressure. It is therefore characterized by an immediate drop in gas temperature (as seen in figure 5-12).

2. When heat transfer is modeled as part of the discharge process, the temperature of the gas falls as the process of discharge progresses, as shown in figures 5-7 and 5-11. Leakage, has a further cooling effect on the discharge process since it lowers the mass flow rate of gas leaving the pump, and also takes away enthalpy from the discharge stream, as observed from the lower discharge temperatures in the graphs on figures 5-7 and 5-11.

3. The outer pocket's discharge process differs from that of the inner pocket principally in that its mean gas temperature is higher than that for the inner pocket. As a result, the discharge process for the outer pocket proceeds identical to that for the inner pocket except for the fact that it remains hotter than gas in the inner pocket throughout the process.

4. It should be pointed out that the very act of choosing the discharge temperature of the pump is an iterative process, since the discharge temperature of the pump

is directly determined by all the heat transfer and thermodynamic processes that occur in the pump. In our simulations, we choose discharge temperatures that provide an overall energy balance on the gas side processes of the pump.

## 5.6 Conclusions

In this chapter, we described the results of the distributed parameter model of a scroll pump paying specific attention to two specific operating conditions, namely $ARI-C$ and $CHEER$. The lessons drawn from the simulations are however, applicable to most other operating conditions as well. Our simulations showed us that leakage as well as heat transfer were important sources of irreversibility at suction, and that both therefore needed to be incorporated into a lumped parameter model of the scroll pump. We observed that the effects of heat transfer on closed process irreversibility were quite negligible and that it was reasonable to ascribe all closed cycle irreversibility to leakage in a lumped parameter model. We observed that the inner and the outer pockets differed in performance owing to the increased heat transfer and leakage that gas in the outer pocket is subject to. As a result, the mass flow rates and volumetric efficiencies of the outer pocket are lower than those of the inner pocket. The pressure profiles in the two pockets of the scroll pump are however found to be nearly identical. We simulated a variety of operating conditions and estimated correlations for leakage into suction, and into the closed process, that are directly applicable to a lumped parameter model of a scroll pump. Leakage into suction was found to be dependent principally on the density of the suction state, while leakage into the closed process was found to depend on the pressure difference across the pump as well as the density of the discharge state.

In studying the heat transfer processes of the wall, we observed that radial conductivity of the scroll base and kissing heat transfer in the scroll wraps played analogous roles and were responsible for the existence of the cold spots associated with the suction port in the scroll pump. We also observed that axial conduction between scroll wraps and base is an important mode of heat transfer especially at the outer

radii of the fixed scroll. This mode of heat transfer tends to bring wrap and base temperatures closer to each other.

**Pump Operating Condition -10/90/10**

(a) Fixed Scroll

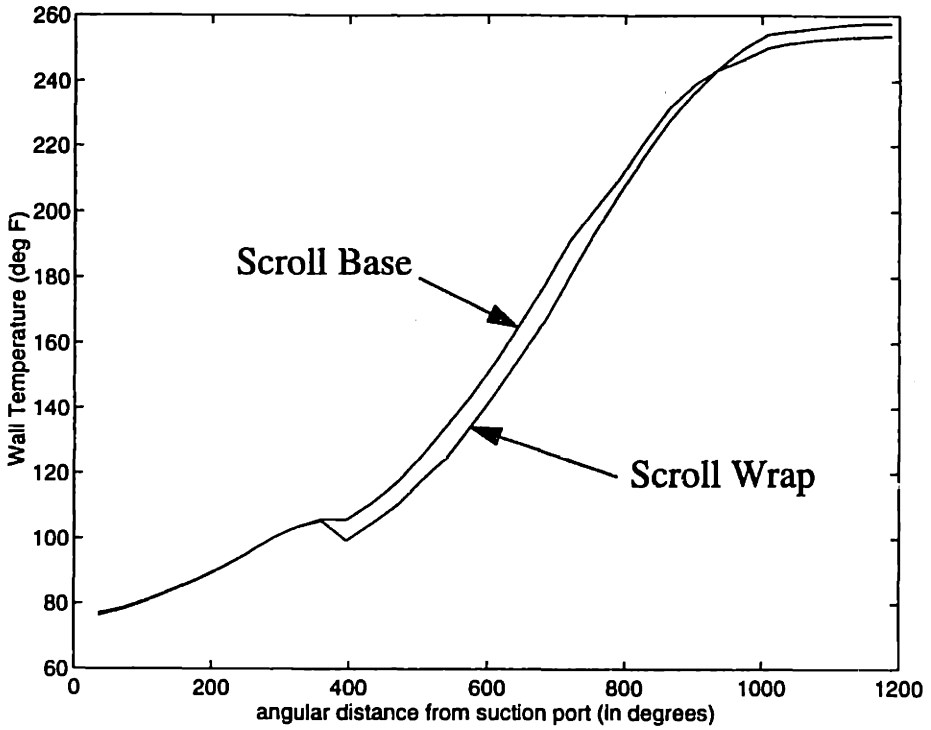


(b) Orbiting Scroll

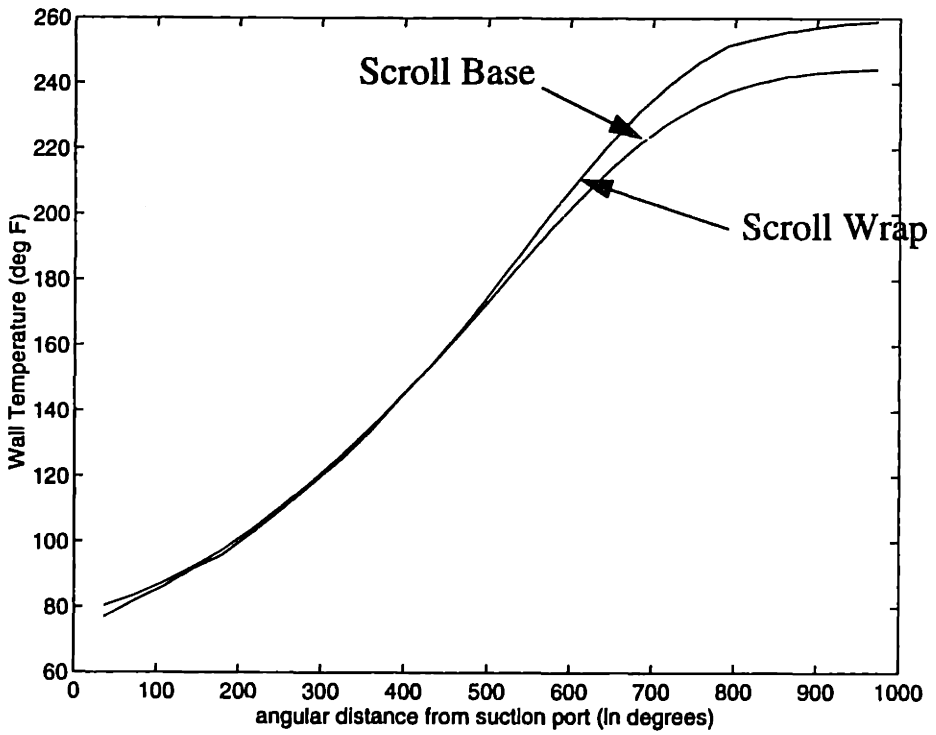


Figure 5-1: Scroll Wall Temperatures (No Radial Conduction, No Axial Conduction, No Kissing Heat Transfer)

**Pump Operating Condition -10/90/10**

(a) Fixed Scroll

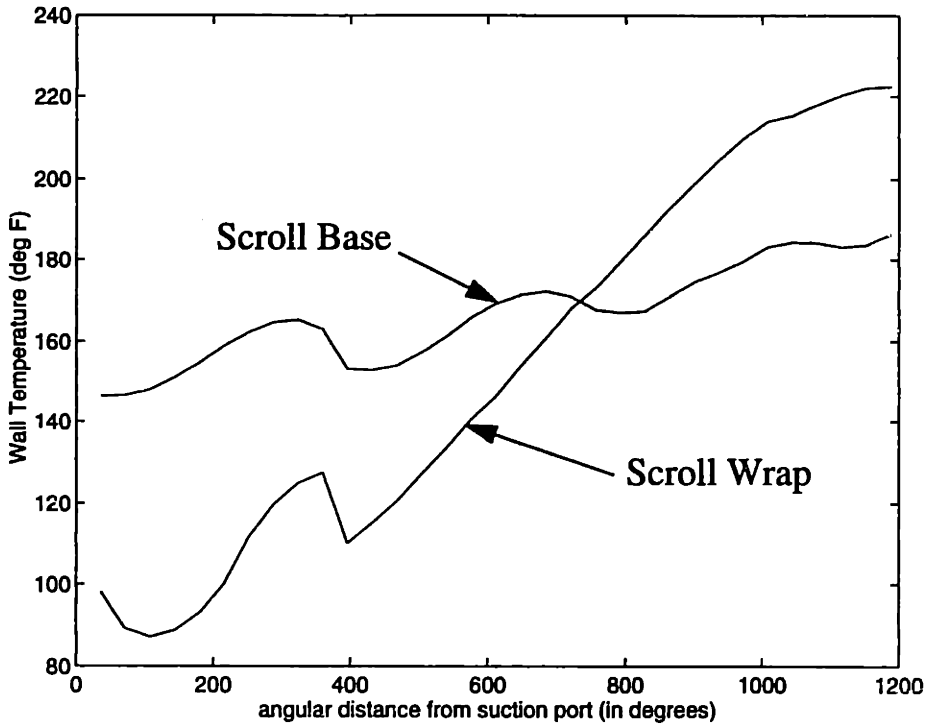


(b) Orbiting Scroll

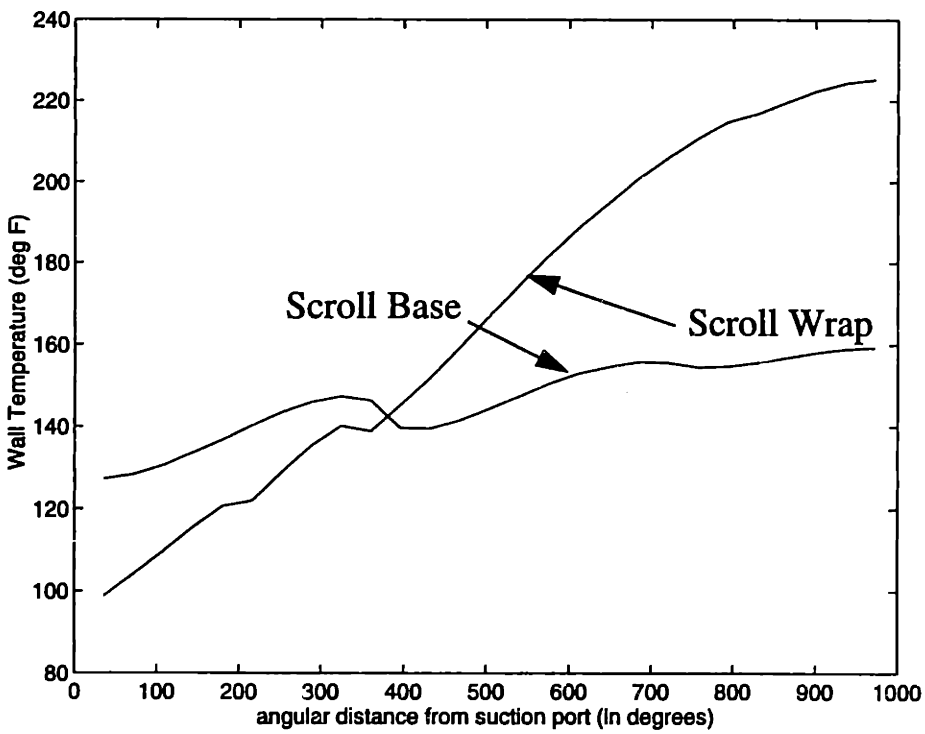


Figure 5-2: Scroll Wall Temperatures (Radial Conduction Allowed, Kissing Heat Transfer Allowed, No Axial Conduction)

**Pump Operating Condition -10/90/10**

(a) Fixed Scroll

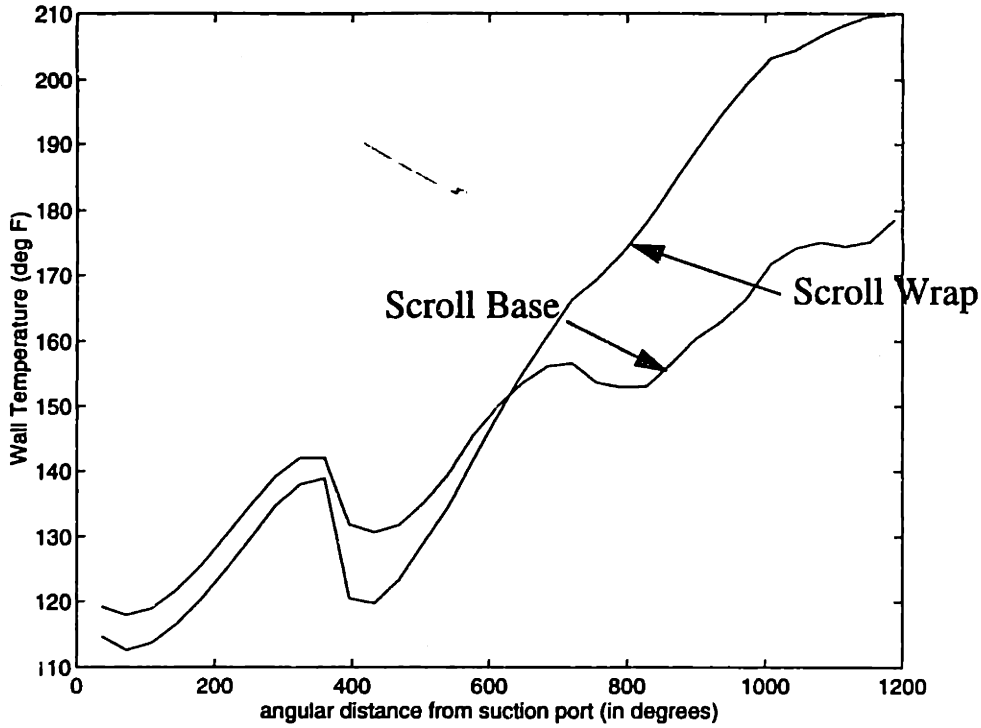


(b) Orbiting Scroll

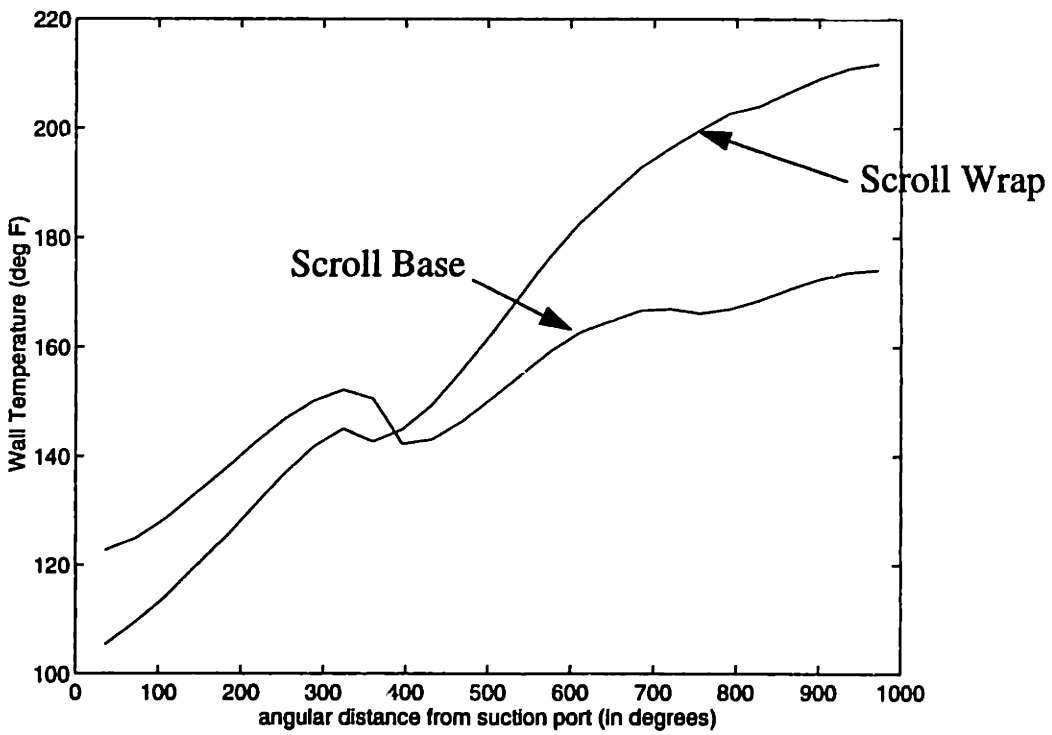


Figure 5-3: Scroll Wall Temperatures
(All Modes of Heat Transfer Allowed)

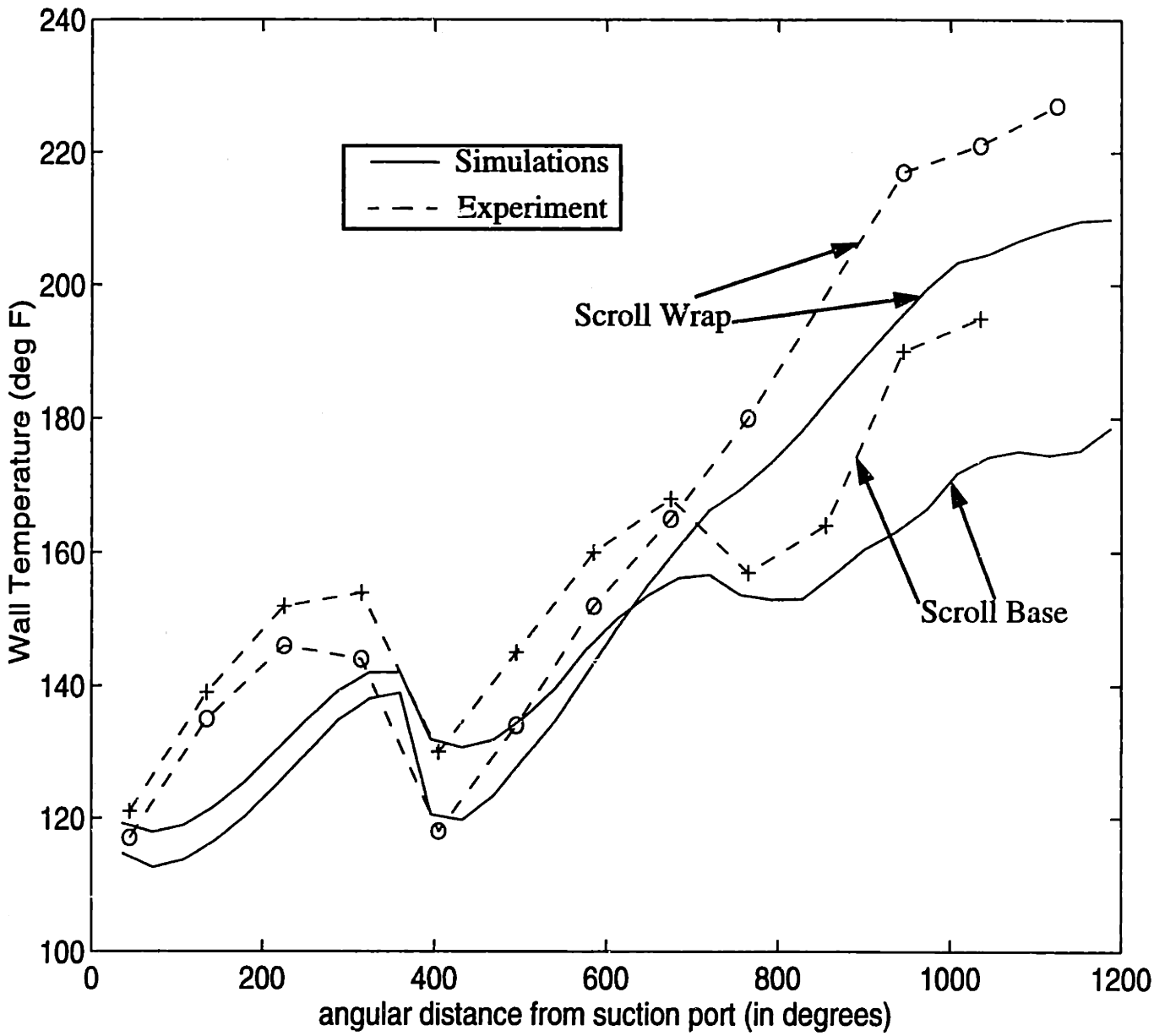


Figure 5-4: Fixed Scroll Wall Temperature Profile - A Comparison of Experimental Data with Simulations.

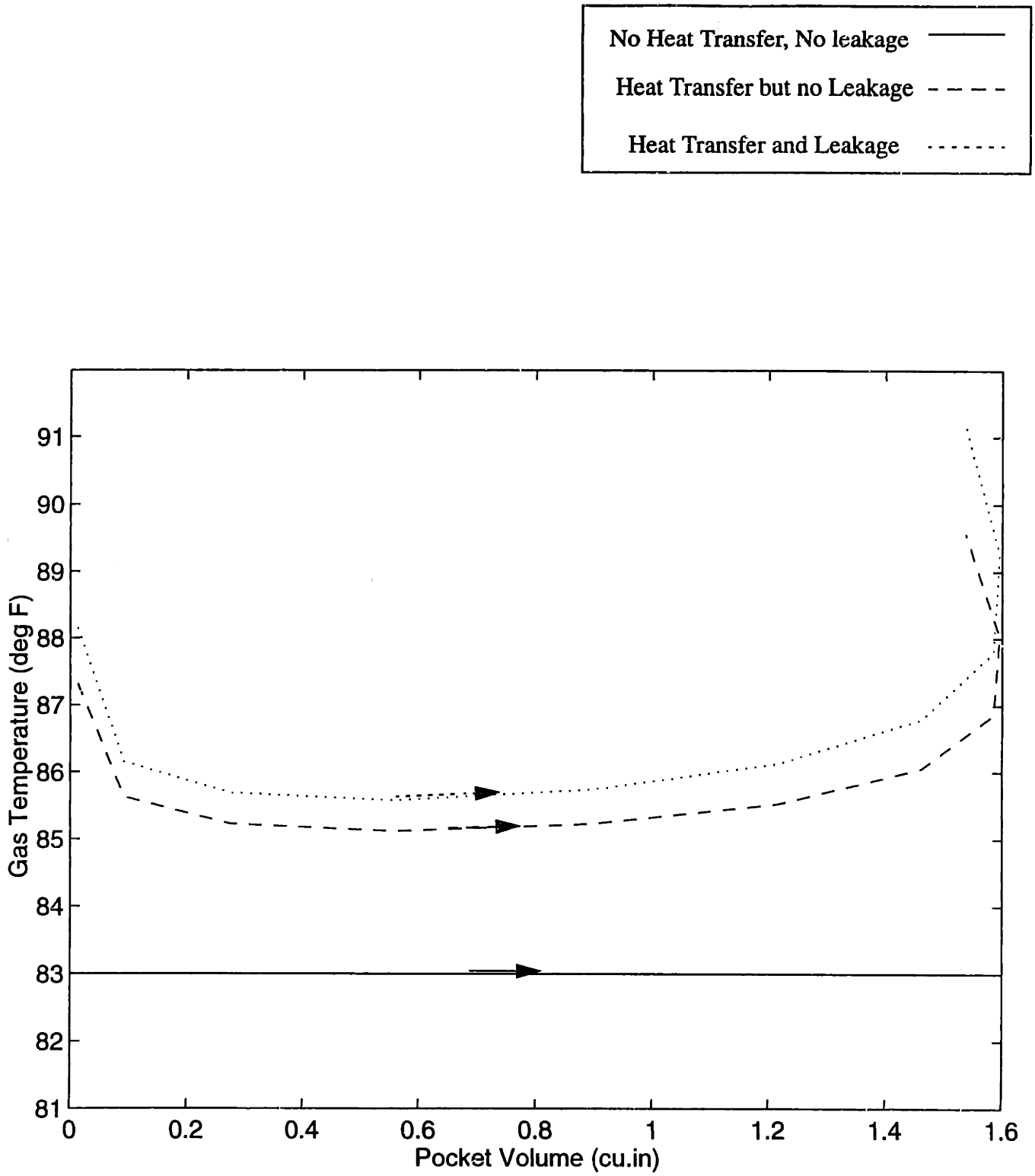


Figure 5-5: Average Gas Temperature Vs. Pocket Volume for Suction Process of ARI-C

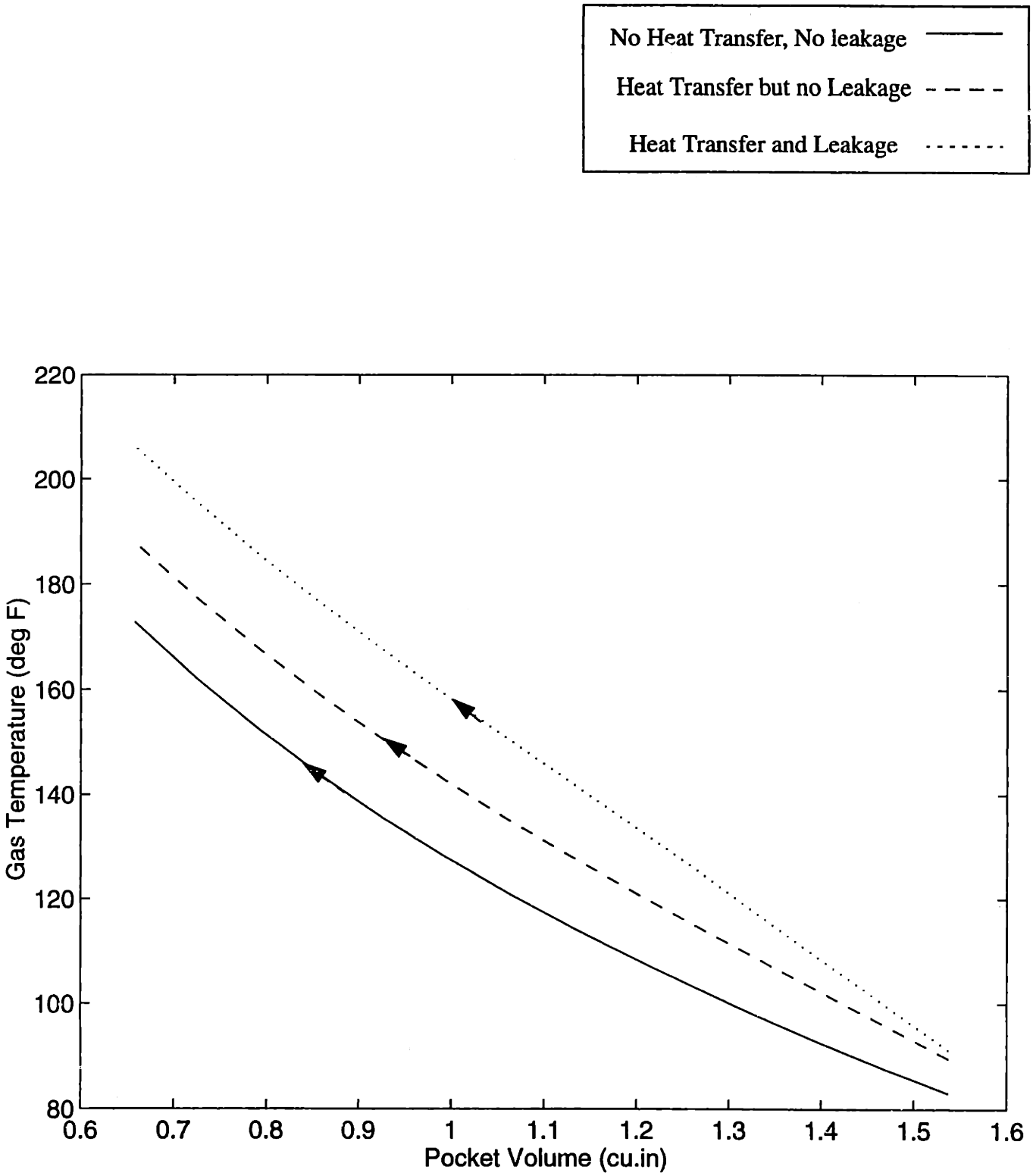


Figure 5-6: Average Gas Temperature Vs. Pocket Volume for Closed Process of ARI-C

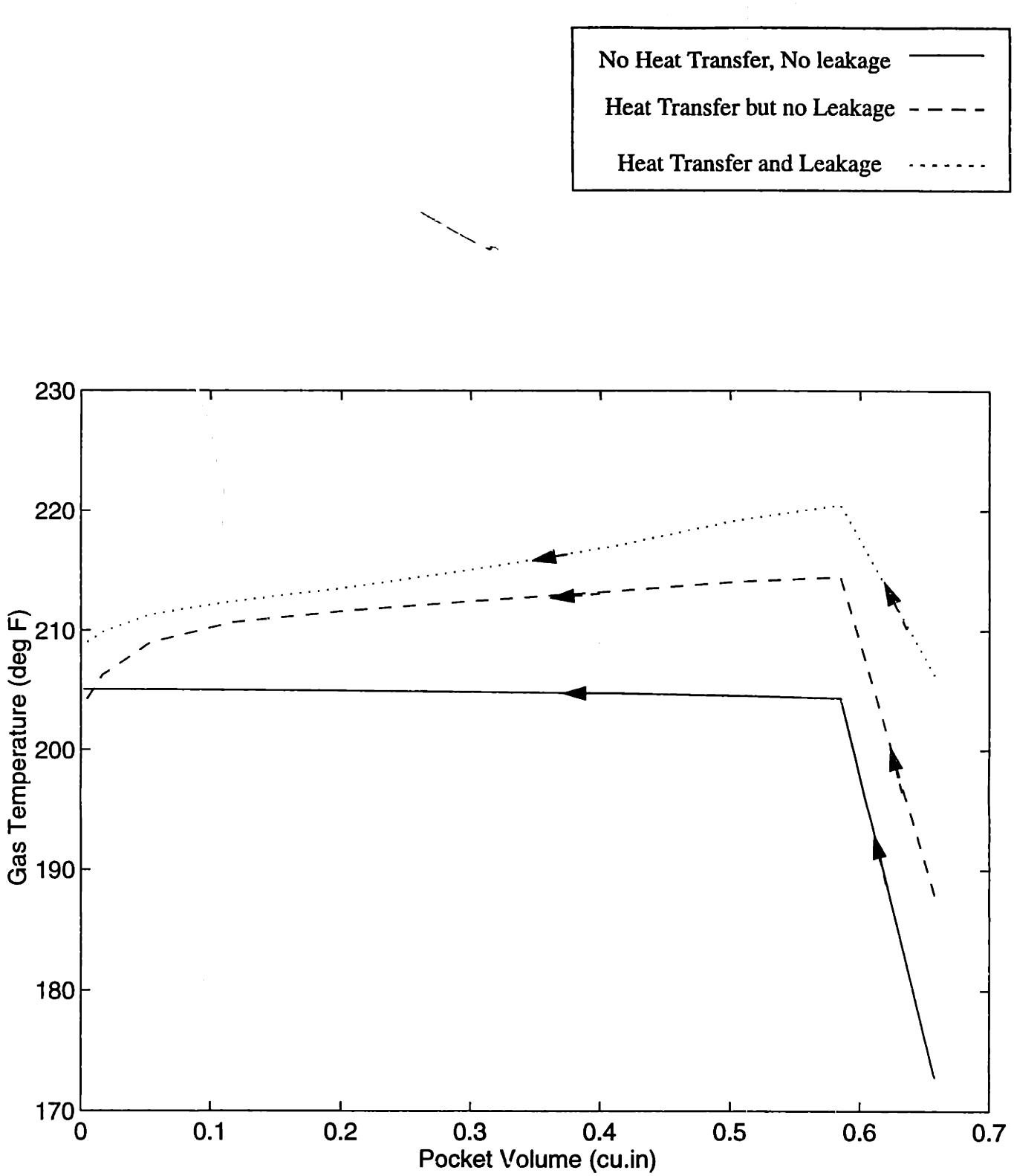


Figure 5-7: Average Gas Temperature Vs. Pocket Volume for Discharge Process of ARI-C

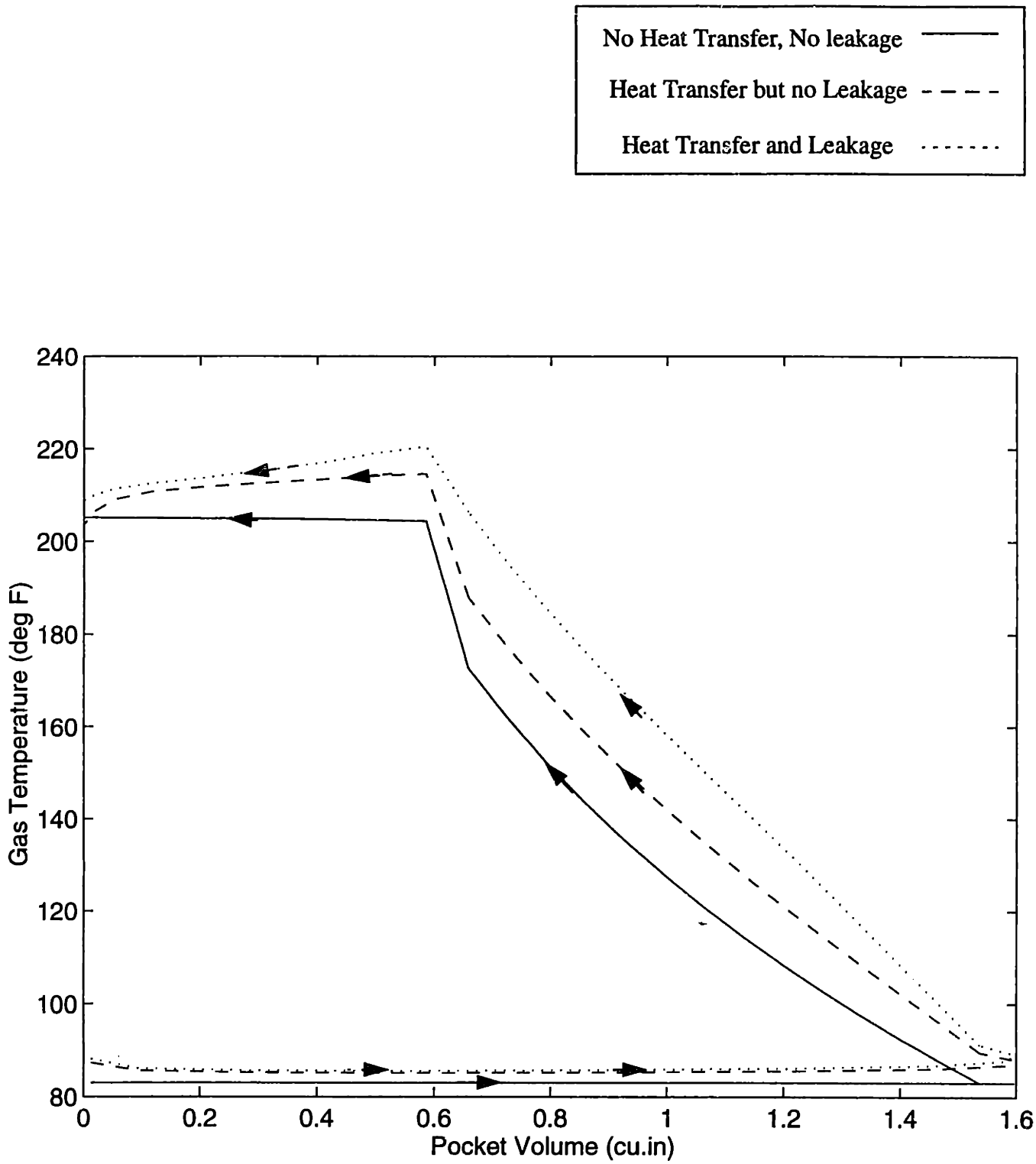


Figure 5-8: Average Gas Temperature Vs. Pocket Volume for Whole Cycle of ARI-C

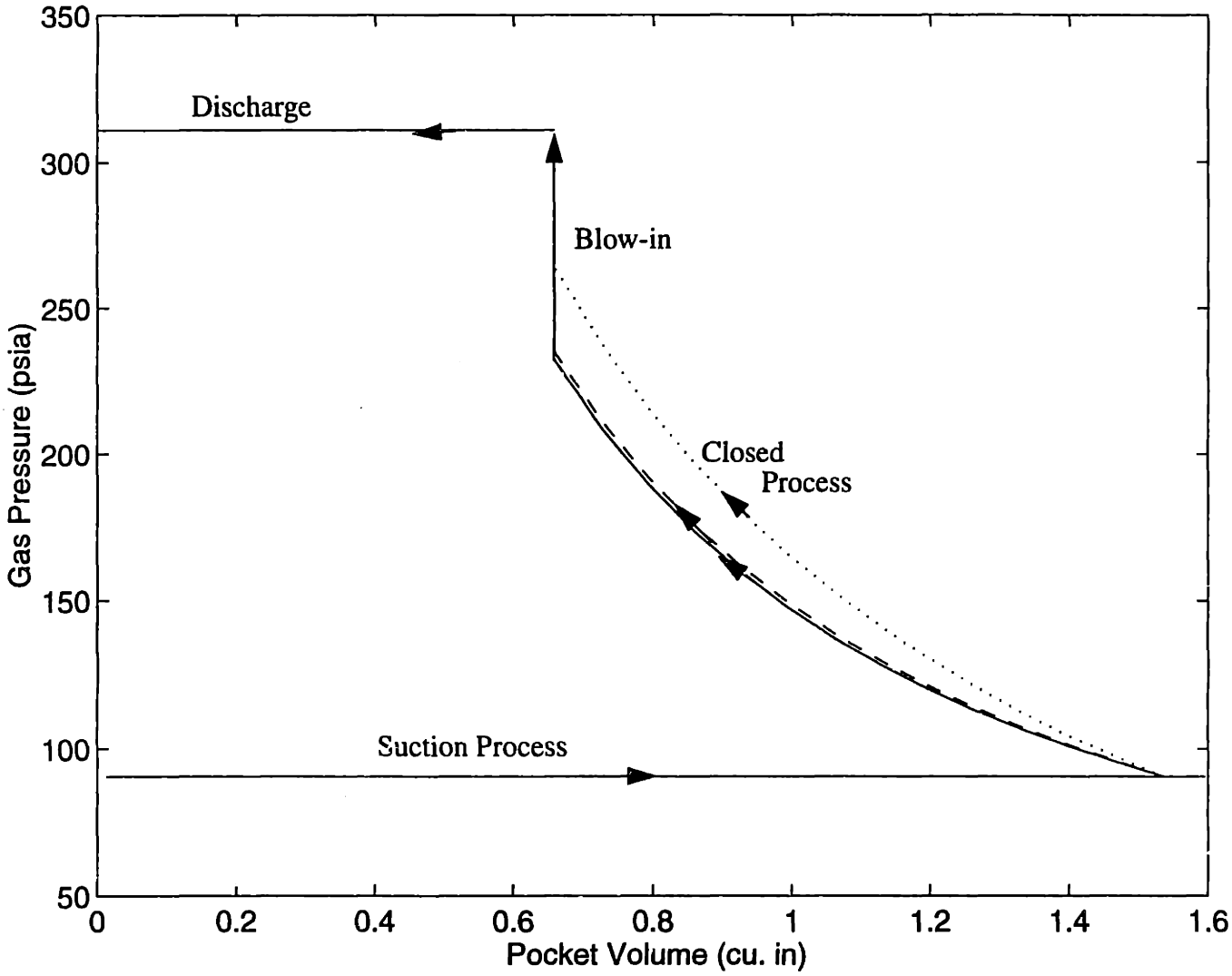


Figure 5-9: Pressure - Volume (P-V) Cycle for ARI-C

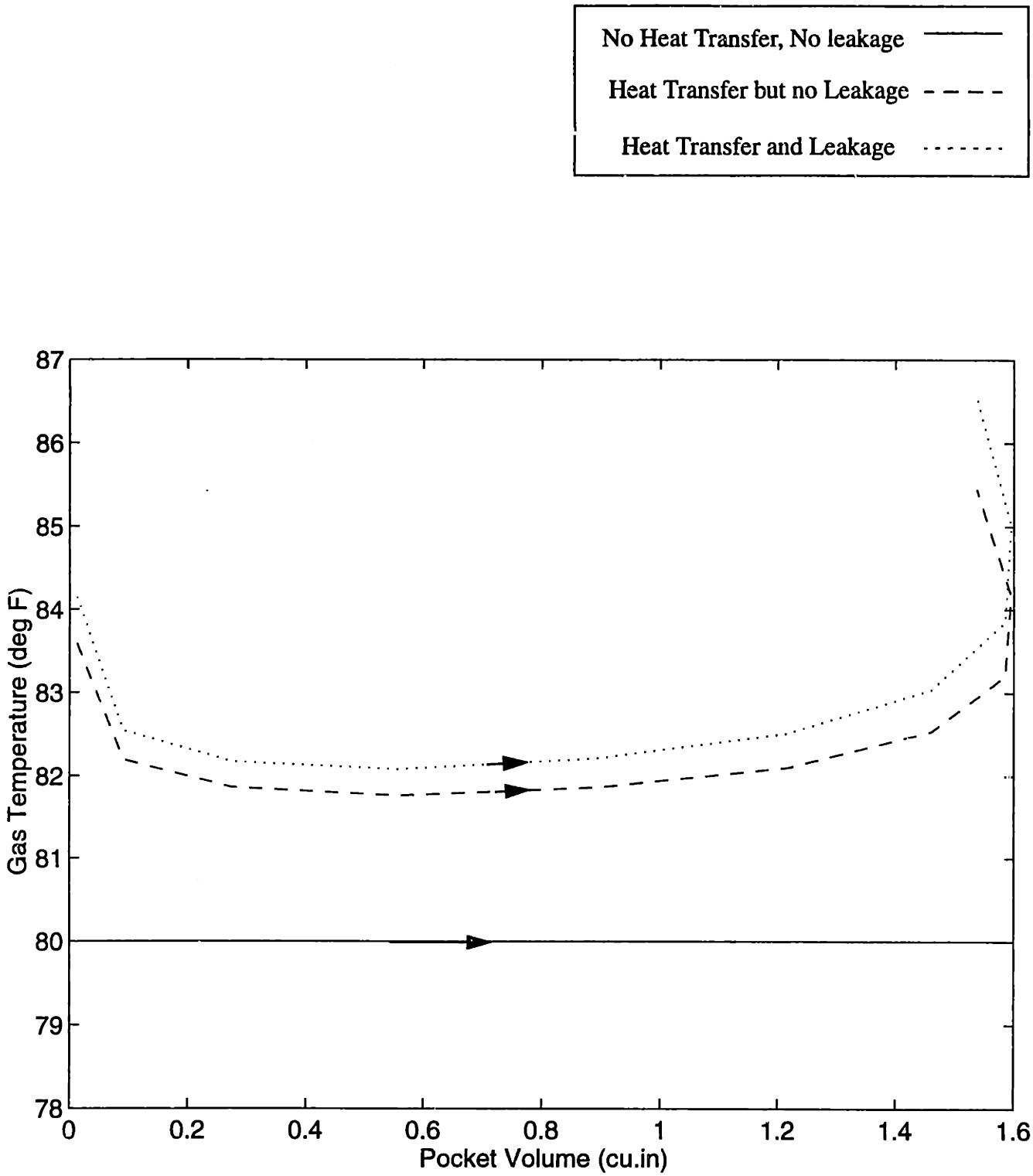


Figure 5-10: Average Gas Temperature Vs. Pocket Volume for Suction Process of CHEER

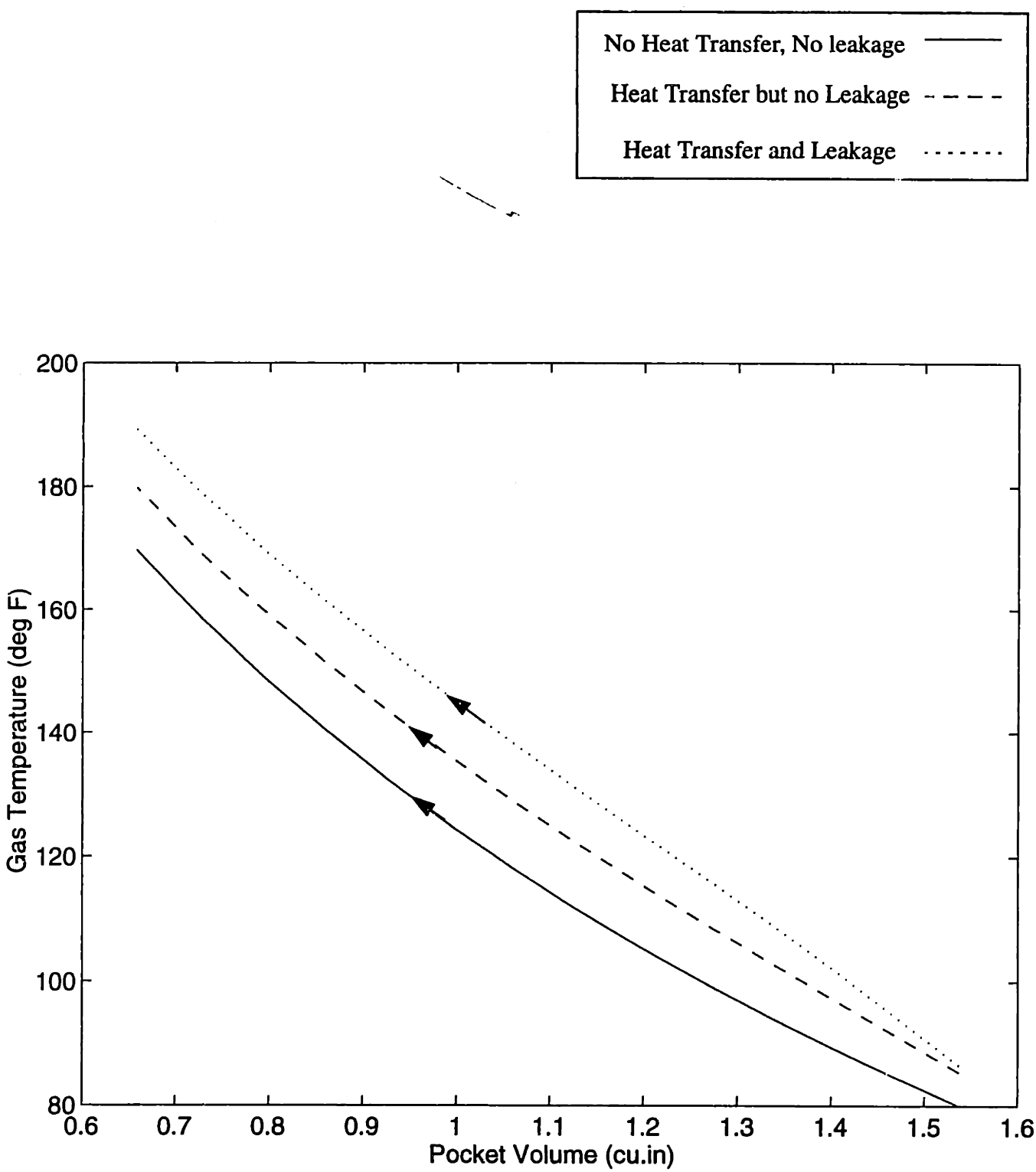


Figure 5-11: Average Gas Temperature Vs. Pocket Volume for Closed Process of CHEER

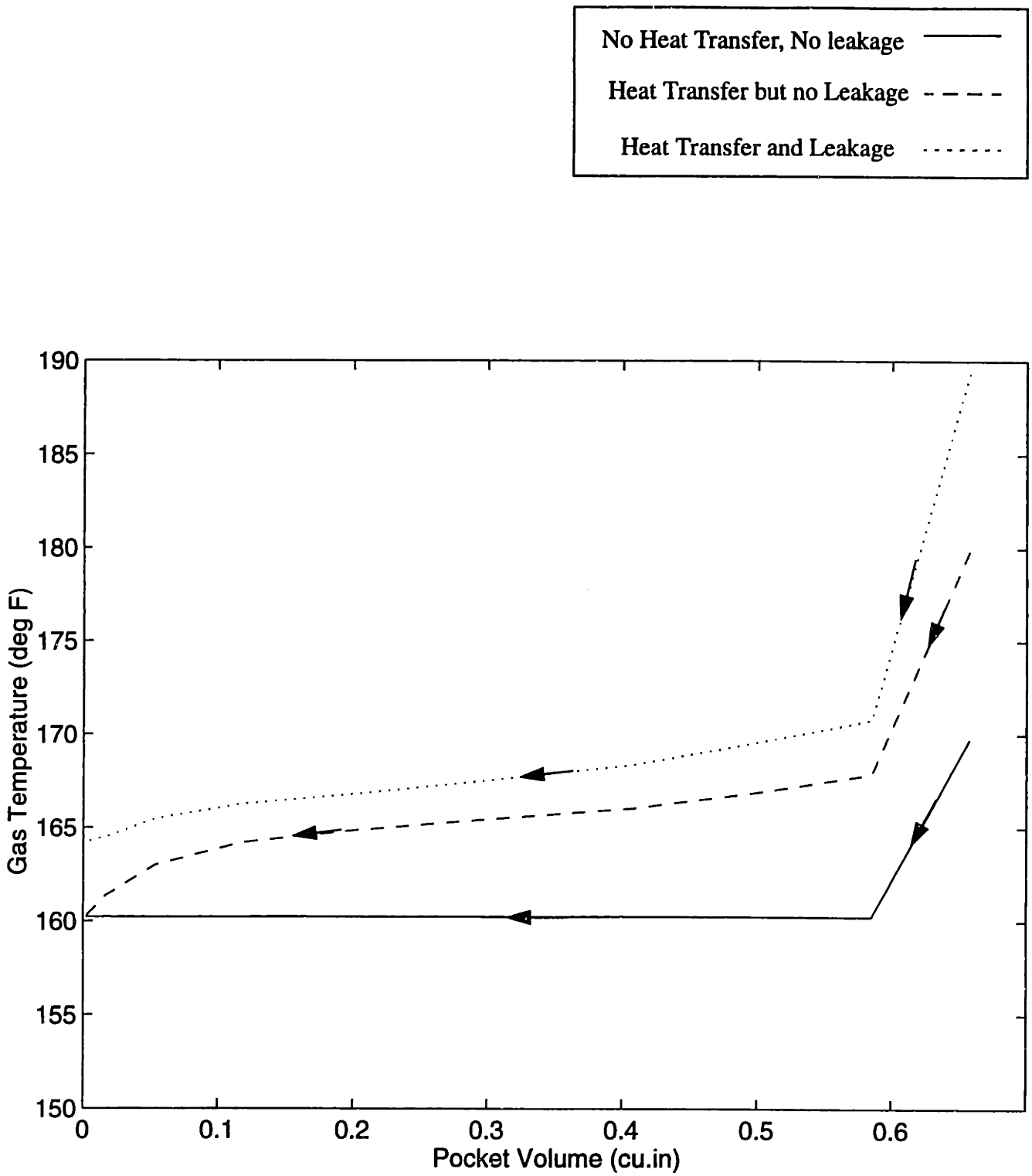


Figure 5-12: Average Gas Temperature Vs. Pocket Volume for Discharge Process of CHEER

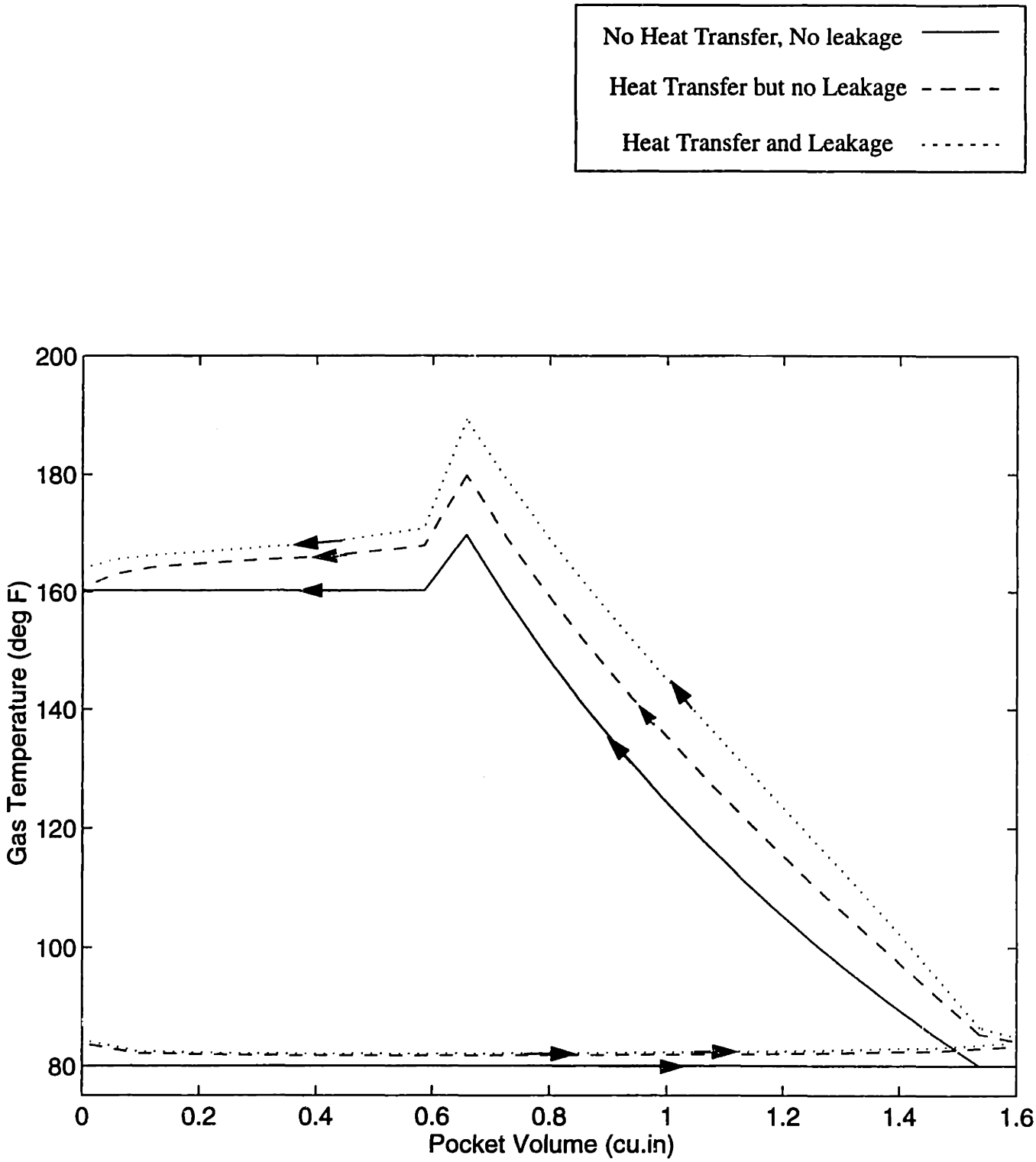


Figure 5-13: Average Gas Temperature Vs. Pocket Volume for Whole Cycle of CHEER

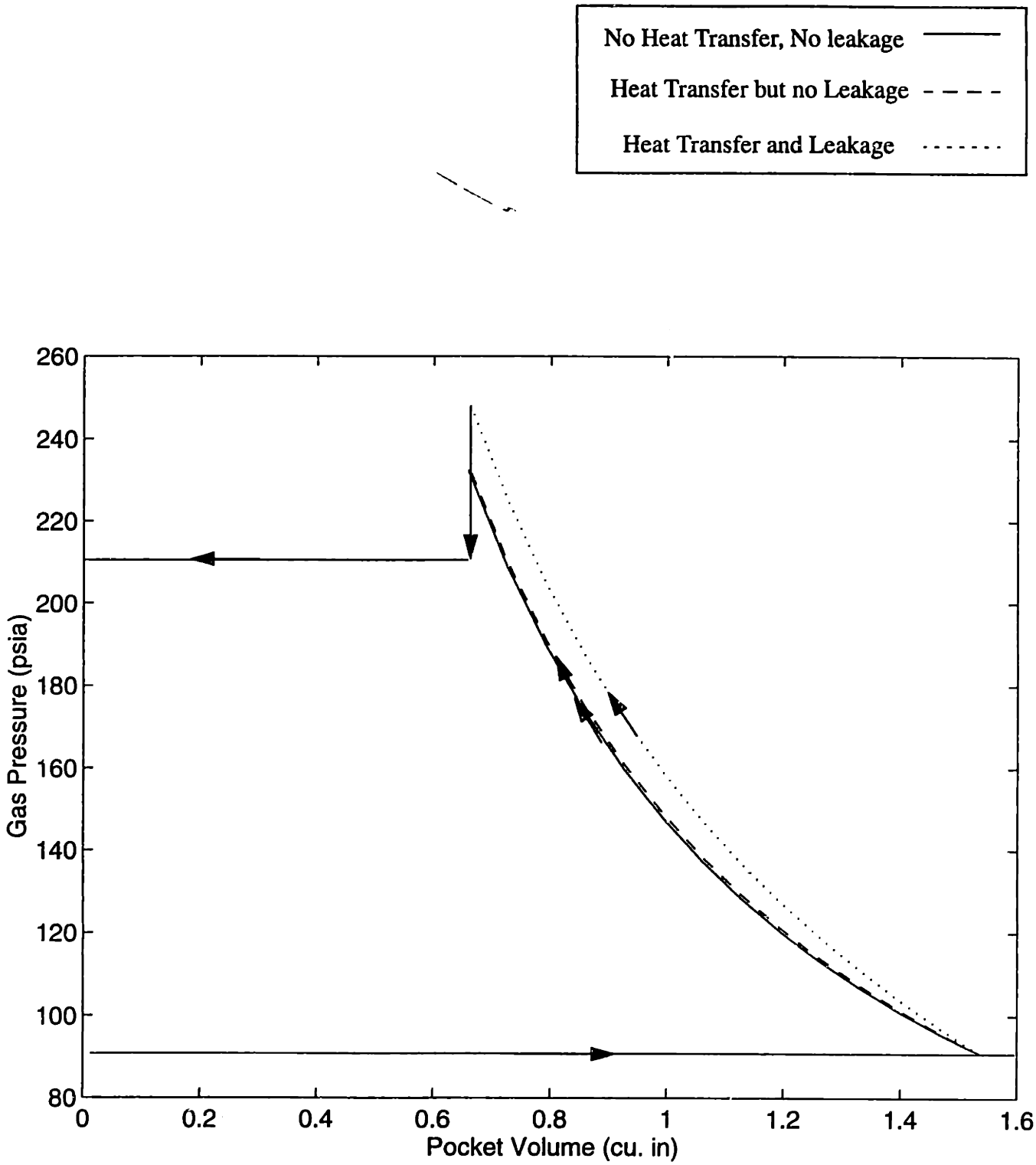


Figure 5-14: Gas Pressure Vs. Pocket Volume (P-V) plot for CHEER

## Table 5-1: Data for ARI-C (45/130/65)

From UTRC data,
TL = 83.0 F, m = 526 lb/hr, TH=204.0 F, n=1.174

Results of Simulation : -
TL = 83.0 F
TH = 200.0 F (Iterated Value)

| Setting | Inner Pocket | Outer Pocket | Pump |
|---|---|---|---|
| No Heat Transfer<br>No Leakage | TL = 83.0 F<br>m = 277.8 lb/hr<br>T1 = 83.0 F<br>T2 = 172 .8 F<br>P2 = 232.6 psia<br>n = 1.092 | TL = 83.0 F<br>m = 277.8 lb/hr<br>T1 = 83.0 F<br>T2 = 172 .8 F<br>P2 = 232.6 psia<br>n = 1.092 | m = 556<br>lb/hr |
| Heat Transfer<br>Allowed, but<br>No Leakage | TL = 80.0 F<br>m = 271.1 lb/hr<br>T1 = 89.6 F<br>T2 = 187.9 F<br>P2 = 237.0 psia<br>n = 1.113 | TL = 88.3 F<br>m = 267.4 lb/hr<br>T1 = 95.0 F<br>T2 = 192.9 F<br>P2 = 236.8 psia<br>n = 1.113 | m = 539<br>lb/hr |
| Heat Transfer<br>and Leakage<br>Allowed | TL = 80.0 F<br>m = 267.6 lb/hr<br>T1 = 91.2 F<br>T2 = 206.3 F<br>P2 = 267.1 psia<br>n = 1.251 | TL = 89.2 F<br>m = 263.4<br>T1 = 97.5 F<br>T2 = 211.0 F<br>P2 = 266.7 psia<br>n = 1.250 | m = 531<br>lb/hr |

Leakage Data : -

| Leakage Location | Inner Pocket | Outer Pocket | Outer Suction Pathway |
|---|---|---|---|
| Into Suction | 2.65 lb/hr | 2.68 lb/hr | 1.30 lb/hr |
| Into Closed Process | 27.55 lb/hr | 27.04 lb/hr | na |

State L = Suction Start, State 1 = Suction End, State 2 = Closed Process End, State H = Discharge
m = mass flow rate, n = polytropic coefficient

## Table 5-2: Data for CHEER (45/100/65)

From UTRC data,
TL = 80.0 F, m = 548 lb/hr, TH=160.0 F, n=1.171

Results of Simulation : -
TL = 80.0 F
TH = 165.0 F (Iterated Value)

| Setting | Inner Pocket | Outer Pocket | Pump |
|---|---|---|---|
| No Heat Transfer<br>No Leakage | TL = 80.0 F<br>m = 279.9 lb/hr<br>T1 = 80.0 F<br>T2 = 170 .0 F<br>P2 = 232.45 psia<br>n = 1.091 | TL = 80.0 F<br>m = 279.9 lb/hr<br>T1 = 80.0 F<br>T2 = 170 .0 F<br>P2 = 232.45 psia<br>n = 1.091 | m = 560<br>lb/hr |
| Heat Transfer<br>Allowed, but<br>No Leakage | TL = 80.0 F<br>m = 277.0 lb/hr<br>T1 = 85.4 F<br>T2 = 179.9 F<br>P2 = 235.0 psia<br>n = 1.104 | TL = 84.3 F<br>m = 274.9 lb/hr<br>T1 = 89.9 F<br>T2 = 183.8 F<br>P2 = 234.9 psia<br>n = 1.103 | m = 552<br>lb/hr |
| Heat Transfer<br>and Leakage<br>Allowed | TL = 80.0 F<br>m = 273.9<br>T1 = 86.5 F<br>T2 = 189.3 F<br>P2 = 250.1 psia<br>n = 1.176 | TL = 84.9 F<br>m = 269.9<br>T1 = 91.5 F<br>T2 = 193.3 F<br>P2 = 249.8 psia<br>n = 1.174 | m = 544<br>lb/hr |

Leakage Data : -

| Leakage Location | Inner Pocket | Outer Pocket | Outer Suction Pathway |
|---|---|---|---|
| Into Suction | 2.52 lb/hr | 2.54 lb/hr | 1.30 lb/hr |
| Into Closed Process | 15.88 lb/hr | 15.33 lb/hr | na |

State L = Suction Start, State 1 = Suction End, State 2 = Closed Process End, State H = Discharge
m = mass flow rate, n = polytropic coefficient

## Table 5-3: Table of Leakage Mass Flow rates into Suction

| Pump Setting | Inner Pocket (lb/hr) | Outer Pocket (lb/hr) | Outer Suction Pathway (lb/hr) | Total Leakage (lb/hr) | Pump ΔP (psia) | Suction Temp (deg F) |
|---|---|---|---|---|---|---|
| -10/90/10 | 1.02 | 1.03 | 0.50 | 2.55 | 151.9 | 56.0 |
| 10/110/30 | 1.49 | 1.50 | 0.80 | 3.79 | 193.6 | 68.0 |
| 25/90/45 | 1.81 | 1.83 | 0.95 | 4.59 | 119.6 | 69.0 |
| 40/110/60 | 2.36 | 2.39 | 1.20 | 5.95 | 152.8 | 79.0 |
| 45/120/65 | 2.60 | 2.62 | 1.30 | 6.52 | 183.9 | 84.0 |
| 55/150/75 | 3.15 | 3.17 | 1.50 | 7.82 | 288.9 | 97.0 |

## Table 5-4: Table of Leakage Mass Flow Rates into Closed Process

| Pump Setting | Inner Pocket (lb/hr) | Outer Pocket (lb/hr) | Total Leakage (lb/hr) | Pump ΔP (psia) | Discharge Temp (deg F) |
|---|---|---|---|---|---|
| -10/90/10 | 15.89 | 15.70 | 31.59 | 151.9 | 260.0 |
| 10/110/30 | 21.13 | 20.87 | 42.00 | 193.6 | 248.0 |
| 25/90/45 | 13.37 | 15.02 | 30.39 | 119.6 | 175.0 |
| 40/110/60 | 20.49 | 20.04 | 40.53 | 152.8 | 185.0 |
| 45/120/65 | 23.68 | 23.15 | 46.83 | 183.9 | 195.0 |
| 55/150/75 | 35.15 | 34.55 | 69.70 | 288.9 | 233.0 |

# Chapter 6

# Conclusions

## 6.1 Overview

The objective of this thesis is to understand the sources of irreversibility in a scroll pump and to provide a ,modeling tool with which to predict scroll pump operation. Towards that end, we described a lumped parameter model of the processes of a scroll pump in chapter 2 of the thesis. In describing the lumped parameter model, a number of assumptions were made and the presence of a novel form heat transfer (kissing heat transfer) postulated. In chapter 3 of the thesis, we performed analysis of heat transfer phenomena within a scroll pump and provided experimental verification of kissing heat transfer in scroll pumps. Since it is not possible with absolute certainty to validate all the assumptions of the lumped parameter model experimentally, we developed a distributed parameter model of the scroll pump in chapter 4. The results of the model (from chapter 5) validated the assumptions of the lumped parameter model, and also helped provide a physically consistent lumped parameter formulation of internal leakage in the scroll pump. In the section that follows, we briefly summarize each part of the thesis, followed finally by a section on suggestions for future work in scroll pump modeling.

## 6.2 Summary

### 6.2.1 Lumped Parameter Model

The lumped parameter model of a scroll pump was developed as a fast, easy and thermodynamically consistent model of the internal processes of a scroll pump. the model takes the suction state of the pump, the speed of the motor and the the discharge pressure of the pump as inputs and solves for intermediate thermodynamic states, mass flow rates and wall temperatures in the scroll pump. The model was developed to be solved using algebraic equations rather than the partial differential equations that describe gas and wall processes. Sources of irreversibility that have been incorporated into the model are heat transfer between suction side walls and suction gas, leakage of refrigerant into the suction process, leakage of refrigerant into and out of the closed process, blow-in / blow-out processes and heat transfer between discharge gas and pump walls near discharge. Heat is transferred between the pump walls at discharge and the pump walls at suction by a combination of conduction through the metal parts of the scroll and kissing heat transfer. Sources of irreversibility that were neglected in the model include friction

and closed cycle heat transfer. Of the two, friction was easy to dismiss based on experimental data. Experimental data however make it hard to distinguish between leakage and heat transfer phenomena. Kissing heat transfer's existence was also only postulated and not proven.

### 6.2.2 Kissing Heat Transfer

Lumped parameter heat transfer conductance estimations in a scroll pump suggested that heat transfer through transient contact between scroll wraps (kissing heat transfer) was a dominant mode of heat transfer between suction and discharge sides of a scroll pump. Such a mode of heat transfer is characterized by large heat fluxes across the wraps of a scroll pump. Such fluxes would be of large enough magnitude that they could not realistically be explained using convective heat transfer between scroll

wrap walls by convection. A specially instrumented scroll compressor was set up to provide experimental evidence of the presence of kissing heat transfer. Kissing heat transfer coefficients were analytically calculated based on estimation of contact angles by hertzian contact between scroll wraps. Such kissing heat transfer coefficients were found to agree with those estimated from the experiment. Further, the heat fluxes observed across scroll wraps were shown to be too large to be explained by convection between metal and gas in the pump.

### 6.2.3 Distributed Parameter Scroll Pump Model

A distributed parameter model of the internal processes of a scroll pump was developed with a view to gaining a deeper understanding of the various processes at play within a scroll pump. The distributed parameter model solves the partial differential equations governing continuity and energy for the gas in a scroll pump. Since this gas interacts with the metal parts of the pump, the energy interactions to the metal are also separately modeled.

Metal side simulations demonstrated that radial conduction in the base of the scrolls and kissing heat transfer between wraps are crucial in explaining the angular asymmetries in scroll metal temperature profiles as observed in the kissing heat transfer experiment. They also established the importance of axial conduction between the outer periphery of the wraps of the fixed scroll and the base of the fixed scroll.

Gas side simulations helped validate the assumptions of the lumped parameter model. They showed that leakage and heat transfer are crucial sources of irreversibility to the suction processes of a scroll pump. Closed process calculations demonstrated that the bulk of closed cycle irreversibility could be ascribed to leakage and that closed cycle heat transfer could be neglected. The outer suction pathway of the scroll pump causes suction gas to experience heat transfer and leakage even before reaching conjugate portions of the outer pocket. As a result of this pre-suction irreversibility, gas in the outer pocket tends to have a higher suction temperature and lower mass flow rate than that in the inner pocket. Inner and outer pockets of the scroll pump were however found to have nearly identical pressure profiles due to net

leakage into the closed cycle being nearly identical for both pockets. Based on data from a number of simulations of the pump, correlations were developed to obtain the lumped parameter formulation of leakage phenomena in the scroll pump. Leakage into suction was found to depend principally on the suction density, while that into the closed pocket depends on pressure difference across the pump as well as discharge density.

The results from the distributed parameter model raise the confidence and predictive value of the lumped parameter scroll pump model.

## 6.3 Recommendations for Future Work

1. The distributed parameter model assumes a constant convective heat transfer based on pipe flow correlations for heat transfer within the pump. Since the state of fluid in the pump varies between suction and discharge, the convective coefficient is likely to change with location within the scroll pump. Also, the validity of pipe flow correlations was never questioned even for the complex geometry of a scroll pump. Locally variable heat transfer coefficients that are determined from experiments specific to the geometry of a scroll pump would be a major refinement on the distributed parameter model.

2. This thesis demonstrates that small tip clearances in a scroll pump can lead to significant irreversibilities in the machine. Since we now have the ability to predict the scroll wall temperature profile for any operating condition, we might suggest that the dishing of scroll wraps be done with the actual temperature profiles in mind rather than linear formulae.

3. The lumped parameter model can be modified to help evaluate design changes on existing scroll pumps. Changes that might be evaluated are a change in volume ratio of the machine (or indeed variable volume ratios), intermediate cooling of the scroll pump metal, economizer cycles and the incorporation of non-return valves on the discharge side of the pump. Since kissing heat transfer

depends heavily on the material of the pump, the use of alternative materials and coatings may also be evaluated.

4. The utility of the lumped parameter model developed here hinges on its ability to make predictions on other scroll pumps. A modification of the lumped parameter model to predict the performance of the new generation of hybrid scrolls must be undertaken and its predictive ability experimentally evaluated.

5. Finally, it is hoped that the distributed parameter model derived here makes it easy to simulate future generations of thermodynamic machinery at the design stage itself.

# Appendix A

# Algorithm for Lumped Parameter Pump Model

## A.1 Overview

This appendix presents a lumped parameter thermal model of the internal processes of a scroll pump. The basic physics of the model are first briefly described below followed by an algorithm necessary to implement such a model on a computer.

Gas enters the scroll pump at state L (pressure $P_L$, temperature $T_L$), undergoes heat transfer with the fixed scroll wall (temp. $T_{wsuc}$), suffers leakage from the closed process of the machine (leakage mass flow rate of $\dot{m}_{leak,suc}$, and reaches a temperature $T_1$ by the end of the suction process. The suction process is characterized by scroll pocket volume increasing from zero to $V_1$, and work of suction $\dot{W}_{suc}$. For the purpose of the model, friction is assumed to be negligible as is any pressure drop associated with the suction process.

At the end of the suction process, gas is enclosed within a pocket of volume $V_1$, Pressure $P_1$, and temperature $T_1$. The closed pocket undergoes compression to a volume $V_2$. No heat transfer between wall and gas is assumed to take place during the closed process. However, gas of mass flow rate, $\dot{m}_{leak,dis}$ leaks into the closed pocket from the discharge side, while gas of mass flow rate, $\dot{m}_{leak,suc}$ leaks out of the closed process into the suction process of the succeeding scroll pocket. The gas

within the pocket is assumed to obey a polytropic process, so that $PV^n = const$ for any point within the closed process. The enthalpy of leakage into suction is assumed to be at a mean of suction and discharge enthalpies, (in reality close to the enthalpy associated with state 1), while leakage into the closed pocket leaks in with the enthalpy associated with the discharge state. Friction in the closed process is assumed to be negligible.

At the end of the closed process, gas at state 2 ($P_2$, $T_2$) undergoes a blow in or blow out process to equalize pressures with the discharge side, which is at a different pressure $P_H$. The blow in and blow out are assumed to be adiabatic processes. At the end of the blow in / blow out process, gas in the pockets (which are just open) is at state 2' ($P_H$, $V_2$, $T_{2'}$).

During the discharge process, gas at state 2' is discharged into the discharge tube of the compressor. During the process of discharge, the gas gets cooled from a temperature of $T_{2'}$ to the discharge temperature $T_H$. This heat is transferred to the fixed scroll wall at the discharge side, which is at temperature $T_{wdis}$.

Heat that is transferred to the scroll wall at the time of discharge is propagated back to the suction side, where it is transferred to the suction gas. The mode of heat transfer from discharge to suction is a combination of conduction heat transfer, and kissing heat transfer through the walls of the scroll pump.

## A.2 Features of the Model

### A.2.1 Inputs

Evaporator saturation Pressure $P_L$ (in psia)

Condenser saturation pressure $P_H$ (in psia),

Suction temperature (after motor preheating) $T_L$ (in deg F),

Speed of Rotation of motor, $N$ (in rpm)

### A.2.2 Scroll Pump Parameters

Displacement Volume of Pump,

$$V_1 = 3.08\ in^3$$

Volume of Pump at End of Closed Process,

$$V_2 = 1.30\ in^3$$

### A.2.3 Heat Transfer and Leakage Models

Suction Heat Transfer Conductance, $UA_{suc}$

$$UA_{suc} = 0.24\dot{m}^{0.8} \quad Btu/hr/^\circ F$$

Discharge Heat Transfer Conductance, $UA_{dis}$

$$UA_{dis} = 0.12\dot{m}^{0.8} \quad Btu/hr/^\circ F$$

Discharge-Suction Heat Transfer Conductance, $UA_{wall}$ (combination of kissing heat transfer and wall conduction)

$$UA_{wall} = 20.0 \quad Btu/hr/^\circ F$$

Mass Flow rate of leakage into suction, $\dot{m}_{leak,suc}$

$$\dot{m}_{leak,suc} = 4.46\rho_L$$

Mass Flow rate of leakage from discharge, $\dot{m}_{leak,dis}$

$$\dot{m}_{leak,dis} = 1.73\sqrt{\rho_H \Delta P}$$

### A.2.4 Outputs

Mass Flow rate, $\dot{m}$

Pocket Temperature at start of suction, $T_1$

Scroll wall temperature near suction, $T_{wsuc}$

Pocket temperature at end of Closed Process, $T_2$

Pocket pressure at end of closed process, $P_2$

Polytropic constant, $n$ characterizing Closed Process

Blow in / Blow out Mass Flow rate, $\dot{m}'$

Temperature of gas in scroll pocket after blowin/blowout, $T_{2'}$

Wall temperature of scroll near discharge $T_{wdis}$

Discharge gas temperature, $T_H$

Heat Transfer at Suction and Discharge, $\dot{Q}_{suc} = \dot{Q}_{dis}$

Reversible Work of Compression at suction, $\dot{W}_{suc}$

Closed Cycle Reversible Work, $\dot{W}_{poly}$

Reversible Work of Discharge, $\dot{W}_{dis}$

## A.3 Algorithm for Computing Model

In the algorithm that follows, all formulae are presented in such a manner as to be used directly with the units used in the section above. Therefore, numbers that appear in formulae typically are conversion factors.

### A.3.1 Suction

Work of suction is $\dot{W}_{suc}$.

$$\dot{W}_{suc} = -6.426 \times 10^{-3} P_L V_1 N \ Btu/hr$$

1. Guess temperature of fixed scroll near suction, $T_{wsuc}$ (in $^\circ F$)

2. Guess pump discharge temperature, $T_H$ (in $^\circ F$)

3. Guess $\dot{m}$ (in $lb/hr$)

4. Compute Leakage into suction, $\dot{m}_{leak,suc}$ (in $lb/hr$)

$$\dot{m}_{leak,suc} = 4.46\rho_L$$

Specific enthalpy of suction leakage is $h_{leak,suc}$ (in $Btu/hr/°F$)

$$h_{leak,suc} = \frac{h_L + h_H}{2}$$

5. Compute conductance of suction heat transfer

$$UA_{suc} = 0.24\dot{m}^{0.8} \quad Btu/hr/°F$$

6. Initially, guess temperature $T_1 = T_{wsuc} - 0.1$ (in $°F$)

7. Compute log mean temperature difference for suction heat transfer, $(\Delta T_{lm})_{suc}$ (in $°F$)

$$(\Delta T_{lm})_{suc} = \frac{T_1 - T_L}{log\frac{(T_{wsuc}-T_L)}{(T_{wsuc}-T_1)}}$$

Calculate $\dot{Q}_{suc}$ (in $Btu/hr$) through two different ways:

$$\dot{Q}_{suc1} = (UA)_{suc} \cdot (\Delta T_{lm})_{suc}$$

$$\dot{Q}_{suc2} = \dot{m} \cdot (h_1 - h_L) + \dot{m}_{leak,suc} \cdot (h_1 - h_{leak,suc})$$

If $\dot{Q}_{suc1} \neq \dot{Q}_{suc2}$, decrement $T_1$ by $0.1°F$ and repeat step 7 until convergence occurs.

8. Recalculate $\dot{m}$ (in $lb/hr$) using the pocket temperature $T_1$.

$$\dot{m}_{calc} = \frac{V_1}{12^3} \cdot \frac{60N}{v_1} - \dot{m}_{leak,suc}$$

where

$$v_1 = v(P_L, T_1)$$

If $\dot{m}_{calc} \neq \dot{m}$, then set $\dot{m} = \dot{m}_{calc}$ and loop back to step 5.

Repeat until convergence occurs.

At end of step 8, we should have consistent values for $\dot{m}$, $\dot{Q}_{suc}$ and $T_1$.

### A.3.2 Closed Process

1. Calculate leakage into closed process from discharge $\dot{m}_{leak,dis}$.

$$\dot{m}_{leak,dis} = 1.73\sqrt{\rho_H \Delta P}$$

Specific enthalpy of leakage into closed process is $h_{leak,dis}$

$$h_{leak,dis} = h_H$$

Net enthalpy of leakage into closed cycle is $H_{leak}$ where

$$H_{leak} = \dot{m}_{leak,dis} h_{leak,dis} - \dot{m}_{leak.suc} h_{leak,suc}$$

Net mass of leakage into closed cycle is $\dot{m}_{leak}$ where

$$\dot{m}_{leak} = \dot{m}_{leak,dis} - \dot{m}_{leak,suc}$$

2. Iterate on $P_2$, such that

$$(\dot{m} + \dot{m}_{leak,dis})u_2 - (\dot{m} + \dot{m}_{leak,suc})u_1 = \dot{W}_{poly} + H_{leak}$$

Here,

$$\dot{W}_{poly} = 6.426 \times 10^{-3} \frac{P_L {V_1}^n}{n-1} [{V_2}^{n-1} - V_1]^{n-1} N \ Btu/hr$$

where,

$$n = \frac{log\frac{P_2}{P_1}}{log\frac{V_1}{V_2}}$$

State 2 here is determined by $(P_2, v_2)$ where

$$v_2 = \frac{V_2}{12^3} \cdot \frac{60N}{\dot{m} + \dot{m}_{leak}}$$

Outputs of this calculation are $P_2$, $T_2$, $\dot{W}_{poly}$ and $n$.

### A.3.3 Blow in / Blow out

#### Blow in

If $P_2 < P_H$, then blow in occurs.

Calculate $\dot{m}'$ such that

$$(\dot{m} + \dot{m}_{leak,dis})u_2 + \dot{m}'h_H = (\dot{m} + \dot{m}_{leak,dis} + \dot{m}')u_{2'}$$

Here, state $2'$ is specified by $(P_H, v_{2'})$ where

$$v_{2'} = \frac{V_2}{12^3} \cdot \frac{60N}{\dot{m} + \dot{m}_{leak,dis} + \dot{m}'}$$

#### Blow out

If $P_2 > P_H$, then blow out occurs. (For blow out scenarios, $\dot{m}' = 0$).

Calculate state $2'$ such that

$$(\dot{m} + \dot{m}_{leak,dis})(u_{2'} - u_2) = -6.426 \times 10^{-3} P_H(V_{2'} - V_2)N$$

where

$$V_{2'} = \frac{v_{2'}}{60N} \cdot 12^3(\dot{m} + \dot{m}_{leak,dis})$$

State $2'$ here is characterized by $(P_H, v_{2'})$

### A.3.4 Discharge

Work of Discharge, $\dot{W}_{dis}$

$$\dot{W}_{dis} = 6.426 \times 10^{-3} P_H V_2 N \ Btu/hr$$

Compute Discharge - Suction Wall Heat Transfer Conductance,

$$UA_{wall} = 20.0 \ Btu/hr/^\circ F$$

1. Compute $T_{wdis}$, as $\dot{Q}_{suc} = \dot{Q}_{dis} = \dot{Q}_{wall}$

$$T_{wdis} = \frac{\dot{Q}_{suc}}{UA_{wall}} + T_{wsuc}$$

2. Compute Discharge Heat Transfer Conductance.

$$UA_{dis} = 0.12\dot{m}^{0.8} \quad Btu/hr/^\circ F$$

Calculate logmean temperature difference for discharge heat transfer.

$$(\Delta T_{lm})_{dis} = \frac{T_{2'} - T_H}{log\frac{T_{2'} - T_{wdis}}{T_H - T_{wdis}}}$$

Compute Discharge Heat transfer through two different ways.

$$\dot{Q}_{dis1} = (\dot{m} + \dot{m}_{leak,dis} + \dot{m}')C_p(T_{2'} - T_H)$$

$$\dot{Q}_{dis2} = (UA)_{dis} \cdot (\Delta T_{lm})_{dis}$$

If $\dot{Q}_{dis1} \neq \dot{Q}_{dis2}$, change $T_H$.

$$T_H = T_{2'} - \frac{\dot{Q}_{dis2}}{(\dot{m} + \dot{m}_{leak,dis} + \dot{m}')C_p}$$

Go back to step 3 of the Suction Process, and redo calculations till convergence occurs.

3. Check if $\dot{Q}_{dis} = \dot{Q}_{suc}$. If not, change $T_{wsuc}$.

$$T_{wsuc} = T_{wsuc} + \frac{\dot{Q}_{dis} - \dot{Q}_{suc}}{(UA)_{wall}}$$

Loop back to step 2 of the suction calculations, and redo calculations till convergence occurs. At the end of this step, the pump model should be complete.

## A.4 Conclusion

At the end of the calculations, all outputs of the model should be available and the pump model thermodynamically self-consistent. It must be noted that this is only one algorithm to solve the lumped parameter pump model. It is quite conceivable that there are other algorithms that are less prone to instability and that converge faster.

# Appendix B

# Friction as a Source of Closed Cycle Entropy Generation

## B.1 Overview

In this appendix, we use experimental data from a specially instrumented scroll compressor [8] to determine the magnitude of friction in a scroll compressor. We then show that the magnitudes of friction thus obtained are too small for friction to be the principal determinant of the polytropic coefficient and end states of the closed process of the scroll compressor. We also demonstrate that the magnitude of friction necessary to fully explain closed cycle irreversibility would be so large as to grossly undermine scroll compressor performance, a fact that is not supported by experimental data. The principal outcome of this appendix is that we stopped considering friction to be a very major source of scroll pump inefficiency and therefore dropped it from our subsequent analysis.

## B.2 Analysis of UTRC's Data

An intricate experiment conducted by a research team at United Technologies Research [8] measured power consumption, motor speed, metal and oil temperatures, refrigerant mass flow rate, as well as cyclical Pressure Volume ($P - V$) data for a

scroll compressor under a variety of operating conditions. This data can be used in conjunction with a motor electrical loss distribution model ([11]), and a bearing loss model to determine the magnitude of friction in the pump. Pump $P-V$ data from the experiment can also be used to estimate the frictional work necessary to account for all of scroll pump closed cycle irreversibility.

### B.2.1 Estimation of Pump Frictional Work

The total electrical power that is consumed by a scroll compressor, ($\dot{W}_{elec}$) is the sum of the mechanical power that is output by the motor of the compressor ($\dot{W}_{mech}$) and its electrical losses, ($\dot{W}_{elec-losses}$).

$$\dot{W}_{elec} = \dot{W}_{mech} + \dot{W}_{elec-losses}$$

While electrical power is directly measured from the experiment, electrical losses can be predicted with the aid of a motor loss distribution model, which takes the winding temperatures and slip (or speed) of the motor as inputs.

The mechanical power ($\dot{W}_{mech}$) put out by the motor is in turn the sum of the mechanical power consumed by the pump ($\dot{W}_{pump}$) and the mechanical losses, $\dot{W}_{bearings}$ associated with the bearings of the compressor. Here, the use of a bearings loss model enables us to determine the magnitude of the pump mechanical power, $\dot{W}_{pump}$.

$$\dot{W}_{mech} = \dot{W}_{pump} + \dot{W}_{bearings}$$

The total mechanical power consumed by the scroll pump can itself be attributed to two sources, namely the indicated work associated with gas compression ($\dot{W}_{PdV}$) and pump friction ($\dot{W}_{pump-fric}$). The indicated work associated with compression can now be calculated simply by finding the area under the $P-V$ curve of the pump, which is possible because of the fact that the experiment experimentally measures pump pocket pressure as a function of pocket position (and volume). Pump friction, then is simply the residual work after the indicated work is subtracted from pump

mechanical work.

$$\dot{W}_{pump-fric} = \dot{W}_{pump} - \dot{W}_{PdV}$$

Thus, we are able to arrive at a semi-experimental estimate of pump mechanical friction. Table $B-1$ presents the results of such an estimation for five scroll compressor operating conditions, while figure $B-1$ shows a schematic of the power consumption laws that we used in estimating pump friction.

### B.2.2 Closed Cycle Irreversibility

Experimental data from the $P-V$ cycle of a scroll pump suggests that the closed process of the pump follows a polytropic process, which can be characterized by $PV^n = const.$ The exponent $n$ is found in general to be greater than the isentropic exponent $\Gamma$, indicating an increase in entropy in the closed process. Here, we estimate the frictional work that would be necessary to explain all of the deviation of the closed process from entropy.

For a closed process that takes a pump from state 1 to state 2, and which suffers no source of irreversibility other than pump friction, the energy balance corresponding to the ends of the closed process is as shown below.

$$\dot{m}(u_2 - u_1) = \dot{W}_{poly} + \dot{W}_{fric,closed}$$

Here, $\dot{m}$ is the experimentally measured mass flow rate of refrigerant into the compressor, while state 1 is estimated assuming that pressure of the pump pocket does not rise (or fall) during suction. State 2 is then estimated with the assumption of no leakage into the closed process. $\dot{W}_{poly}$ is the $P-dV$ work associated with the closed process and can be calculated as follows:

$$\dot{W}_{poly} = \frac{1}{\tau}\int PdV = \frac{1}{\tau}\frac{P_1 {V_1}^n}{n-1}[{V_2}^{n-1} - V_1]^{n-1}$$

where $n$ is the polytropic exponent of the closed process, while $\tau$ is the time-period of rotation of the motor. $V_1$ and $V_2$ are the volumes of the scroll pump pockets

associated with the start and end of the closed process respectively, while $P_1$ and $P_2$ are the corresponding gas pressures. The frictional work that would be necessary to explain all of the deviation of the closed process from isentropy is then simply the difference of the increase in closed cycle internal energy and the closed cycle polytropic work.

$$\dot{W}_{fric,closed} = \dot{m}(u_2 - u_1) - \dot{W}_{poly}$$

Table $B-2$ shows the values of closed cycle pump friction estimated for the same 5 operating conditions as table $B-1$. As observed from the tables, the estimates of closed cycle pump friction on table $B-2$ are much larger than those on table $B-1$. In fact, some of the estimates of closed cycle pump friction in table $B-2$ are even larger than the experimental measurements of total electrical power consumption of the compressor. Clearly, if pump friction were the principal source of closed cycle irreversibility, the power consumption of the compressor would have been found to be significantly higher. The fact that experimental estimates of overall pump friction (from table $B-1$) are much smaller than the estimates of table $B-2$ suggests that pump friction is in reality fairly unimportant. The principal source of closed process irreversibility is therefore not pump friction.

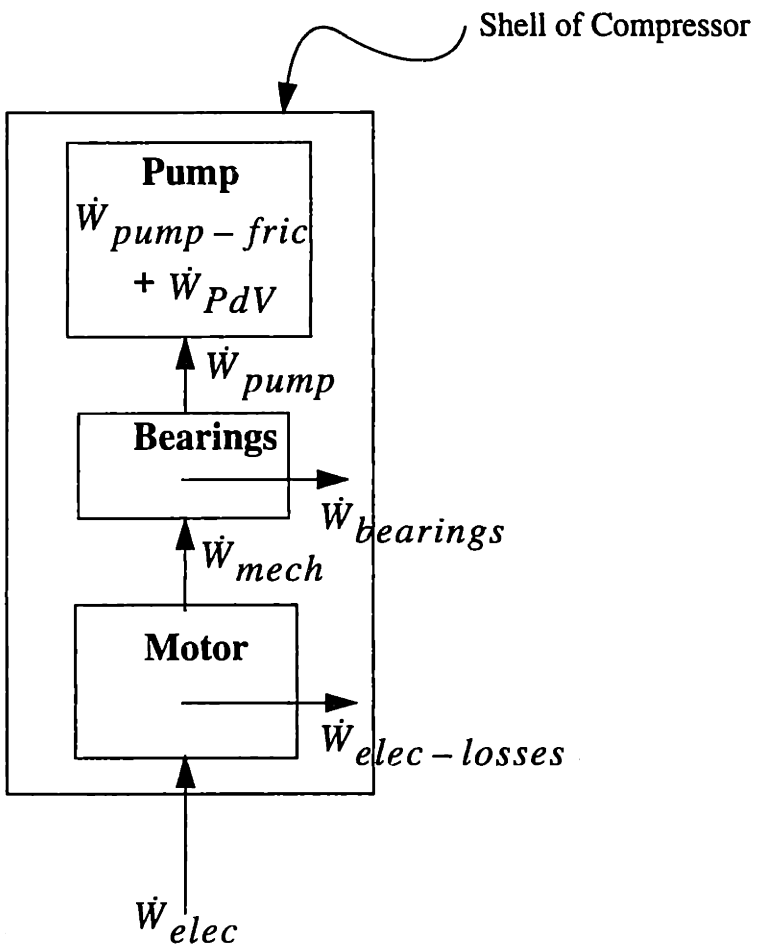


**Figure B-1: Power Balance on Hermetic Shell of Compressor**

| Operating Condition | $W_{elec}$ (Btu/hr) | $W_{elec\text{-}losses}$ (Btu/hr) | $W_{bearings}$ (Btu/hr) | $W_{PdV}$ (Btu/hr) | $W_{pump\text{-}fric}$ (Btu/hr) |
|---|---|---|---|---|---|
| -10/90/10 | 7782 | 1184 | 341 | 5408 | 849 |
| 10/110/30 | 9608 | 1358 | 341 | 7282 | 627 |
| 25/90/45 | 7765 | 1174 | 341 | 5254 | 996 |
| 45/120/65 | 10225 | 1375 | 341 | 7871 | 638 |
| 55/150/75 | 14324 | 2188 | 341 | 11645 | 150 |

Table B-1: Estimation of Pump Friction from Experimental Data

| Operating Condition | *Poly Coeff. (n)* | *Mass Flow Rate (lb/hr)* | *Wpoly* (Btu/hr) | $m\,(u_2\text{-}u_1)$ (Btu/hr) | $W_{fric,closed}$ (Btu/hr) |
|---|---|---|---|---|---|
| -10/90/10 | 1.333 | 163 | 2305 | 5295 | 2990 |
| 10/110/30 | 1.379 | 252 | 3567 | 9435 | 5868 |
| 25/90/45 | 1.180 | 370 | 4381 | 5616 | 1235 |
| 45/120/65 | 1.193 | 530 | 6254 | 8803 | 2549 |
| 55/150/75 | 1.313 | 608 | 7705 | 16829 | 9124 |

Table B-2: Estimation of Frictional Work Necessary to Account for all of Closed Process Irreversibility

# Appendix C

# P-V data for Closed Cycle

## C.1 Overview

In this appendix, we look at raw $P-V$ data corresponding to the closed processes of the $ARI-C$ and $CHEER$ operating conditions. This data was collected from a specially instrumented scroll compressor by researchers at UTRC [8]. We plot the pressure volume data for these two operating conditions on a log-log curve and demonstrate that the points all follow a process described by $PV^n = const$, where the exponent $n$ is fairly constant for the whole process. We regress the logarithm of pressure against the logarithm of volume and demonstrate that the statistical fit of a line through all the points is very good.

We also regress points corresponding to the start of the closed process separately from those corresponding to the end of the closed process. Results of the two regressions show that for both conditions, the polytropic coefficient for early parts of the cycle is greater than that for later parts of the cycle. However, the difference in polytropic coefficients is not sufficient tc account for closed process irreversibility completely with heat transfer. Significant closed process heat transfer would imply that $n > \gamma$ for early parts of the closed process (near suction), but $n < \gamma$ for later parts of the closed process (near discharge). Our regressions, however show that $n > \gamma$ throughout the closed process. Hence, if all closed process irreversibility were to be accounted for by heat transfer, such heat transfer would be unidirectional (into

the pocket) throughout the closed process. Unidirectional heat transfer, however is unphysical given that walls of the pump are hotter than the gas at the start of the closed process, but cooler than it at the end of the closed process.

The observed variation of closed process polytropic coefficient is consistent with leakage being the principal source of closed cycle irreversibility. The pressure difference associated with leakage into early parts of the closed process is greater than that associated with later parts of the closed process. This is so because leakage into the closed process is sourced principally at the discharge pressure. As a result, more leakage of mass occurs into the closed process at earlier portions of the closed process than the later portions. Thus, while entropy of the gas in the closed process is constantly increasing due to leakage, the rate of its increase diminishes as we go from the start to the end of the closed process.

Figure C-1 plots the P-V data for the *ARI* operating conditions, while figure C-2 plots that corresponding to the *CHEER* operating condition.

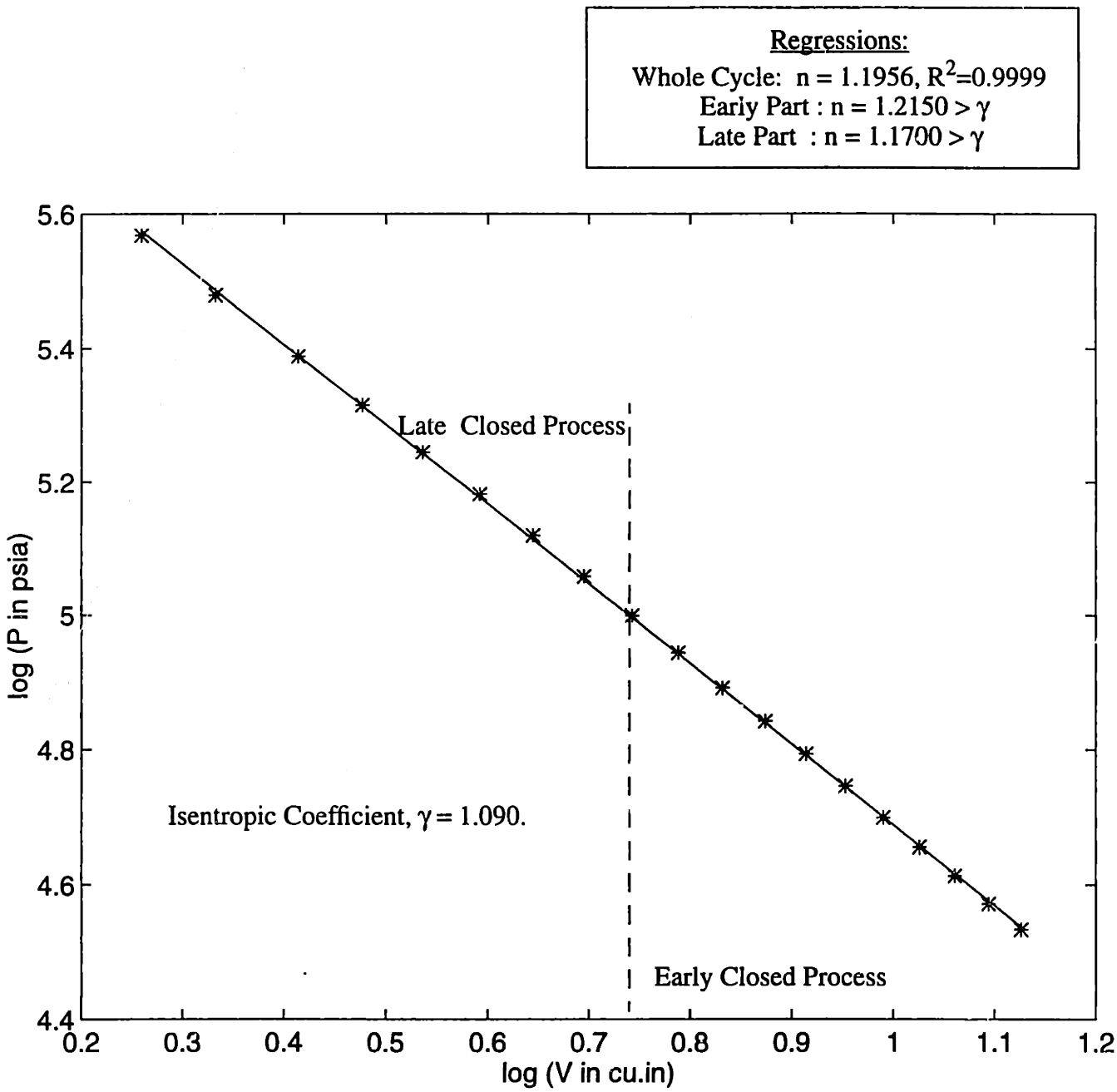


Figure C-1: log(P) Vs log(V) for ARI-C Operating Condition

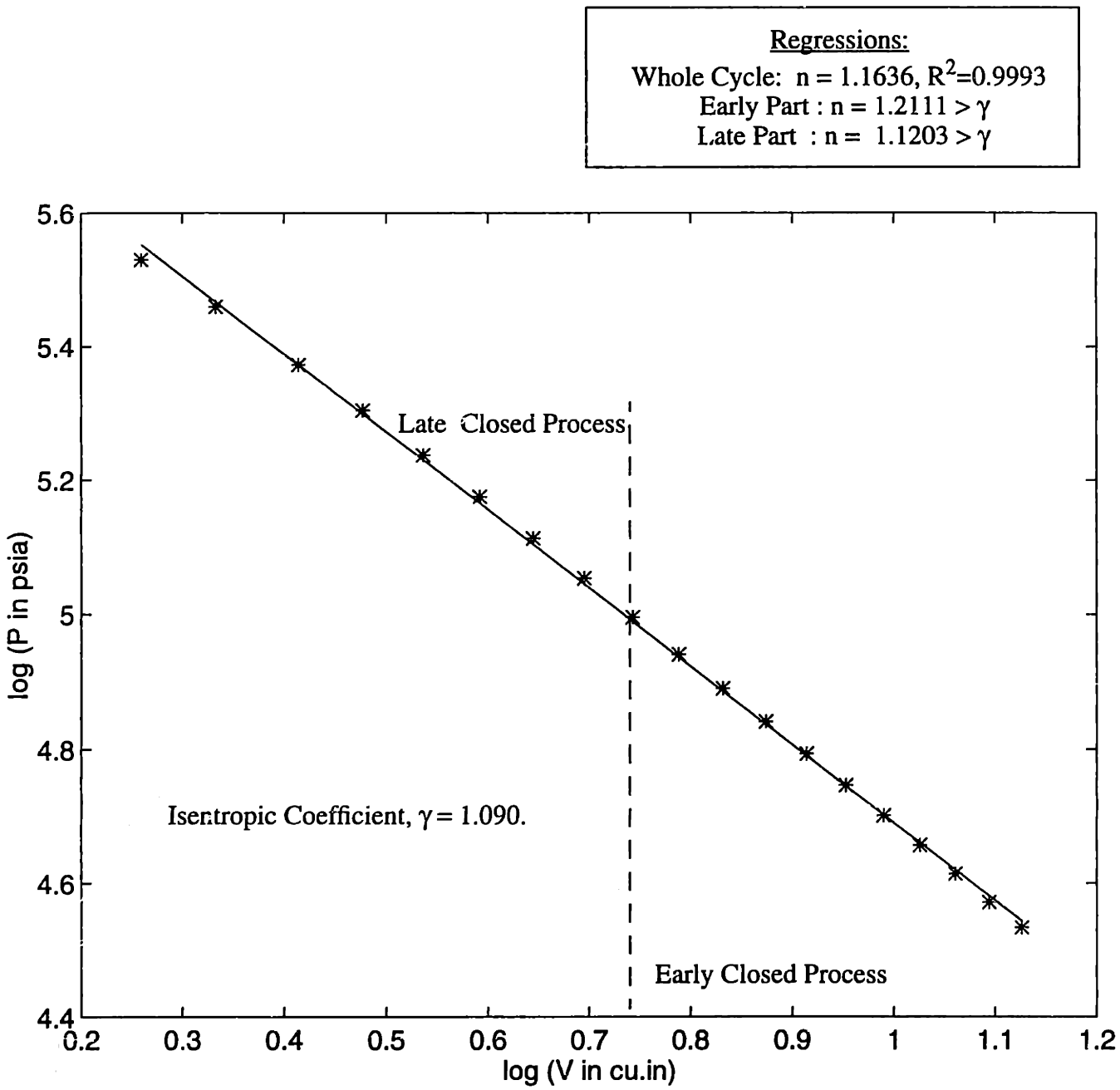


Figure C-2: log(P) Vs log(V) for CHEER Operating Condition

# Appendix D

# Leakage as a Source of Closed Cycle Entropy Generation

## D.1 Overview

In this appendix, we use data from UTRC's [8] experiment to estimate net leakage from the discharge side of the pump that would be necessary to account for all the deviation of the closed process from isentropy. Thereafter, we plot the calculated leakage mass flow rate versus pressure difference across the compressor and demonstrate that the net leakage mass flow rate does seem to be proportional to the pressure difference across the pump. Since such a dependence of leakage on pressure difference makes physical sense and since we are unable to account for closed process irreversibility using heat transfer and friction, we conclude that friction must be the principal source of closed process irreversibility in the scroll pump.

## D.2 Calculation of Leakage Mass Flow Rate

The energy balance for a closed polytropic process with leakage as the sole source of irreversibility is as shown below.

$$(\dot{m} + \dot{m}_{leak})u_2 - \dot{m}u_1 = \dot{W}_{poly} + \dot{m}_{leak}h_H$$

Here, $\dot{m}_{leak}$ is the net leakage of mass from pump discharge into the closed process. We neglect any leakage of mass out of the closed process into suction and assume that all leakage mass comes in with the specific enthalpy $h_D$ associated with discharge. $\dot{m}$ is the experimentally measured mass flow rate of refrigerant through the system while states 1 and 2 are the start and end of the closed process. $\dot{W}_{poly}$ is the $P - dV$ work associated with the polytropic process.

$$\dot{W}_{poly} = \frac{1}{\tau}\int PdV = \frac{1}{\tau}\frac{P_1 V_1{}^n}{n-1}[V_2{}^{n-1} - V_1]^{n-1}$$

As with appendix $B$, the state 1 of the gas at the start of the closed process is calculated assuming no rise/fall of gas pressure during suction and assuming no leakage of gas into suction (i.e.) using the displacement rate of the pump and the mass flow rate through the system.

$$v_1 = \frac{V_1}{\dot{m} \cdot \tau}$$

$$T_1 = T(P_1, v_1)$$

State 2 on the other hand is affected by the level of leakage and is therefore not known a priori. Through a process of iteration, we calculate the leakage mass flow rates that satisfy the energy equation associated with the closed process as well as the continuity equation associated with state 2 (since the mass of gas in the pocket has risen due to leakage).

$$v_2 = \frac{V_2}{(\dot{m} + \dot{m}_{leak}) \cdot \tau}$$

$$T_2 = T(P_2, v_2)$$

## D.3 Leakage vs $\Delta P$

Figure D-1 shows a plot of the calculated leakage mass flow rate versus the pressure difference of the pump. As seen from the figure, there is a clear dependence of leakage mass flow rate upon the pressure difference across the pump. Such a dependence

makes physical sense because any internal leakages that occur in the pump are likely to occur across gaps between wraps and tips and at pinch points across pressure differences that in general mirror those across the pump. From the figure, it is also clear that the fit of the regression is not perfect (only 76due to a variety of reasons. First of all, we are erroneous in ascribing all closed process irreversibility to leakage when we know that there will be small portions of the irreversibility that have to be ascribed to heat transfer and friction. Secondly, in the spirit of a lumped parameter model, we have neglected any leakage that may occur from the closed cycle to suction instead assuming that all leakage occurs from the discharge side of the pump to the closed process. Thirdly, we have assumed that the closed process is perfectly represented by a polytropic process when in fact, closed cycle polytropic coefficient does vary a little bit locally within the closed process. The principal idea behind the plot (and the regression) here is simply to demonstrate a physical plausible mechanism of leakage within a scroll pump.

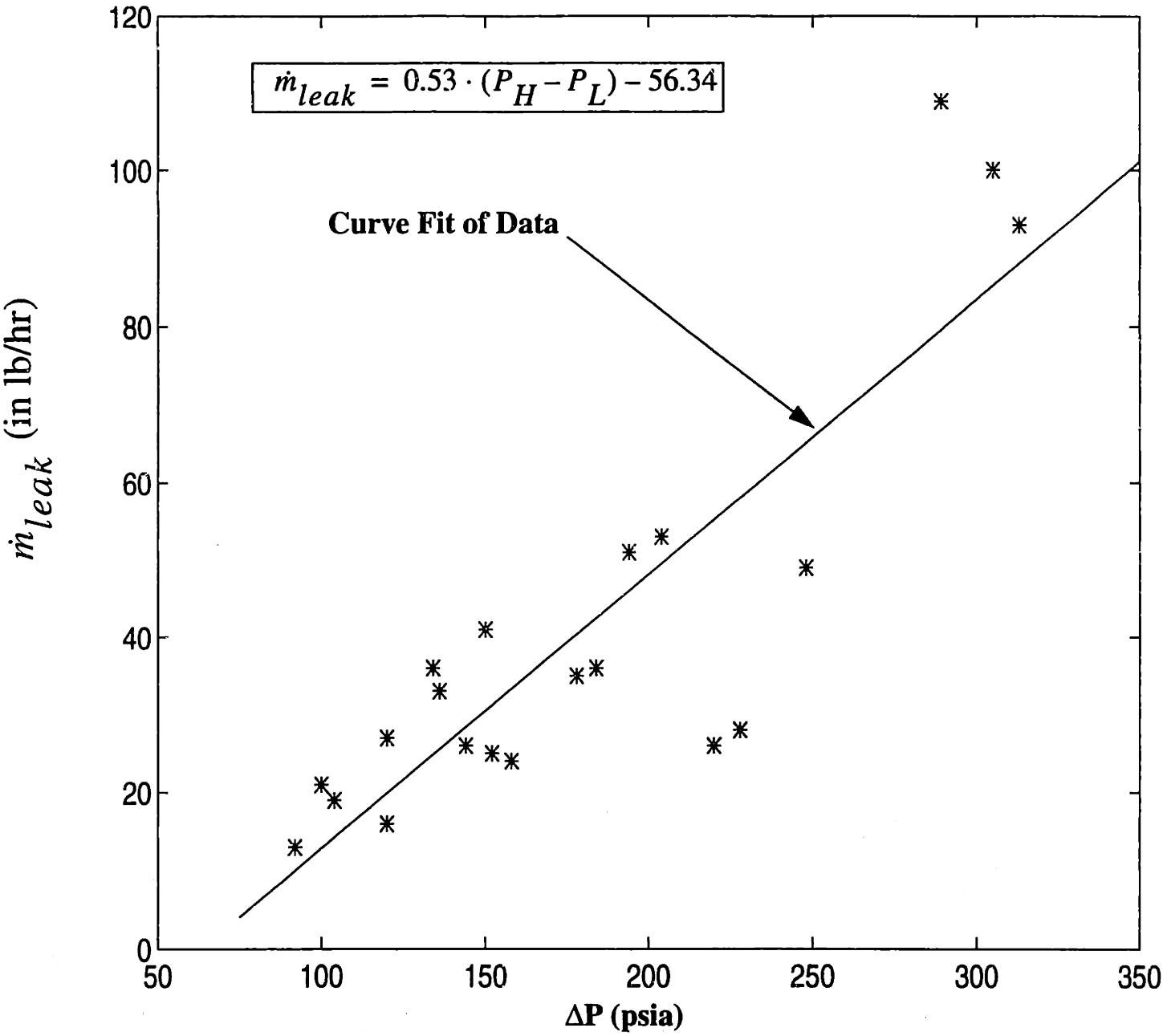


Figure D-1: Calculated Leakage Vs ΔP

# Bibliography


[1] Vedat S. Arpaci. *Conduction Heat Transfer.* Ginn Press, 1991.

[2] James W. Bush and Wayne P. Beagle. Derivation of general relation governing the conjugacy of scroll profiles. *Proceedings of the Purdue Compressor Conference*, 1992.

[3] James W. Bush, Wayne P. Beagle, and Mark E. Housman. Maximizing scroll compressor displacement using generalized wrap geometry. *Proceedings of the Purdue Compressor Conference*, 1994.

[4] Leon Creux. Rotary engine. *U. S. Patent 801, 182*, 1905.

[5] J. Gallagher, M. McLinden, and M. Huber. *NIST Thermodynamic Properties of Refrigerants and Refrigerant Mixtures, Version 3.0.* U.S. Department of Commerce, 1991.

[6] Frank P. Incropera and David P. Dewitt. *Fundamentals of Heat and Mass Transfer, Second Edition.* John Wiley and Sons, 1985.

[7] Patrick Cheong-Yu Leung. *Thermal analysis of an oil and R-22 cooled compressor motor.* M.S. Thesis, Massachusetts Institute of Technology, 1995.

[8] Anthony J. Marchese. *An Experimental Investigation into the Thermal, Mechanical, Electrical, Pressure, and Stability Characteristics of the Carrier 3 Ton Scroll Compressor.* Advanced Compressor Technology, United Technologies Research Center, 1992.

[9] Haluk Tolga Ozgen. *Investigation of Motor Heat Transfer in Hermetic Scroll Compressors.* M.S. Thesis, Massachusetts Institute of Technology, 1996.

[10] Raymond J. Roark and Warren C. Young. *Formulas for Stress and Strain, Fifth Edition.* Mc-Graw Hill and Company, 1975.

[11] Steve Umans. Steady-state, lumped parameter model for capacitor run, single-phase induction motors. *Proceedings of IEEE-IAS Annual Meeting, Denver, CO,* 1994.

[12] W. R. Zimmerman. A general approach to using a stiff equation solver to integrate a system of partial differential equations. *Numerical Methods for Partial Differential Equations, 11,* 1995.